UNIVERSITA' DEGLI STUDI DI PAVIA

Dipartimento di Biologia e Biotecnologie

"L. Spallanzani"

Celiac disease and autophagy: new functional perspectives in diagnosis and treatment

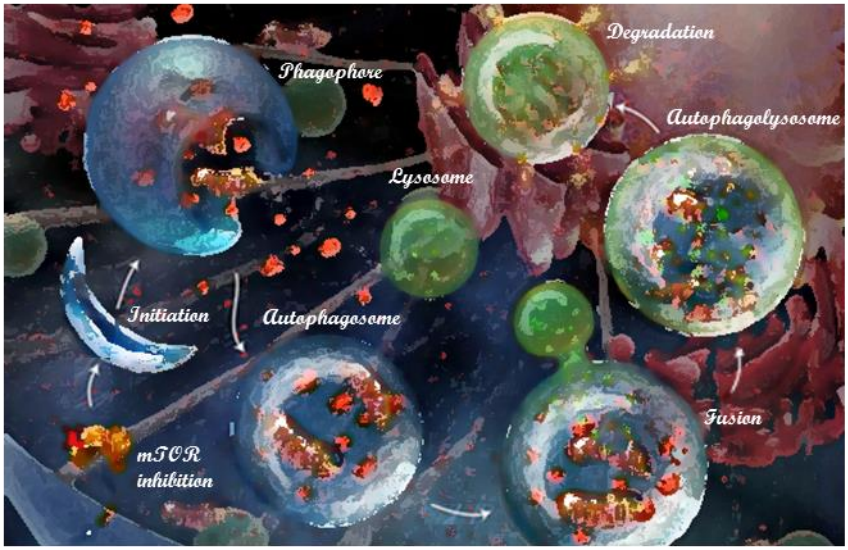

Federico Manai

Dottorato di Ricerca in
Genetica, Biologia Molecolare e Cellulare
XXIX Ciclo – A.A. 2013-2016

UNIVERSITA' DEGLI STUDI DI PAVIA

Dipartimento di Biologia e Biotecnologie

"*L. Spallanzani*"

Celiac disease and autophagy: new functional perspectives in diagnosis and treatment

Federico Manai

Supervised by Prof. Sergio Comincini

Dottorato di Ricerca in
Genetica Biologia Molecolare e Cellulare
XXIX Ciclo – A.A. 2013-2016

Abstract

Celiac disease (CD) is the most common inflammatory disease of the intestine. It is a chronic systemic autoimmune disorder affecting the small bowel of genetic susceptible individuals. CD is triggered by the ingestion of gluten, a storage protein present in wheat, barley and rye.

CD frequency in the general population of Europe and United States is approximately 1% whereas in Finland and Sweden it reaches peaks of respectively 2% to 3%. In Italy, the estimated prevalence is 0.7%, however the number of patients currently undiagnosed seems to be largely superior to known cases.

The only effective therapy is a gluten-free diet (GFD). Nevertheless, 7 to 30% of all patients is not responsive to GFD because inadvertent ingestion of gluten.

The two major challenges about CD concern diagnosis and treatment. Auto-antibodies in the serum represent a valuable tool for CD diagnosis, but a percentage of patients remains elusive because of the presence of mild symptoms. Moreover, despite international established guidelines, there is still controversy about the use of endoscopy as the essential step in CD diagnosis. Nowadays, the attention of the researchers has shifted in the identification of new non-invasive diagnostic biomarkers. Because of their characteristics, microRNAs (miRNAs) have been emerged as promising candidate not only in CD field but also for other disorders, such as Crohn disease and ulcerative colitis. The issues concerning the GFD have prompted researchers to investigate for alternative treatments. Currently, two pharmacological agents are investigated in late clinical trials as non-dietary treatments for CD.

Autophagy is a cellular process that is implicated in immunity and autoimmunity as well as in the degradation of protein aggregates. Impairment of autophagic flux contributes to the pathogenesis of several disorders characterized by the accumulation of toxic protein aggregates, such as Alzheimer and Parkinson disease.

Accordingly, a collaborative study was born with the Pediatric Auxology Unit and the Pediatric Surgery Unit of the Fondazione IRCCS Policlinico San Matteo. Thus, the first resulted aim of this Thesis is to investigate the role of key autophagic genes and of their regulatory miRNAs sequences as new candidate biomarkers in CD. For this purpose, blood and intestinal biopsies were collected by an exploratory cohort of pediatric CD patients and controls matched for sex and age. The obtained results suggest

that the investigated autophagy-related genes and miRNAs could have a potential diagnostic power to distinguish between CD patients and controls. Moreover, specific expression profiles could be use for CD patients' stratification.

The role of autophagy in the metabolism of gliadin was then studied in an *in vitro* model obtained with Caco-2 cells and modulation of this cellular process was performed in order to counteract the toxicity of these peptides. The results indicate that autophagy is implicated in gliadin degradation and that impairment of this process affects the release of gliadin outside the cells by exocytosis. On the other hand, autophagy induction leads to gliadin degradation, decreases its secretion and confers a proliferative advantage to cells.

On the whole, these preliminary results indicate that the study of autophagy could be interesting for the search of new diagnostic biomarkers. The finding that autophagy is implicated in gliadin metabolism will possibly allow the identification of new therapeutical approaches based on the modulation of this cellular process.

Acknowledgements

This study was carried out in the laboratory of Functional Oncogenomics at the Department of Biology and Biotechnology - University of Pavia in collaboration with the Pediatric Auxology Unit and the Pediatric Surgery Unit of the Fondazione IRCCS Policlinico San Matteo of Pavia.

I want to thank Prof. Sergio Comincini for leading me during these years in his laboratory. As the good teacher described by Anatole France, he awakened the natural curiosity of my young mind for the purpose of satisfying it afterwards. I would dedicate to him this sentence of Henry Adams: “A teacher affects eternity; he can never tell where his influence stops”. I want to thank also all the Funcional Oncogenomics laboratory staff for the continuous human and professional support, in particular many thanks to Mariarita Lillo and Valentina Fermi (the ‘Ferlillo’ girls), Sabrina Commissario, Carolina Martinelli, Sara Adrasto and the new entries Fabio Gabriele, Martina Morandi and Blanca Fabre. A special thank to my friends and colleagues Marta Esposito, Ibrahim Bitar, Alice Mazzagatti, Stefania Brandini and Mirella Bensi.
Thank also to all the collaborator in Policlinico S. Matteo, particularly Prof. Mauro Bozzola, Prof. Gloria Pelizzo and Dr. Cristina Meazza.

Finally, I want to thank all the people that contributed to achieving this goal. A big thank to my mom and my brother to whom I dedicate this PhD thesis.

Abbreviations

AGA Anti-gliadin antibodies
APC Antigen presenting cell
ATG Autophagy-related protein
ATI Amylase/trypsin inhibitor
CD Celiac disease
DC Dendritic cell
DGP Deaminated gliadin peptides
EMA Endomysial antibodies
ESPGHAN European society for pediatric gastroenterology hepatology and nutrition
FDA Food and drug administration
GFD Gluten-free diet
HLA Human leukocyte antigen
IBD Inflammatory bowel disease
IEC Intestinal epithelial cell
IEL Intraepithelial lymphocyte
Ig Immunoglobulin
LAK Limphokine-activated killer
MHC Major histocompatibility complex
miRNA microRNA
mTOR Mammalian target of rapamycin
NCGS Non celiac gluten sensitivity
NRCD Non responsive celiac disease
PT-gliadin Peptic-tryptic gliadin
RCD Refractory celiac disease
RT-PCR Real-Time PCR
siRNA small interfering RNA
TG2 Transglutaminase 2
TLR Toll-like receptor
TNFα Tumor necrosis factor α
UC Ulcerative colitis

Contents

1. Introduction and review of the literature

1.1 Celiac disease

Celiac disease (CD), also referred as celiac sprue and gluten-sensitive enteropathy in medical literature, is a chronic systemic autoimmune disease of the small intestine. It was considered as a gastrointestinal disorder of childhood for a long period of time, until Vilppula and colleagues (2008; 2009) demonstrated that adults can also develop CD. This disease results from an immune response, in genetically susceptible individuals, to ingested dietary gluten and its related peptides in the form of wheat, barley and rye cereals and other environmental factors (Di Sabatino and Corazza, 2009).

1.1.1 Epidemiology

Originally considered as a rare disease, it is now known that CD is one of the most common inflammatory disorders of the small bowel, affecting people all over the world. The emergence of highly sensitive and specific serological tests have substantially helped to identify the true prevalence of CD (Fasano and Catassi, 2012). In Europe and United States, the mean frequency of CD in the general population is approximately 1% with some regional differences, the reason for which remains elusive. The prevalence of CD is as high as 2% to 3% in Finland and Sweden, whereas it is only 0.2% in Germany, although these areas share a similar distribution to causal factors (level of gluten intake and frequency of HLA-DQ2 and -DQ8) (Mustalahti *et al.* 2010; Fasano *et al.* 2003). In Italy, the estimated prevalence is 0.7%, but the number of patients currently undiagnosed seems to be largely superior to known cases. Indeed, about 100,000 people have been diagnosed with CD, but it is believed that there are at least another 500,000 undiagnosed cases. This phenomenon is related to the presence of prevalent forms of CD with nonspecific symptoms. Furthermore, the prevalence of CD is higher in first-degree relatives of CD patients (10-15%) (Bozzola *et al.* 2014). The new epidemiology of CD shows an increase in the percentage of cases in Western countries and a high incidence in other areas of the world. This disease is common in North Africa and Middle East: particularly, CD prevalence reaches 5.6% in a population of Western Sahara, the Saharawi, of Arab-Berber origin. The reason of this frequency is still unclear but it may be due to strong genetic predisposition and dietary

changes (Catassi *et al.* 2015). For what concern Asia, epidemiology of CD is confined to India, despite the diagnosis is still difficult because of malnutrition. The frequency seems to be higher in the northern part of the country, the so-called celiac belt, in which the CD prevalence is 1.04% and overall sero-prevalence is 1.44% (Makharia *et al.* 2011). Two recent geoepidemiological studies showed the paradoxical distribution of CD prevalence and its causative factors in the world. The major CD-predisposing haplotype (HLA-DQ2) has a high frequency in Middle East (countries consuming more wheat) compared with Europe (countries consuming less wheat) in which there is a higher prevalence of CD (Abadie *et al.* 2011). To explain these findings, Lionetti and Catassi (2014) suggested that the diffusion of CD and its causative factors occurred in different times and that the current high prevalence of CD is the result of a positive selection of CD-predisposing haplotypes in wheat-consuming population started in the Neolithic period (**Figure 1 and 2**).

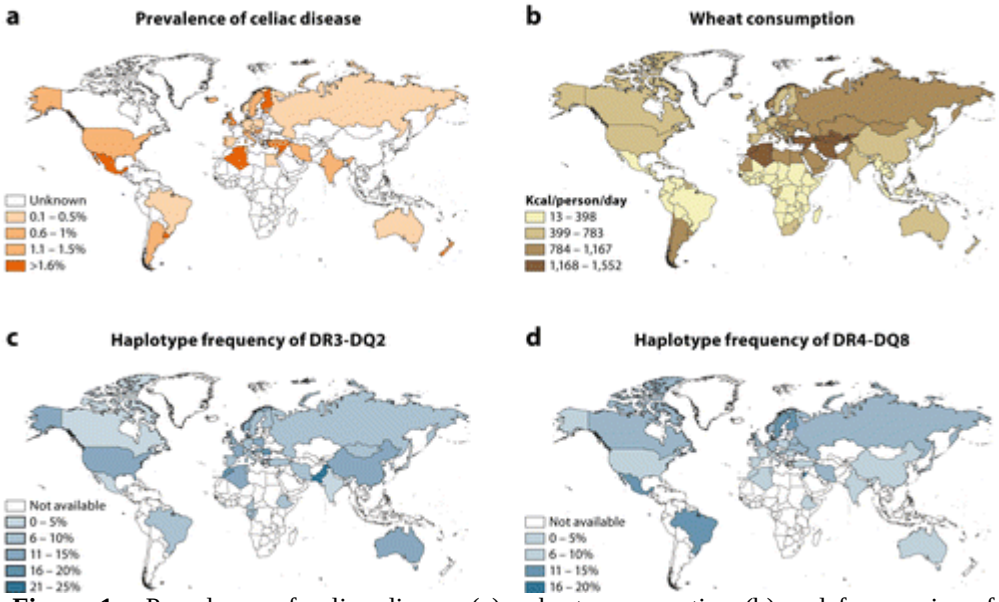

Figure 1: Prevalence of celiac disease (a), wheat consumption (b) and frequencies of HLA-DQ2 and HLA-DQ8 (c and d) worldwide (Abadie *et al.* 2011).

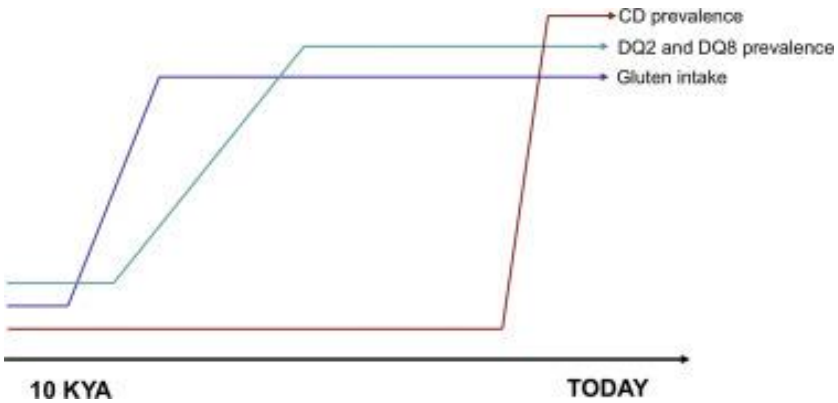

Figure 2: Model of CD diffusion during time. Gluten intake increased during the agriculture revolution in Middle East and Europe, followed by an increase in HLA-DQ2/DQ8 aplotypes due to positive selection. The prevalence of CD in modern time was triggered by other environmental changes (Lionetti and Catassi, 2014).

1.1.2 Genetic risk

CD is a complex disorder with a non-Mendelian pattern of inheritance, involving human leukocyte antigen (HLA) genes and non-HLA genes. Genetic linkage studies show that the primary genetic predisposing factors are the HLA-DQ alleles on chromosomes 6p21.3 (CELIAC1), which encodes for paralogues of the α and β chain of the major histocompatibility complex class II (MHC II). This complex binds peptides derived from antigens that access the endocytic route of antigen presenting cells (APC) and presents them on the cell surface for recognition by the CD4+ T-cells. Most of the patients with CD have a variant of DQ2 (DQA1*05-DQB1*02) and a minority of patients a variant of DQ8 (DQA1*03-DQB1*0302) (Sollid *et al.* 1989, 1993). Vader *et al.* (2003) demonstrated that only HLA-DQ2.5 can present a large repertoire of gluten peptides compared with HLA-DQ2.2, which can present only a subset of these peptides. Some rare individuals inherit alleles that code for half of the DQ2-/DQ8- heterodimer (DQA1*05 or DQB1*02 but not both), underlining the importance of HLA-DQ molecules in the genetic susceptibility to CD (Karell *et al.* 2003). HLA-DQ2 on the membrane of antigen-presenting cells (APC) has a key role in CD by presenting gluten peptides to pathogenic CD4+ T-cells in the *lamina propria* of the small bowel (Arentz-Hansen *et al.* 2000). Although the HLA-DQ locus shows a consistent involvement in CD over the global population, it is carried by approximately one third of Caucasians, suggesting the existence of other genes involved in the development of CD. Other genetic factors have been reported:

- CELIAC2 (5q31-33), which contains cytokine gene clusters (Greco *et al.* 1998)
- CELIAC3 (2q33.2), which encodes for CTLA4, a member of the immunoglobulin superfamily and a costimulatory molecule on activated T-cells (Djilali-Saiah *et al.* 1998). Hunt *et al.* (2005) suggested that some variants of this gene could mediate loss of tolerance to gluten and related peptides in CD.
- CELIAC4 (19p13.1), which encodes for the myosin IXB variant (Van Belzen *et al.* 2003). A defect in this gene may be involved in the perturbation of intestinal mucosal homeostasis and consequent

defects in the barrier property before the onset of the inflammatory response (Monsuur *et al.* 2005)

- CELIAC6 (4q27), a region that encompassed the KIAA1109, TENR, IL2 and IL21 genes (Van Heel *et al.* 2007). In particular, IL2 and IL12 are both implicated in intestinal inflammation.
- CELIAC8 (2q11-q12), a region which contains the IL18RAP and IL18R1 genes (Hunt *et al.* 2008). IL18 plays a key role in the mucosal inflammation after interferon-γ (IFN-γ) synthetizing induction by T-cells. IL18RAP and IL18R1 encode respectively for the β and α chain of the IL18 receptor: in particular, IL18RAP is over-expressed in unstimulated T-cells and NK cells of CD patients.
- CELIAC9 (3p21), a large cluster of chemokine receptor genes that includes CCR1, CCR2, CCRL2, CCR3, CCR5 and XCR1 (Hunt *et al.* 2008)
- CELIAC10 (3q25-q26), which encodes for the IL12A gene (Hunt *et al.* 2008). This gene codifies the IL12 p35 subunit of IL12 p70, an heterodimeric cytokine that induces interferon-γ-secreting Th1 cells.
- CELIAC12 (6q25.3), which contains the Rho GTPase-activating protein TAGAP, generally involved in cytoskeletal modifications (Hunt *et al.* 2008)
- CELIAC13 (12q24), a region that encompassed the SH2B3 gene, strongly expressed in the small bowel of CD patients (Hunt *et al.* 2008). This protein links T-cells receptor activation to PLC-γ-1, GRB2 and PI3K.

A second-generation genome-wide association study (Dubois *et al.* 2010) identified other CD predisponsing genes implicated in immune functions (BACH2, CCR4, CD80, CIITA-SOCS1-CLEC16A, ICOSLG and ZMIZ1) or thymic T-cells selection (ETS1, RUNX3, THEMIS and TNFRSF14).

1.1.3 Environmental factors

CD develops after the ingestion of prolin-rich and glutamine-rich proteins in genetically susceptible host. Other environmental cofactors can contribute to CD onset.

Gluten

Gluten is a mixture of storage proteins present in wheat, barley, rye, oat and all their species and hybrids, such as spelt, kamut and triticale. These proteins are joined with starch in the endosperm of various types of grains and are necessary for plant germination. Gluten contains hundreds of proteins (called prolamins), in the form of mono-, oligo- or polymers linked by interchain disulphide bonds, rich in proline and glutamine. Wheat prolamins are called gliadins and glutenins, prolamins from barley are hordeins and prolamins from rye and oat are, respectively, secalins and avenins (Wieser, 2007). Gluten is appreciated for its viscoelastic properties. For what concern wheat, gliadins and glutenins show different soluble properties: in fact, gliadin is the alchol soluble component of gluten whereas glutenin is insoluble. Gliadins can be subdivided into four different types, according to their aminoacid sequences and composition and their MWs: ω5-, ω1,2-, α/β- and γ-gliadins (Wieser, 1996).

Type	MW×10^{-3}	Proportions[a] (%)	Partial amino acid composition (%)				
			Gln	Pro	Phe	Tyr	Gly
ω5-Gliadins	49–55	3–6	56	20	9	1	1
ω1,2-Gliadins	39–44	4–7	44	26	8	1	1
α/β-Gliadins	28–35	28–33	37	16	4	3	2
γ-Gliadins	31–35	23–31	35	17	5	1	3
x-HMW-GS	83–88	4–9	37	13	0	6	19
y-HMW-GS	67–74	3–4	36	11	0	5	18
LMW-GS	32–39	19–25	38	13	4	1	3

a According to total gluten proteins.

Figure 3: Gluten protein types. HMW-GS and LMW-GS indicate, respectively, high- and low-molecular-weight glutenins (Wieser *et al.* 1996).

Several gliadin epitopes show immunogenic and toxic properties. These epitopes present multiple Pro and Gln residues that give rise to the following characteristics (Kim *et al.* 2004):

1. Resistance to proteolysis by gastric, pancreatic and intestinal proteases
2. These peptides have a particular conformation due to the high level of Pro residues that is the conformation preferentially adopted by MHC class II ligands
3. Selected Gln residues are target for deamination by tissue transglutaminase (TG2) in normal conditions. These modifications lead to an increased immunogenicity

There are two epitopes that are more immunogenic than others: the immunodominant PFPQPQLPY and PQPQLPYPQ in the α2-gliadin fraction (Hausch *et al.* 2002). These two epitopes are present together with the epitope PYPQPQLPY in the immunodominant 33mer peptide, LQLQPFPQPQLPYPQPQLPYPQPQLPYPQPQPF (residues 57-89) (Shan *et al.* 2002).

Other factors

Recent studies have shown that CD patients have differences in their intestinal microbiota composition compared with healthy controls (Nistal *et al.* 2012, Di Cagno *et al.* 2011). Schippa *et al.* (2010) demonstrated also the existence of a microbial signature among untreated CD patients and patients under gluten-free diet. Human microbiota is also able to affect gluten metabolism. Caminero *et al.* (2016) showed that *Pseudomonas aeruginosa*, an opportunistic pathogen in CD patients, can cleave the proteolytic resistant 33mer peptide through the action of the protease LasB, thus increasing its immunogenic properties. On the contrary, *Lactobacillus* spp. in mice show fast and effective gluten metabolism leading to a decrease in its toxicity. These studies and others suggest a key role of human gut microbiota and correlated environmental factors (e.g. antibiotics) in the modulation of gluten tolerance (Cenit *et al.* 2015).

1.1.4 Pathophysiology

Gluten peptides can be translocated across intestinal epithelium to the *lamina propria* through two different mechanisms. Transcytosis is an intestinal apical-to-basal uptake mechanism of macromolecules. The immunodominant 33mer peptide in CD patients preferentially uses this mechanism to translocate (Schumann *et al.* 2008) as the contribution of the paracellular pathway seems to be negligible (Ménard *at al.* 2012), despite gliadin is able to alter zonulin expression, increasing intestinal permeability (Drago *et al.* 2006). Matysiak-Budnik and colleagues (2008) demonstrated that gliadin peptides, including the 33mer and p31-55, can also undergo a protected transport in CD by retrotranscytosis of SIgA through the Tf receptor (CD71). In active CD, in fact, IgA are high concentrated in the apical membrane of small bowel epithelia and can form high molecular weight complexes with gliadin peptides that have a strong affinity to CD71, which is up-regulated because of villous atrophy and consequent iron-deficiency anemia. Gluten peptides are modified by the enzymatic activity of extracellular TG2, whose levels and activity raise after tissue injury (Siegel *et al.* 2008). TG2 is able to deamidate non-charged glutamine into negatively charged glutamate acid, thus increasing the overall negative charge of gliadin and improving its binding affinity to HLA-DQ2/DQ8 molecules (Molberg *et al.* 1998). These molecules are present in the membrane of APCs including dendritic cells (DCs), that migrate in lymphoid tissues and mesentheric lymph nodes after the recognition of gliadin peptides (Bernardo, 2013). As a consequence, DCs present gliadin-antigen to $CD4^+$-naïve T-cells promoting the repertoire expansion of gluten-specific Th1/Th17 pro-inflammatory T-cells with a concomitant production of IFN-γ, TNF-α, IL-18 and IL-21. These cells expressed the $\alpha_4\beta_7$ integrin, essential to migrate in the gut (Escudero-Hérnandez *et al*. 2016). IFN-γ leads to an increased expression of HLA-DQ2/DQ8 and, as a result, to an increased gluten peptides presentation. This self-amplifiyng loop is further exacerbated by the release of TG2 as a result of the gluten-specific $CD4^+$ T-cells action (Tjon *et al.* 2010).

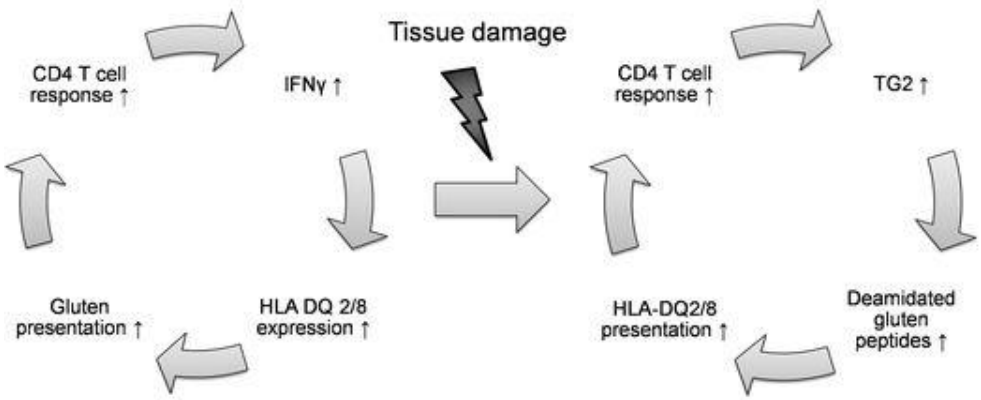

Figure 4: Mechanism of phatogenesis of CD. HLA-DQ2$^+$ and HLA-DQ8$^+$ individuals present native gluten peptides on APC to CD4+ T-cells. The release of INF-γ increased the expression of HLA-DQ2/DQ8. The consequent inflammation leads to tissue damage and the release of TG2, which is able to deamidate native gluten peptides and expand their repertoire. CD4+ T-cells response is enhanced and more IFN-γ is produced, thus increasing the inflammatory response (Tjon *et al.* 2010).

In active CD, the release of IFN-γ increases the number of CD8$^+$ TCRαβ$^+$ and TCRγδ$^+$ intraepithelial lymphocytes (IELs) with innate-like lymphokine-activated killer (LAK) activities, expressing the CD94/NKG2C and NKG2D receptors (Meresse *et al.* 2006). At the same time, intestinal epithelial cells (IECs) over-expressed the ligands of CD94/NKG2C and NKG2D, respectively MICA and HLA-E as response to the stress caused by IL-15. The interaction between IELs and IECs through their receptors and ligands produces the release of IFN-γ and cytolysis, worsening the tissue damage. IL-15 plays a key role in promoting IECs perforin-granzyme-dependent lysis by IELs (Meresse *et al.* 2004). CD4$^+$ T-cells can also interact with B-cells during their maturation to produce specific TG2 and gluten antibodies (Escudero-Hérnandez *et al*. 2016). There is still debate whether the innate immune response at IECs level precedes or not the adaptive immune response in the *lamina propria.* IL-15 action is more pronounced in refractory celiac disease (RCD) patients, in which the uncontrolled over-expression of this cytokine promotes the clonal proliferation of aberrant IELs that increases the tissue epithelial damage

(Mention *et al.* 2003). The commensal microbiota, which is altered in CD patients, also exerts a role in promoting CD pathogenesis. *Bacteroides fragilis*, which is present at high levels in CD patients' mucosa, is able to digest gluten producing toxic peptides (Sánchez *et al.* 2012). Also other species of bacteria such as *Staphylococcus*, *Clostridium* and *Escherichia* are increased in CD patients (Nadal *et al.* 2007). Therefore, the microbiota seems to be implicated in the modulation of the intestinal immune response and also in the maintenance of oral tolerance. It is still unclear if intestinal dysbiosis is a cause or a consequence of the pathogenesis of CD.

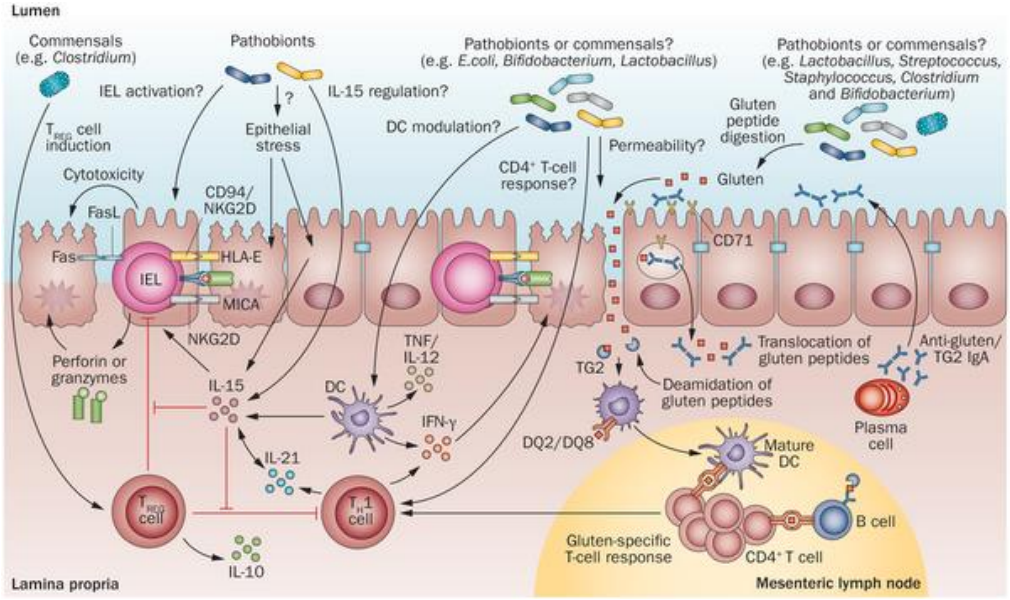

Figure 5: Gluten peptides translocate the epithelial barrier via transcellular or paracellular mechanisms. TG2 deamidates native gluten peptides in the *lamina propria*, allowing the uptake of deamidated gliadin peptides by DCs. A proinflammatory gluten-specific CD4+ T-cells response is induced, characterized by IFN-γ, IL-21, anti-gliadin and anti-TG2 antibodies production. Increased epithelial cell stress can upregulate stress molecules on the membrane (HLA-E, MICA/B) and induce IL-15 production. IL-15 can induce IEL proliferation and activation leading to cytotoxic killing of epithelial cells and consequent tissue damage. Human gut microbiota might contribute to CD development by influencing different processes, such as IELs activation or up-regulation, DCs maturation and proinflammatory cytokine production, intestinal permeability modulation, gluten peptides digestion, and induction of CD4+ T-cells responses (Verdu *et al.* 2015).

1.1.5 Clinical aspects

Dietary gluten intake in CD patients causes inflammatory injuries to the mucosa of the small intestine that leads to villous atrophy. A serious consequence of this condition is related to a severe malabsorption syndrome that is currently rare (Farrell and Kelly, 2002). Clinical manifestations of CD can vary according to age groups. Classic symptoms affecting intestine, characterized by a general onset in childhood, are steatorrhea, abdominal distention and pain, flatulence, dyspesia whereas extraintestinal symptoms are caused by malabsorption, such as failure to thrive and short stature (D'Amico *et al.* 2005). Other extraintestinal symptoms, that can have onset in adulthood, are anemia, osteoporosis, epilepsy, gluten ataxia, diabetes, dermatitis herpetiformis and liver disease (Green *et al.* 2005; Rampertab *et al.* 2006). The onset of these symptoms from gluten exposure requires days or weeks compared to other conditions, such as wheat allergy (minutes-hours) and non-celiac (non-allergy) gluten sensivity (NCGS) (hours-days). Time from gluten exposure to symptoms appearing is one of the criteria for the differential diagnosis of CD (Schuppan *et al.* 2015). According to the clinical manifestation, CD has been described with great agreement by Ludvigsson *et al.* (2013):

- Typical CD: this definition takes into account the historical symptomatology in CD patients due to malabsorption (diarrhea and/or malnutrition) or to malabsorption syndrome (all the symptoms described above). Clinical presentation has changed over time and this definition now referred to most frequently encoutered form of CD.
- Asymptomatic or silent CD: patients do not manifest any common CD symptom, even in response to direct questioning. These individuals are diagnosed during the enrollment in general screening programs for the detection of CD.
- Atypical or non-classical CD: this definition describes patients with gluten-induced enterophaty and no weight loss. On the contrary, this individuals present one or more of the symptoms described above.

Authors argue that the term atypical CD should not be used because some CD patients may fulfill the requirements for non-classic CD.

- Refractory CD (RCD): despite patients are under gluten-free diet, symptoms of malabsorption and villous atrophy continue to persist. RCD can be divided in two cathegories: RCD1 (normal immunophenotype), that usually responds to GFD and pharmacological supports (corticosteroids), and RCD2, with incomplete response to clinical menagement and poor prognosis characterized by increased risk to develop ulcerative jejunitis and enterophaty-associated T-cell lymphoma (EATL) (Rishi *et al.* 2016).
- Latent CD: there are several definitions of this term but generally refers to those patients that have normal intestinal mucosa but positive serology. This term is in general discouraged.
- Potential CD: this term refers to those individuals with positive serology, normal intestinal mucosa but an increased risk to develop the disease. Some physicians prefer to use this term for patients with also an increased number of IELs in the villi.

Di Sabatino and Corazza (2013) underlined the necessity to clarify some points on the Oslo definition in order to avoid ambiguities and classify undefined conditions.

1.1.6 Diagnosis and clinical management

The first-line of investigation to diagnose CD is represented by serological blood tests (**Table 1**). Immunoglobulin A (IgA) anti-tissue transglutaminase (tTG) is the preferential test used to diagnose CD, with a sensibility of 94% and a specificity of 97%. This test is performed in patients over 2 years of age. Other tests are recommended in case of IgA deficiency: anti-tTG IgG and IgG anti deamidated gliadin peptides (DGP), the latter gives better performances in patients under 2 years of age. Analysis of anti-endomysial (EMA) IgA, which has a sensibility >90% and a specificity of 90%, is used as a confirmatory test (Rubio-Tapia *et al.* 2013). All serological tests should be performed in patients on gluten-containing diet. These tests are dependent by the level of histological lesions: CD patients with a low

intestinal damage may present seronegative results. Typing of HLA-DQ2/DQ8 is a usefull test to confirm or exclude CD diagnosis in patients with an equivocal histopathological result or to rule out CD in other at-risk groups (Kaukinen *et al.* 2002).

Test	Mean sensibility	Mean specificity	Use
Anti-tTG IgA	94%	97%	Test
Anti-tTG IgG	Variable (12-99%)	Variable (86-99%)	IgA deficiency
Anti-EMA IgA	>90%	99%	Confirmatory test
Anti-DGP IgG	>90%	>90%	IgA deficiency and children < 2 years
HLA-DQ2/DQ8	91%	54%	High negative predictive value

Table 1: Serological tests used in clinical practice for CD diagnosis. Sensibility and specificity values are reported together with the specific use in the diagnostic process.

Upper endoscopy with duodenal biopsy is used as confirmation of diagnosis in patients with positive serology or negative serology but high suspicious of CD. Generally, two bioptic specimens are collected from the duodenal bulb and four from the distal duodenum (Rubio-Tapia *et al.* 2013). One of the two hallmarks in a biopsy derived from a CD patients is IELs infiltration. Currently the threshold number of IELs suggesting for CD is still controversial. A cut-off value of 20-25 IELs per 100 enterocytes has been proposed compared to the old one of >40 IELs per 100 enterocytes (Abadie *et al.* 2012). The second hallmark is represented by villous atrophy, a consequence of mucosal inflammation. The histopathological changes were categorized for the first time by Marsh (1992) and then modified by Oberhuber and colleagues (1999) as follow:

- M0: normal villous
- M1: increase of IELs
- M2: increase of IELs and glandular crypt hyperplasia
- M3a: partial villous atrophy
- M3b: substantial villous atrophy

- M3c: total villous atrophy

This classification has been recently semplified by Corazza and colleagues (2007) according to villous morphology:

- A: non-atrophic
- B1: atrophic, villous-crypt ratio <3:1
- B2: atrophic, villi no longer detectable

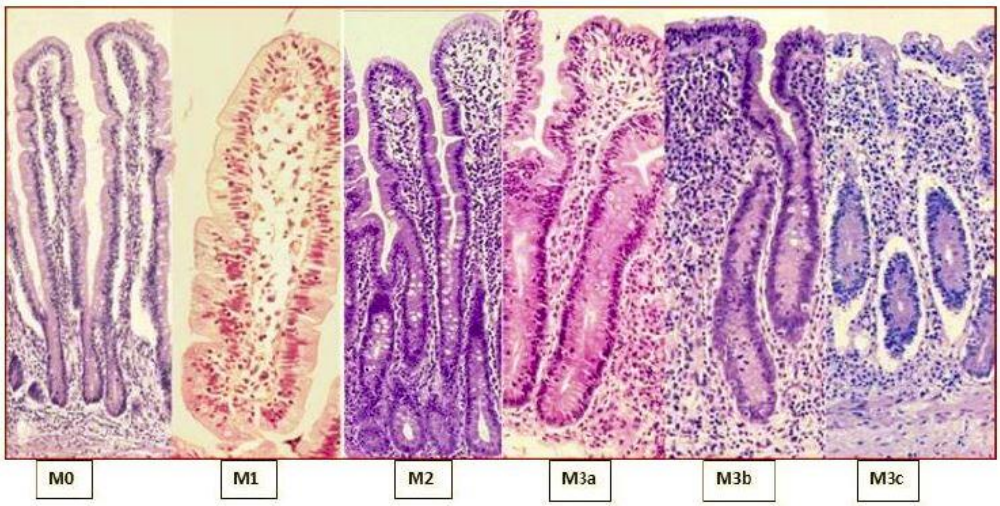

Figure 6: Marsch modified classification. M0: normal villous, M1: increase of IELs, M2: increase of IELs and granular crypt hyperplasia, M3a: partial villous atrophy, M3b: substantial villous atrophy, M3c: total villous atrophy.

Marsh modified (Oberhuber)	Histologic criterion			Corazza
	Increased intraepithelial lymphocytes[a]	Crypt hyperplasia	Villous atrophy	
Type 0	No	No	No	None
Type 1	Yes	No	No	Grade A
Type 2	Yes	Yes	No	
Type 3a	Yes	Yes	Yes (partial)	Grade B1
Type 3b	Yes	Yes	Yes (subtotal)	
Type 3c	Yes	Yes	Yes (total)	Grade B2

[a] >40 intraepithelial lymphocytes per 100 enterocytes for Marsh modified (Oberhuber); >25 intraepithelial lymphocytes per 100 enterocytes for Corazza.

Figure 7: Comparison of the histologic classifications used in CD diagnosis (Rubio-Tapia *et al.* 2013).

Nowadays, the only effective therapy consists in a gluten-free diet (GFD), that is a diet containing a low level of gluten. The Codex Alimetarius defines that a diet with less than 20 p.p.m. of gluten can be considered gluten-free. Non-responsive celiac disease (NRCD) affects 7 to 30% of all patients and it is not responsive to GFD. This condition can be due by inadvertent ingestion of gluten or other causes, such as other food intolerancies. These patients are treated with an adjust GFD, which excludes gluten contamination and causes of other intolerancies. 1-2% of CD patients suffer of RCD that is treated with GFD adjuvanted by a pharmacological therapy based on steroids or immunosuppressants, such as azathioprine. These patients are also treated in order to prevent the effects of micronutrient malabsorption (Rubio-Tapia *et al.* 2013).

1.1.7 Non-celiac gluten sensitivity

Non-celiac gluten sensitivity (NCGS) is a gluten-related disorder recently re-discovered, although the existence of this condition is known from the ’80. This disease is characterized by a heterogeneous pattern of intestinal symptoms that overlaps other conditions, such as irritable bowel syndrome (IBS), and extra-intestinal symptoms (Catassi *et al.* 2013). The pathophysiology of NCGS is still unclear. It seems like the immunological mechanisms causing NCGS do not depend by the presence of IgE as in wheat allergy or in an adaptive immune response as in CD. The innate immune response may be due by the increase in the duodenal mucosa of Toll-like receptor 2 (TLR2) and a down-regulation of FOXP3, a T-regulatory cell marker (Elli *et al.* 2015). Other molecules could play a key role in triggering NCGS. Amylase/trypsin inhibitors (ATIs) are water soluble proteins that belong to globulins. Junker and colleagues (2012) demonstrated that ATIs CM3 and 0.19 promote an immune response in monocytes, macrophages and DCs through the activation of TLR4. The formation of (TLR4)-MD2-CD14 complex leads to the release of pro-inflammatory cytokines and chemokines, such as TNF-α, IL-8 and MCP1. Actually, there are no serological tests to identify NCGS patients (Shuppan *et al.* 2015).

1.2 Autophagy

All eukaryotic cells are able to digest their cytoplasmic content through different processes that undergo the general term autophagy (from the Greek words *auto* meaning 'self' and *paghein* meaning 'to eat'). Autophagy includes different form of digestive pathways that are: macroautophagy, microautophagy, chaperone-mediated autophagy and non-canonical autophagy. Generally, the term autophagy refers to macroautophagy: this process depends on specialized autophagy-related proteins (ATGs) and is able to digest different targets, such as organelles, large aggregates of proteins and microorganisms (Deretic *et al.* 2013). This process was discovered in 1957 by Clark observing irregular vacuoles in mice kidney tubule cells containing different kind of materials, including mitochondria. This vacuoles, originally called 'dense bodies', were also described by Novikoff and colleagueá (1956) through electron microscopy (TEM). Subsequently, Ashford and Porter (1962) demonstrated that the administration of glucagon to hepatocytes from rats increases the presence of these 'dense bodies'. According to these evidence, Deter and De Duve (1967) coined the term autophagy to refer to double-membrane vesicles containing portion of cytoplasm and organelles. The first description of the autophagosome formation was made one year later by Arstila and Trump (1968). Because of glucagon role in increasing autophagy, this process was originally described as a response to nutrients deprivation (Pfeifer and Warmuth-Metz, 1983). In addition to starvation, autophagy is implicated in a variety of processes to maintain cellular homeostasis. Important physiological functions are protein turnover, control of organelles quality and number and digestion of damaged organelles (Ravikumar *et al.* 2010). Autophagy plays also a key role in direct microorganisms and viruses clearance, in control of inflammation through the inhibition of the inflammosome, antigen presentation, T-cells homeostasis and secretion of immune mediators (Deretic *et al.* 2013). Autophagy impairment is crucial in several diseases, in particular proteopathies, such as Alzheimer disease (Yu *et al.* 2005), Parkinson disease (Winslow *et al.* 2010) and Huntington disease (Martinez-Vincente *et al.* 2010). As described above, there are four types of autophagy:

- Macroautophagy: organelles or other cargos (proteins, lipids or nucleic acids) are sequestred in the autophagosome, a double-membrane vesicle, and delivered to the lysosome for degradation (Ravikumar *et al.* 2010).
- Microautophagy: small cytosolic materials are degraded after their engulfment in lysosomes through membrane invagination (Santambrogio and Cuervo, 2011).
- Chaperone-mediated autophagy: proteins with the specific sequence KFERQ are recognised by Hsc70 (70 Kda heat shock cognate protein) and then degraded by lysosomes action (Kaushik *et al.* 2011).
- Non-canonical autophagy: under specific circumstances autophagosome formation in macroautophagy can bypass the canonical steps. Currently, two non-canonical pathways have been described: beclin-1 indipendent autophagy and a pathway that bypass the action of ATG5, ATG7 and LC3 (Codogno *et al.* 2011).

Although autophagy was initially described in mammalian cells, the understanding of the molecular mechanism has been reached after genetic analysis in *Saccaromyces cerevisiae*. Tsukada and Ohsumi (1993) isolated and characterized the first mutant defective in autophagy, *apg1*. After this discovery, several other laboratories worked to find other genes implicated in the autophagy pathway, also in other organisms. Nowadays, 37 autophagy-related genes (ATGs) have been described, exerting a function in different steps of the pathway (Ohsumi *et al.* 2014).

1.2.1 Autophagic pathway

Autophagy consists of six different steps, that are: 1) initiation, 2) nucleation or phagophore formation, 3) Atg5-Atg12 conjugation, interaction with Atg16L and multimerization at the phagophore, 4) LC3 processing and insertion, 5) capture of random/selective targets for degradation and 6) fusion of the autophagosome with the lysosome.

1. Initiation: in mammals, the phagophore does not origin *de novo* but derives from the membrane of the endoplasmic reticulum (ER)

and/or the *trans*-Golgi and endosomes (Axe *et al.* 2008). Autophagy induction is triggered by different stimuli that repress mTOR, a protein that belongs to the PI3K family. mTOR is the catalitic subunit of two distinct complexes: mTORC1, which consists of Raptor, Deptor, PRAS40 and GβL/mLst8, and mTORC2, that contains Rictor, GβL/mLst8, Sin1, PPR5/protor and Deptor. The complex that is responsible for autophagy activation is mTORC1 whereas mTORC2, wrongly considered insensitive to rapamycine at the beginning, is involved in other cellular functions. Active mTORC1 inhibits autophagy through the binding and subsequent phosphorilation of the ULK complex, which is composed by ULK1/2, Atg13, FIP200 and Atg101. ULK1/2 can exert is kinase activity after mTORC1 inhibition by different mechanisms, such as starvation or rapamycine interaction, that cause the dissociation of this protein from the ULK complex. It seems that ULK complex exerts its action upstream the Atg14L-hVPS34 (PIK3C3) complex and leads to the accumulation of PI(3)P on the target membrane. Deprivation of nutrients promotes ULK complex activation so that it can phosphorilate Ambra1 leading to the release of PIK3C3 complex with the consequent PI(3)P generation (Jung *et al.* 2010; Di Bartolomeo *et al.* 2010).

2. Nucleation: this step is mediated by the action of Beclin-1, which belongs to PIK3C3 complex together with PIK3C3, p150, Ambra1, UVRAG or Atg14L. Beclin-1 allows the binding of PIK3C3 with several regulators. Beclin-1 can interact through the presence of a BH3 domain with Bcl-2 and Bcl-X_L, which are able to decrease the binding of Beclin-1 with PIK3C3 complex. Several autophagy-inducing stimuli, such as starvation, are able to disrupt the Bcl-2/Beclin-1 complex through the JNK1-mediated phosphorilation of Bcl-2 or the DAPk-mediated phosphorilation of Beclin-1 (He and Levine, 2010). The PIK3C3-mediated generation of PI(3)P recruits other autophagy-related proteins: WIPI1/2 (orthologs of Atg8), Atg2 and DFCP1 (Polson *et al.* 2010).

3. Atg5/Atg12 conjugation: two ubiquitin-like conjugation systems are implicated in autophagosome expansion. The first mechanism includes the activation of Atg12 mediated by Atg7, an E1-like enzyme. Atg12 is then transferred to Atg10, an E2-like enzyme, for the conjugation with Atg5. A 800 kDa multimeric complex is then created after the interaction of Atg12-Atg5 with Atg16L (Mizushima *et al.* 2003). The function of this complex is to bind the autophagosome membrane inducing the curvature and determining LC3 lipidation as well as the interaction of Atg12 with Atg3 (Fujita *et al.* 2008).
4. LC3 processing: the second ubiquitin-like conjugation system involved LC3 (microtubule-associated protein 1A/1B-light chain 3). LC3 is cleaved by Atg4, a cysteine protease, and this exposes a glycine at the C-terminal end, to generate LC3B-I. Then, Atg7 promotes the ATP-dependent activation of the C-terminal glycine. Subsequently, activated LC3B-I is transferred to Atg3, an E2-like enzyme. Atg16L complex acts as a scaffold to transfer LC3 (homolog of Atg8) from Atg3 to phosphatidylethanolamine (PE). LC3-PE, also known as LC3-II, is localized on the autophagosome membrane and is an autophagy-specific marker. After vesicle formation, LC3B-II is removed by the outer autophagosomal membrane, in a process called deconjugation, which is mediated by Atg4. LC3B-II remains associate with the inner autophagosomal membrane and is partially degraded after fusion with lysosome (Wirawan *et al.* 2012). Other molecules co-localize with LC3B-II, i.e. GABARAP and GATE16 (Kabeya *et al.* 2004).
5. Cargo recognition: Damaged organelles or protein aggregates are sequestred into autophagosomes in a specific way. Selectivity is achieved through autophagy receptors, which recognize cargos tagged with LC3-interacting regions (LIRs). LIR motifs interact with autophagy modifier proteins of the LC3/GABARAP family. In yeast five receptors have been described, while in mammals more than two dozen autophagy receptors were identified. The most prevalent

autophagy targeting signal in mammals is the modification of cargos through ubiquitination. Most of the currently autophagy receptors harbour both Ub-binding domain (UBDs) and LIRs. p62/SQSTM1 (sequestosome-1) is an adaptor molecule that promotes turnover of poly-Ub targets. Selective autophagy receptors lack a clear specialization but often cooperate with each other in selecting a specific cargo: NRB1 interacts with p62 for the sequestration of protein aggregates and peroxisomes. OPTN and NDP52 interact with p62 during xenophagy (Stolz *et al.* 2014).

6. Fusion with lysosome: Autophagosomes can fuse with early or late endosomes to become amphisomes or can also be directly targeted to the lysosomes along the microtubules. The outer autophagosomal membrane fuses with the lysosome, releasing the inner autophagosomal membrane and its contents into the lysosomal lumen. Several proteins are involved in these fusion events, including LAMP2, the UVRAG-C-Vps tethering complex, Rab, HOPS, SNAREs, AAA ATPases, LC3, FYCO1 and the ESCRT machinery (Tong *et al.* 2010). After the fusion with the lysosome, the autophagic body is disintegrated and its cargo is degraded by lysosomal hydrolases and lipases. Subsequently, lysosomal efflux transporters (i.e. Atg22 in yeast, not yet identified in mammals), mediate the release of the resulting amino acids, fatty acids and nucleosides back into the cytosol (Yang *et al.* 2006).

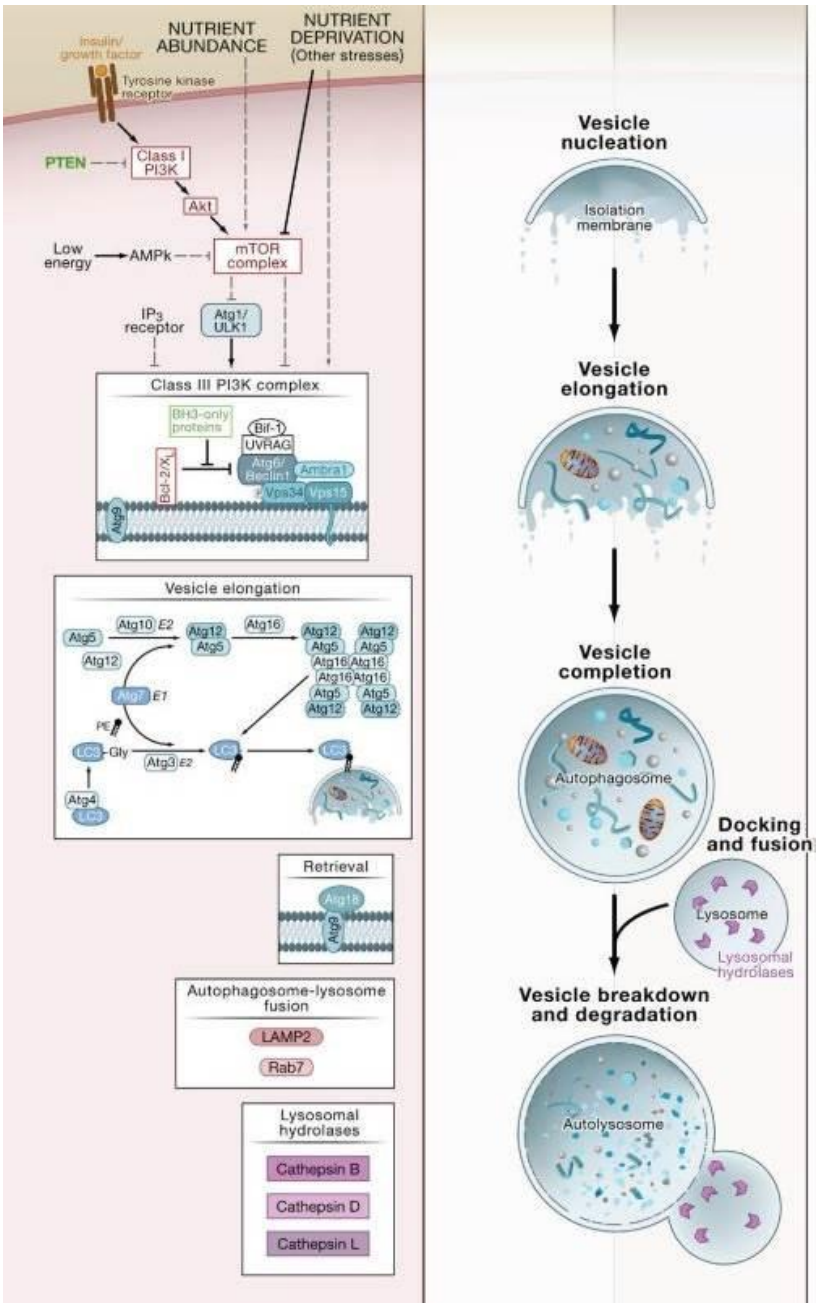

Figure 8: Overview of the autophagic pathway. Autophagy is stimulated by nutrient

deprivation, or other stimuli, such as deprivation of insulin and other growth factors or low energy. The initial step of vesicle nucleation is characterized by the activation of the class III PI3K (Vps34) to generate phosphatidylinositol 3-phosphate (PI3P) on the target membrane. This activation depends on the formation of a multiprotein complex that includes Atg6/Beclin 1, Vps15, UVRAG, Bif-1 and Ambra1. Vesicles elongation and completion processes are based on two evolutionarily conserved ubiquitin-like conjugation systems. The first pathway involves the covalent conjugation of Atg12 to Atg5, with the help of Atg7 and Atg10 whereas the second pathway involves the conjugation of phosphatidylethanolamine (PE) to a glycine (Gly) residue of LC3 by the sequential action of the protease Atg4, Atg7 and Atg3. This lipid conjugation leads to the conversion of the soluble form of LC3 (named LC3-I) to the autophagic vesicle-associated form, LC3-II. Once autophagosomes are formed, they undergo progressive maturation by fusion with lysosomes, forming autolysosomes. This fusion is not well characterized but involves the integral lysosomal membrane protein LAMP-2 and the GTP-binding protein Rab7 (Levine and Kroemer, 2008).

1.2.2 Autophagy regulation

Autophagy is induced by a variety of stress stimuli, including nutrient depletion, energy stress, pathogens-associated molecular patterns (PAMPs) and danger-associated molecular patterns (DAMPs), hypoxia and anoxia, redox stress, ER stress and mitochondrial damage. The induction of autophagy by all these stimuli involves different but partially overlapped pathways.

Nutrient deprivation and energy stress: Nutrient depletion is the most potent known physiological inducer of autophagy. The induction of autophagy in mammalian cell cultures recurs within minutes, with maximal levels in presence of concominant depletion of nutrients (i.e. aminoacids and glucose) and growth factors (i.e. serum). Starvation-induced autophagy is regulated by several molecules including mTOR, AMPK and sirtuins (i.e. Sirt1 and Sirt2). Sirt1 is a NAD-dependent deacetylases that acts on Atg5, Atg7, LC3 (Lee *et al.* 2008) and FOXO3, the transcription factor forkhead box O3a. Depletion of growth factors (i.e. serum deprivation) inhibits Akt and induces FOXO3 through a different mechanism. This transcription factor enhances the expression of several pro-autophagic molecules, such as ULK2, Beclin1, VPS34, Bnip3, ATG12, LC3 and GABARAP (Mammucari

et al. 2007). Serum deprivation induces also the dissociation of Sirt2 and FOXO1, thus promoting its acetylation and interaction with Atg7 (Zhao *et al.* 2010). Depletion of growth factors, such as insulin or insulin-like growth factors, inhibits mTORC1 through multiple mechanisms. In fact, Akt becomes catalitically active in response to growth factors, due to the sequential stimulation of class I PI3K and PDK1. Furthermore, growth factors activate Ras, stimulating a cascade involving Raf-1, MEK1/2 and ERK1/2. The tuberous sclerosis complex 1/2, TSC1/TSC2, is phosphorylated by Akt and ERK1/2; Akt activates also Raptor, thus inducing mTOR activation (Neufeld, 2010). AMPK plays a crucial role not only in starvation but also in energy depletion. This kinase monitors the energy status of the cells by sensing the AMP:ATP ratio. In nutrient deprivation conditions and/or energy stress, AMPK and Sirt1 engage in a coordinated positive amplification loop, the "Sirt1-AMPK cycle" that promotes autophagy. Sirt1 mediates the deacetylation of the AMPK-upstream kinase LKB1, promoting its translocation in the nucleus and AMPK activation. AMPK can indirectly stimulate Sirt1 by the reduction of NAM and the increase of NAD^+. Autophagy is induced through the AMPK-mediated phosphorylation of TSC2 and Raptor, leading to mTORC1 inhibition. Another mechanism involves the phosphorylation of ULK1 by AMPK (Ruderman *et al.* 2010; Kim *et al.* 2011).

ER stress: The major ER stress pathway, the unfolded protein response (UPR), is a potent stimulus for autophagy. This response is mediated by PERK, ATF6 and IRE1, which are normally bound and inactivated by BiP/GRP78. PERK and ATF6 can induce autophagy, while IRE1 acts as a negative regulator. Particularly, PERK mediates the phosphorylation of eIF2α, which activates the transcription factor ATF4, thus leading to the transcriptional activation of LC3 and Atg5 (He and Klionsky, 2009; Milani *et al.* 2009).

Hypoxia and anoxia: Hypoxia and anoxia (oxigen concentration of <3% and <0.1%, respectively) are two stimuli that can induce autophagy. Hypoxia-induced autophagy depends on HIF, while anoxia-induced autophagy is HIF-indipendent. When the oxygen concentration is below 5%, the HIF heterodimer becomes stabilized and activates the transcription

of BNIP3 and BNIP3L, two proteins that can disrupt the binding between Beclin1 and Bcl-2 (Bellot *et al.* 2009). In cases of severe hypoxia or anoxia, autophagy is induced by the protein DJ-1 with an unknown mechanism, by a stimulation of a PDGFR-dependent pathway and by AMPK (Mazure and Pouyssegur, 2010).

Redox stress: Oxidative stress can induce autophagy through different mechanisms. Exogenous hydrogen peroxide can activate PERK, leading to the stimulation of eIF2α, or can inhibit mTOR directly (Liu *et al.* 2008). Redox stress can also stimulate autophagy through the action of p53. This transcription factor can transactivate several autophagy inducers including DRAM1 and Sestrin2, the latter is able to bind the TSC1/TSC2-AMPK complex. p53 plays a dual role in autophagy regulation, acting as a tonic inhibitor when present in the cytoplasm (Green and Kroemer, 2009).

Mitochondrial damage: The autophagic recognition of depolarized mitochondria is mediated by a refined voltage sensor, involving the mitochondrial kinase, PINK1. This kinase rapidly accumulates on mitochondrial surface after its depolarization, allowing the recruitment of the E3 ubiquitin ligase Parkin. Parkin promotes the ubiquitination of several mitochondrial substrates, i.e. VDAC1, and rectruits p62/SQSTM1, thus leading to mitophagy (Narendra *et al.* 2010).

Immunity and inflammation: Autophagy plays a crucial role also in immunity and inflammation. Several stimuli that depend on the cellular response to pathogens are able to induce autophagy. DAMPs, such as DNA complexes, ATP and high-mobility group box 1 protein (HMGB1), can induce autphagy. Particularly, Tang and colleagues (2010) demonstrated that HMGB1 is able to disrupt the binding of Beclin1 with Bcl-2 and can also stimulate autophagy by interacting with its receptor RAGE. TLRs and autophagy cooperate in the response against PAMPs. It was demonstrated, for example, that Toll-like receptor 4 (TLR4) signalling leads to ubiquitination of Beclin1 by the E3 TNF receptor-associated factor 6 (TRAF6). As a result of this process, Bcl-2 releases Beclin1, which becomes active. Also ULK1 is ubiquitinated by TRAF6, underlining the key role of this enzyme in autophagy regulation (Shi and Kehrl, 2010; Nazio *et*

al. 2013). Inflammatory cytokines are involved in autophagy activation: for example, IL-1β induces autophagy through the downstream recruitment of TRAF6, while INF-γ activates the autophagic process through the phosphorylation of Beclin1 mediated by DAPk1 (Zalkvar *et al.* 2009; Shi *et al.* 2012). Other cytokines, i.e. IL-4 and IL-13, inhibit autophagy in a contest dependent manner: they occur through Akt signalling when autophagy is induced by starvation, while are STAT6-dependent when autophagy is induced by IFN-γ (Harris *et al.* 2007).

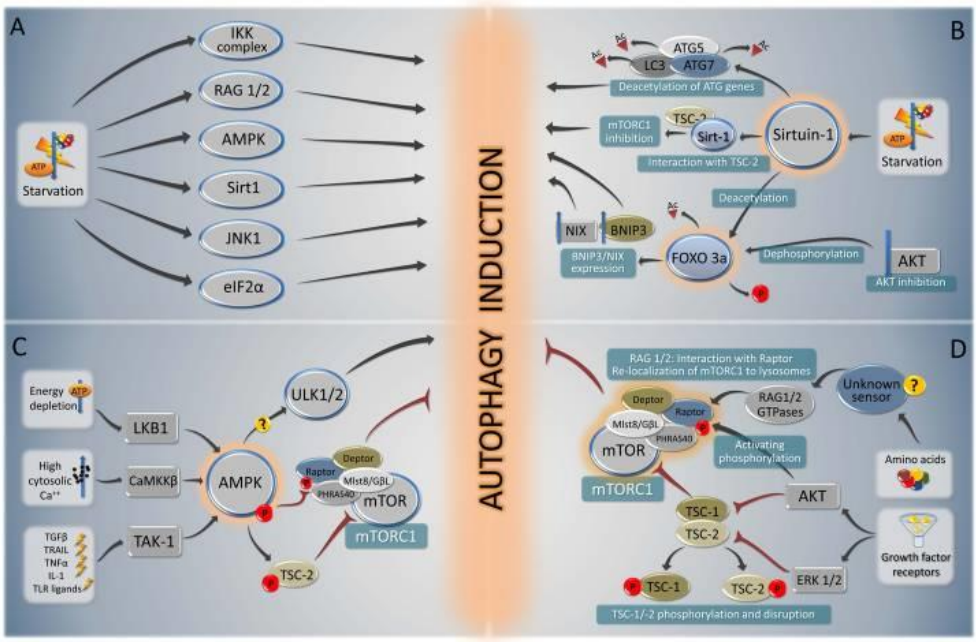

Figure 9: Schematic representation of the autophagic induction due to starvation, energy depletion and lack of aminoacids. (A) Principal effectors induced by nutrient starvation. (B) Starvation activates Sirtuin-1, which can induce autophagy through three different mechanisms: deacetylation of ATGs proteins (Atg7, Atg5 and LC3), deacetylation of FOXO3 and consequent transcription of NIX and Bnip3 and interaction with TSC-2, thus inhibiting mTORC1. (C) Energy depletion leads to LKB1 deacetylation mediated by Sirt1 and, as a consequence, to the activation of AMPK. Other kinases can activate AMPK, i.e. CaMKKβ and TAK-1. (D) Aminoacids depletion induces RAG1/2 through an unknown mechanism, thus activating mTORC1. (Kroemer *et al.* 2010).

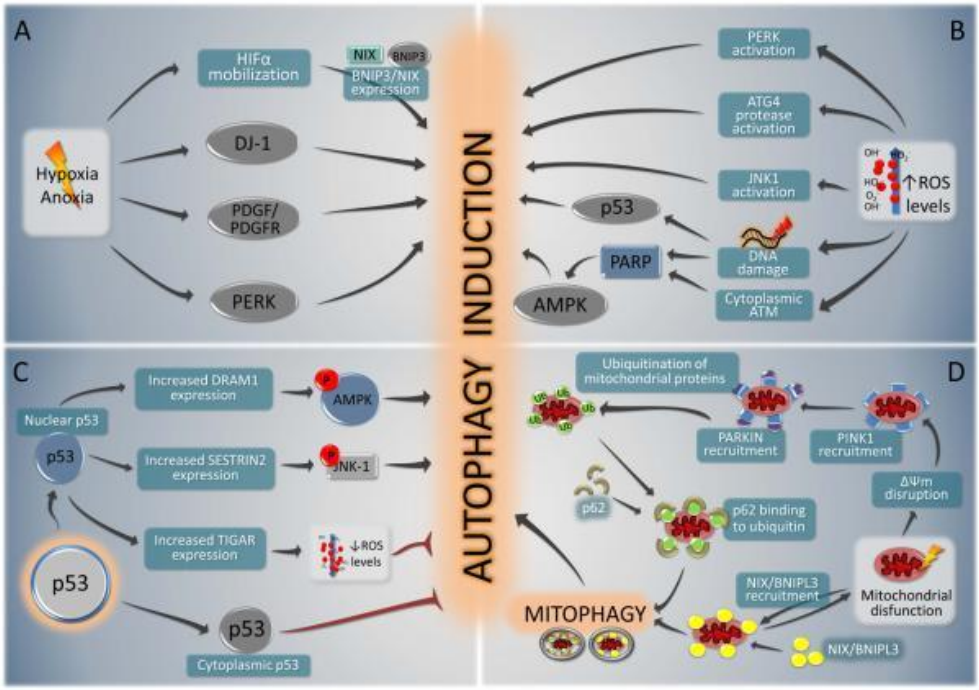

Figure 10: Autophagy induction due to different stress stimuli. (A) Hypoxia and anoxia can activate autophagy through HIF, DJ-1, PDGF pathway and PERK. (B) Increased ROS levels can trigger the activation of PERK, JNK1 and ATG4, thus inducing autophagy. The DNA damage caused by ROS activates the checkpoint responses mediated by p53 and ATM, which are able to induce the autophagic pathway. (C) Particularly, p53 increases the expression levels of Sestrin2 and DRAM1, which phosphorylate respectively JNK-1 and AMPK leading to their activation. (D) Mitophagy is triggered by Δψm disruption, a signal for PINK recruitment. This allows the action of Parkin and the ubiquitination of mitochondrial proteins (Kroemer *et al.* 2010).

1.2.3 Autophagy and autoimmune diseases

Autophagy plays a crucial role in the pathogenesis of several autoimmune diseases. Crohn disease is an inflammatory bowel disease (IBD) caused by a combination of environmental, immune and bacterial factors in genetically susceptible individuals. It has been demonstrated that genetic polymorphisms in the genes *ATG16L* and *IRGM* confer a strong predisposition to Crohn disease development (Scharl *et al.* 2012). Despite

this strong association, the role played by Atg16L in Crohn disease pathogenesis is still unclear, because of the lack of knowledge about the functions that Atg16L exerts in the autophagic pathway. However, it is clear that Atg16L is able to suppress the inflammatory process: Atg16L-deficient mice are highly susceptible to colitis induced by dextran sulphate sodium. The symptoms developed by these mice can be treated with injections of anti-IL-1β and IL-18 antibodies (Saitoh *et al.* 2008). Recently, SNPs in the *ULK1* gene have been indentified to increase susceptibility to Crohn disease, thus demonstrating that autophagy contributes to the pathogenesis of this disease (Henckaerts *et al.* 2011). The autophagic protein Atg5 is implicated in the development of systemic lupus erythematosus (SLE), multiple sclerosis (MS) and rheumatoid arthritis (RA). SLE is an autoimmune disease in which the immune system of the patient attacks healthy tissues. Five SNPs, identified near to and in the *ATG5* locus, are associated with SLE initiation and/or development even if the pathogenetic mechanism is still unclear (SLEGEN, 2008). Recenlty, it has been demonstrated that T-cells in SLE patients are autoreactive and autophagy promotes their survival and contributes to their persistence in autoimmune conditions (Gros *et al.* 2012). MS is a demyelinating disease that affects the brain and the spinal cord. Changes in the expression of Atg5 correlate also with immune-mediated myelin injury in MS mice and in patients. Particularly, Atg5 is over-expressed in circulating T-cells of relapsing-remitting MS (RRMS) patients compared with healty controls and in T-cells in the inflammatory sites of the brain. Atg5 over-expression seems to extend T-cells survival and proliferation during active disease; moreover it seems to correlate with the severity of the disease in mice models (Alirezaei *et al.* 2009). In RA, anti-citrullinated protein antibodies (ACPAs) are the most powerful biomarkers that allow the diagnosis of this disease. During inflammation, the arginine residues of self-proteins are converted in citrullin by the enzymes peptidylarginine deiminase (PADs), in a process known as citrullination, thus leading to an immune response. Presentation of these peptides is blocked after treatment with 3-methyladenine or reducing Atg5 expression, confirming a key role of autophagy in RA pathogenesis (Ireland and Unanue, 2011).

1.3 MicroRNAs

Small RNAs are 20-30 nucleotides in lenght and can associate with Argonaute (AGO) family proteins. There are three main classes of small RNAs: microRNA (miRNA), short interfering RNA (siRNA) and PIWI-interacting RNA (piRNA). miRNAs constitute the dominant class of small RNAs in somatic tissues. These molecules are able to bind target mRNAs through base pairing, while AGO proteins induce translational repression, mRNA deadenylation and mRNA decay. The miRNA-binding site is generally in the 3' UTR region of mRNAs, whereas in miRNAs the domain at the 5' UTR (nucleotide position 2 to 7) is crucial for target recognition and is known as "miRNA seed". More than 60% of human genes contain at least one miRNA-binding site, underlining the importance of these molecules in several cellular processes (Ha and Kim, 2014). In 1993, in the nematode *C. elegans*, was discovered the first miRNA, Lin-4, a heterochronic gene that controls the temporal development pattern of all larval stages. Lin-4 transcript negatively regulates the expression of *Lin-14* through its 3' UTR region: this interaction decreases the expression level of *Lin-14*, which encodes for a protein that specifies the division timings of specific group of cells (Lee *et al.* 1993). The second discovered miRNA in 2000 was Let-7, another heterochronic gene in *C. elegans*. This small RNA is able to control the L4-to-adult transition of larval development, regulating Lin-14, Lin-28, Lin-41 and Daf-12 through their 3' UTR (Reinhart *et al.* 2000). Dysregulation of miRNAs biogenesis and/or regulation is associated with numerous diseases, i.e. cancer and neurodegenerative disorders (Ha and Kim, 2014).

1.3.1 miRNAs biogenesis and regulation

Human miRNAs sequences are mainly located in introns of non-coding or coding transcripts, but some miRNAs are present in the exonic regions. Several miRNA loci constitute polycistronic transcriptional units that are generally co-transcribed (Lee *et al.* 2002). Regulation of miRNAs transcription is still unclear due to the scarcity of annotated miRNA TSS and promoters. Specifically, miRNA gene expression depends on the identification of promoter regions in order to identify the transcription

factors involved in this process. However, it was demonstrated that CpG islands and enrichment of the H3K4me3 characterized the promoter of miRNAs similarly to protein-coding gene promoters (Schanen and Li, 2011). RNA Pol II and associated transcription factors promote the transcription of miRNAs and it is known that a large number of miRNAs and their target genes are co-expressed under different conditions and co-regulated by the same transcriptional factors (Lee *et al.* 2004). Transcription gives rise tipically to a sequence of 1 Kb, known as pri-miRNA that contains a stem-loop structure of 32-35 bp in which mature miRNA is embedded. Maturation of the pri-miRNA is promoted by the action of a complex called microprocessor, composed by the nuclear RNase III Drosha and the essential cofactor DGCR8 (known as Pasha in *D. melanogaster*) (Denli *et al.* 2004). Drosha is a protein of ~ 120 kDa that mediates the cut of the stem-loop region, leading to the release of a small hairpin-shaped RNA of ~65 nt (i.e. pre-miRNA). This action is performed by two tandem RNase III domains (RIIIDs) in the C-terminus that dimerize intramolecularly to create the processing center. pri-miRNAs are recognized through the ds-RNA binding domain (dsRBD) of Drosha and the addition activity of DGCR8. The hairpin cutting occurs 11 bp away from the basal junction between ssRNA and dsRNA and 22 bp away from the apical junction linked to the terminal loop (Han *et al.* 2004, 2006). The microprocessor complex is composed also by other proteins, such as the containing DEAD-box RNA helicase p68, p72, NF90 and NF45 (Gregory *et al.* 2004). The p68/p72 and NF90/NF45 complexes have been shown to alter the miRNA processing efficiency for specific miRNAs and, particularly, endogenous p68/p72 facilitate Drosha processing of a subset of pri-miRNAs based on reduced mature miRNA levels (Fukuda *et al.* 2007). On the other hand, the NF90/NF45 complex acts as a negative regulator in the miRNAs processing pathway: it as been shown that over-expression of NF90/NF45 causes accumulation of various pri-miRNAs, whereas depletion of NF90 leads to a decrease in pri-miRNAs levels and an increase in mature miRNAs (Sakamoto *et al.* 2009). Terminal loop binding proteins can enhance Drosha activity, as in the case of hn-RNP-A1 and miR-18a: this protein is able to bind the target pri-miRNA and relax the stem region, thus facilitating the interaction with Drosha/DGCR8 (Michlewski *et al.* 2008). Following microprocessor activity, pre-miRNA is exported in the cytoplasm in order to

complete its maturation. The export is carried out by the protein exportin 5 (EXP5) that forms a complex with Ran-GTP and the pre-miRNA. After the translocation through the nuclear pore complex, GTP is hydrolyzed and the complex is disassembled with the releasing of the pre-miRNA (Bohnsack *et al.* 2004). Cytoplasmic pre-miRNA processing is performed by Dicer. This ~ 200 kDa protein is a RNA III-type endonuclease that, similarly to Drosha, has two tandem RIIIDs in the C-terminus forming its catalytic site. The N-terminal helicase recognizes pre-miRNA by interacting with the terminal loop (Zhang *et al.* 2004; Tsutsumi *et al.* 2011). The cleavage site of Dicer is located at 21-25 nt from the 3' end of dsRNAs (3'-counting rule). In mammals an additional mechanism to process pre-miRNA is the 5'-counting rule (Macrae *et al.* 2006; Park *et al.* 2011). This process generates a small RNA duplex with a mismatch in the guide strand at nucleotide position 8-11 (Gregory *et al.* 2005). Dicer interacts with some cofactors belonging to the dsRBDs protein family, such as TRBP and PACT. These cofactors are not essential for miRNAs processing but facilitates the assembling (Haase *et al.* 2005). Phosphorylated TRBP stabilizes the Dicer-containing complex and is also able to modulate processing efficacy of some pre-miRNAs. In fact, this protein is a substrate for MAPK and ERK phopshorylation, leading to the preferential up-regulation of growth-promoting miRNAs, such as miR-17, miR-20a and miR-92 (Paroo *et al.* 2009). Other RNA-binding proteins can regulate the processing of various pre-miRNA. KSRP is known as a key mediator of AU-rich element (ARE)-directed mRNA decay, facilitating the recruitment of the degradation machinery on ARE-containing mRNAs (Gherzi *et al.* 2004). This protein is also a component of both Drosha and Dicer complexes and promotes the biogenesis of a subset of miRNAs, i.e. let-7a and miR-21. KSRP binds the terminal loop of its target pri- and/or pre-miRNA and induces Drosha and Dicer activity through a protein-protein interaction (Trabucchi *et al.* 2009). Other proteins have been described to modulate miRNAs processing by binding of the terminal loop. Lin28 impairs processing of pri- and pre-miRNAs from the Let-7 family reducing Drosha and Dicer activity and inducing uridylation of pre-miR by TUT4, the terminal urydyl transferase 4 (Newman *et al.* 2008; Heo *et al*. 2009). The activity of Dicer is modulated also by negative feedback loops as in the case of Let-7 miRNA. Specifically, human *DICER1* mRNA contains a binding site for Let-7,

resulting in a regulation between Dicer and its product Let-7 (Tokumaru *et al.* 2008). The small RNA duplex produced by Dicer is subsequently loaded onto an AGO protein to form the RNA-induced silencing complex (RISC). The loading is mediated by the binding of the 5'-monophosphate of the guide RNA with the interface of the MID and PIWI domains of AGO proteins. Subsequently, the 3' end of the guide RNA reaches the PAZ domain, strengthening the binding between the small RNA duplex and the AGO protein (Elkayam *et al.* 2012). After the loading, the pre-RISC complex removes the passenger strand to generate the mature RISC. Human AGO2, and as a consequence RISC, is localized in distinct cytoplasmatic foci, called processing bodies (P-bodies) (Sen and Blau, 2005). The localization of AGO2 into these P-bodies is regulated by MAPKAPK2 or 4PH, which increase also AGO2 stability (Qi *et al.* 2008; Zeng *et al.* 2008). The RISC complex promotes the post-transcriptional gene silencing through different mechanisms. The cap-dependent initiation of translation is inhibited by affecting eIF4F cap recognition together with the Cup repressor protein. The RISC complex can also inhibit the 40S ribosomal subunit recruitment and /or the formation of the 80S ribosomal complex. The activity of ribosomes can be inhibit also during the elongation phase, causing the formation of incomplete peptides and their consequent degradation. Furthermore, RISC is able to recruit on the target mRNAs decapping (DCP1/DCP2) and/or deadenylating enzymes leading to messenger destabilization (Li and Rana, 2014).

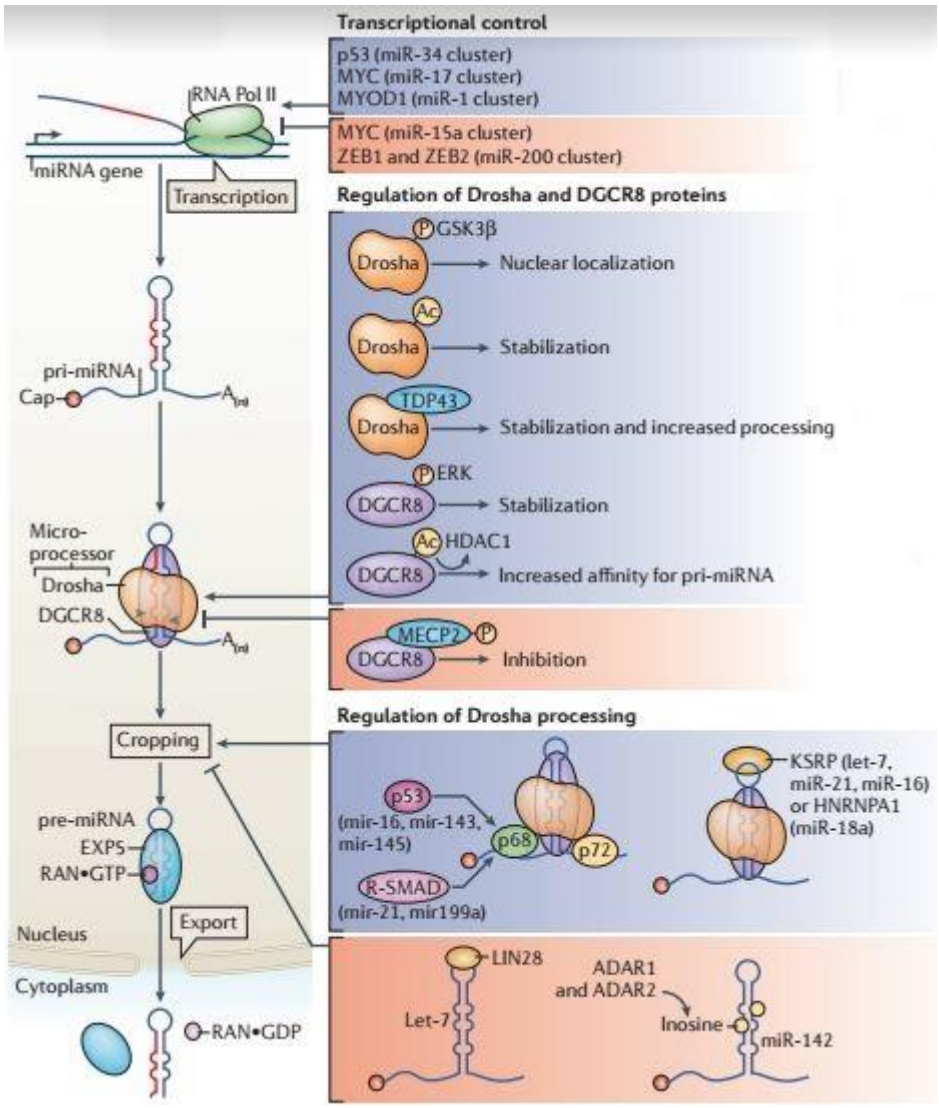

Figure 11: Overview of miRNA gene transcription and microprocessor processing. The miRNA gene is transcribed by RNA pol II and the pri-miRNA is processed by Drosha and its cofactor DGCR8. The cropping is also mediated by other proteins, such as p68 and p72. The resulting pre-miRNA is exported in the cytoplasm by the action of EXP5 and Ran-GTP (Ha and Kim, 2014).

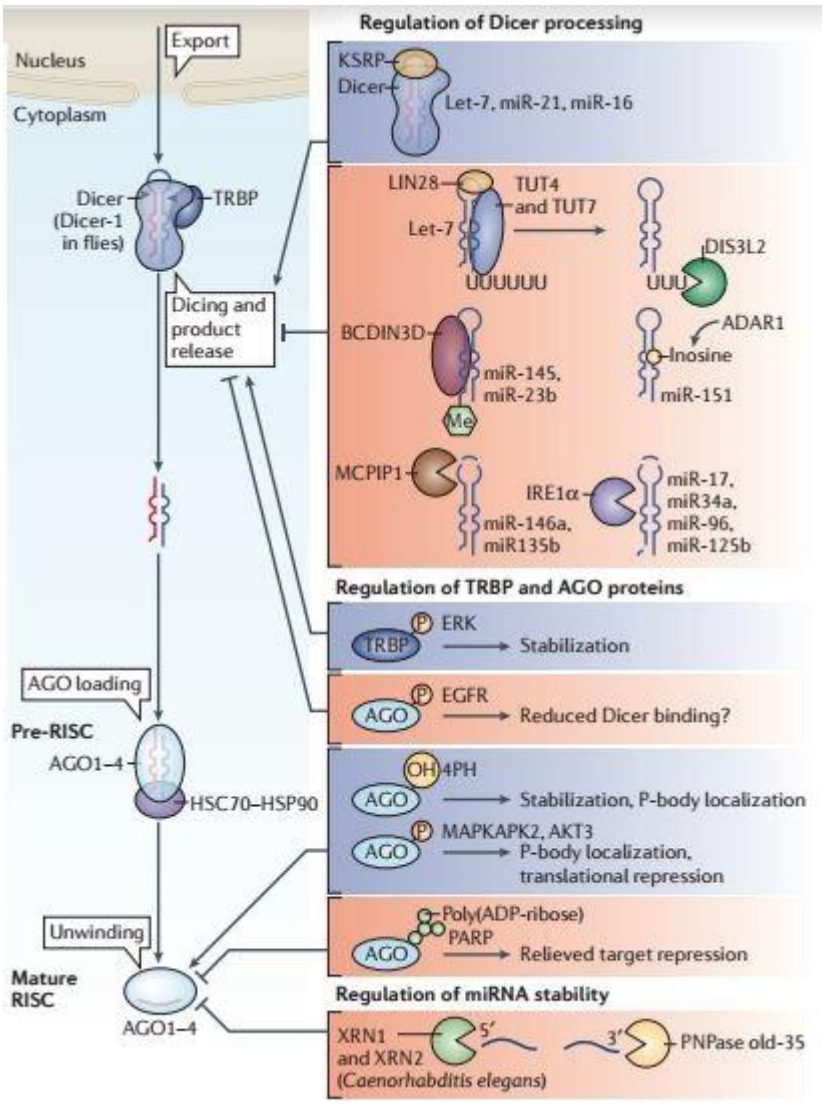

Figure 12: Overview of Dicer processing and RISC assembly. Once exported in the cytoplasm, pre-miRNA is processed by Dicer and its cofactor TRBP. The mature miRNA is then loaded in the RISC complex, composed by AGO1-4 and HSC70-HSC90. The mature RISC complex promotes the RNA silencing through different mechanisms (Ha and Kim, 2014).

1.3.2 miRNAs potential as biomarkers

In clinical context, an ideal biomarker should fit a number of criteria stated also by FDA: it should be non-invasive, highly specific and sensitive, predictive (long half-life in sample and proportional to degree of severity of pathology), robust (rapid and accurate detection) and translatable. Currently, biomarkers that are used in clinical practice are proteins in the blood of patients affected by a particular disease/condition, such as troponin, carcinoembryonic antigen (CEA), prostate specific antigen (PSA) and aminotransferases (ALT and AST). Because of their stability in different body fluids, miRNAs can be very usefull in disease diagnosis and prognosis, as well as in the prediction of therapeutic response. Specifically, miRNA levels can be detected with various methods, i.e. PCR, in blood, plasma, serum, urine and saliva of patients with different diseases. It was described that Let-7 expression is reduced in lung cancer; moreover low levels of Let-7 correlate with a significant shorter survival rate (Takamizawa *et al.* 2004). Other examples are miR-141, whose serum levels can distinguish advanced prostate cancer patients from healthy individuals, the miR-126:miR-182 ratio in urine of patients with bladder cancer and miR-125a and miR-200a in the saliva of oral squamous cell carcinoma patients (Mitchell *et al.* 2008; Hanke *et al.* 2010; Park *et al.* 2009). The importance of miRNAs as diagnostic biomarkers is not limited in cancer but also in other pathologies, such as viral infections, cardiovascular diseases, neurodegenerative disorders, diabetes and metabolic diseases (Wang *et al.* 2016). Since miRNAs are aberrantly expressed in several diseases, targeting of miRNAs might be a new interesting therapeutic approach. Nowadays, there are different methods that can be used in order to counteract miRNAs dysregulation, such as RNA sponges and antisense oligonucleotide (ASOs). miRNAs sponges are mRNAs with multiple artificial miRNA-binding sites, which can sequester the over-expressed target miRNA leading to the expression of the mRNA of interest (Ebert and Sharp, 2010). miRNAs that are up-regulated should be targeted using anti-miRNAs, specific modified ASOs. A class of anti-miRNAs is represented by antagomir, which are cholesterol-conjugated to facilitate cellular uptake and their protection against the binding of serum proteins. Other approaches that have been studied *in vivo* are oligos

modified with the locked nucleic acid (LNA) or the 2'-O-methoxyethyl (MOE) phosphorothioate chemistry. Both these derivatives have been evaluated in clinical trials. In case of miRNAs reduction the solution should be the use of miRNA mimics, in order to increase the concentration of the target miRNA. However, this approach needs to be investigated *in vivo*. It has been described that tetracycline-inducible shRNAs are able to decrease the activity of Drosha and Pasha, thus providing an indirect methodology to modulate miRNAs expression. However, this mechanism should be controlled since down-regulation of this pathway will have an effect on all miRNAs (van Rooij *et al.* 2008).

2. Aims of the research

The principal aims of my PhD project were to search for novel autophagy-related biomarkers for CD diagnosis and to establish an *in vitro* cell model to evaluate the importance of the autophagy process to counteract gluten toxicity. The goal of physicians is to remove endoscopy and biopsy analysis from the CD diagnostic path because of the risks and the invasiveness of this practice. The search of new molecular markers or signature to improve CD diagnosis and/or patients' stratification is therefore encouraged. miRNAs have emerged as promising non-invasive biomarkers in many diseases and are implicated in the regulation of several cellular processes, including autophagy. Since autophagy plays a crucial role in immunity and inflammation, in this work the expression of two autophagic genes and their negative miRNA regulators was investigated in order to find statistically significant differences between pediatric CD patients and control subjects matched for sex and age.

In the second part of the Thesis, autophagy was studied in a CD *in vitro* model to investigate its involvement in gliadin metabolism and the modulation of this process was assayed to prevent gliadin extracellular spread. Gliadin peptides have sticky properties and are able to spontaneously form aggregates that are endocyted by cells. This characteristic is common to other toxic proteins responsible for different diseases, such as Alzheimer and Parkinson disease, and autophagy impairment plays a crucial role in the pathogenesis of these disorders, thus leading to an inability to digest these protein aggregates. Particularly, autophagy was modulated through molecular and pharmacological approaches to reduce the release of gliadin aggregates outside the cells.

3. Materials and Methods

Subjects

In this study pediatric patients were enrolled in collaboration with the Pediatric Auxology Unit and the Pediatric Surgery Unit of the Fondazione IRCCS Policlinico San Matteo over the last two years. This study was approved by the Ethical Committee of Fondazione IRCCS Policlinico San Matteo and a written informed consent was obtained from the parents of all the subjects.

The cohort of subjects submitted to CD screening was divided into two groups, as described in **Table 2**.

Parameters	Group 1 (CD patients)	Group 2 (Controls)
N°	25	33
Sex	11 M, 14 F	16 M, 17 F
Age	9.4 ± 4.4	9.4 ± 3.9
Height SDS	0.5 ± 1.6	-0.31 ± 1.48
BMI SDS	-0.88 ± 1.29	-0.80 ± 1.99
Positive serological test for CD (anti-tTG IgA/IgG and/or anti-EMA IgA)	25/25	0/33
Confirmatory biopsy for CD	25/25	0/33

Table 2: Clinical and serological data of the patients enrolled in the study. Height and body mass index (BMI) are indicated as standard deviation scores.

CD patients were enrolled for the concomitant presence of symptoms (anemia, short stature, gastrointestinal symptoms given by malabsorption). Positive serological tests and histological analysis of the biopsies confirmed the CD diagnosis. Control patients were referred to clinicians for other reasons not related to CD. Some of them underwent upper gastrointestinal endoscopy for other clinical purposes, such as gastroesophageal reflux, esophageal varices, gastritis or *H.pylori* infection. The exclusion criteria were dysmorphic syndromes, chromosomal abnormalities and chronic

conditions causing growth retardation. A total of 105 specimens were collected, specifically 56 peripheral blood samples and 49 intestinal biopsies. Blood samples were collected from 33 controls and 23 untreated CD patients whereas biopsies were collected from 24 controls and 25 untreated CD patients, divided into Marsch 3B and 3C pathological grading (Oberhuber, 2000).

Sample collection

Peripheral blood (3 ml for each sample) was collected in EDTA tubes whereas duodenal specimens (5-10 mm^3 for each biopsy) were collected in 1.5 ml of TRIzol reagent. Both type of tissues were stored at -80°C until RNA extraction.

Real-Time PCR expression analysis

Total RNA was extracted from blood and biopsies with TRIzol reagent according to the manufactorer's intructions. Before RNA extraction, biopsies were homogenized with TissueRuptor (Qiagen). RNA quantification was performed using Quant-it RNA Assay (Invitrogen). miRNAs cDNA was obtained using a sequence-specific hairpin-primer and amplified using the TaqMan MicroRNA Assays kit (Applied Biosystems). *ATG7* and *BECN1* cDNA were obtained using random hexamers primers (Applied Byosystems) as reported in Comincini *et al.* (2013). Sequence specific primers were then used to amplify cDNAs with TaqMan Universal Master Mix II, no UNG (Applied Biosystems). Real-Time PCR was performed using 5 ng of each cDNA and using the MiniOpticon Real-Time PCR System (Biorad) platform. Samples were analyzed in duplicate and subjected to 40 amplification cycles of 95°C for 15 min and 60°C for 1 min. All data were normalized to the *BACT* gene and relative quantification with $2^{-\Delta\Delta Ct}$ method was employed to calculate relative changes in gene expression using an internal calibrator (control sample) obtained calculating the mean of all the controls (Livak and Schmittgen, 2001). All the relative quantification values were checked for the presence of outliers and far-out values. The samples with relative quantification values very far by mean were analyzed a second time and the outliers were verified as real. As the

deletion of outliers is a controversial practice especially for relatively small cohorts, all the statistical analyses were performed including also the samples with outliers and far-out values.

Statistical analysis

The MedCalc software (https://www.medcalc.org/) was used to perform the Mann-Whitney U test, the receiver operating characteristic (ROC) curve analysis, the heatmaps and one-way ANOVA. The Orange data mining software (http://orange.biolab.si/, University of Ljubljana) was used for the nomograms and the classification trees using a Naive Bayes learner/classifier and a classification tree learning algorithm. Differences were considered statistically significant when $P < 0.05$.

Cell cultures

Caco-2 cells are a well known *in vitro* model of CD due to their characteristics resemble that of the human small intestinal mucosa. These cells were used as the main cell line to study the molecular response to PT-gliadin while HeLa cells were selected as an outgroup. Caco-2 and HeLa cells from American Type Culture Collection (ATCC) were cultured and maintained in DMEM (Euroclone) supplemented with (or without in serum deprivation experiments) 10% FBS, 100 units/ml penicillin, 0.1 mg/ml streptomycin and 1% L-glutamine and kept at 37°C in a 5% CO_2/95% air atmosphere. Most of the experiments were performed in plates of 6-12-24 wells adding different amount of cells, depending on each experiment requirements. Treatments with rapamycin (Sigma) were conducted at different concentration (5-10-20 µM).

PT-gliadin preparation

Gliadin from wheat (Sigma) was digested as described by Gujral *et al.* 2015 to a final concentration 1 g/ml. In detail, gliadin was firstly dissolved in 500 ml 0.2 N HCl for 2 h at 37 °C with 1 g pepsin (Sigma). The resultant peptic digest was further digested by addition of 1 g trypsin (Sigma), after pH adjusted to 7.4 using 2 N NaOH and the solution was incubated at 37 °C for

4 hours with a vigorous agitation. Finally, the mixture was boiled to inactivate enzymes for 30 min and stored at -20°C. Ovalbumin (Sigma) at 1 g/ml was used as an additional external protein for internalization and cell toxicity studies. PT-gliadin or ovalbumin were then administered directly to the cells.
For PT-gliadin Alexa Fluor 488 labelling, an initial purification of PT-gliadin was performed using affinity chromatography-purification G50 columns (Amersham). The resulted proteins were resuspended in PBS and quantified through Qubit^{TM} Fluorometer (Invitrogen). The final concentration was 1.12 mg/ml. 100 µg of proteins were then labelled with Alexa Fluor 488 by Alexa Fluor Microscale labelling kit (Molecular Probes) according to manufacturer's instructions. A same amount of ovalbumin was labelled following the same protocol.

Trypan blue exclusion assay

Trypan blue exclusion assay was used to evaluate cell viability after PT-gliadin administration. 10^5 cells were seeded in duplicate in 24-well plates with the administration of PT-gliadin (500 µg/ml). Cells viability was monitored at 24 and 48 hours p.t. Viable cells were counted adding 0.1 ml of Trypan blue dye 0.4% (Biorad) to 1 ml of cells in order to distinguish dead cells (blue) and live cells. Cells counting was performed with a hemacytometer.

Electron miscoscopy observations

Electron microscopy analysis was performed according to Fassina *et al.* 2012. HeLa and Caco-2 cells (10^6) were grown in complete DMEM medium supplied with digested gliadin (200 µg/ml) arriving to 2.5 ml as final volume. At 24 hours p.t. cells were harvested by centrifugation at 800 rpm for 3 min and fixed with 2% glutaraldehyde in DMEM, for 2 hours at room temperature. Cells where then rinsed overnight in PBS (pH 7.2) and then post-fixed in 1% aqueous OsO_4 for 2 hours at room temperature. Cells were pre-embedded in 2% agarose in water, dehydrated in acetone and finally embedded in epoxy resin (Electron Microscopy Sciences, EM-bed812). Ultrathin sections (50-60 nm) were collected on formvar-carbon-

coated nickel grids and stained with uranyl acetate and lead citrate. The specimens were observed with a Zeiss EM900 transmission electron microscope (TEM) equipped with a 30 µm objective aperture and operating at 80 kV.

Immunofluorescence analysis

Immunofluorescence assays were performed according to Sbalchiero *et al.* 2008. Primary antibodies anti-gliadin (Abcam) and anti-Limp1 (Santa Cruz) were diluted 1:30 and used to trace the gliadin uptake and internalization into vesicles. Species-specific Alexa Fluor 488 and Alexa Fluor 633 secondary conjugated antibodies (1:100) (Invitrogen) were then employed. Cells cultured on coverlips were washed three times with PBS and fixed with 4% paraformaldehyde-PBS, pH 7.4, for 15 min at room temperature. Cells were incubated for 1 hour with primary antibodies diluted in PBS + 5% non-fat milk powder (w/v). Cells were then washed with PBS and incubated for 1 hour with secondary antibodies in PBS + 5% non-fat milk powder. Coverlips were then washed three times with PBS and treated with ProLong Gold antifade reagent with DAPI (Invitrogen) according to the manufacturer's instructions and finally mounted onto glass slides. Fluorescence signals were detected using a fluorescence light inverted microscope (Nikon Eclipse TS100, Japan) with a 100x oil immersion objective.

Acridine orange staining

Monitoring and visualization of acidic vesicles was performed using an acidotropic dye, i.e. acridine orange (ext. 500nm – emis. 525 nm) according to Klionsky *et al.* 2016. Acridine orange was added at the final concentration of 1 µg/ml in Caco-2 and HeLa cultures in presence or absence of unlabelled gliadin 10 min before its fluorescent visualization. As already widely documented, lysosomes emitted in the red range because of the protonation of the dye caused by the acidic content of these vesicles. Red fluorescent spots are indicative of a higher intravesicular acidic content. Autophagosomes and lysosomes can also be distinguish according to their shape and size since the formers are more heterogeneous and bigger in

dimensions (Paglin *et al.* 2001; Kanzawa *et al.* 2003; Wilson *et al.* 2011; Zhao *et al.* 2016). An inverted fluorescence microscope (Eclipse Nikon TS100) was employed for live cells monitoring using 40x magnification.

LC3B-GFP autophagosome analysis

For autophagosome detection, cells were seeded at the density of 5 x 10^4 cells/well in 24-multiwell plates. After 24 hours cells were transducted with BacMam LC3B-GFP or with BacMam LC3B(G120A)-GFP with a multiplicity of infection (MOI) equal to 30, according to Premo Autophagy Sensor kit (ThermoFisher). LC3B-GFP signal was monitored at 24 and 48 hours p.t. using and inverted fluorescence microscope (40 x magnification, Eclipse Nikon TS100) as described in Fassina *et al.* (2012).

Immunoblotting analysis

Cells were cultured in 6-multiwell plates and collected at different interval times (2-4-24-48-72 hours). Cells were tripsinized 10 min at 37ºC, centrifuged 10 min at 14800 rpm and dried pellets were kept at -80ºC upon protein extraction. Cells were lysated in ice-cold RIPA buffer (150 mM NaCl, 50 mM Tris-HCl pH8.0, 0.5% sodium deoxycholate, 1% Nonidet P40, 0.1% sodium dodecylsulphate) and supplemented with Complete Mini protease inhibitor cocktail 7X (Roche). Protein extracts were quantified using the Quant-it Protein Assay Kit (Invitrogen). Proteins (30-50 µg) were added with Laemmli sample buffer (2% SDS, 6% glycerol, 150 mM β-mercaptoethanol, 0.02% bromophenol blue and 62.5 mM TRIS-HCl pH 6.8), denatured for 5 minutes at 95°C and separated on 12% or 15% SDS-PAGE according to the protein size. After electrophoresis, proteins were transferred onto nitro-cellulose membrane Hybond-C Extra (GE Healthcare), using the semi-dry blotter TE70 PWR apparatus (GE Healthcare). Membranes were blocked 1 hour with 5% non-fat milk in TBS (138 mM NaCl, 20 mM TrisOH pH 7.6) containing 0.1% Tween 20 and incubated over-night at 4°C with primary antibodies LC3-II, ATG3, ATG7, BECN1 (Cell Signalling) diluted at 1/3000 in 5% non-fat milk in TBS, BACT (Cell Signalling) was diluted at 1/10000 in 5% non-fat milk in TBS. Species-specific peroxidase-labelled ECL secondary antibodies (Cell

Signalling Technology, 1/10000 dilution) were used in 5% non-fat milk in TBS (Barbieri *et al.* 2011). Protein signals were revealed using the ECL Advance Western Blotting Detection Kit (GE Healthcare) by means of Chemidoc (BIORAD) instrument. Protein expression was quantified by densitometric analysis with ImageJ software (http://rsbweb.nih.gov/ij/) according to the guidelines.

Fluorimetric analysis

For gliadin secretion assays, medium of cells treated with Alexa-Fluor 488 labelled PT-gliadin was collected and quantified in its fuorescent emission spectrum by Qubit™ Fluorometer (Invitrogen) at different times after PT-gliadin administration. Since Alexa Fluor 488 emission/excitation spectra (ext. 492nm – emis. 517 nm) is nearly overlapping with that specific for Qubit™ DNA HS analysis (ext. 485nm – emis. 530 nm), fluorimetric variations were measured employing Qubit instrument as an effective and specific fluorimeter. The presence of gliadin-488 in the medium following different *in vitro* modulation of the autophagy process was evaluated. Specifically, cells were seeded at the density of 2 x 10^4 cells/well in 24-multiwell plates and incubated for 24 hours with PT-gliadin labelled with Alexa Fluor 488. Cells were wash once with PBS and the medium was replaced with complete DMEM FBS 10% or with starved DMEM 0% FBS. After additional 24 and 48 hours, medium was collected and assayed in fluorescent content by Qubit™.

Cell transfection

To down-regulate *BECN1* expression, Caco-2 cells were transiently transfected with Lipofectamine® RNAiMAX (Invitrogen) reagent coupled with a pool of validated si*BECN1* (si16537, si16538 and si16539) sequences at the final concentration of 2.5 µM. Transfection was performed with 0.5 µl of Lipofectamine for each well. 24 hours after transfection, PT-gliadin was added to the transfected and control cells and silencing was monitored through *BECN1* immunoblotting at 48 and 72 hours p.t.

4. Results

The results reported in this PhD Thesis are organized into two parts: the former (Part A) related to the identification of markers for CD diagnosis, the latter (Part B) to the establishment of an *in vitro* cell model to evaluate the contribution of the autophagy process to counteract some cytotoxic features of the gliadin peptides.

Part A

Identification of autophagy genes/miRNAs associated with celiac disease

To identify novel molecular markers useful to increase sensitivity and specificity in pediatric CD patients' diagnosis, the expression levels of key autophagy genes and their regulatory miRNAs were analyzed. Specifically, *BECN1* and miR-30a (Zhu *et al.* 2009), *ATG7* and miR-17 (Comincini *et al.* 2013) were investigated. To this purpose, relatively quantitative Real-Time PCR was performed on blood and intestinal biopsies derived from exploratory cohorts of pediatric CD patients with active disease compared with controls, as described in Materials and Methods. In **Figure 13** are reported the notched box-and-whisker plots of the expression levels of the analyzed genes/miRNAs in both tissues. Among the investigated targets, miR-17 showed the greatest variability in the blood of both CD patients and controls (**Panels A** and **B**). Moreover, the lowest variability was observed for *ATG7* in the blood of controls and *BECN1* in the blood of CD patients. As reported in **Panels C** and **D**, *ATG7* showed the highest variability compared with *BECN1*, whose variability is low.

A

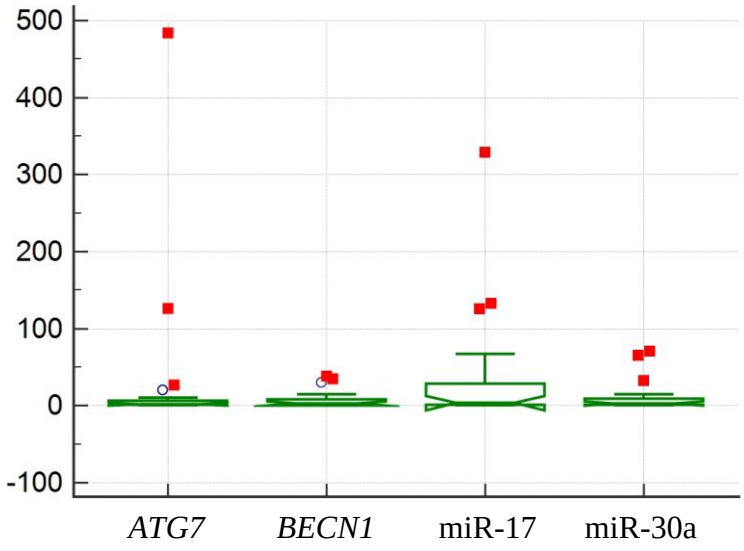
500
400
300
200
100
0
-100
ATG7
BECN1
miR-17
miR-30a

B

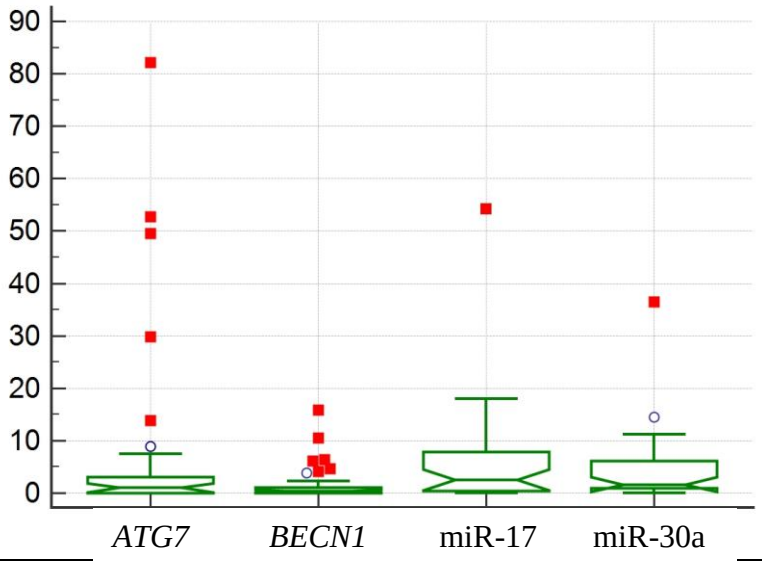
90
80
70
60
50
40
30
20
10
0
ATG7
BECN1
miR-17
miR-30a

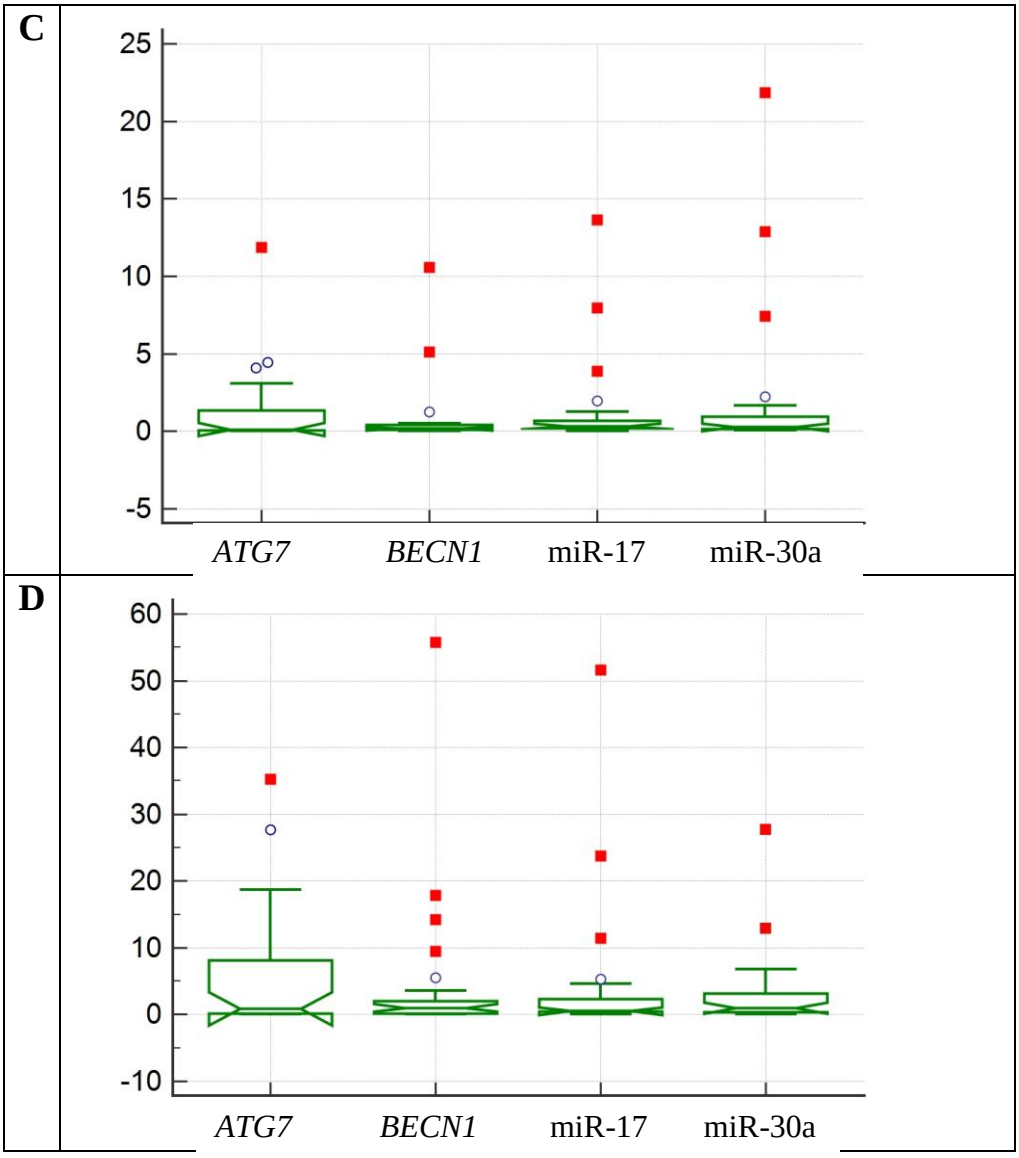

Figure 13: Notched box-and-whisker plots of the expression values obtained by Real-Time PCR from the blood of CD patients (A) and controls (B). The values obtained from the biopsies of CD patients (C) and controls (D) are reported below. In Y axis are reported the obtained relative expression values. Outliers (circles) and far-out values (squares) are indicated.

To assess the presence of statistically significant differences in genes/miRNAs expression levels between CD patients and controls, the non-parametric Mann-Whitney U test was performed. Differences were considered statistically significant when P-value < 0.05. The results are reported in **Table 3**.

Tissue	Gene/miRNA	Z-score	P-value
Peripheral blood	*ATG7*	2.13	0.2585
	BECN1	2.34	0.0189*
	miR-17	1.13	0.2557
	miR-30a	1.51	1.1310
Intestinal biopsy	*ATG7*	2.41	0.0159*
	BECN1	2.48	0.0129*
	miR-17	2.09	0.0365*
	miR-30a	2.16	0.0302*

Table 3: P-values and Z-scores obtained adopting the Mann-Whitney U test. The asterisks indicate statistical significant results (P-value < 0.05).

In blood, only *BECN1* showed statistically significant differences between the two analyzed groups (P-value = 0.0189). Conversely, in intestinal biopsies all the investigated targets showed statistically significant differences between CD and control subjects.

Bioinformatics performance of the investigated targets as potential CD biomarkers

To further assess the diagnostic capability of the investigated autophagy-related genes/miRNAs to distinguish CD *vs* control subjects, the receiver operating characteristics (ROC) curve analysis was performed (**Table 4**). In blood, *BECN1* ROC curve revealed a fair diagnostic property, with area under the ROC curve (AUC) value of 0.683 (P = 0.012). The sensitivity and specificity values associated to this curve were 65.22 and 74.29%, respectively. In intestinal biopsies, similar levels within a fair-range of sensitivity and specificity were reported for *ATG7*, *BECN1*, miR-17 and miR-30a.

Tissue	Gene/miRNA	AUC	C.I. 95%	P-value	Sensitivity	Specificity
Peripheral blood	*ATG7*	0.603	0.46-0.73	0.1723	78.26	47.06
	BECN1	0.683	0.54-0.79	0.012*	65.22	74.29
	miR-17	0.605	0.46-0.73	0.1822	34.78	97.06
	miR-30a	0.632	0.49-0.75	0.0754	56.52	67.65
Intestinal biopsy	*ATG7*	0.697	0.55-0.81	0.007*	64.00	69.23
	BECN1	0.703	0.55-0.82	0.0068*	88.00	57.69
	miR-17	0.671	0.52-0.79	0.0274*	56.00	84.62
	miR-30a	0.677	0.53-0.80	0.0238*	72.00	69.23

Table 4: Receiver operating characteristic (ROC) curve analysis. Confidential intervals (95%), sensitivity and specificity percentage values are reported. The asterisks indicate statistical significant results (P-value < 0.05).

Classification of CD patients and controls through the expression levels of the autophagy-related markers

To determine whether the investigated genes/miRNAs were able to effectively distinguish CD/control subjects and to eventually stratify CD patients, a supervised multivariate analysis was conducted. Initially, a classification tree was created on the expression values detected in the blood of CD patients and controls. As reported in **Figure 14**, two branches containing 12 subgroups were obtained, as indicated by capital letters (A-N). The algorithm mainly considered miR-17 and *BECN1* relative expression cut-off values to create apical classification subgroups. In particular, D, F and M subgroups homogeneously classified 16/23 CD patients (69.56%) whereas subgroups G and I were mainly composed of CD patients. Particularly, G was composed of three CD patients and one control, while two CD patients and one control belonged to subgroup I. Similarly, subgroups A, B, H and L homogenously classified 28/33 controls (84.84%),

whereas C was composed mostly of controls. Specifically, C was composed of two controls and one CD patient. Lastly, the subgroup N included one CD patient and one control.

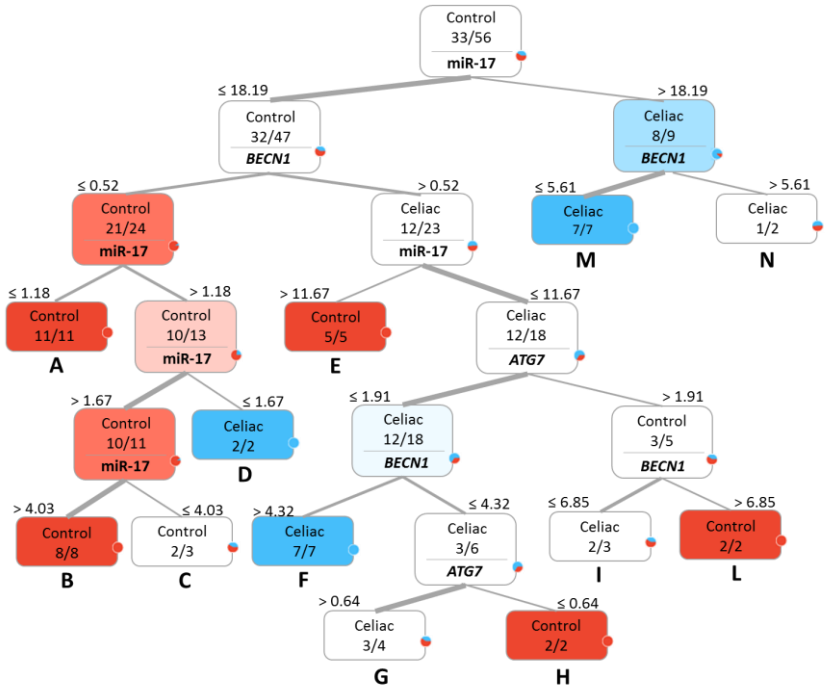

Figure 14: Classification tree obtained using the expression levels of analyzed genes and miRNAs in blood. CD patients are indicated in blue, controls in red. Resulting classes are highlighted by capital letters.

A classification tree was also created for samples derived from intestinal biopsies. As reported in **Figure 15**, 11 subgroups were obtained, again indicated by the capital letters. Five of them (i.e. B, E, G, H and L) homogeneously classified 22/25 CD patients (88%). Similarly, A, D and M grouped 19/24 controls (79.16%), whereas the subgroups F and I were composed of two controls and one CD patient. As reported, the expression levels of all the analyzed genes/miRNAs were employed to build the classification tree. Next, an unsupervised analysis was conducted employing relative gene expression data to correctly classify CD and control subjects. In particular, the classification tree algorithm, which is an example of greedy algorithm that follows the problem solving heuristic of making the locally optimal choice at each stage (Quinlan, 1986), was assayed to calculate the probability of each subject to be correctly classified in accordance with the initial diagnosis. Using the expression levels of the genes/miRNAs detected in the blood only four subjects (i.e. 10, 29, 36 and 56) were misclassified, as reported in **Table 5**. In the case of biopsies, only three subjects were misclassified (i.e. 7, 15 and 49), as indicated in **Table 6**.

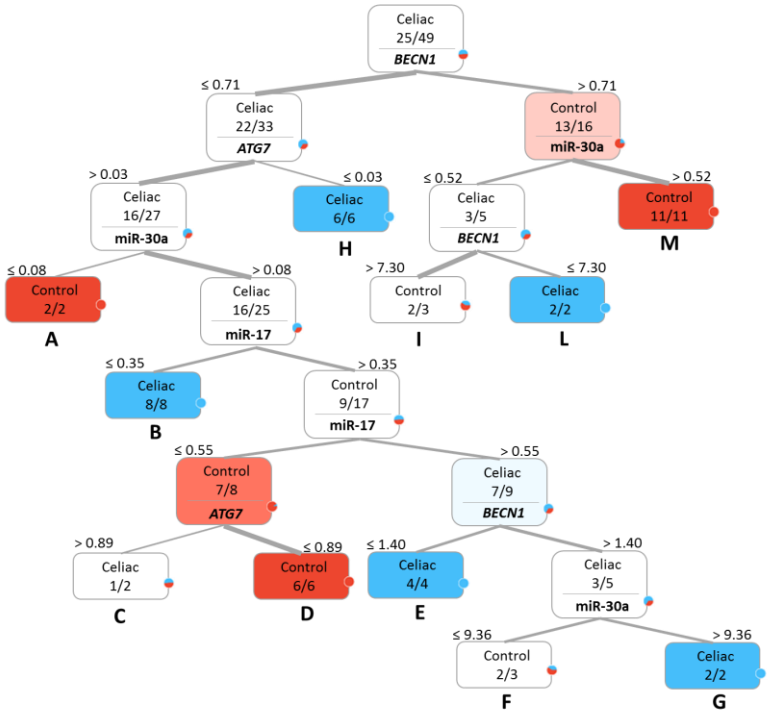

Figure 15: Classification tree obtained using the expression levels of analyzed genes and miRNAs in biopsies. CD patients are indicated in blue, controls in red. Resulting classes are highlighted by capital letters.

Unsupervised analysis for blood samples			
Subject	**Diagnosis**	**CD *vs* control probability**	**Classification**
1	Celiac disease	1.00 : 0.00	Celiac disease
2	Celiac disease	0.50 : 0.50	Celiac disease
3	Celiac disease	0.67 : 0.33	Celiac disease
4	Celiac disease	1.00 : 0.00	Celiac disease
5	Celiac disease	1.00 : 0.00	Celiac disease
6	Celiac disease	1.00 : 0.00	Celiac disease
7	Celiac disease	0.75 : 0.25	Celiac disease
8	Celiac disease	1.00 : 0.00	Celiac disease
9	Celiac disease	1.00 : 0.00	Celiac disease
10	Celiac disease	0.33 : 0.67	Control *
11	Celiac disease	0.67 : 0.33	Celiac disease
12	Celiac disease	1.00 : 0.00	Celiac disease
13	Celiac disease	1.00 : 0.00	Celiac disease
14	Celiac disease	1.00 : 0.00	Celiac disease
15	Celiac disease	1.00 : 0.00	Celiac disease
16	Celiac disease	0.75 : 0.25	Celiac disease
17	Celiac disease	1.00 : 0.00	Celiac disease
18	Celiac disease	1.00 : 0.00	Celiac disease
19	Celiac disease	0.75 : 0.25	Celiac disease
20	Celiac disease	1.00 : 0.00	Celiac disease
21	Celiac disease	1.00 : 0.00	Celiac disease
22	Celiac disease	1.00 : 0.00	Celiac disease
23	Celiac disease	1.00 : 0.00	Celiac disease
24	Control	0.00 : 1.00	Control
25	Control	0.00 : 1.00	Control
26	Control	0.00 : 1.00	Control
27	Control	0.00 : 1.00	Control
28	Control	0.00 : 1.00	Control
29	Control	0.50 : 0.50	Celiac disease *
30	Control	0.00 : 1.00	Control
31	Control	0.00 : 1.00	Control
32	Control	0.00 : 1.00	Control

33	Control	0.00 : 1.00	Control
34	Control	0.00 : 1.00	Control
35	Control	0.00 : 1.00	Control
36	Control	0.67 : 0.33	Celiac disease *
37	Control	0.00 : 1.00	Control
38	Control	0.00 : 1.00	Control
39	Control	0.00 : 1.00	Control
40	Control	0.00 : 1.00	Control
41	Control	0.33 : 0.67	Control
42	Control	0.00 : 1.00	Control
43	Control	0.33 : 0.67	Control
44	Control	0.00 : 1.00	Control
45	Control	0.00 : 1.00	Control
46	Control	0.00 : 1.00	Control
47	Control	0.00 : 1.00	Control
48	Control	0.00 : 1.00	Control
49	Control	0.00 : 1.00	Control
50	Control	0.00 : 1.00	Control
51	Control	0.00 : 1.00	Control
52	Control	0.00 : 1.00	Control
53	Control	0.00 : 1.00	Control
54	Control	0.00 : 1.00	Control
55	Control	0.00 : 1.00	Control
56	Control	0.75 : 0.25	Celiac disease *

Table 5: Unsupervised analysis using of the subjects using the expression values of genes/miRNAs in the blood. CD *vs* control probability was calculated (second column) in order to compare the obtained classification with the diagnosis. Asterisks highlighted misclassified subjects.

Unsupervised analysis for intestinal biopsies			
Subject	**Diagnosis**	**CD *vs* control probability**	**Classification**
1	Celiac disease	1.00 : 0.00	Celiac disease
2	Celiac disease	1.00 : 0.00	Celiac disease
3	Celiac disease	1.00 : 0.00	Celiac disease

4	Celiac disease	1.00 : 0.00	Celiac disease
5	Celiac disease	1.00 : 0.00	Celiac disease
6	Celiac disease	1.00 : 0.00	Celiac disease
7	Celiac disease	0.33 : 0.67	Control *
8	Celiac disease	1.00 : 0.00	Celiac disease
9	Celiac disease	1.00 : 0.00	Celiac disease
10	Celiac disease	1.00 : 0.00	Celiac disease
11	Celiac disease	1.00 : 0.00	Celiac disease
12	Celiac disease	1.00 : 0.00	Celiac disease
13	Celiac disease	1.00 : 0.00	Celiac disease
14	Celiac disease	1.00 : 0.00	Celiac disease
15	Celiac disease	0.33 : 0.67	Control *
16	Celiac disease	1.00 : 0.00	Celiac disease
17	Celiac disease	1.00 : 0.00	Celiac disease
18	Celiac disease	1.00 : 0.00	Celiac disease
19	Celiac disease	1.00 : 0.00	Celiac disease
20	Celiac disease	1.00 : 0.00	Celiac disease
21	Celiac disease	0.50 : 0.50	Celiac disease
22	Celiac disease	1.00 : 0.00	Celiac disease
23	Celiac disease	1.00 : 0.00	Celiac disease
24	Celiac disease	1.00 : 0.00	Celiac disease
25	Celiac disease	1.00 : 0.00	Celiac disease
26	Control	0.00 : 1.00	Control
27	Control	0.00 : 1.00	Control
28	Control	0.00 : 1.00	Control
29	Control	0.00 : 1.00	Control
30	Control	0.00 : 1.00	Control
31	Control	0.00 : 1.00	Control
32	Control	0.33 : 0.67	Control
33	Control	0.00 : 1.00	Control
34	Control	0.00 : 1.00	Control
35	Control	0.33 : 0.67	Control
36	Control	0.00 : 1.00	Control
37	Control	0.00 : 1.00	Control
38	Control	0.00 : 1.00	Control

39	Control	0.00 : 1.00	Control
40	Control	0.00 : 1.00	Control
41	Control	0.00 : 1.00	Control
42	Control	0.00 : 1.00	Control
43	Control	0.00 : 1.00	Control
44	Control	0.00 : 1.00	Control
45	Control	0.33 : 0.67	Control
46	Control	0.00 : 1.00	Control
47	Control	0.33 : 0.67	Control
48	Control	0.00 : 1.00	Control
49	Control	0.50 : 0.50	Celiac disease *

Table 6: Unsupervised analysis of the subjects using the expression values of genes/miRNAs in the intestinal biopsies. CD *vs* control probability was calculated (second column) in order to compare the obtained classification with the diagnosis. Asterisks highlighted misclassified subjects.

Nomograms analysis

To determine the relative contribution of each genes/miRNAs in determining the CD diagnostic performance, a Naive Bayesian nomogram analysis was performed (Partin *et al.* 1993). Relative expression genes/miRNAs values and probability to identify CD *vs* controls were compared. The expression profiles of the investigated targets were represented in order of their relative positive influence in determining an increased probability of CD identification, specifically set on P = 0.8. In blood samples, as reported in **Figure 16**, gene expression trends were nearly monotonic. An increase in the expression levels of one or more of these markers was therefore nearly proportional to the increase in probability of a correct CD identification.

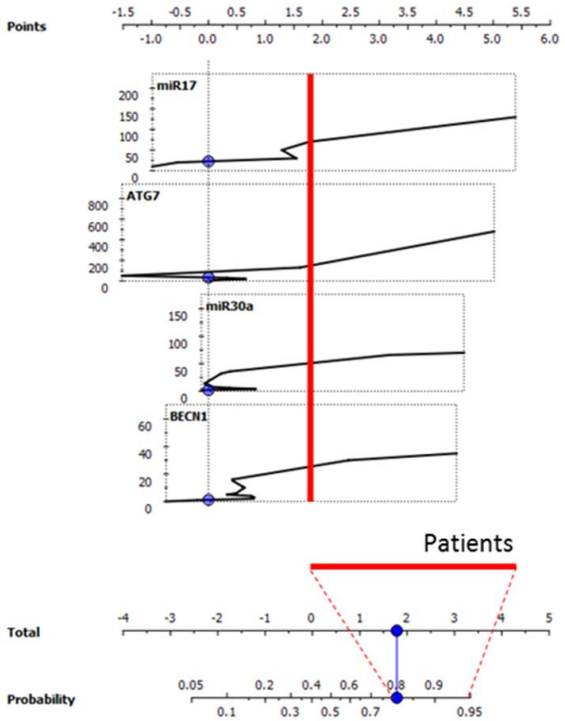

Figure 16: Nomogram (lower graph) created considering the relative expression values of the analyzed genes/miRNAs in the peripheral blood specimens (upper). The red line evidences the portion of the curves (on the right side of each) that confers a high probability (P > 0.8), in correspondence of the identified relative expression values, to correctly classify a celiac condition.

As shown in **Figure 17**, in biopsies, *ATG7* showed an opposite trend compared to blood, it was nearly monotonic, with however the important exception of the portion under the curve relative to established CD probability threshold (P = 0.8). *BECN1* displayed a relatively complex expression trend, similar in its linearity and its decreasing profile to *ATG7*. The portion of the curve that determine a high celiac diagnostic probability was linear compared with *ATG7*. Differently, miRNAs exhibited very complex curves, with higher scores (log odds ratio) in correspondence of low expression values, suggestive of decreasing expression levels associated with higher probability of CD.

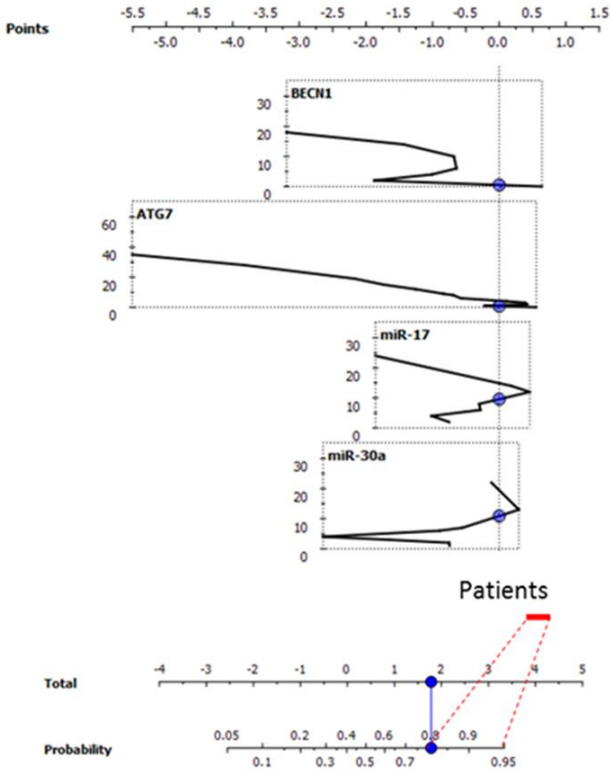

Figure 17: Nomogram (lower graph) created considering the relative expression values of the analyzed genes/miRNAs in the intestinal biopsies (upper). The red line evidences the portion of the curves (on the right side of each) that conferes a high probability (P > 0.8), in correspondence of these identified relative expression values, to correctly classify a celiac condition.

BECN1 showed opposite expression trends in the two investigated tissues in CD patients and controls

To better discriminate the presence of significant down or up-regulation of the investigated autophagy related markers between CD patients and controls, heatmaps were created taking into account 43 samples of which both blood and biopsies specimens were collected; these were clinically subdivided into 22 CD patients and 21 controls. As illustrated in **Figure 18**,

an opposite trend of *BECN1* expression in both tissues was found. Specifically, over-expression of *BECN1* was predominantly detected in the blood of CD patients compared with controls while biopsies showed an opposite trend.

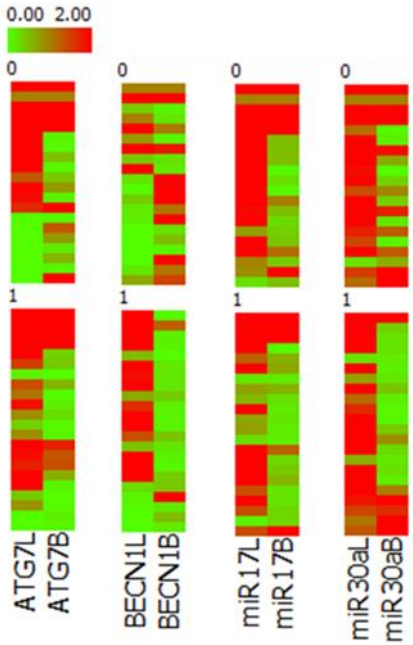

Figure 18: Heatmaps of the expression of investigated genes and miRNAs. CD diagnosis is indicated with 1, controls with 0. Down-regulation is highlighted in green while up-regulation in red. Cut-off value = 1. The letter L indicates the blood tissue (L = leukocytes) whereas B indicates intestinal biopsies (B = biopsy).

These evidence were further highlighted in **Figure 19** graphs. Histograms were then created to deeply analyze these differences (**Figure 20**). *BECN1* resulted over-expressed in the blood of 20% of controls versus 63.63% of CD patients. An opposite situation was observed at the level of the intestine, in which *BECN1* was significantly over-expressed in controls (55%) compared with CD patients (9.09%) ($P < 0.001$, ANOVA two-ways). The same analyses were performed on the other investigated targets without statistically significant results (data not shown).

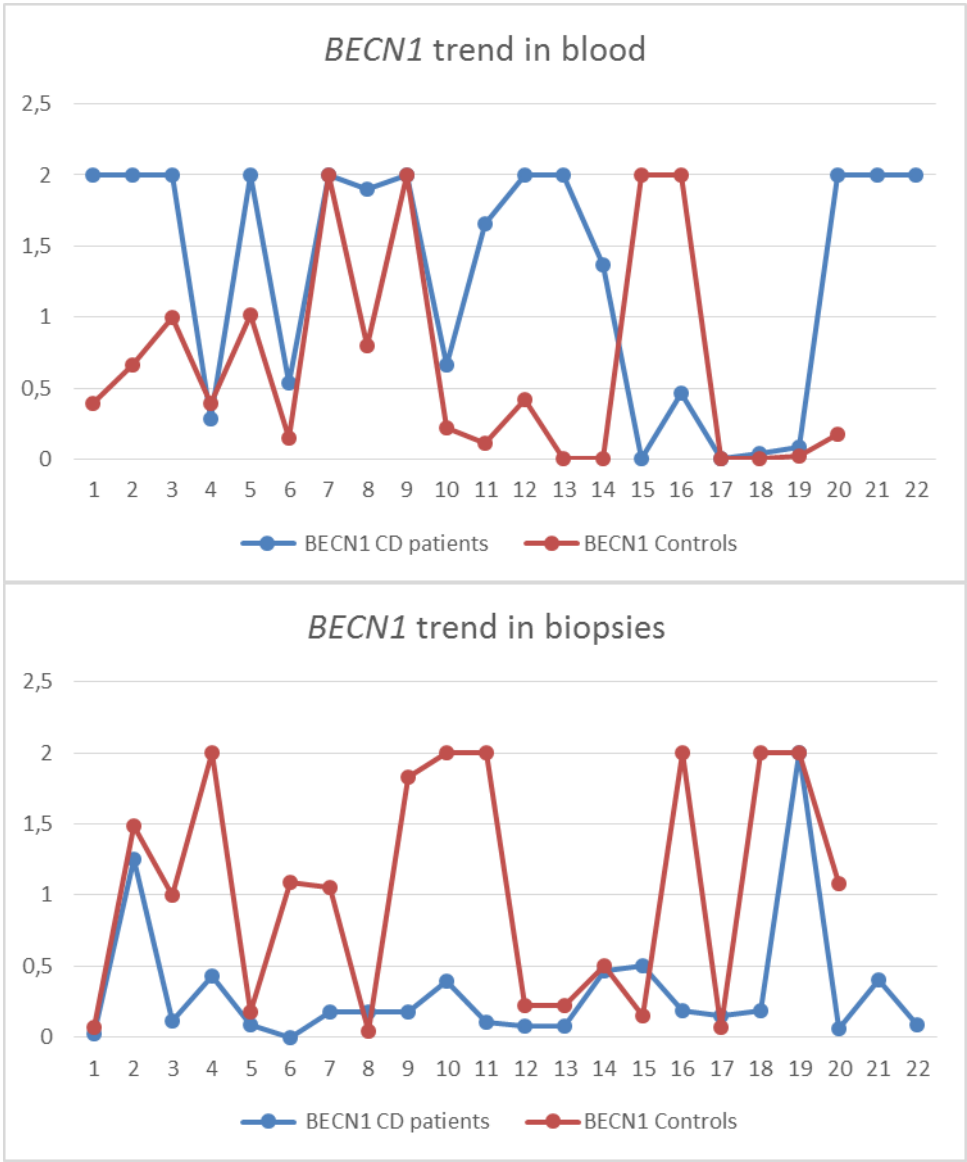

Figure 19: *BECN1* expression trends in blood and biopsies of CD patients compared with controls. On the Y axis, 1 indicate the basal level of expression, 2 the over-expression and 0 the down-regulation. On X axis, the labels of the analyzed samples.

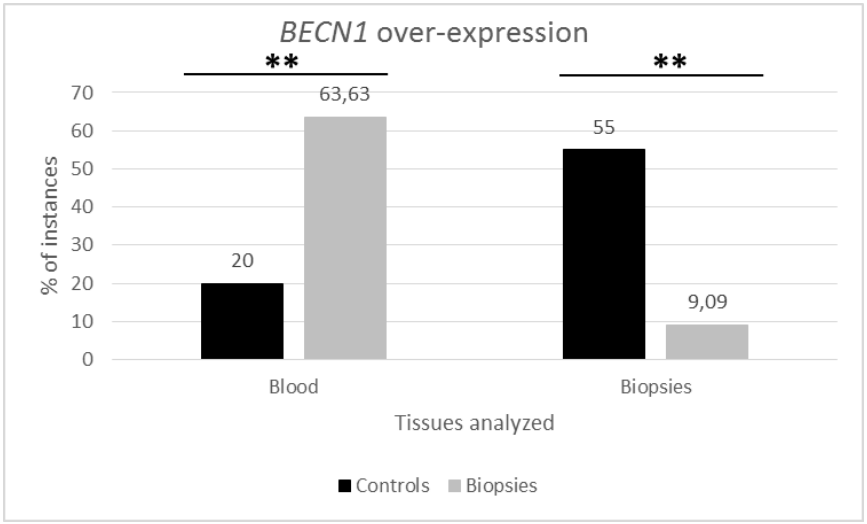

Figure 20: Histograms reporting the percentage of subjects with *BECN1* over-expression in both tissues taking into account their diagnosis. The asterisks indicated statistically significant differences ($P < 0.001$, two-ways ANOVA).

Part B

Gliadin affects viability and is internalized into growing cells

To investigate the morphological and functional effects of gliadin to epithelial cells, human colon carcinoma cell line Caco-2 was assayed in viability and in morphological changes. HeLa cells were adopted as an outgroup control. As a preliminary experiment, cells were cultured in complete DMEM and treated with PT-gliadin at different concentration (0.5 – 1 mg/ml) and their viability was assayed by Trypan blue exclusion test after 24 and 48 hours p.t. (**Figure 21**). Both cell lines exhibited a significant reduction in viability ($P < 0.001$, ANOVA One-way), mainly induced at the first assayed interval of time (i.e. 24 hours p.t.).

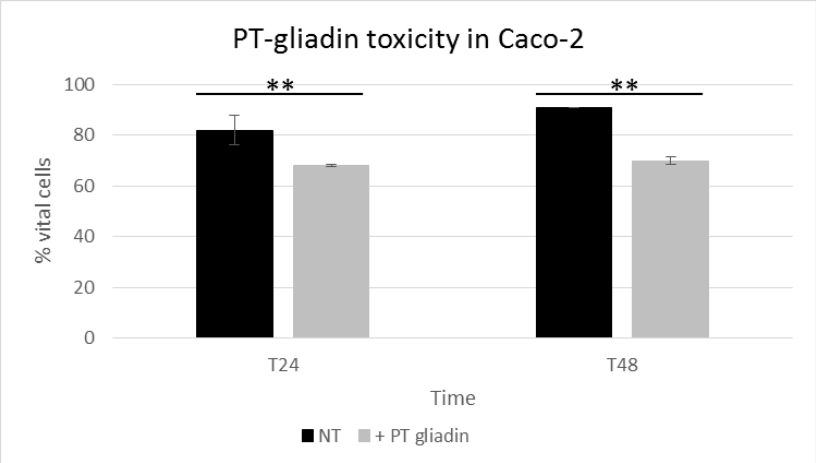

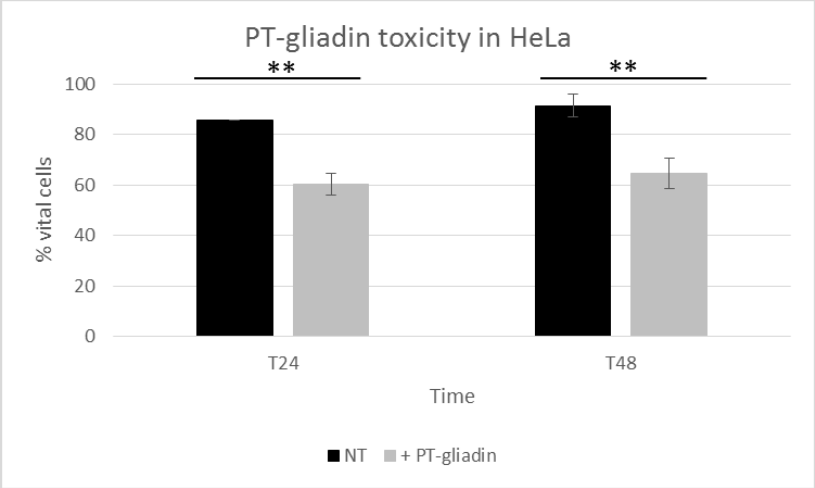

Figure 21: Viability of Caco-2 and HeLa cells treated with PT-gliadin (500 µg/ml)) compared with non treated (NT) negative controls. Viability was measured with trypan blue exclusion test. One-way ANOVA was used to determine the statistical differences between the observed values of vital cells ($P < 0.001$).

The effects of gliadin in living cells were also monitored through optical microscope evaluations at different time intervals (24-48-72 hours p.t.). As exemplified in **Figure 22**, at 24 hours p.t., PT-gliadin spontaneously formed large extracellular aggregates that can be visualized even at lower magnifications. These aggregates were also visible in proximity or associated with plasma membranes and within large intracellular vesicles. Importantly, the number and shape of vesicles were significantly reduced in untreated cells.

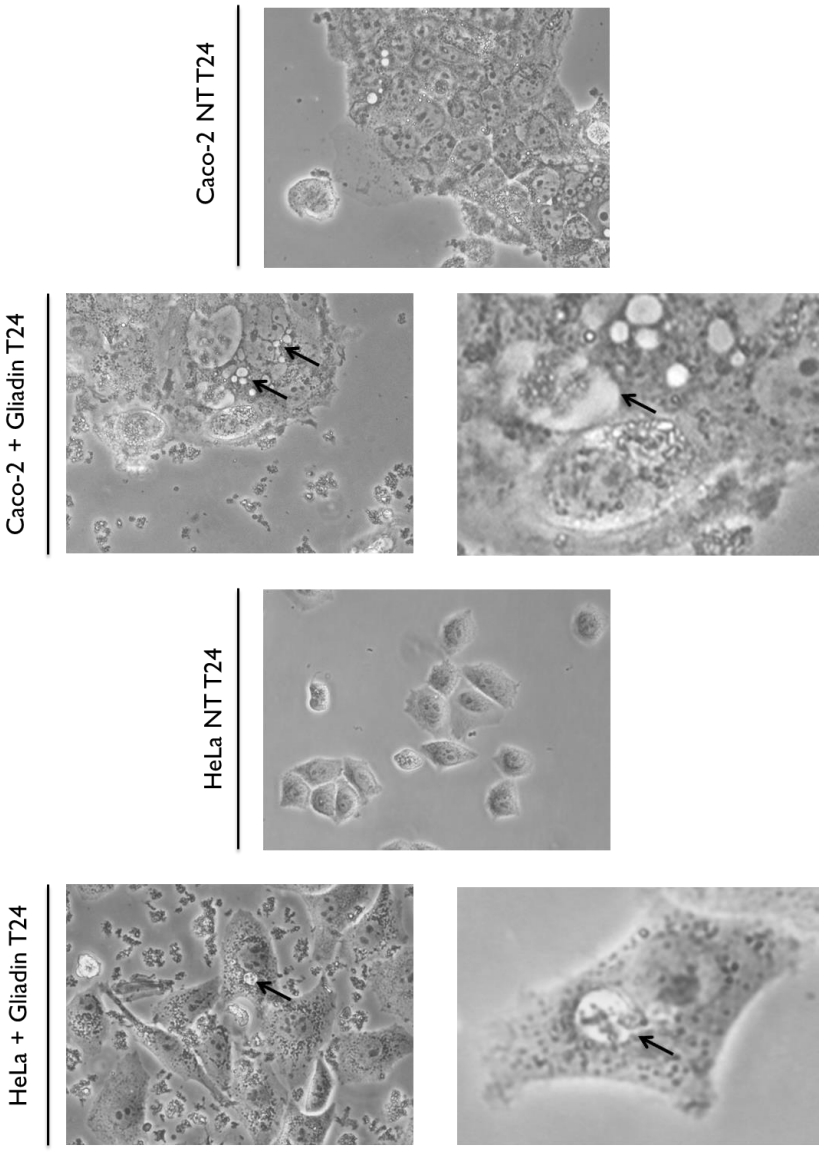

Figure 22: Caco-2 and HeLa cells treated with PT-gliadin and visualized at 24 hours p.t. On the left of the panel visualization was performed at 10X of magnification whereas on the right at 40X. Asterisks indicate extracellular gliadin aggregates, while arrows show vesicles containing exogenous material.

To deeply investigate and better characterized the content of the vesicles, electron microscopy observations were conducted on HeLa treated with gliadin. As shown in **Figure 23** two different types of vesicles, likely autophagosomes, were evidenced. One containing gliadin-like aggregates, the other showing partially digested materials or without appreciable contents.

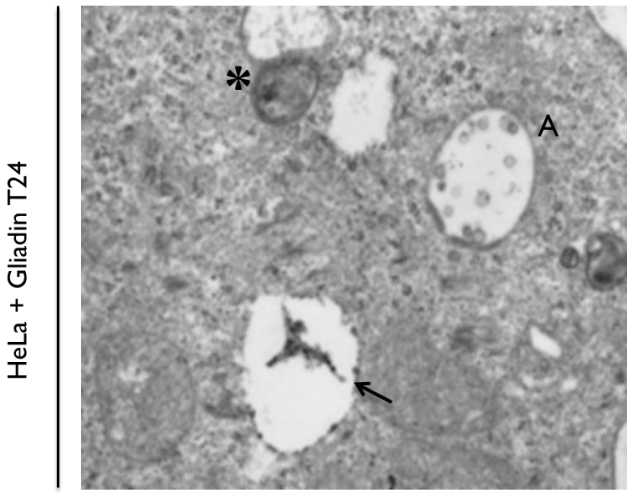

Figure 23: TEM observation at 2000X magnification. PT-gliadin (200 µg/ml) was administered to HeLa cells in suspension at 37ºC for 30 min before plating. Cells were fixated 24 hours after and visualized. The black arrow and the asterisk indicate, respectively, an autophagosome with a gliadin-like aggregate and the fusion with a lysosome. The letter A indicates an autophagosome with digested materials.

To monitor the kinetic of gliadin cellular uptake, immunofluorescence experiments were performed on fixed Caco-2 and HeLa using anti-gliadin and secondary conjugated Alexa-488 antibodies. After 30 minutes of gliadin administration, fluorescent signals were localized in correspondence of plasma membranes, while after 4 hours p.t. intracellular signals were detected (**Figure 24**, Panel A). The possible involvement of the vesicles containing PT-gliadin in a degradative pathway was subsequently investigated. The recruitment of lysosomes was studied through the use of a primary antibody against Limp2, a lysosomal integral membrane protein. As shown in **Figure 24**, panel B, anti-Limp2 signal roughly co-localized with the anti-gliadin ones, showing also a relatively high accumulation of

lysosomes in correspondence to the internalized PT-gliadin content.

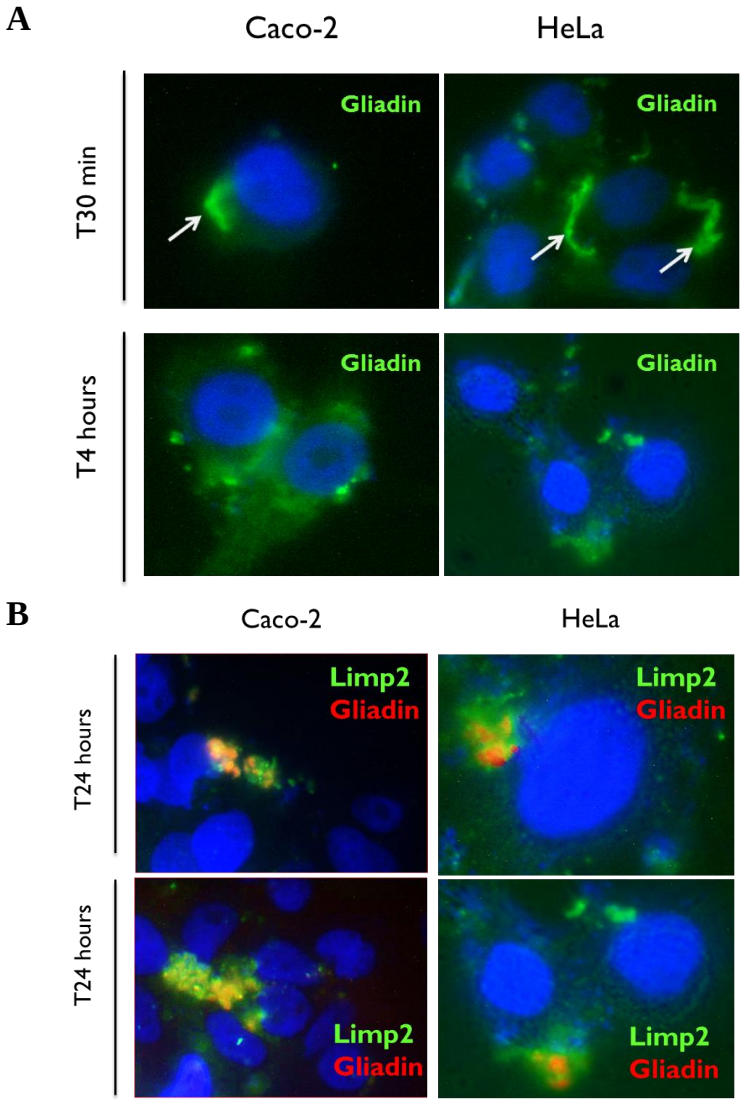

Figure 24: Caco-2 and HeLa cells were grown on sterilized glasses in 3 ml plates and treated with gliadin (500 µg/ml). Fixation was performed at 30 min, 4 and 24 hours p.t. Observations were done using inverted microscope Eclipse Nikon TS100, 100X oil immersion objective. PT-gliadin was revealed by 488-Alexa-Fluor488 (A), or Alexa-Fluor633 (B) and nuclei by DAPI.

The vesicles containing PT-gliadin are addressed to a degradative pathway involving autophagy

As reported, autophagy converges with endocytosis since autophagosomes may fuse with vesicles involved in the endocytic pathway (Gordon *et al*. 1992; Liou *et al.* 1997). Considering the internalization of PT-gliadin through the endocytic pathway and the increase in the number of lysosomes and their substantial recruitment in the same cytoplasmatic area, acridine orange (AO) fluorescent dye was used to detect autophagosomes, that can be distinguished from lysosomes according to their shape and size. Specifically, cells were incubated with PT-gliadin (0.5 mg/ml) and, at the end of the scheduled time interval, stained with AO (1 µg/ml) and compared with untreated ones at different times. As shown in **Figure 25 A** and **B**, Caco-2 treated with PT-gliadin, similarly with HeLa, showed an increase in the number of red spots already at 4 hours p.t. in the initial phases of cells attachment, suggesting a fast uptake of the peptides from the medium. Following the investigated time intervals, Caco-2 cells markedly showed an increase in acidic red/yellow-spectrum emitting large vesicles: as widely documented (Klionsky *et al*. 2016), the shape and the red-yellow appearance, due to intra-vesicular pH acidic variation, were indicative of autophagosomes. These vesicles were also surrounded by smaller red vesicles, likely lysosomes, suggesting an activation of a degradative autophagic process.

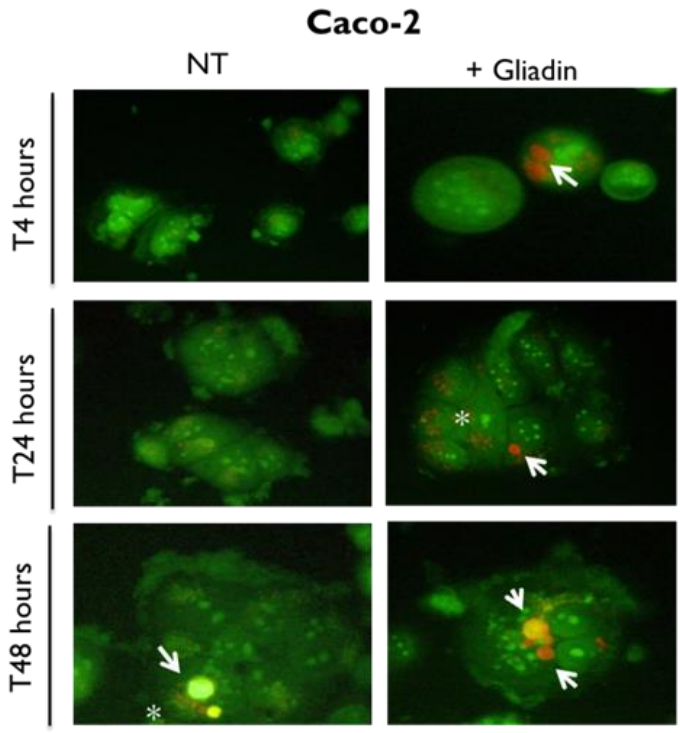

Figure 25 A: Caco-2 cells were treated with gliadin (500 µg/ml) or without (NT). Before visualization (15 minutes), acridine orange (1 µg/ml) were added in each condition. Observations were done using inverted microscope Eclipse Nikon TS100, 40X magnification. White arrows pointed large acidic vesicles that, according to their shape and emission spectra, were likely autophagosomes. Asterisks indicated recruitment of lysosomes.

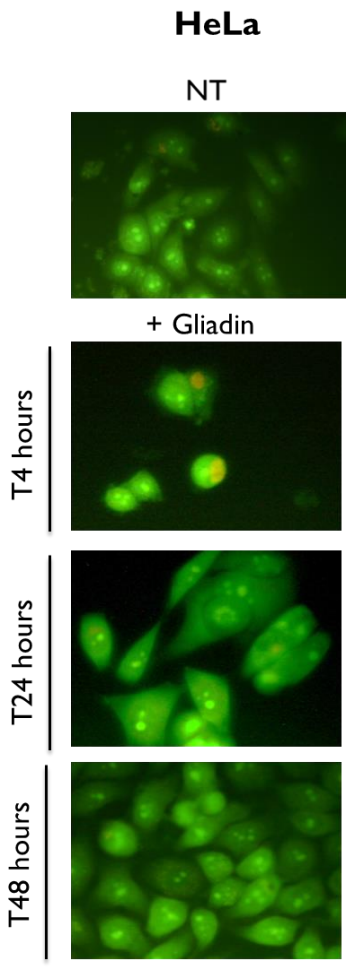

Figure 25 B: HeLa cells were treated with gliadin (500 µg/ml) or without (NT). Before visualization (15 minutes), acridine orange (1 µg/ml) were added in each condition. Observations were done using inverted microscope Eclipse Nikon TS100, 40X magnification. White arrows pointed large acidic vesicles that, according to their shape and emission spectra, were likely autophagosomes. Asterisks indicated recruitment of lysosomes.

Alltogether, a significant lysosomes recruitment and an increase in size and number of autophagosome-like vesicles, mostly in Caco-2 cells, suggested the activation of the autophagy process by PT-gliadin administration. Therefore, an immunoblotting analysis of the expression of key autophagy proteins (i.e. LC3, ATG7, Beclin1 and ATG3) was performed (**Figure 26**). As quantified by BACT normalized densitometric analysis (**Figure 27**), Caco-2 and HeLa cells displayed a different ATGs expression profile following PT-gliadin administration: notably, in Caco-2, a general increase of LC3-II, Beclin1, ATG7 and ATG3 expression was reported, compared to untreated cells. Differently, HeLa exhibited a marked downregulation of ATG proteins.

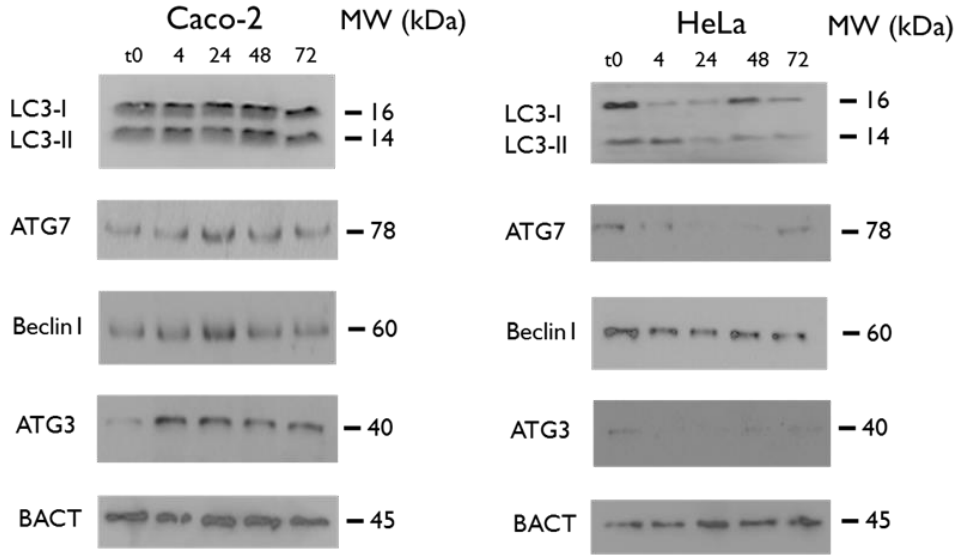

Figure 26: ATGs immunoblotting analysis in Caco-2 and HeLa cells after PT-gliadin administration. Molecular weights (MW) expressed in kDa are reported.

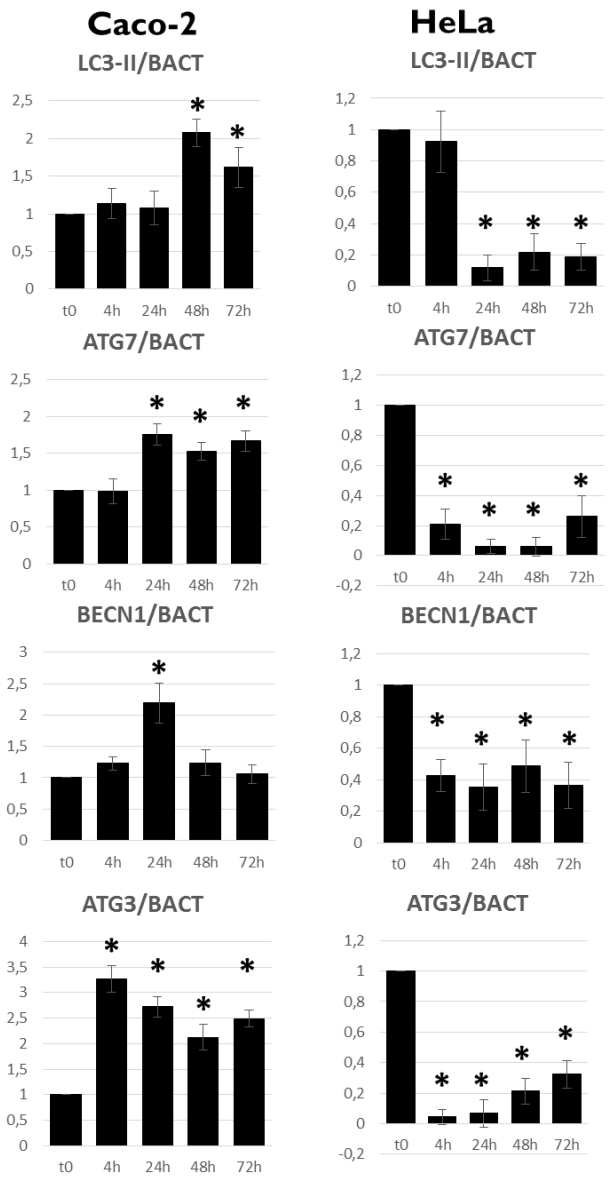

Figure 27: Densitometric analysis of ATGs expression in Caco-2 and HeLa cells after PT-gliadin administration. Experiments were performed in triplicates and normalized using BACT and finally referred to untreated (t0) cells. Bars indicate SD. Asterisks indicate statistical significant differences (ANOVA, One-way, $p<0,0001$).

To verify the specificity of PT-gliadin in activation of the autophagy process, cells were assayed with equal amount of a different exogenous protein like egg-ovalbumin (OVA). Primarily, PT-gliadin and OVA proteins were covalently labelled with the green-fluorescent dye Alexa Fluor 488 (thus producing GLIA-488 and OVA-488), in order to better monitor their internalization in Caco-2 and HeLa living cells. Purified unlabelled or labelled proteins were then visualized after electrophoresis (**Figure 28**, left and central panels). GLIA-488 exhibited a heterodispersed pattern ranging from 20-40 kDa, similar to the unlabelled PT-gliadin, while OVA-488 had the expected 40 kDa molecular weight. Noticeably, only GLIA-488 was visible when administered in growing cells, due to its tendency to form large aggregates (**Figure 28**, right panel)

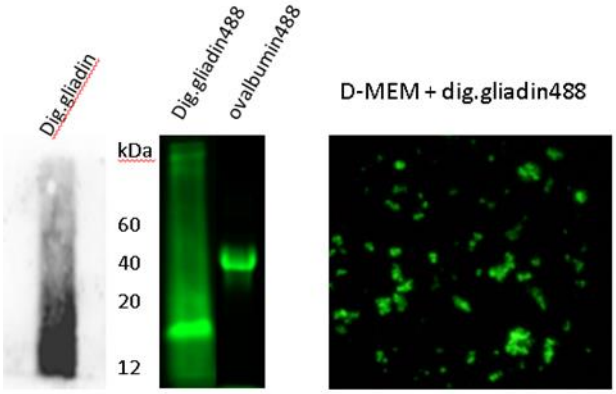

Figure 28: On the left, immunoblotting assay showing PT-gliadin fragments after peptic-tryptic digestion. In the middle, SDS-PAGE showing labelled GLIA-488 and OVA-488. On the right, GLIA-488 aggregates in DMEM growing conditions.

Then, GLIA-488 was administered (10 µg/ml) to growing cells to directly estimate internalization and intracellular degradation processes (**Figure 29**). Immediately before the end of the scheduled at 24 hours p.t., cells were washed twice with PBS and the medium (containing extracellular GLIA-488) was replaced with a fresh one. Following next fluorescent microscope visualization, cells exhibited a similar degree of internalization of GLIA-488 aggregates in correspondence of large vesicles. In the next time intervals, Caco-2 released fluorescent protein aggregates in the medium, while HeLa stored longer the fluorescence proteins within long-term

vesicles, over 72 hours p.t. Importantly, according to microscope evaluations, the release of GLIA-488 into the medium was not due to whole cellular degradation processes produced by membrane rupture events, rather by exocytic pathways.

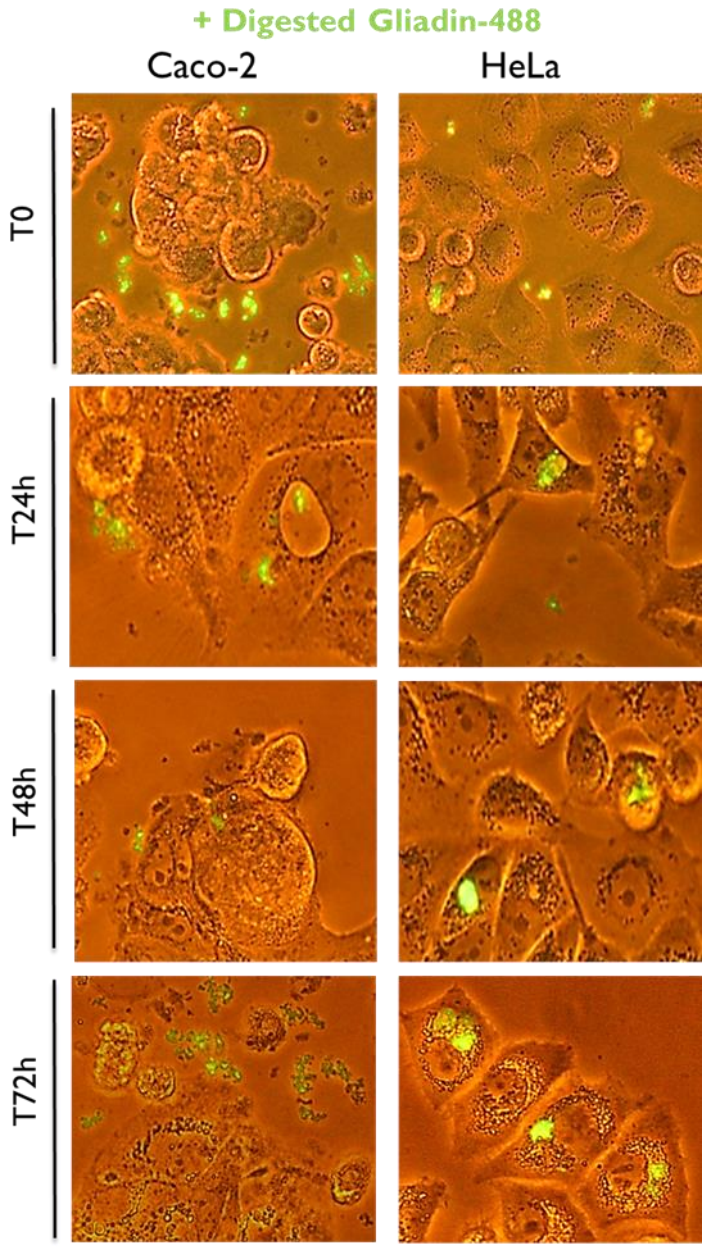

Figure 29: Caco-2 and HeLa cells incubated with GLIA-488. Observations were done at different times using inverted microscope Eclipse Nikon TS100, 40X magnification.

Differently, OVA-488 at the same concentration (10 µg/ml) was not detectable by inverted fluorescent microscope. Similarly to the previous experiments, this labelled protein did not alter cellular morphology and viability (data not shown).

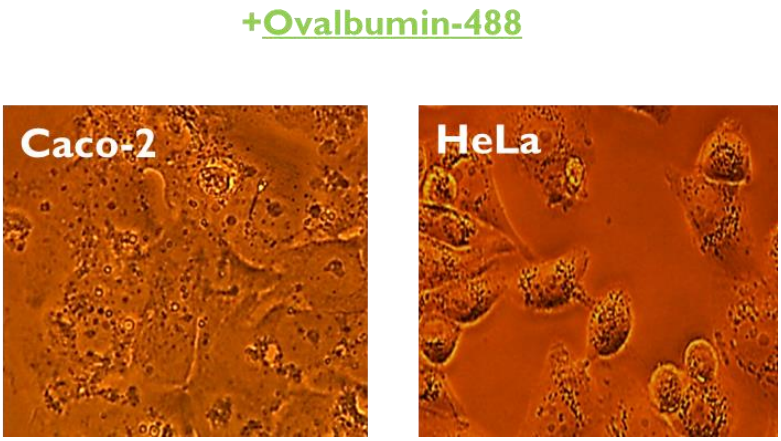

Figure 30: Caco-2 and HeLa incubated with OVA-488 and observed with the fluorescent inverted microscope Eclipse Nikon TS100, 40X magnification.

Autophagy activation was then investigated in cells treated with OVA evaluating LC3-II/BACT ratio at different time intervals (**Figure 31**). Of note, differently from PT-gliadin administration, cells showed a nearly constitutive expression of LC3-II (**Figure 32**).

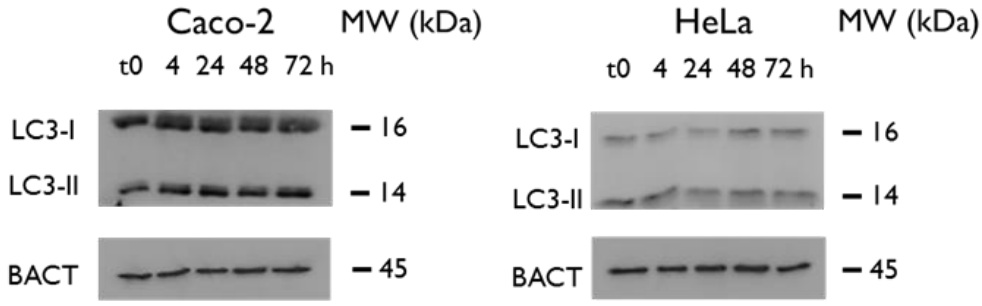

Figure 31: Immunoblotting assays on Caco-2 and HeLa cells treated with OVA-488 of LC3-II; β-actin (BACT) was used as housekeeping protein. Molecular weights (MW) in kDa are reported.

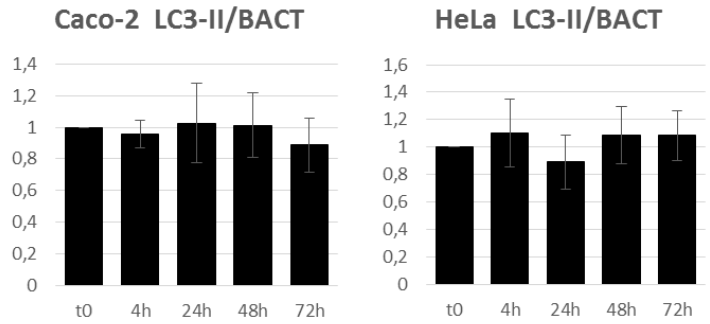

Figure 32: LC3-II densitometric analysis, normalized to BACT are referred to untreated (t0) cells. Experiments were performed in triplicates. Bars indicate SD.

Serum deprivation induces autophagy activation increasing PT-gliadin degradation

According to the above reported results, cells gave rise to different response to PT-gliadin administration; Caco-2 increased acidic vesicles synthesis, reasonably autophagosomes, along with a significant lysosomes recruitment and polarization within the cell. However, after the longest incubation interval assayed, i.e. 72 hours p.t., PT-gliadin was partly released in the medium, forming aggregates, thus suggesting an incomplete degradative autophagic process. Differently, HeLa cells internalized gliadin into large vesicles, without an apparent activation of the catabolic process. It was reported that serum starvation can activate autophagy in cultured mammalian cells (Mizushima and Komatsu, 2011). To evaluate if serum starvation activated autophagy, autophagosomes induction was monitored in living cells by transduction with a baculovirus expressing LC3B-GFP, known to be localized in correspondence of nascent membranes of the autophagosomes. As reported in **Figure 33**, serum deprivation produced, 24 hours post transduction, large intracellular vesicles, whose membrane layers were fluorescent to GFP; also, thick and rought particles were visible within the lumen, strongly suggesting these vesicles as active autophagosomes. Noticeably, Caco-2 cells seemed to well tolerate even for longer periods (i.e. 24-48 hours) the absence of serum as compared with other human cancer cell lines, more sensitive to FBS (Comincini, personal

communication).

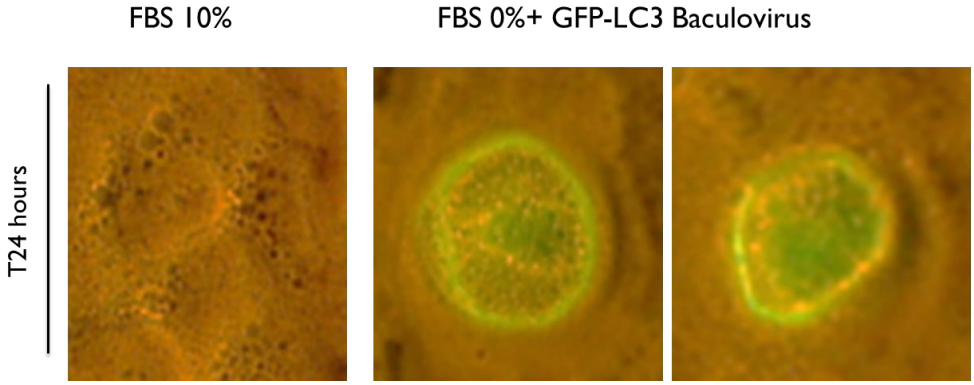

Figure 33: Visualization of autophagosomes in Caco-2 cells treated with PT-gliadin and transfected with baculovirus 24 hours p.t. The optical microscope observation were performed using Eclipse Nikon TS100.

To further confirm the autophagy activation through the serum deprivation protocol, Caco-2 cells, challenged with or without FBS, were incubated with AO dye. Again, AO fluorescence properties were adopted to visualize acidic vesicles in the cytoplasm. As exemplified in **Figure 34**, according to microscope evaluations, the absence of FBS from the medium for 48 hours did not alter significantly the morphology of the cells that maintained their attachment to the growing support (lower panels). Particularly, lower fluorescent microscopic panels highlighted a clear increase in number and shape of red acidic vesicles within FBS 0% cells, surrounded by lysosomes. Intravesicular acidic pH differences (color shift from red to yellow) was scored.

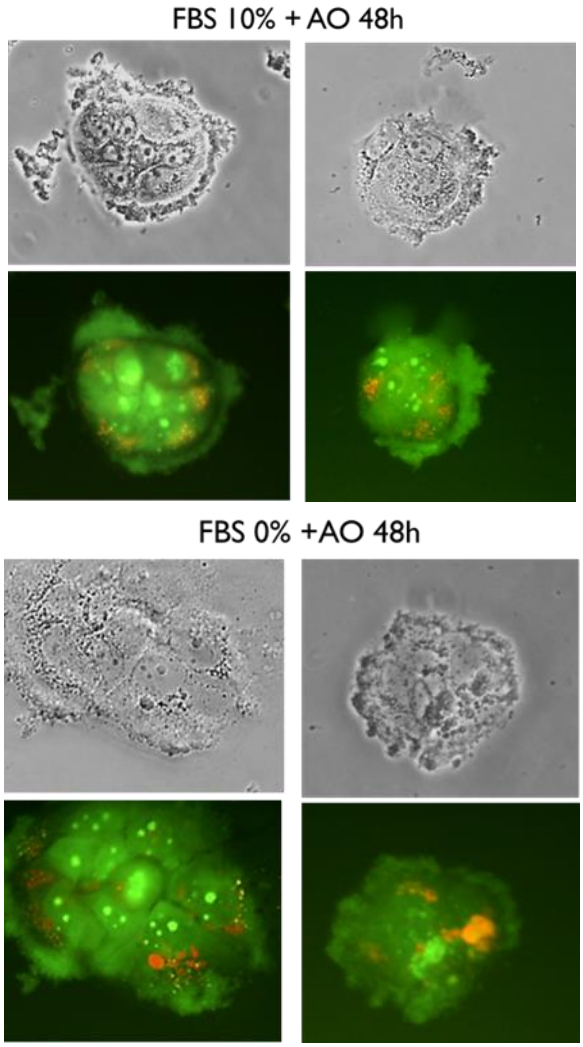

Figure 34: Visualization through acridine orange (AO) staining of acidic vesicles in Caco-2 cells treated with PT-gliadin (500 µg/ml) in DMEM with or without 10% FBS. AO (1 µg/ml) was added after 48 hours p.t. immediately before the microscope visualization (Eclipse Nikon TS100).

An immunoblotting analysis was then used to further confirm the above mentioned data and to directly assay autophagy activation after PT-gliadin administration along with serum deprivation. In particular, autophagy activation was again measured through the BACT normalized levels of LC3-II whereas lysosomes amount indirectly through the expression of Lamp-1 (Lysosomial-associated membrane protein-1). As illustrated in **Figures 35** and **36**, serum deprivation resulted in a direct increase in the amount of LC3-II and Lamp1 proteins, compared to untreated cells. Specifically, LC3-II expression levels increased with a peak at 24 hours post starvation treatment whereas the Lamp-1 showed its highest expression at 48 hours p.t. Furthermore, LC3-II and Lamp-1 levels exhibited a decrease after the peak reached at their respective times, but the proteins expression remained higher compared with non-starved cells at t0.

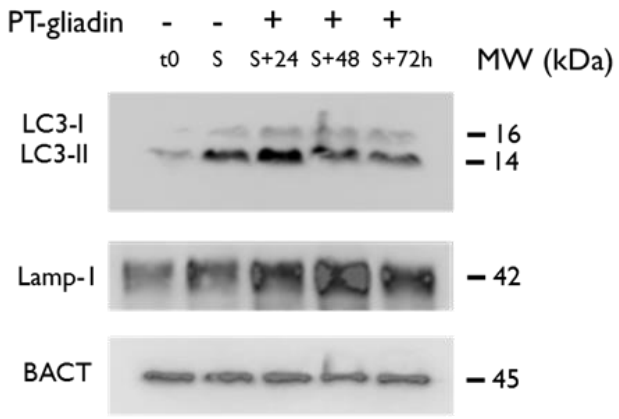

Figure 35: LC3 and Lamp-1 immunoblotting analysis of Caco-2 cells treated with PT-gliadin (500 μg/ml) and following different time intervals of serum deprivation starvation. Molecular weights (MW) of the proteins are reported in kDa.

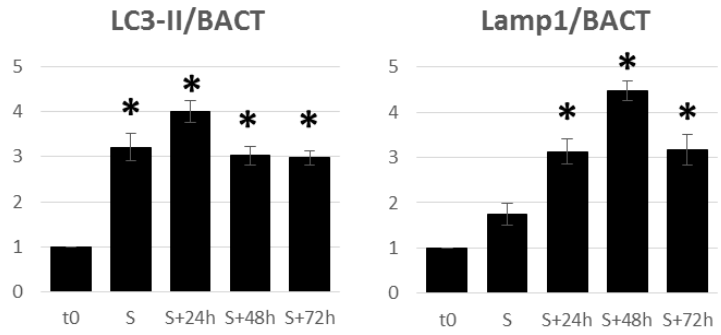

Figure 36: Densitometric analysis of LC3-II and Lamp-1 normalized expression in Caco-2 cells under serum deprivation in presence of PT-gliadin. Experiments were performed in triplicates. Bars indicate SD. Asterisks indicate statistical significant differences (ANOVA, One-way, P<0,0001).

Serum deprivation decreases PT-gliadin secretion and conferes a proliferative advantage

To deeply investigate the cellular response to PT-gliadin in serum deprivation conditions, Caco-2 cells were treated with GLIA-488 in normal medium (NT) and in a starved one (0% FBS) and then monitored for 48 hours. Internalization and secretion of GLIA-488 was studied through fluorimetric analyses of the respective media at 48 hours and 72 p.t. As shown in **Figure 37**, cells internalized GLIA-488. Differently, at 48 hours p.t. medium from cells with FBS 10% showed higher amount of fluorescent aggregates. Media from cells cultivated with or without FBS were then collected and fluorescence amount was assayed by fluorimetric analysis, as described in the Methods. As reported in right panel of **Figure 37**, serum deprivation resulted in a significant decrease (p<0,001, ANOVA One-Way) of extracellular release of GLIA-488. Finally, in both cultures the medium was replaced with a normal one to study the viability recovery of the cells. Observations were performed 24 hours later (72 hours post starvation treatment) at optical microscope. Starved cells exhibited the typical Caco-2 morphology and were able to form the colonies, whereas non-starved cells showed severe and irreversible morphological alteration and cellular debris due to the toxic effect exerted by PT-gliadin (**Figure 38)**.

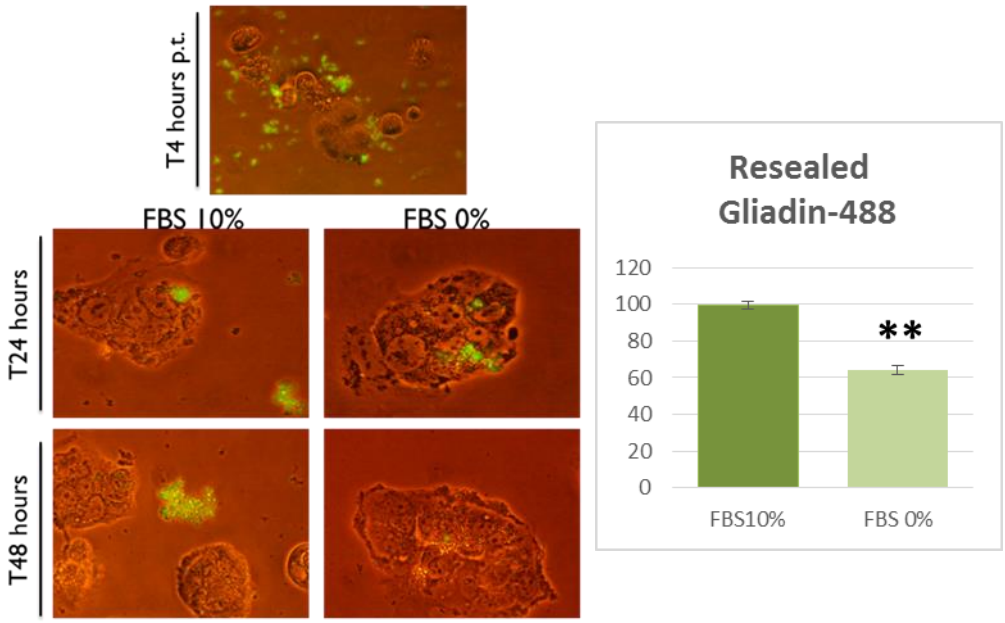

Figure 37: PT-gliadin (GLIA-488) secretion analyses. On the left, microscope (Eclipse Nikon TS100) observation at 40X of Caco-2 cells treated with GLIA-488 (10 µg/ml) in DMEM with or without 10% FBS. On the right, results of the fluorimetric analysis on the collected medium at 48 hours p.t. The measurements (triplicates) were performed using QubitTM Fluorometer. Fluorescence, in arbitrary units, is reported in the ordinate. SD and Anova-one way significance (P<0,001) are reported.

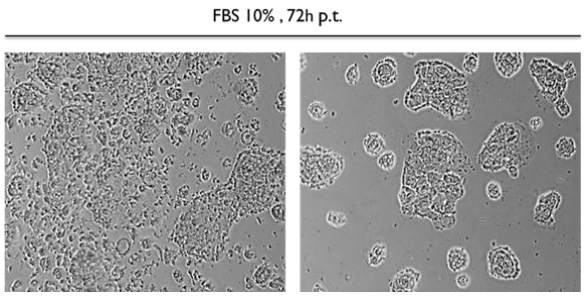

Figure 38: Proliferative monitoring (10X magnification) of Caco-2 cells 72 hours after starvation treatment and 24 hours after medium refreshment. On the left, Caco-2 previously grown in normal DMEM whereas Caco-2 treated with serum starvation deprivation are reported on the right.

Serum deprivation increases PT-gliadin degradation decreasing its extracellular secretion

To directly demonstrate that the scored decrease in PT-gliadin secretion was due to an increased intracellular degradation process, Caco-2 cells were incubated as before with GLIA-488 and grown in normal medium (NT, FBS 10%) or in a 0% FBS medium. As before, media after 24 and 48 hours p.t. were subjected to fluorimetric analysis (**Figure 39**, left panel): as a result, a significant reduction of extracellular fluorescence was observed, mostly following a serum deprivation for 48 hours. Subsequently, cells were recovered and their total proteins were extracted, quantified and electrophoresed. As a result, the amount of GLIA-488 markedly decreased following the time of serum deprivation (**Figure 39**, right panel).

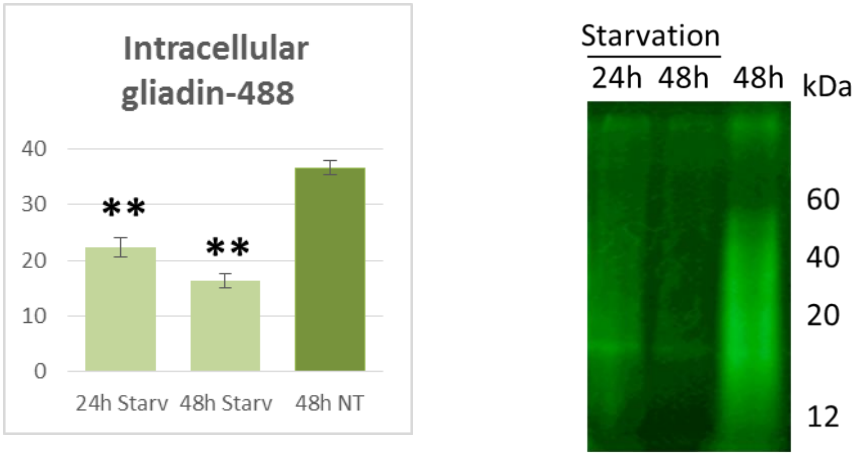

Figure 39: PT-gliadin (GLIA-488) degradation assay. On the left, fluorimetric analysis on the collected media at different times by QubitTM Fluorometer. On the right, SDS-PAGE of total isolated proteins showing GLIA-488 fluorescence. Molecular weights (kDa) are reported. Fluorescence, in arbitrary units, is reported in the ordinate.

Modulation of autophagy through rapamycin is not effective and leads to cellular toxicity

As widely reported, Caco-2 cells are a well characterized intestinal *in vitro* model used for permeability assays of drugs and chemical compounds (Hubatsch *et al.* 2007). Therefore, pharmacological modulation of autophagy was performed. Firstly, Caco-2 cells were assayed in inducing autophagosomes with different rapamycin concentrations (i.e 5, 10 and 20 µM), a well known mTOR inhibitor, capable of promoting autophagy (Noda and Ohsumi, 1998). After 24 hours p.t., acidic autophagosomes were scored similarly for the different concentrations employed, after AO incubation and fluorescent analysis as previously reported (**Figure 40**).

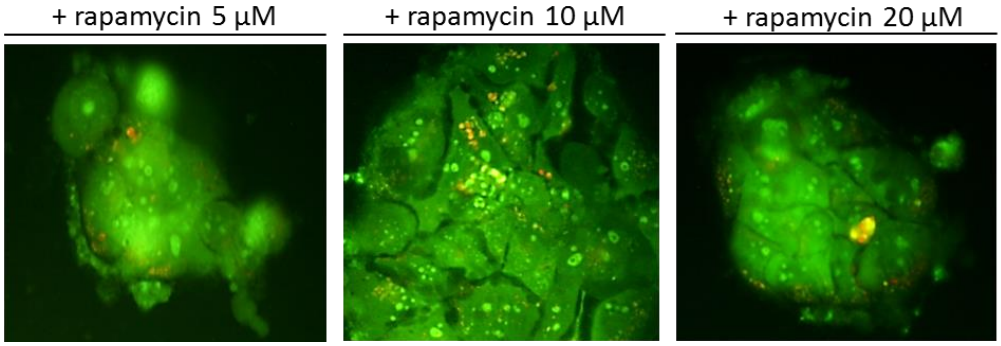

Figure 40: Induction of autophagy in Caco-2 cells using different concentration of rapamycin (5, 10 and 20 µM). Visualization was performed with acridine orange (1 µg/ml) and through microscope observations using inverted microscope Eclipse Nikon TS100, 40X magnification.

In parallel, Caco-2 cells were grown in normal medium in presence of GLIA-488 (10 µg/ml) with the same rapamycin concentrations and compared with cells treated with GLIA-488 but without rapamycin (NT). Cells were monitored through microscope observation at 24 hours and fluorimetric analyses were perfomed on the collected media. Caco-2 cells showed no toxicity when treated with rapamycin 5 µM and GLIA-488 was internalized as described in previous experiments, although extracellular aggregates were detected in the same amount of NT cells (**Figure 41**). Moreover, at higher doses of rapamycin, morphological alterations and

decrease in viability were observed in Caco-2 cells in a dose-dependent manner. Compared with the results obtained with the serum deprivation protocol, no significant decrease of PT-gliadin (GLIA-488) secretion was detected by fluorimetric analysis, as reported in **Figure 41**.

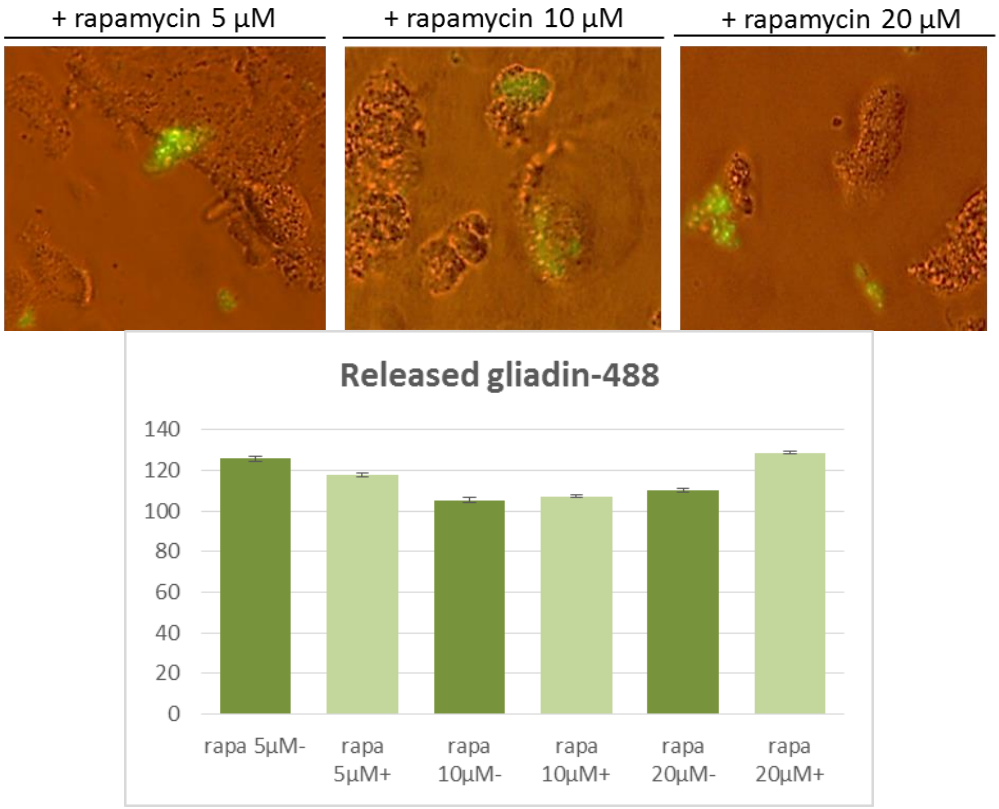

Figure 41: PT-gliadin (GLIA-488) secretion analyses after rapamycin treatment (24 hours). On the top, Caco-2 cells treated with GLIA-488 with rapamycin at different concentrations (5, 10 and 20 µM). Inverted microscope Eclipse Nikon TS100, 40X magnification was used for the visualization. Below, release of GLIA-488 measured through fluorimetric analyses (QubitTM Fluorometer). Fluorescence, in arbitrary units, is reported in the ordinate. SD, resulted from triplicate experiments, are indicated.

Then, immunoblotting was performed to deeply investigate autophagy activation after administration of rapamycin. Caco-2 cells were grown in

normal DMEM with GLIA-488 (10 µg/ml) and a single-dose administration of rapamycin (5 µM), that did not showed toxic effects in previous experiments. Expression levels of LC3-II were studied at different times (i.e. T24 and T48) as well as fluorimetric measurements were performed. As shown in **Figure 42** (panels A and B), LC3-II normalized levels slightly increased at 24 and more significantly at 48 hours p.t. compared with the untreated cells (NT) while no significative differences were detected between cells treated with PT-gliadin and with the combination of PT-gliadin and rapamycin. As reported by the histogram in **Figure 42** (panel C) no decrease of PT-gliadin secretion was detected by fluorimetric analysis at both investigated times, comparing untreated- with rapamycin-treated cells.

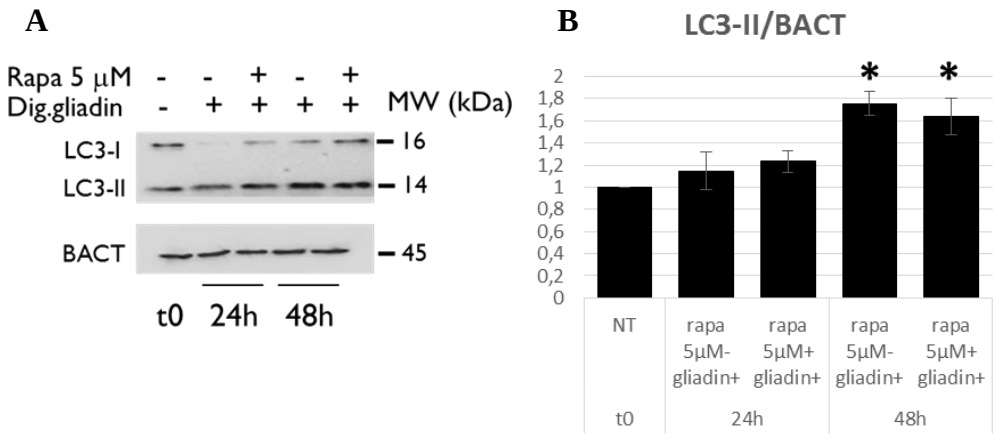

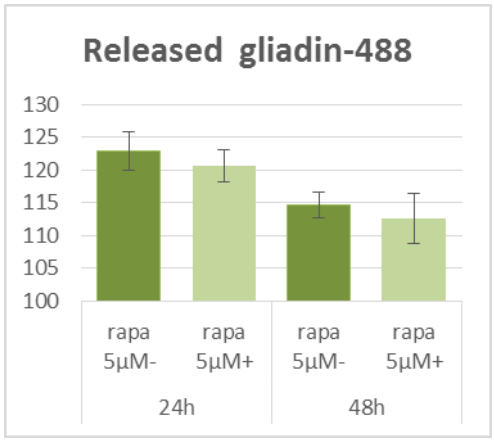

Figure 42: Modulation of autophagy with rapamycin in presence of PT-gliadin (GLIA-488) and secretion analysis. (A) immunoblotting assay for LC3-II expression and (B) relative densitometric analysis. LC3-II was normalized with BACT levels. (C) Fluorimetric analysis results of GLIA-488 extracellular release measured by QubitTM Fluorometer. SD (resulted from triplicate experiments) are indicated.

Down-regulation of autophagy through si*BECN1* do not affect PT-gliadin secretion

To study the effect of autophagy down-regulation in the cellular response to PT-gliadin internalization, silencing through siRNAs toward a key *ATG* was performed. Therefore, Caco-2 cells were initially transfected using a pool of validated siRNAs sequences against *BECN1*. Cellular toxicity was investigated through optical microscope observations at different times (T24, T48 and T72) and MTT assay (data not shown). An immunoblotting was performed to evaluate protein levels of BECN1 and LC3-II in order to confirm autophagy down-regulation. As shown in **Figure 43**, BECN1 levels decreased over time thus confirming silencing efficacy. Similarly, LC3-II levels decreased as a consequence of BECN1 silencing showing that autophagy was down-regulated as expected.

A

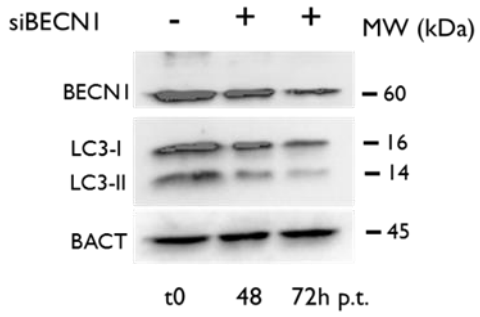

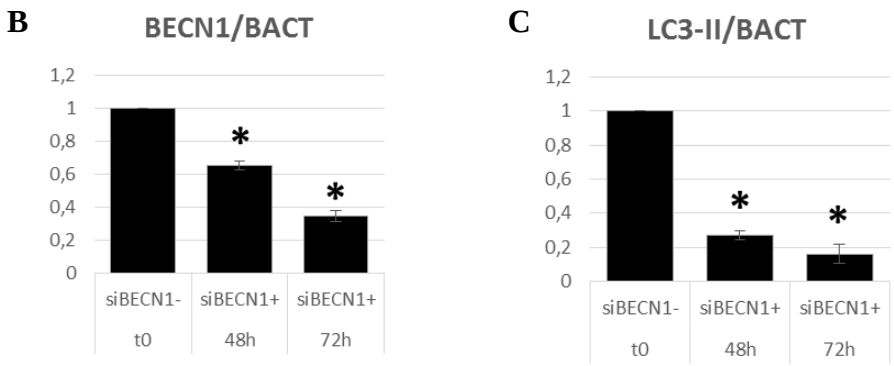

Figure 43: Effect of *BECN1* silencing in Caco-2 cells. (A) immunoblotting analysis for BECN1, LC3-II, BACT protein expression. Molecular weight (MW) are reported in kDa. (B, C) Relative densitometric analyses, SD (resulted from triplicate experiments) and significance (P < 0,001, Anova-one way) was reported.

Then, the same experiment was conducted in presence of GLIA-488 to study PT-gliadin degradation and secretion. Particularly, cells were trasfected with *siBECN1* and after 24 hours GLIA-488 (10 μg/ml) was added. Cells were observed at optical microscope at T48 and T72 and fluorimetric analysis was performed on the collected media. As shown in **Figure 44**, Caco-2 cells transfected with si*BECN1* showed morphological alterations and a general reduction of proliferation capability compared to control cells. Moreover, autophagy inhibition through si*BECN1* did not produce any significant differences in the amount of secreted GLIA-488.

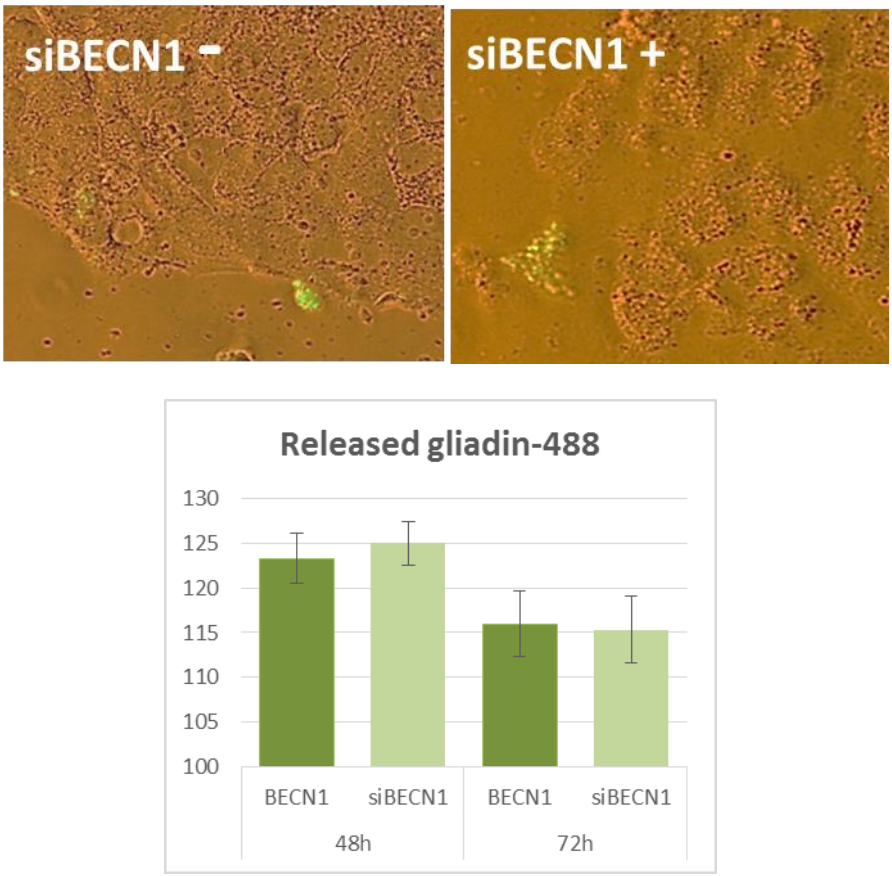

Figure 44: Effect of *BECN1* silencing in Caco-2 cells treated with PT-gliadin (GLIA-488). On the top, microscope observation of Caco-2 cells trasfected or not with si*BECN1* in presence of GLIA-488. Below, results of the secretion analysis obtained through fluorimetric analyses by QubitTM Fluorometer (SD, resulted from triplicate experiments are indicated).

5. Discussion

Celiac disease (CD) is an immune-mediated systemic disorder of the small intestine elicited by gluten and related prolamins in genetically susceptible individuals and characterized by the presence of different clinical manifestations (D'Amico *et al.* 2005; Green *et al.* 2005). Currently, there are two main issues about CD concerning diagnosis and treatment. According to ESPGHAN guidelines, auto-antibodies in serum represents a valuable tool for identifying new celiac patients presenting with only mild gastro-intestinal symptoms, non-specific general complaints or extra-intestinal manifestations, or for screening asymptomatic subjects (Giersiepen *et al.* 2012). Small intestinal biopsy histology has long been considered an essential step for CD diagnosis. Gastrointestinal endoscopy is invasive, costly and associated with risks for the patients. Researchers have therefore explored the possibility of CD diagnosis without endoscopy or biopsy analyses (Kelly *et al.* 2015). ESPGHAN guidelines proposed that in children and adolescents with signs or symptoms suggestive of CD and high anti-TG2 titers with levels ten times higher compared with normal ones, the probability of villous atrophy is high thus allowing CD diagnosis without biopsies. However, Schirru *et al.* (2014) described a two years old female affected by acute viral gastroenteritis with anti-TG2 levels of more than ten times the upper limit of normal, positivity for EMA, AGA-IgA, AGA-IgG and the at-risk HLA genotype. Hence, the identification of new molecular markers seems to be necessary to bypass this critical issue and to improve CD diagnostic algorithm in order to classify potential CD patients. From a diagnostic point of view, microRNAs (miRNAs) have also recently emerged as promising non-invasive biomarkers in several autoimmune disorders, also affecting the intestine. miRNAs are small non-coding RNA molecules that can modulate gene expression at the post-transcriptional level. miRNAs bind to complementary sequences of specific targets of messengers RNA, which can interfere with protein synthesis. As discuss in the Introduction, miRNAs have a number of intrinsic characteristics that make them attractive as biomarkers. The field of circulating miRNAs (cmiRNAs) has generated a great interest and has been growing at an exponential rate with more than 2000 publications now published on the subject. Biological fluids are rich in cmiRNAs that can act as surrogate

markers to biopsy-based sampling. Liquid biopsies based on circulating cell-free tumor DNA (ctDNA) or cmiRNAs hold great clinical promise in many field, such as cancer and autoimmune disorders (Larrea *et al.* 2016). cmiRNAs in the serum of Crohn disease patients were identified as novel biomarkers (Zahm *et al.* 2011). In this study was investigated a panel of 24 miRNAs, including four miRNAs previously described as associated with colonic and ileal Crohn disease (Wu *et al.* 2010). These examined serum miRNAs displayed encouraging diagnostic utility, showing high sensitivity and specificity. Recently, six serum miRNAs were identified in the serum of Crohn disease patients (active and inactive disease versus controls) and 25 miRNAs in the serum of ulcerative colitis (UC) patients. Particularly, miR-29a is over-expressed in the peripheral blood of UC patients and is also a strong potential novel non-invasive biomarker for colorectal cancer (Iborra *et al.* 2013). Benderska and colleagues (2015) demonstrated that miR-26b over-expression at the intestinal level could serve as a biomarker to distinguish between ulcerative colitis-associated carcinogenesis and sporadic cancer types, showing that miRNAs can be useful in patients' stratification. Similar approaches have been performed for CD providing encouraging results. Buoli Comani and colleagues (2015) demonstrated that miRNAs and their gene targets showed an altered expression in duodenal mucosa and plasma of CD pediatric patients, and these alterations could be different from adult ones. Some miRNAs can also distinguish different clinical CD phenotypes according to the level of deregulation (Vaira *et al.* 2014). Other works demonstrated the key role of miRNAs in the pathogenesis of CD (Capuano *et al.* 2011; Magni *et al.* 2014). In particular, Capuano and colleagues (2011) demonstrated that high levels of miR-449a targeted and reduced both NOTCH1 and KLF4 in the small intestine of CD patients, leading to an impaired differentiation and maturation of goblet cells. Despite the studies of miRNAs in CD are scarce compared with other pathologies, current evidence suggest that miRNAs deserve further studies because of their role as potential non-invasive biomarkers. Moreover, miRNAs could identify particular classes of patients, thus contributing to a custom clinial menagement (Bascuñán-Gamboa *et al.* 2014). In relation to therapeutic options, the main issues associated with CD treatment concerns costs, patients education, motivation and follow-up. The only effective therapy is a gluten free diet (GFD) that is a diet containing less than 20

p.p.m. of gluten. Patients affected by refractory celiac disease (RCD) are treated with GFD adjuvanted pharmachological therapy based on steroids or immunosuppressants, i.e. azathioprine. Burden of a GFD, i.e. the degree of difficulties to following the treatment, is higher than other common intestinal diseases (Leffler *et al.* 2016). A large proportion of patients report inadvertent or deliberate exposure to gluten and non-responsive celiac disease if frequent in CD patients diagnosed in adulthood (Hall *et al.* 2013; Hollon *et al.* 2013). Hence, novel alternative treatments or adjunctive therapies to GFD are strongly suggested. Currently, there are only two agents, ALV003 and Larazotide acetate, in late clinical trials as candidates of non-dietary treatments for celiac therapy. ALV003 is composed by two recombinant, orally administered, gluten specific proteases that are able to reduce the small intestinal mucosal injury caused by the administration of gluten, while Larazoide acetate is an oral peptide that modulates intestinal tight junctions reducing symptoms in patients in response to gluten (Gottlieb *et al.* 2015).

In this PhD thesis, novel biomarkers, related to the autophagy process, were investigated in peripheral blood and intestinal biopsies of patients with active CD compared with non-CD subjects matched for age and sex. As already introduced, autophagy process is important in host defence against intracellular and extracellular pathogens, metabolic syndromes, immune cell homeostasis, antigen processing and presentation, and maintenance of tolerance (reviewed in Levine et al. 2011; Deretic et al. 2013). Furthermore, autophagy is involved in other pathological conditions, such as IBDs (Lapaquette *et al*. 2010). In particular, Lu *et al.* (2014) demonstrated that miR-106b and miR-93 can modulate ATG16L1 expression. Reduction in autophagy process leads to a defective autophagy-dependent eradication of intracellular bacteria, thus contributing to Crohn disease pathogenesis. Some evidence suggested that tissue transglutaminase (TG2), whose activity is implicated in CD, is a key regulator of cross-talk between autophagy and apoptosis. Specifically, knock-out of the endogenous *TG2* gene in MEF cells resulted in a significant exacerbation of caspase 3 activity and PARP cleavage in response to apoptotic stimuli. The same cells showed the accumulation of LC3-II isoform following autophagy induction. Therefore, TG2 transamidating activity plays a protective role against death stimuli leading to caspase 3 suppression as well as PARP cleavage upon apoptosis

induction. Furthermore, MEF mutants were unable to catalyze the final steps in autophagosome formation during autophagy (Rossin *et al.* 2012). Moreover, *Tg2* knock-out mice displayed impaired autophagy and accumulated ubiquitinated protein aggregates upon starvation. TG2 physically interacts with p62 targeting cytosolic abnormal polypeptides that escape proteasome-dependent degradation to inclusion in bodies called 'aggresomes', subsequently degraded by autophagy (D'Eletto *et al.* 2012). Rajaguru and collaborators (2013) reported an increase in the expression of LC3-II in dendritic cells, which plays an important role presenting the gliadin-antigen to $CD4^+$-naïve T-cells. In line with these recent contributions, this PhD thesis is oriented to decipher if key autophagy executory genes and their miRNAs regulators showed variations associated with CD status. Lastly, in the second part of the Thesis, *in vitro* studies aimed to modulate the autophagy process were assayed to specifically counteract gliadin toxicity.

In the first part of the work, specimens were collected from 25 CD patients and 33 control subjects, subdivided as described in Material and Methods. All the samples were analyzed through Real-Time PCR for two essential autophagic genes (*ATG7* and *BECN1*) and two miRNAs (miR-17, miR-30a). As introduced before, BECN1 and ATG7 are key proteins implicated in autophagy, respectively in the nucleation phase and in autophagosome elongation. Among all the miRNAs that play a role in autophagy regulation, miR-30a and miR-17 were investigated because of their experimental validation as negative regulators of the autophagic process. Particularly, miR-30a is able to negatively regulate BECN1 expression resulting in decrease autophagic activity. Moreover, it was demonstrated that treatment of different cancer cell lines with miR-30a mimic and antagomir could respectively decrease and increase BECN1 expression (Zhu *et al.* 2009). A similar approach was used on T98G glioblastoma cells to demonstrate that miR-17 negatively regulates ATG7 (Comincini *et al.* 2013). For all these reasons, this work investigated these two validated miRNAs and their target genes. Relatively quantitative Real-Time-PCR was performed on blood and intestinal biopsies derived from these exploratory cohorts of pediatric CD patients and controls and the relative expression genes/miRNAs values were statistically analyzed. The non-parametric Mann-Whitney U test and the ROC curves analyses were performed (Motawi *et al.* 2015; Wang *et al.*

2015; Regazzo *et al.* 2016). In the peripheral blood, the expression levels of *BECN1* differed significanlty between patients and controls. The area under the ROC curve confimed the levels of expression of *BECN1* as a parameter that can fairly distinguish between the two diagnostic groups (diseased/normal), with a specificity of 74.29 and a sensitivity of 65.22. The differences in the levels of expression were confirmed by the ROC analyses and the area under the ROC curve highlighted the property to distinguish between patients and controls. In this case, *ATG7* and *BECN1* presented the highest significance level P, respectively 0.007 and 0.0068, compared with those obtained for miRNAs. Particularly, the expression of miR-30a at bioptic level might give the best performance in distinguishing between patients affected by CD and other conditions because of its sensitivity and specificity values. To determine whether the investigated genes/miRNAs were able to effectively distinguish and stratify the patients in the two cohorts, a supervised multivariate analysis was conducted. Classification trees were used based on decision tree learning model. This is a method commonly used in data mining with the goal of generalizing known structure to apply to new sets of data (Rokach and Maimon, 2014). In blood, miR-17 constituted the first node of the tree, determining together with *BECN1* levels a first class (M) of CD patients. The other classes are determined by the algorithm taking into account all the candidate targets excluded miR-30a. The CD patients homogeneously classified were 16/23 (69.56%) suggesting that peripheral blood guaranteed a discreet performance in patients' stratification. Classification tree obtained for biopsies homogeneously classified 22/25 CD patients (88%) in five groups (B, E, G, H and L) using the relative expression values of *ATG7*, *BECN1* and their negative regulators, miR-17 and miR-30a. Analysis of intestinal biopsies seemed to be a more promising approach compared with blood analysis for CD patients' stratification. In intestinal biopsies, the decision tree learning model used all the genes/miRNAs previously identified by Mann-Whitney U test and ROC analyses to create these CD classes, strengthening the idea that all these candidate targets might have good performances in CD patients' identification and stratification. Subsequently, it was evaluated the ability of the algorithm to correctly classify all the subjects according to the initial diagnosis. The number of subjects correctly classified were 52/56 in the case of blood and 46/49 in the case of intestinal

biopsies. The number of subjects misclassified by the classification tree in the blood and biopsies was, respectively, four and three. Particularly, one false negative and three false positive were obtained in the blood, whereas two false negative and one false positive were obtainted in intestinal biopsies. These results highlighted the capability of these genes/miRNAs to correctly identify and classify CD patients and controls. Then, a nomogram was created for both tissues using the Orange software to evaluate the relative contribution of each genes/miRNAs in determining an increase in the celiac CD diagnostic probability performance. A Naive Bayesian nomogram analysis uses a Naive Bayes classifier (NBC). This tool is a method to visualize a NBC that clearly exposes the quantitative information on the effect of attribute values to class probabilities and uses simple graphical objects (points, rulers and lines) that are easier to visualize and comprehend (Mozina *et al.* 2004). A nomogram is a dynamic supervised statistic tool used to analyze continuous and categorical variables together. The algorithm associates to each continuous variable a score and a probability to the disease/ physiological state. This tool was used also in other pathological contests, i.e. glioblastoma subtyping (Comincini et al. 2007 and 2009). This prediction tool is used in clinical practice to assess the risk for a particular pathology taking into account specific characteristic of the patient. Currently, the Memorial Sloan Kettering Cancer Center of New York uses this intrument for different kind of cancers, i.e. prostate, breast, ovarian and melanoma (https://www.mskcc.org/nomograms). In peripheral blood, high rate of CD patients' identification was determined by the increase of *ATG7* and *BECN1* levels as well as by an increase in miR-17 and miR-30a expression. Although Mann-Whitney U test and ROC analyses did not identify any miRNAs as able to distinguish between CD patients and controls, miR-17 played an important role in increasing CD likelihood compared with *BECN1*. In biopsies, the nomograms did not detect any gene or miRNA capable to determine a significant increase in CD probability. Finally, heatmaps were created in order to find particular expression signatures in CD patients. *BECN1* resulted to be over-expressed in the blood of CD patients whereas it was down-regulated in the biopsies of the same subjects. Over-expression of *BECN1* might be linked to the role of autophagy in immunity. This cellular process regulates the secretion of immune mediators, such as IL-1β, IL-6, IL-8 and IL-18. Autophagy up-

regulation during the immune response leads to the high secretion of these pro-inflammatory cytokines. Moreover, a feedback loop increases autophagy up-regulation through the action of different mediators: for example, IFN-γ promotes the action of DAPk1 leading to BECN1 activation and IL-1β activates TRAF6, a member of the complex TRAF6-BECN1-Ambra1 to limit inflammosome activity (Zalkvar *et al.* 2009; Shi *et al.* 2012). On the other side, gliadin toxicity on intestinal epithelial cells could be due by autophagy impairment as suggested by *BECN1* down-regulation detected in biopsies. As described in the Introduction, this process is implicated in the clearance of exogenous proteins and misfolded protein aggregates, both in physiological and pathological conditions. Basing on the described evidence, a parsimonious interpretation model of the expression results was proposed:

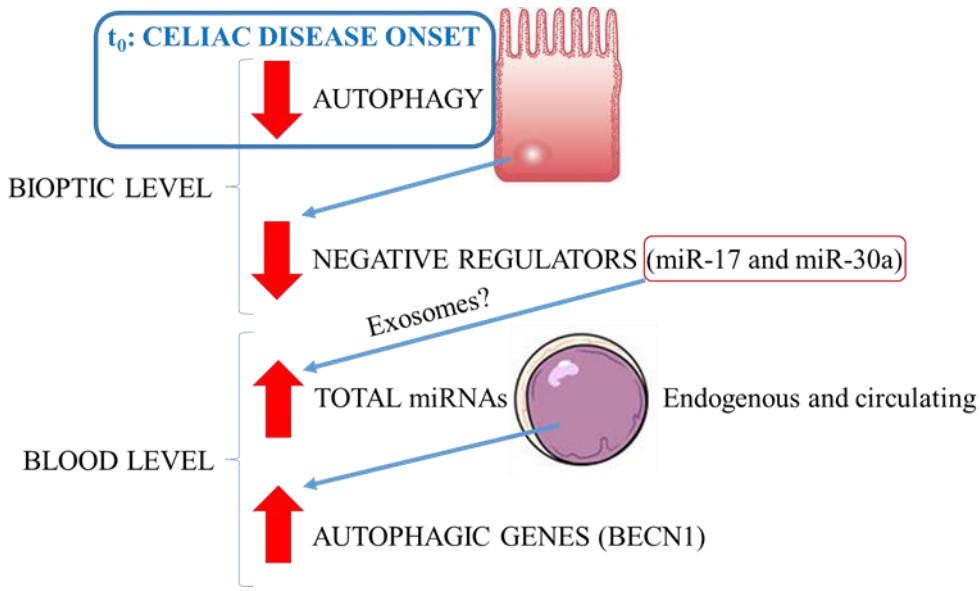

Figure 45: Interpretative model of autophagy status as inferred by ATGs and miRNAs investigated expression profiles in the intestine and in peripheral blood of CD patients.

As shown in **Figure 45**, celiac disease onset would correspond with an autophagy impairment in epithelial cells of the intestine, mainly caused by *BECN1* down-regulation as evidenced by heatmaps analyses. The decrease in the expression of miR-17 and miR-30a could be explained as the result of

a compensatory mechanism triggered by this pathological loss of homeostasis in the autophagic process, in order to counteract autophagy down-regulation. miR-30a and miR-17 decreasing could be also mediated by the release of these miRNAs in the extracellular space through exosomes (Zhang *et al.* 2015), thus in part explaining the high levels detected in the blood. According to the heatmap analyses, *BECN1* was over-expressed in the blood of CD patients, leading to autophagy up-regulation. These evidence are consistent with the involvement of autophagy in the inflammatory responses, as described before. Furthermore, *BECN1* over-expression could be also due to a cellular compensation to maintain autophagy homeostasis after the possible exosome-mediated release of miR-17 and miR-30a from the epithelial cells. Certainly, these preliminary results merit further investigations to confirm the diagnostic power of these autophagic genes/miRNAs and this preliminary interpretative model. The analyzed genes/miRNAs should be investigated in a larger cohort to strengthen the results obtained in this study. Particularly, the statistical resolution of data mining and machine learning analyses, i.e. classification trees and nomograms, depends on the size of the analyzed cohort. Moreover, an immunoblotting analysis should be performed to study BECN1 protein levels to confirm autophagy down-regulation in the intestine of CD patients, thus validating the interpretative model proposed before.

In the second part of the Thesis, *in vitro* experiments were conducted to elucidate autophagy involvement in the cellular response to PT-gliadin administration. To this purpose Caco-2 cells were employed: these cells represent not only a well established model for polarised epithelial transport but also they show physiological similarities with small bowel enterocytes (Hidalgo *et al.* 1989; Sambuy *et al.* 2005). For all these reasons, Caco-2 cells constitute a well-known and characterized CD *in vitro* model (Stoven *et al.* 2013). On the contrary, HeLa cervical cancer cells were adopted as an experimental outgroup. As a first approach, both cell lines were treated with PT-gliadin at different concentration and monitored dayly through optical microscope observations. A marked, concentration-dependent, toxicity was observed and the reduction of cell viability was confirmed with trypan blue exclusion test. These results were useful to determine the PT-gliadin concentration for subsequent experiments. Furthermore, microscope

observations showed that PT-gliadin can form sticky and large extracellular aggregates as already reported. This biochemical property can be explained by the presence of glutamine and proline-rich repetitive regions in the N-terminal of gliadin proteins. The importance of these repetitive regions in determining the sticky properties of gliadin was demonstrated by the use of deletion mutant of γ-gliadin. These mutants, lacking the entire N-terminal region, are not able to aggregate (Rosenberg *et al.* 1993). Gliadin aggregates were visible through optical microscope observation at low magnification and electron microscope analysis confirmed the complex structure of these protein aggregates. As already demonstrated, Caco-2 cells are able to endocyte gliadin peptides and segregate them into early endosomal compartments (Zimmermann *et al.* 2014; Zimmer *et al.* 2010). Moreover, Barone and colleagues (2010) demonstrated that gliadin peptide p31-43 can interfere with endocytic vesicles maturation. The data presented in this Thesis confirmed PT-gliadin internalization through endocytosis and confinement of this exogenous material into large autophagic vesicles. Along with autophagic process activation, the increase in the lysosomes population is suggestive of a degradative endocytic pathway (Appelqvist *et al.* 2013). The endocytic pathway crosstalks with autophagy and autophagosomes fuse with endosomes after large exogenous protein uptake (Gordon *et al.* 1992; Liou *et al.* 1997). The first clues on the involvement of autophagy after gliadin uptake derived from fluorescent analysis of cells incubated with the acidotrophic acridine orange dye. This method is useful to visualize acidic vesicles, i.e. lysosomes and autophagosomes, because of the emission changes dependent to pH conditions. Acridine orange dye emits orange/red light in presence of the low pH inside these vesicles. It is possible to distinguish between lysosome and autophagosomes according to their shape and size. This method is able to highlighted only late autophagic vacuols, i.e. autolysosomes, but not autophagosomes because they are not acidic compartments (Klionsky *et al.* 2016). Other approaches should be used together with acidotrophic dyes, such as electron microscopy, which is able to reveal the morphology of autophagic structures at a resolution of nm range. Another method used to investigate autophagy is the detection of LC3-II over-expression through immunoblotting. LC3, a protein implicated in phagophore elongation and closure, is the most widely used marker for autophagy activation. Despite its reliability, LC3-II levels depend on the

cellular contest and do not change in a predictable manner: a high autophagic flux could determine low LC3-II levels. For this reason, other autophagy-related proteins should be investigated together with LC3, i.e. ATG7 and/or BECN1, to determine autophagy induction (Klionsky *et al.* 2016). Considering these recommendation, autophagy involvement was initially investigated through the use of acridine orange but confirmed by means of complementary approaches. Caco-2 and HeLa cells showed a different behavior. The results collected for Caco-2 suggested that these cells internalized PT-gliadin and confined it in autophagosomes, accomplished by an increase of recruitment of lysosomes. After 24 hours cells actively continued their degradative attempt against the exogenous material, increasing the biosynthesis of lysosomes as a normal response due to the accumulation of undigested material (Appelqvist *et al.* 2013). After 48 hours the number of vesicles resembling autophagosomes slightly increased in number compared with treated cells at 24 hours. However, the yellow emissions of these vesicles indicated a decrease in their acid content, which may mean a temporary blockage of the degradative lysosomal response. This impairment in the process seemed to indicate the incapacity to completely digest PT-gliadin, which is stored inside the cells. Vesicles containing PT-gliadin were detected days after the incorporation suggesting that Caco-2 were not able to complete metabolize and degrade large amounts of PT-gliadin. On the other hand, HeLa cells seemed to store PT-gliadin inside their cytoplasm in long-term vesicles that remained stable but catabolically inactive. Because inner autophagy activation seemed feasible according to the acidic vesicles scored, molecular complementary approaches were needed. To this purpose, protein expression of validated autophagic markers was evaluated by immunoblotting according to Klionsky *et al.* (2016). Every cell present a basal autophagy level essential to maintain cell homeostasis and crucial for important function, such as damaged organelles and misfolded proteins degradation. Caco-2 cells displayed a much higher basal autophagy compared with other cell lines, i.e. HeLa (Pettersen *et al.* 2016). This characteristic could suggest that Caco-2 cells are more prone to use autophagy as a degradation system for PT-gliadin. Results from immunoblotting assays correlated with acridine orange observations, thus confirming that autophagy is implicated in the cellular response against gliadin endocytosis. Moreover, HeLa cells showed a down-

regulation of this process after PT-gliadin administration strengthening the idea that these cells were not able to digest the toxic peptides through autophagy because of its low basal levels. Subsequently, in order to understand whether these cellular responses were triggered by PT-gliadin due to its particular biochemical properties, the uptake and toxicity process were compared using a different exogenous protein as identical egg-ovalbumin. This protein is normally used as negative control in endocytic and toxicity assays (Martucci *et al.* 2003). Specifically, PT-gliadin and ovalbumin were covalently labelled with Alexa Fluor 488 (generating GLIA-488 and OVA-488, respectively) in order to performed comparison of the uptake and traffick of the proteins within growing cells. GLIA-488 gave rise to large aggregates, both outside and inside cells. Differently, no fluorescent signals of identical amount of OVA-488 protein were detected in the medium and inside cells. This could be related to the fact that ovalbumin is a protein that does not form large aggregates as PT-gliadin and the absence of signals in the medium may be due to an insufficient sensitivity of the microscope in detecting fluorescent monomeric proteins. Alternatively, the absence of ovalbumin fluorescent signals inside cells could be due by a poor internalization of the protein. Immunoblotting analysis show a slight increase in LC3-II levels in Caco-2 cells that may indicate a certain degree of internalization of ovalbumin which triggers autophagy to degrade the endocyted materials. On the contrary, HeLa cells showed a decreased trend after 24 hours p.t. Alltogether, these observations are coherent with the idea that PT-gliadin can perturb cellular homeostasis and proliferation of the cultures due to its characteristics, compared with other proteins (i.e. ovalbumin). This effect may be the result of PT-gliadin ability to give raise to aggregates that are resistant to degradation. Specifically, gliadin peptides are exceptionally resistant to enzymatic processing due to their proline-rich epitopes (Hausch *et al.* 2002). Gliadin biochemical behavior shows similarities to other toxic peptides that are able to form cytoplasmic toxic aggregates leading to cell death, such as β-amyloid and α-synuclein. It is known that impairment of autophagy leads to exocytosis of peptides that can not be degraded, as in the case of Parkinson disease, through a novel secretory pathway named ‘exophagy’, which involves the intermediate compartments of autophagy (Lee *et al.* 2013). Moreover, the secreted peptides could be internalized by other cells thus

perpetuating the toxic effect of gliadin in neighboring cells. Starting from this hypothesis, secretion was investigated using PT-gliadin covalently labelled with Alexa Fluor 488 and treating both cell lines. Fluorescent green spots were detected inside Caco-2 cells confirming PT-gliadin internalization process and, after the replacement of the medium, fluorescent extracellular aggregates were observed after next time intervals. The release of potentially toxic peptides from Caco-2 cells could be attributed to secretion processes that expel them when cells can not complete degradation and in part to cell death and destruction of the membranes. According to the hypothesis that toxic and sticky peptides are extruded through 'exophagy' as a consequence of autophagy failure, the obtained results suggested that Caco-2 secreted PT-gliadin in a similar way when they were not able to complete the internal degradation of these peptides. This hypothesis is enforced by the fact that autophagy was active at initial stages and further incresead after gliadin internalization in Caco-2 cells, as an attempt to catabolize the exogenous proteins. Conversely, HeLa cells have the tendency to store great amounts of PT-gliadin because of autophagy down-regulation appeared less efficient in secreting these aggregated peptides. Thus, autophagy modulation experiments have been carried out starting with serum deprivation, a known factor to induce different autophagic cellular responses (Kroemer *et al.* 2010; Shang *et al.* 2011; Lin *et al.* 2012; Chen *et al.* 2014; Sui *et al.* 2015). Autophagy induction through starvation was primarily confirmed transducing cells with baculovirus expressing LC3B-GFP chimera: this approach enabled to directly visualize large autophagic vesicles. Autophagosomes induced by serum deprivation were also confirmed by immunoblotting of their membrane constitutive protein LC3-II and by AO staining. According to experimental data, serum deprivation treatment was able to reduce PT-gliadin secretion and to confere proliferative advantage to cells compared with non-starved ones. These results can be explained by the fact that nutrient deprivation potentiates autophagy to digest PT-gliadin, promoting a clearance of the toxic intracellular protein. All these evidence were further confirmed treating Caco-2 cells with GLIA-488 in normal medium or in a starved one (0% FBS) to perform fluorimetric analysis on the collected media and through a fluorescent elecrophoresis visualization of the intracellular proteins. Fluorimetric analysis confirmed previous results showing a decrease in PT-

gliadin secretion during time compared with non-starved cells and electrophoresis analysis displayed a progressive degradation of GLIA-488 once internalized by starved cells. Then, a well established pharmacological approach with rapamycin to induce autophagy was tested. Rapamycin, an inhibitor of mTOR (Ballou and Lin, 2008), was used at different concentrations to induce autophagy in Caco-2 cells treated with GLIA-488. Increase in autophagy was preliminarily confirmed using acridine orange. A significant, dose-dependent, toxic effect was diplayed after the administration of rapamycin to cells in presence of PT-gliadin and no decrease in fluorescent PT-gliadin secretion was detected. To investigate autophagy activation and protein secretion during time, immunoblotting analysis and fluorimetric measurements were performed using the lowest and non-toxic concentration of rapamycin. The results showed no induction of autophagy, thus explaining the absence of decreasing in PT-gliadin secretion. Since most of sporadic colorectal cancers (CRC) exhibited high levels of activated Akt, Gulhati and colleagues (2009) investigated the role of downstream mTORC1 and mTORC1 on CRC growth. This study demonstrated that Caco-2 and other cells, i.e. SW480, are relatively resistant to different doses of rapamycin (2, 10 and 50 mM) compared with other human CRC lines and that their proliferation do not decrease after treatment with this compound. In analogy, the results reported above seemed to indicate that rapamycin treatment was not suitable to modulate autophagy Caco-2 cells. Finally, to interfere with the functionality of autophagy process, the down-regulation of *BECN1* gene was performed. As described in the literature, silencing of *BECN1*, or other key autophagy genes, provide an effective strategy in autophagy pathway blockage (Zeng *et al.* 2006; Li *et al.* 2014; Zanotto-Filho *et al.* 2015; Klionsky *et al.* 2016). A significant transient silencing was confirmed by immunoblotting assay, while no effects on PT-gliadin secretion were detected. These results seems to indicate that autophagy inhibition do not negatively affect cellular response to gliadin toxic effect. This experiment suggested that even partially inhibiting the autophagy process, this did not affect the capability of the cells to eventually reduce the release of PT-gliadin. It is likely that Caco-2 cells, in a context of autophagy inactivation, can store PT-gliadin within inactive autophagic vesicles and further release and spread their content to other cells.

6. Conclusions and Perspectives

In conclusion, in this PhD thesis it was demonstrated that the study of autophagy could be promising at different levels in CD research. Indeed, expression levels of key autophagic genes (*ATG7* and *BECN1*) and miRNAs (miR-17 and miR-30a) in the peripheral blood and intestinal biopsies can fairly distinguish between CD patients and controls. This positive feature made these genes and miRNAs interesting candidates as novel non-invasive biomarkers in CD field, thus recommending further investigations on larger cohorts to assess their potential diagnostic power. An enlarged panel of several miRNAs implicated in autophagy might be investigated in the blood of CD patients in order to find other interesting candidate as biomarkers. Moreover, the present study highlighted a possible role for these autophagy targets in CD patients' stratification, especially at the bioptic level. In addition, the creation of nomograms as supporting tools to assist in CD diagnosis, particularly in potential CD, seems to be clinically relevant. Additional analyses might be performed in specific cellular types to deeply investigate the role of autophagy in CD. Specifically, leukocytes population might be finely characterized in order to demonstrate the contribution of each cell subtype in determining the levels of the analyzed genes/miRNAs. Furthermore, according to the interpretative model described before, exosomes content analyses might be conducted, thus determining a profile of endogenous and circulating miRNAs in the peripheral blood of CD patients. The results reported in the second part of this PhD Thesis demonstrated an involvement of autophagy in gliadin metabolism. Autophagy is a complex intracellular degradation system that plays a crucial role in several physiological and pathological mechanisms, such as protein aggregates degradation. Once internalized, gliadin biochemical behavior resembles that of the toxic proteins causing protein conformational diseases. In this work the evidence provided suggest that gliadin is endocyted by cells and addressed to autophagosomes for its degradation but, despite autophagy activation, cells are not able to completely metabolize and degrade these peptides. It was also demonstrated that autophagy modulation through serum deprivation is able to give a proliferative advantage to cells increasing gliadin degradation and decreasing its exocytosis, thus limiting the toxic effects of these peptides on neighboring cells. Other mechanisms

of autophagy activation, i.e. rapamycin administration, were invastigated without any interesting results. Autophagy impairment in gliadin-exposed cells was also confirmed by transient *BECN1* silencing. Future work, along this line of research, might be directed to investigate other pharmacological autophagic inducers and, more importantly, autophagy modulation in dendritic cells (DC). Particularly, these cells play a crucial role in CD pathogenesis and, as already known, HLA-antigen presentation is mediated by autophagy (Crotzer and Blum, 2009). Interestingly, Di Sabatino and colleagues (2007) demonstrated that DC were increased in the mucosa of untreated CD patients. Moreover, different levels of LC3-II were detected in DC derived from duodenal biopsies of CD patients compared with normal controls (Rajaguru *et al.* 2013). A further interesting perspective might be a more exhaustive study of the beneficial effect of serum deprivation in DC and in other *in vitro* model, i.e. organ cultures. Recently, the health benefits of fasting have been highlighted in different fields: it has a role in adaptive cellular response against oxidative stress and inflammation. In particular, it was also demonstrated that intermittent or periodic fasting in humans helps to reduce obesity, hyperthension, rheumatoid arthritis and confers protection to cancer (Longo and Mattson, 2014). Moreover, it was described that fasting and particular protein dietary regimens optimize longevity, sensitize tumors to chemotherapy and protect against its side effects both in mice models and humans (Di Biase *et al*. 2016; Di Biase and Longo, 2015; Levine *et al.* 2014; Safdie *et al.* 2012; 2009). These considerations might be a starting point to investigate fasting in the treatment of CD, therefore giving rise to a novel therapeutic approach. In conclusion, with this work, it was demonstrated that genes and miRNAs involved in autophagy might have a potential diagnostic power useful for CD diagnosis and for the creation of clinical predictive tools. Moreover, this cellular pathway is involved in gliadin metabolism and its modulation could be a promising strategy in CD treatment.

Finally, although the complexity of this disease and its clinical menagement, this study might present new interesting perspectives in CD diagnosis and therapy reasearch.

References

Abadie V, Discepolo V, Jabri B. Intraepithelial lymphocytes in celiac disease immunopathology. Semin Immunopathol. 2012;34(4):551-566.

Abadie V, Sollid LM, Barreiro LB, Jabri B. Integration of genetic and immunological insights into a model of celiac disease pathogenesis. Annu Rev Immunol. 2011;29:493-525.

Alirezaei M, Fox HS, Flynn CT, Moore CS, Hebb AL, Frausto RF, Bhan V, Kiosses WB, Whitton JL, Robertson GS, Crocker SJ. Elevated ATG5 expression in autoimmune demyelination and multiple sclerosis. Autophagy. 2009;5(2):152-158.

Appelqvist H, Wäster P, Kågedal K, Öllinger K. The lysosome: from waste bag to otential therapeutic target. J Mol Cell Biol. 2013;5(4):214-226.

Arentz-Hansen H, Körner R, Molberg O, Quarsten H, Vader W, Kooy YM, Lundin KE, Koning F, Roepstorff P, Sollid LM, McAdam SN. The intestinal T cell response to alpha-gliadin in adult celiac disease is focused on a single deamidated glutamine targeted by tissue transglutaminase. J Exp Med. 2000;191(4):603-612.

Arstila AU, Trump BF. Studies on cellular autophagocytosis. The formation of autophagic vacuoles in the liver after glucagon administration. Am J Pathol. 1968;53(5):687-733.

Ashford TP, Porter KR. Cytoplasmic components in hepatic cell lysosomes. J Cell Biol. 1962;12:198-202.

Axe EL, Walker SA, Manifava M, Chandra P, Roderick HL, Habermann A, Griffiths G, Ktistakis NT. Autophagosome formation from membrane compartments enriched in phosphatidylinositol 3-phosphate and dynamically connected to the endoplasmic reticulum. J Cell Biol. 2008;182(4):685-701.

Ballou LM, Lin RZ. Rapamycin and mTOR kinase inhibitors. J Chem Biol. 2008;1(1-4):27-36.

Barbieri G, Palumbo S, Gabrusiewicz K, Azzalin A, Marchesi N, Spedito A, Biggiogera M, Sbalchiero E, Mazzini G, Miracco C, Pirtoli L, Kaminska B, Comincini S. Silencing of cellular prion protein (PrPC) expression by DNA-antisense oligonucleotides induces autophagy-dependent cell death in glioma cells. Autophagy. 2011;7(8):840-853.

Barone MV, Nanayakkara M, Paolella G, Maglio M, Vitale V, Troiano R, Ribecco MT, Lania G, Zanzi D, Santagata S, Auricchio R, Troncone R, Auricchio S.

Gliadin peptide P31-43 localises to endocytic vesicles and interferes with their maturation. PLoS One. 2010;5(8):e12246.

Bascuñán-Gamboa KA, Araya-Quezada M, Pérez-Bravo F. MicroRNAs: an epigenetic tool to study celiac disease. Rev Esp Enferm Dig. 2014;106(5):325-333.

Bellot G, Garcia-Medina R, Gounon P, Chiche J, Roux D, Pouysségur J, Mazure NM. Hypoxia-induced autophagy is mediated through hypoxia-inducible factor induction of BNIP3 and BNIP3L via their BH3 domains. Mol Cell Biol. 2009;29(10):2570-2581.

Benderska N, Dittrich AL, Knaup S, Rau TT, Neufert C, Wach S, Fahlbusch FB, Rauh M, Wirtz RM, Agaimy A, Srinivasan S, Mahadevan V, Rümmele P, Rapti E, Gazouli M et al. miRNA-26b Overexpression in Ulcerative Colitis-associated Carcinogenesis. Inflamm Bowel Dis. 2015;21(9):2039-2051.

Bernardo D. Human intestinal dendritic cells as controllers of mucosal immunity. Rev Esp Enferm Dig. 2013;105(5):279-290.

Bohnsack MT, Czaplinski K, Gorlich D. Exportin 5 is a RanGTP-dependent dsRNA-binding protein that mediates nuclear export of pre-miRNAs. RNA. 2004;10(2):185-191.

Bozzola M, Meazza C, Nastasio S, Maggiore G. Celiac disease: an update. 2014. Nova Science Publisher, New York, USA

Buoli Comani G, Panceri R, Dinelli M, Biondi A, Mancuso C, Meneveri R, Barisani D. miRNA-regulated gene expression differs in celiac disease patients according to the age of presentation. Genes Nutr. 2015;10(5):482.

Caminero A, Galipeau HJ, McCarville JL, Johnston CW, Bernier SP, Russell AK, Jury J, Herran AR, Casqueiro J, Tye-Din JA, Surette MG, Magarvey NA, Schuppan D, Verdu EF. Duodenal bacteria from patients with celiac disease and healthy subjects distinctly affect gluten breakdown and immunogenicity. Gastroenterology. 2016; S0016-5085(16)34713-8.

Capuano M, Iaffaldano L, Tinto N, Montanaro D, Capobianco V, Izzo V, Tucci F, Troncone G, Greco L, Sacchetti L. MicroRNA-449a overexpression, reduced NOTCH1 signals and scarce goblet cells characterize the small intestine of celiac patients. PLoS One. 2011;6(12):e29094.

Catassi C, Gatti S, Lionetti E. World perspective and celiac disease epidemiology. Dig Dis. 2015;33(2):141-146.

Catassi C, Bai JC, Bonaz B, Bouma G, Calabrò A, Carroccio A, Castillejo G, Ciacci C, Cristofori F, Dolinsek J, Francavilla R, Elli L, Green P, Holtmeier W, Koehler P et al. Non-Celiac Gluten sensitivity: the new frontier of gluten related disorders. Nutrients. 2013;5(10):3839-3853.

Cenit MC, Olivares M, Codoñer-Franch P, Sanz Y. Intestinal Microbiota and Celiac Disease: Cause, Consequence or Co-Evolution? Nutrients. 2015;7(8):6900-6923.

Chen R, Zou Y, Mao D, Sun D, Gao G, Shi J, Liu X, Zhu C, Yang M, Ye W, Hao Q, Li R, Yu L. The general amino acid control pathway regulates mTOR and autophagy during serum/glutamine starvation. J Cell Biol. 2014;206(2):173-182.

Clark Sl Jr. Cellular differentiation in the kidneys of newborn mice studies with the electron microscope. J Biophys Biochem Cytol. 1957;3(3):349-362.

Codogno P, Mehrpour M, Proikas-Cezanne T. Canonical and non-canonical autophagy: variations on a common theme of self-eating? Nat Rev Mol Cell Biol. 2011;131:7-12.

Comincini S, Allavena G, Palumbo S, Morini M, Durando F, Angeletti F, Pirtoli L, Miracco C. microRNA-17 regulates the expression of ATG7 and modulates the autophagy process, improving the sensitivity to temozolomide and low-dose ionizing radiation treatments in human glioblastoma cells. Cancer Biol Ther. 2013;14(7):574-586.

Comincini S, Ferrara V, Arias A, Malovini A, Azzalin A, Ferretti L, Benericetti E, Cardarelli M, Gerosa M, Passarin MG, Turazzi S, Bellazzi R. Diagnostic value of PRND gene expression profiles in astrocytomas: relationship to tumor grades of malignancy. Oncol Rep. 2007;17(5):989-996.

Comincini S, Paolillo M, Barbieri G, Palumbo S, Sbalchiero E, Azzalin A, Russo MA, Schinelli S. Gene expression analysis of an EGFR indirectly related pathway identified PTEN and MMP9 as reliable diagnostic markers for human glial tumor specimens. J Biomed Biotechnol. 2009;2009:924565.

Corazza GR, Villanacci V, Zambelli C, Milione M, Luinetti O, Vindigni C, Chioda C, Albarello L, Bartolini D, Donato F. Comparison of the interobserver reproducibility with different histologic criteria used in celiac disease. Clin Gastroenterol Hepatol. 2007;5(7):838-843.

Crotzer VL, Blum JS. Autophagy and its role in MHC-mediated antigen presentation. J Immunol. 2009;182(6):3335-3341.

D'Amico MA, Holmes J, Stavropoulos SN, Frederick M, Levy J, DeFelice AR, Kazlow PG, Green PH. Presentation of pediatric celiac disease in the United States: prominent effect of breastfeeding. Clin Pediatr (Phila). 2005;44(3):249-258.

D'Eletto M, Farrace MG, Rossin F, Strappazzon F, Giacomo GD, Cecconi F, Melino G, Sepe S, Moreno S, Fimia GM, Falasca L, Nardacci R, Piacentini M. Type 2 transglutaminase is involved in the autophagy-dependent clearance of ubiquitinated proteins. Cell Death Differ. 2012;19(7):1228-1238.

Denli AM, Tops BB, Plasterk RH, Ketting RF, Hannon GJ. Processing of primary microRNAs by the Microprocessor complex. Nature. 2004;432(7014):231-235.

Deretic V, Saitoh T, Akira S. Autophagy in infection, inflammation and immunity. Nat Rev Immunol. 2013;13(10):722-737.

Deter RL, De Duve C. Influence of glucagon, an inducer of cellular autophagy, on some physical properties of rat liver lysosomes. J Cell Bio. 1967;33:437-449.

Di Bartolomeo S, Corazzari M, Nazio F, Oliverio S, Lisi G, Antonioli M, Pagliarini V, Matteoni S, Fuoco C, Giunta L, D'Amelio M, Nardacci R, Romagnoli A, Piacentini M, Cecconi F et al. The dynamic interaction of AMBRA1 with the dynein motor complex regulates mammalian autophagy. J Cell Biol. 2010;191(1):155-168.

Di Biase S, Longo VD. Fasting-induced differential stress sensitization in cancer treatment. Mol Cell Oncol. 2015;3(3):e1117701.

Di Biase S, Lee C, Brandhorst S, Manes B, Buono R, Cheng CW, Cacciottolo M, Martin-Montalvo A, de Cabo R, Wei M, Morgan TE, Longo VD. Fasting-mimicking diet reduces HO-1 to promote T cell-mediated tumor cytotoxicity. Cancer Cell. 2016;30(1):136-146.

Di Cagno R, De Angelis M, De Pasquale I, Ndagijimana M, Vernocchi P, Ricciuti P, Gagliardi F, Laghi L, Crecchio C, Guerzoni ME, Gobbetti M, Francavilla R. Duodenal and faecal microbiota of celiac children: molecular, phenotype andmetabolome characterization. BMC Microbiol. 2011;11:219.

Di Sabatino A, Corazza GR. Some clarification is necessary on the Oslo definitions for coeliac disease-related terms. Gut. 2013;62(1):182.

Di Sabatino A, Corazza GR. Coeliac disease. Lancet. 2009;373(9673):1480-1493.

Di Sabatino A, Pickard KM, Gordon JN, Salvati V, Mazzarella G, Beattie RM, Vossenkaemper A, Rovedatti L, Leakey NA, Croft NM, Troncone R, Corazza GR, Stagg AJ, Monteleone G, MacDonald TT. Evidence for the role of interferon-alfa production by dendritic cells in the Th1 response in celiac disease. Gastroenterology. 2007;133(4):1175-1187.

Djilali-Saiah I, Schmitz J, Harfouch-Hammoud E, Mougenot JF, Bach JF, Caillat-Zucman S. CTLA-4 gene polymorphism is associated with predisposition to coeliac disease. Gut. 1998;43(2):187-189.

Drago S, El Asmar R, Di Pierro M, Grazia Clemente M, Tripathi A, Sapone A, Thakar M, Iacono G, Carroccio A, D'Agate C, Not T, Zampini L, Catassi C, Fasano A. Gliadin, zonulin and gut permeability: Effects on celiac and non-celiac intestinal mucosa and intestinal cell lines. Scand J Gastroenterol. 2006;41(4):408-419.

Dubois PC, Trynka G, Franke L, Hunt KA, Romanos J, Curtotti A, Zhernakova A, Heap GA, Adány R, Aromaa A, Bardella MT, van den Berg LH, Bockett NA, de la Concha EG, Dema B et al. Multiple common variants for celiac disease influencing immune gene expression. Nat Genet. 2010;42(4):295-302.

Ebert MS, Sharp PA. MicroRNA sponges: progress and possibilities. RNA. 2010;16(11):2043-2050.

Elli L, Roncoroni L, Bardella MT. Non-celiac gluten sensitivity: time for sifting the grain. World J Gastroenterol. 2015;21(27):8221-8226.

Elkayam E, Kuhn CD, Tocilj A, Haase AD, Greene EM, Hannon GJ, Joshua-Tor L. The structure of human argonaute-2 in complex with miR-20a. Cell. 2012;150(1):100-110.

Escudero-Hernández C, Peña AS, Bernardo D. Immunogenetic pathogenesis of celiac disease and non-celiac gluten sensitivity. Curr Gastroenterol Rep. 2016;18(7):36.

Fasano A, Catassi C. Clinical practice. Celiac disease. N Engl J Med. 2012 ;367(25):2419-2426.

Fasano A, Berti I, Gerarduzzi T, Not T, Colletti RB, Drago S, Elitsur Y, Green PH, Guandalini S, Hill ID, Pietzak M, Ventura A, Thorpe M, Kryszak D, Fornaroli F et al. Prevalence of celiac disease in at-risk and not-at-risk groups in the United States: a large multicenter study. ArchIntern Med. 2003;163(3):286-292.

Farrell RJ, Kelly CP. Celiac sprue. N Engl J Med. 2002;346(3):180-188.

Fassina L, Magenes G, Inzaghi A, Palumbo S, Allavena G, Miracco C, Pirtoli L, Biggiogera M, Comincini S. AUTOCOUNTER, an ImageJ JavaScript to analyze LC3B-GFP expression dynamics in autophagy-induced astrocytoma cells. Eur J Histochem. 2012;56(4):e44.

Fujita N, Itoh T, Omori H, Fukuda M, Noda T, Yoshimori T. The Atg16L complex specifies the site of LC3 lipidation for membrane biogenesis in autophagy. Mol Biol

Cell. 2008;1 (5):2092-2100.

Fukuda T, Yamagata K, Fujiyama S, Matsumoto T, Koshida I, Yoshimura K, Mihara M, Naitou M, Endoh H, Nakamura T, Akimoto C, Yamamoto Y, Katagiri T, Foulds C, Takezawa S et al. DEAD-box RNA helicase subunits of the Drosha complex are required for processing of rRNA and a subset of microRNAs. Nat Cell Biol. 2007;9(5):604-611.

Gherzi R, Lee KY, Briata P, Wegmüller D, Moroni C, Karin M, Chen CY. A KH domain RNA binding protein, KSRP, promotes ARE-directed mRNA turnover by recruiting the degradation machinery. Mol Cell. 2004;14(5):571-583.

Giersiepen K, Lelgemann M, Stuhldreher N, Ronfani L, Husby S, Koletzko S, Korponay-Szabó IR; ESPGHAN Working Group on Coeliac Disease Diagnosis. Accuracy of diagnostic antibody tests for coeliac disease in children: summary of an evidence report. J Pediatr Gastroenterol Nutr. 2012;54(2):229-241.

Gordon PB, Høyvik H, Seglen PO. Prelysosomal and lysosomal connections between autophagy and endocytosis. Biochem J. 1992;283 (Pt 2):361-369.

Gottlieb K, Dawson J, Hussain F, Murray JA. Development of drugs for celiac disease: review of endpoints for Phase 2 and 3 trials. Gastroenterol Rep (Oxf). 2015;3(2):91-102.

Greco L, Corazza G, Babron MC, Clot F, Fulchignoni-Lataud MC, Percopo S, Zavattari P, Bouguerra F, Dib C, Tosi R, Troncone R, Ventura A, Mantavoni W, Magazzù G, Gatti R et al. Genome search in celiac disease. Am J Hum Genet. 1998;62(3):669-675.

Green PH. The many faces of celiac disease: clinical presentation of celiac disease in the adult population. Gastroenterology. 2005;128(4 Suppl 1):S74-78.

Green DR, Kroemer G. Cytoplasmic functions of the tumour suppressor p53. Nature. 2009;458(7242):1127-1130.

Gregory RI, Chendrimada TP, Cooch N, Shiekhattar R. Human RISC couples microRNA biogenesis and posttranscriptional gene silencing. Cell. 2005;123(4):631-640.

Gregory RI, Yan KP, Amuthan G, Chendrimada T, Doratotaj B, Cooch N, Shiekhattar R. The Microprocessor complex mediates the genesis of microRNAs. Nature. 2004;432(7014):235-240.

Gros F, Arnold J, Page N, Décossas M, Korganow AS, Martin T, Muller S.

Macroautophagy is deregulated in murine and human lupus T lymphocytes. Autophagy. 2012;8(7):1113-1123.

Gujral N, Suh JW, Sunwoo HH. Effect of anti-gliadin IgY antibody on epithelial intestinal integrity and inflammatory response induced by gliadin. BMC Immunol. 2015;16:41.

Gulhati P, Cai Q, Li J, Liu J, Rychahou PG, Qiu S, Lee EY, Silva SR, Bowen KA, Gao T, Evers BM. Targeted inhibition of mammalian target of rapamycin signaling inhibits tumorigenesis of colorectal cancer. Clin Cancer Res. 2009;15(23):7207-7216.

Ha M, Kim VN. Regulation of microRNA biogenesis. Nat Rev Mol Cell Biol. 2014;15(8):509-524.

Haase AD, Jaskiewicz L, Zhang H, Lainé S, Sack R, Gatignol A, Filipowicz W. TRBP, a regulator of cellular PKR and HIV-1 virus expression, interacts with Dicer and functions in RNA silencing. EMBO Rep. 2005;6(10):961-967.

Hall NJ, Rubin GP, Charnock A. Intentional and inadvertent non-adherence in adult coeliac disease. A cross-sectional survey. Appetite. 2013;68:56-62.

Han J, Lee Y, Yeom KH, Nam JW, Heo I, Rhee JK, Sohn SY, Cho Y, Zhang BT, Kim VN. Molecular basis for the recognition of primary microRNAs by the Drosha-DGCR8 complex. Cell. 2006;125(5):887-901.

Han J, Lee Y, Yeom KH, Kim YK, Jin H, Kim VN. The Drosha-DGCR8 complex in primary microRNA processing. Genes Dev. 2004;18(24):3016-3027.

Hanke M, Hoefig K, Merz H, Feller AC, Kausch I, Jocham D, Warnecke JM, Sczakiel G. A robust methodology to study urine microRNA as tumor marker: microRNA-126 and microRNA-182 are related to urinary bladder cancer. Urol Oncol. 2010;28(6):655-661.

Harris J, De Haro SA, Master SS, Keane J, Roberts EA, Delgado M, Deretic V. T helper 2 cytokines inhibit autophagic control of intracellular Mycobacterium tuberculosis. Immunity. 2007;27(3):505-517.

Hausch F, Shan L, Santiago NA, Gray GM, Khosla C. Intestinal digestive resistance of immunodominant gliadin peptides. Am J Physiol Gastrointest Liver Physiol. 2002;283(4):G996-G1003.

He C, Klionsky DJ. Regulation mechanisms and signaling pathways of autophagy. Annu Rev Genet. 2009;43:67-93.

He C, Levine B. The Beclin 1 interactome. Curr Opin Cell Biol. 2010;22(2):140-149.

Henckaerts L, Cleynen I, Brinar M, John JM, Van Steen K, Rutgeerts P, Vermeire S. Genetic variation in the autophagy gene ULK1 and risk of Crohn's disease. Inflamm Bowel Dis. 2011;17(6):1392-1397.

Heo I, Joo C, Kim YK, Ha M, Yoon MJ, Cho J, Yeom KH, Han J, Kim VN. TUT4 in concert with Lin28 suppresses microRNA biogenesis through pre-microRNA uridylation. Cell. 2009;138(4):696-708.

Hidalgo IJ, Raub TJ, Borchardt RT. Characterization of the human colon carcinoma cell line (Caco-2) as a model system for intestinal epithelial permeability. Gastroenterology. 1989;96(3):736-749.

Hollon JR, Cureton PA, Martin ML, Puppa EL, Fasano A. Trace gluten contamination may play a role in mucosal and clinical recovery in a subgroup of diet-adherent non-responsive celiac disease patients. BMC Gastroenterol. 2013;13:40.

Hubatsch I, Ragnarsson EG, Artursson P. Determination of drug permeability and prediction of drug absorption in Caco-2 monolayers. Nat Protoc. 2007;2(9):2111-2119.

Hunt KA, Zhernakova A, Turner G, Heap GA, Franke L, Bruinenberg M, Romanos J, Dinesen LC, Ryan AW, Panesar D, Gwilliam R, Takeuchi F, McLaren WM, Holmes GK, Howdle PD et al. Newly identified genetic risk variants for celiac disease related to the immune response. Nat Genet. 2008;40(4):395-402.

Hunt KA, McGovern DP, Kumar PJ, Ghosh S, Travis SP, Walters JR, Jewell DP, Playford RJ, van Heel DA. A common CTLA4 haplotype associated with coeliac disease. Eur Hum Genet. 2005;13(4):440-444.

Iborra M, Bernuzzi F, Correale C, Vetrano S, Fiorino G, Beltrán B, Marabita F, Locati M, Spinelli A, Nos P, Invernizzi P, Danese S. Identification of serum and tissue micro-RNA expression profiles in different stages of inflammatory bowel disease. Clin Exp Immunol. 2013;173(2):250-258.

International Consortium for Systemic Lupus Erythematosus Genetics (SLEGEN), Harley JB, Alarcón-Riquelme ME, Criswell LA, Jacob CO, Kimberly RP, Moser KL, Tsao BP, Vyse TJ, Langefeld CD, Nath SK, Guthridge JM, Cobb BL, Mirel DB, Marion MC et al. Genome-wide association scan in women with systemic lupus erythematosus identifies susceptibility variants in ITGAM, PXK, KIAA1542 and other loci. Nat Genet. 2008;40(2):204-210.

Ireland JM, Unanue ER. Autophagy in antigen-presenting cells results in presentation of

citrullinated peptides to CD4 T cells. J Exp Med. 2011;208(13):2625-2632.

Jung CH, Ro SH, Cao J, Otto NM, Kim DH. mTOR regulation of autophagy. FEBS Lett. 2010;584(7):1287-1295.

Junker Y, Zeissig S, Kim SJ, Barisani D, Wieser H, Leffler DA, Zevallos V, Libermann TA, Dillon S, Freitag TL, Kelly CP, Schuppan D. Wheat amylase trypsin inhibitors drive intestinal inflammation via activation of toll-like receptor 4. J Exp Med. 2012;209(13):2395-2408.

Kabeya Y, Mizushima N, Yamamoto A, Oshitani-Okamoto S, Ohsumi Y, Yoshimori T. LC3, GABARAP and GATE16 localize to autophagosomal membrane depending on form-II formation. J Cell Sci. 2004;117(Pt 13):2805-2812.

Kanzawa T, Kondo Y, Ito H, Kondo S, Germano I. Induction of autophagic cell death in malignant glioma cells by arsenic trioxide. Cancer Res. 2003;63(9):2103-2108.

Karell K, Louka AS, Moodie SJ, Ascher H, Clot F, Greco L, Ciclitira PJ, Sollid LM, Partanen J; European Genetics Cluster on Celiac Disease. HLA types in celiac disease patients not carrying the DQA1*05-DQB1*02 (DQ2) heterodimer: results from the European Genetics Cluster on Celiac Disease. Hum Immunol. 2003;64(4):469-477.

Kaukinen K, Partanen J, Mäki M, Collin P. HLA-DQ typing in the diagnosis of celiac disease. Am J Gastroenterol. 2002;97(3):695-699.

Kaushik S, Bandyopadhyay U, Sridhar S, Kiffin R, Martinez-Vicente M, Kon M, Orenstein SJ, Wong E, Cuervo AM. Chaperone-mediated autophagy at a glance. J Cell Sci. 2011;124(Pt 4):495-499.

Kelly CP, Bai JC, Liu E, Leffler DA. Advances in diagnosis and management of celiac disease. Gastroenterology. 2015;148(6):1175-1186.

Kim J, Kundu M, Viollet B, Guan KL. AMPK and mTOR regulate autophagy through direct phosphorylation of Ulk1. Nat Cell Biol. 2011;13(2):132-141.

Kim CY, Quarsten H, Bergseng E, Khosla C, Sollid LM. Structural basis for HLA-DQ2-mediated presentation of gluten epitopes in celiac disease. Proc Natl Acad Sci U S A. 2004;101(12):4175-4179.

Klionsky DJ, Abdelmohsen K, Abe A, Abedin MJ, Abeliovich H, Acevedo Arozena A, Adachi H, Adams CM, Adams PD, Adeli K, Adhihetty PJ, Adler SG, Agam G, Agarwal R, Aghi MK et al. Guidelines for the use and interpretation of assays for monitoring autophagy (3rd edition). Autophagy. 2016;12(1):1-222.

Kroemer G, Mariño G, Levine B. Autophagy and the integrated stress response. Mol Cell. 2010;40(2):280-293.

Lapaquette P, Glasser AL, Huett A, Xavier RJ, Darfeuille-Michaud A. Crohn's disease-associated adherent-invasive E. coli are selectively favoured by impaired autophagy to replicate intracellularly. Cell Microbiol. 2010;12(1):99-113.

Larrea E, Sole C, Manterola L, Goicoechea I, Armesto M, Arestin M, Caffarel MM, Araujo AM, Araiz M, Fernandez-Mercado M, Lawrie CH. New concepts in cancer biomarkers: circulating miRNAs in liquid biopsies. Int J Mol Sci. 2016;17(5).

Lee HJ, Cho ED, Lee KW, Kim JH, Cho SG, Lee SJ. Autophagic failure promotes the exocytosis and intercellular transfer of α-synuclein. Exp Mol Med. 2013;45:e22.

Lee RC, Feinbaum RL, Ambros V. The C. elegans heterochronic gene lin-4 encodes small RNAs with antisense complementarity to lin-14. Cell. 1993;75(5):843-854.

Lee Y, Kim M, Han J, Yeom KH, Lee S, Baek SH, Kim VN. MicroRNA genes are transcribed by RNA polymerase II. EMBO J. 2004;23(20):4051-4060.

Lee Y, Jeon K, Lee JT, Kim S, Kim VN. MicroRNA maturation: stepwise processing and subcellular localization. EMBO J. 2002;21(17):4663-4670.

Lee IH, Cao L, Mostoslavsky R, Lombard DB, Liu J, Bruns NE, Tsokos M, Alt FW, Finkel T. A role for the NAD-dependent deacetylase Sirt1 in the regulation of autophagy. Proc Natl Acad Sci U S A. 2008;105(9):3374-3379.

Leffler D, Kupfer SS, Lebwohl B, Bugin K, Griebel D, Lathrop JT, Lee JJ, Mulberg AE, Papadopoulos E, Tomaino J, Crowe SE. Development of celiac disease therapeutics: report of the third gastroenterology regulatory endpoints and advancement of therapeutics workshop. Gastroenterology. 2016;151(3):407-411.

Levine B, Kroemer G. SnapShot: Macroautophagy. Cell. 2008;132(1):162.e1-162.e3.

Levine B, Mizushima N, Virgin HW. Autophagy in immunity and inflammation. Nature. 2011;469(7330):323-335.

Levine ME, Suarez JA, Brandhorst S, Balasubramanian P, Cheng CW, Madia F, Fontana L, Mirisola MG, Guevara-Aguirre J, Wan J, Passarino G, Kennedy BK, Wei M, Cohen P, Crimmins EM, Longo VD. Low protein intake is associated with a major reduction in IGF-1, cancer, and overall mortality in the 65 and younger but not older population. Cell Metab. 2014;19(3):407-417.

Li Y, Luo P, Wang J, Dai J, Yang X, Wu H, Yang B, He Q. Autophagy blockade sensitizes the anticancer activity of CA-4 via JNK-Bcl-2 pathway. Toxicol Appl Pharmacol. 2014;274(2):319-327.

Li Z, Rana TM. Therapeutic targeting of microRNAs: current status and future challenges. Nat Rev Drug Discov. 2014;13(8):622-638.

Lin SY, Li TY, Liu Q, Zhang C, Li X, Chen Y, Zhang SM, Lian G, Liu Q, Ruan K, Wang Z, Zhang CS, Chien KY, Wu J, Li Q, Han J, Lin SC. Protein phosphorylation-acetylation cascade connects growth factor deprivation to autophagy. Autophagy. 2012;8(9):1385-1386.

Lionetti E, Catassi C. Co-localization of gluten consumption and HLA-DQ2 and -DQ8 genotypes, a clue to the history of celiac disease. Dig Liver Dis. 2014;46(12):1057-1063.

Liou W, Geuze HJ, Geelen MJ, Slot JW. The autophagic and endocytic pathways converge at the nascent autophagic vacuoles. J Cell Biol. 1997;136(1):61-70.

Liu L, Wise DR, Diehl JA, Simon MC. Hypoxic reactive oxygen species regulate the integrated stress response and cell survival. J Biol Chem. 2008;283(45):31153-31162.

Livak KJ, Schmittgen TD. Analysis of relative gene expression data using real-time quantitative PCR and the 2(-Delta Delta C(T)) method. Methods. 2001;25(4):402-408.

Longo VD, Mattson MP. Fasting: molecular mechanisms and clinical applications. Cell Metab. 2014;19(2):181-192.

Lu C, Chen J, Xu HG, Zhou X, He Q, Li YL, Jiang G, Shan Y, Xue B, Zhao RX, Wang Y, Werle KD, Cui R, Liang J, Xu ZX. Mir106b and mir93 prevent removal of bacteria from epithelial cells by disrupting ATG16L1-mediated autophagy. Gastroenterology. 2014;146(1):188-199.

Ludvigsson JF, Leffler DA, Bai JC, Biagi F, Fasano A, Green PH, Hadjivassiliou M, Kaukinen K, Kelly CP, Leonard JN, Lundin KE, Murray JA, Sanders DS, Walker MM, Zingone F et al. The Oslo definitions for coeliac disease and related terms. Gut. 2013;62(1):43-52.

Macrae IJ, Zhou K, Li F, Repic A, Brooks AN, Cande WZ, Adams PD, Doudna JA. Structural basis for double-stranded RNA processing by Dicer. Science. 2006;311(5758):195-198.

Magni S, Buoli Comani G, Elli L, Vanessi S, Ballarini E, Nicolini G, Rusconi M,

Castoldi M, Meneveri R, Muckenthaler MU, Bardella MT, Barisani D. miRNAs affect the expression of innate and adaptive immunity proteins in celiac disease. Am J Gastroenterol. 2014;109(10):1662-1674.

Makharia GK, Verma AK, Amarchand R, Bhatnagar S, Das P, Goswami A, Bhatia V, Ahuja V, Datta Gupta S, Anand K. Prevalence of celiac disease in the northern part of India: a community based study. J Gastroenterol Hepatol. 2011;26(5):894-900.

Mammucari C, Milan G, Romanello V, Masiero E, Rudolf R, Del Piccolo P, Burden SJ, Di Lisi R, Sandri C, Zhao J, Goldberg AL, Schiaffino S, Sandri M. FoxO3 controls autophagy in skeletal muscle in vivo. Cell Metab. 2007;6(6):458-471.

Marsh MN. Gluten, major histocompatibility complex, and the small intestine. A molecular and immunobiologic approach to the spectrum of gluten sensitivity ('celiac sprue'). Gastroenterology. 1992;102(1):330-354.

Martinez-Vicente M, Talloczy Z, Wong E, Tang G, Koga H, Kaushik S, de Vries R, Arias E, Harris S, Sulzer D, Cuervo AM. Cargo recognition failure is responsible for inefficient au ophagy in Huntington's disease. Nat Neurosci. 2010;13(5):567-576.

Martucci S, Fraser JS, Biagi F, Corazza GR, Ciclitira PJ, Ellis HJ. Characterizing one of the DQ2 candidate epitopes in coeliac disease: A-gliadin 51-70 toxicity assessed using an organ culture system. Eur J Gastroenterol Hepatol. 2003;15(12):1293-1298.

Matysiak-Budnik T, Moura IC, Arcos-Fajardo M, Lebreton C, Ménard S, Candalh C, Ben-Khalifa K, Dugave C, Tamouza H, van Niel G, Bouhnik Y, Lamarque D, Chaussade S, Malamut G, Cellier C et al. Secretory IgA mediates retrotranscytosis of intact gliadin peptides via the transferrin receptor in celiac disease. J Exp Med. 2008;205(1):143-154.

Mazure NM, Pouysségur J. Hypoxia-induced autophagy: cell death or cell survival? Curr Opin Cell Biol. 2010;22(2):177-180.

Ménard S, Lebreton C, Schumann M, Matysiak-Budnik T, Dugave C, Bouhnik Y, Malamut G, Cellier C, Allez M, Crenn P, Schulzke JD, Cerf-Bensussan N, Heyman M. Paracellular versus transcellular intestinal permeability to gliadin peptides in active celiac disease. Am J Pathol. 2012;180(2):608-615.

Mention JJ, Ben Ahmed M, Bègue B, Barbe U, Verkarre V, Asnafi V, Colombel JF, Cugnenc PH, Ruemmele FM, McIntyre E, Brousse N, Cellier C, Cerf-Bensussan N. Interleukin 15: a key to disrupted intraepithelial lymphocyte homeostasis and lymphomagenesis in celiac disease. Gastroenterology. 2003;125(3):730-745.

Meresse B, Curran SA, Ciszewski C, Orbelyan G, Setty M, Bhagat G, Lee L,

Tretiakova M, Semrad C, Kistner E, Winchester RJ, Braud V, Lanier LL, Geraghty DE, Green PH et al. Reprogramming of CTLs into natural killer-like cells in celiac disease. J Exp Med. 2006;203(5):1343-1355.

Meresse B, Chen Z, Ciszewski C, Tretiakova M, Bhagat G, Krausz TN, Raulet DH, Lanier LL, Groh V, Spies T, Ebert EC, Green PH, Jabri B. Coordinated induction by IL15 of a TCR-independent NKG2D signaling pathway converts CTL into lymphokine-activated killer cells in celiac disease. Immunity. 2004;21(3):357-366.

Michlewski G, Guil S, Semple CA, Cáceres JF. Posttranscriptional regulation of miRNAs harboring conserved terminal loops. Mol Cell. 2008;32(3):383-393.

Milani M, Rzymski T, Mellor HR, Pike L, Bottini A, Generali D, Harris AL. The role of ATF4 stabilization and autophagy in resistance of breast cancer cells treated with Bortezomib. Cancer Res. 2009;69(10):4415-4423.

Mitchell PS, Parkin RK, Kroh EM, Fritz BR, Wyman SK, Pogosova-Agadjanyan EL, Peterson A, Noteboom J, O'Briant KC, Allen A, Lin DW, Urban N, Drescher CW, Knudsen BS, Stirewalt DL et al. Circulating microRNAs as stable blood-based markers for cancer detection. Proc Natl Acad Sci U S A. 2008;105(30):10513-10518.

Mizushima N, Komatsu M. Autophagy: renovation of cells and tissues. Cell. 2011;147(4):728-741.

Mizushima N, Yoshimori T, Ohsumi Y. Role of the Apg12 conjugation system in mammalian autophagy. Int J Biochem Cell Biol. 2003;35(5):553-561.

Molberg O, Mcadam SN, Körner R, Quarsten H, Kristiansen C, Madsen L, Fugger L, Scott H, Norén O, Roepstorff P, Lundin KE, Sjöström H, Sollid LM. Tissue transglutaminase selectively modifies gliadin peptides that are recognized by gut-derived T cells in celiac disease. Nat Med. 1998;4(6):713-717.

Monsuur AJ, de Bakker PI, Alizadeh BZ, Zhernakova A, Bevova MR, Strengman E, Franke L, van't Slot R, van Belzen MJ, Lavrijsen IC, Diosdado B, Daly MJ, Mulder CJ, Mearin ML, Meijer JW et al. Myosin IXB variant increases the risk of celiac disease and points toward a primary intestinal barrier defect. Nat Genet. 2005;37(12):1341-1344.

Motawi TK, Shaker OG, El-Maraghy SA, Senousy MA. Serum microRNAs as potential biomarkers for early diagnosis of hepatitis C virus-related hepatocellular carcinoma in egyptian patients. PLoS One. 2015;10(9):e0137706.

Mozina M, Demsar J, Kattan M, Zupan B. Nomograms for visualization of Naïve Bayes classifier. European Conference on Principles and Practice of Knowledge Discovery

in Databases (PKDD), September 20-24, 2004, Pisa.

Mustalahti K, Catassi C, Reunanen A, Fabiani E, Heier M, McMillan S, Murray L, Metzger MH, Gasparin M, Bravi E, Mäki M; Coeliac EU Cluster, ProjectEpidemiology. The prevalence of celiac disease in Europe: results of a centralized, international mass screening project. Ann Med. 2010;42(8):587-595.

Nadal I, Donat E, Ribes-Koninckx C, Calabuig M, Sanz Y. Imbalance in the composition of the duodenal microbiota of children with coeliac disease. J Med Microbiol. 2007;56(Pt 12):1669-1674.

Narendra D, Kane LA, Hauser DN, Fearnley IM, Youle RJ. p62/SQSTM1 is required for Parkin-induced mitochondrial clustering but not mitophagy; VDAC1 is dispensable for both. Autophagy. 2010;6(8):1090-1106.

Nazio F, Strappazzon F, Antonioli M, Bielli P, Cianfanelli V, Bordi M, Gretzmeier C, Dengjel J, Piacentini M, Fimia GM, Cecconi F. mTOR inhibits autophagy by controlling ULK1 ubiquitylation, self-association and function through AMBRA1 and TRAF6. Nat Cell Biol. 2013;15(4):406-416.

Neufeld TP. TOR-dependent control of autophagy: biting the hand that feeds. Curr Opin Cell Biol. 2010;22(2):157-168.

Newman MA, Thomson JM, Hammond SM. Lin-28 interaction with the Let-7 precursor loop mediates regulated microRNA processing. RNA. 2008;14(8):1539-1549.

Noda T, Ohsumi Y. Tor, a phosphatidylinositol kinase homologue, controls autophagy in yeast. J Biol Chem. 1998;273(7):3963-3966.

Novikoff AB, Beaufay H, De Duve C. Electron microscopy of lysosomerich fractions from rat liver. J Biophys Biochem Cytol. 1956;2(4 Suppl):179-184.

Nistal E, Caminero A, Vivas S, Ruiz de Morales JM, Sáenz de Miera LE, Rodríguez-Aparicio LB, Casqueiro J. Differences in faecal bacteria populations and faecal bacteria metabolism in healthy adults and celiac disease patients. Biochimie. 2012;94(8):1724-1729.

Oberhuber G, Granditsch G, Vogelsang H. The histopathology of coeliac disease: time for a standardized report scheme for pathologists. Eur J Gastroenterol Hepatol. 1999;11(10):1185-1194.

Ohsumi Y. Historical landmarks of autophagy research. Cell Res. 2014;24(1):9-23.

Paglin S, Hollister T, Delohery T, Hackett N, McMahill M, Sphicas E, Domingo D,

Yahalom J. A novel response of cancer cells to radiation involves autophagy and formation of acidic vesicles. Cancer Res. 2001;61(2):439-444.

Park JE, Heo I, Tian Y, Simanshu DK, Chang H, Jee D, Patel DJ, Kim VN. Dicer recognizes the 5' end of RNA for efficient and accurate processing. Nature. 2011;475(7355):201-205.

Park NJ, Zhou H, Elashoff D, Henson BS, Kastratovic DA, Abemayor E, Wong DT. Salivary microRNA: discovery, characterization, and clinical utility for oral cancer detection. Clin Cancer Res. 2009;15(17):5473-5477.

Paroo Z, Ye X, Chen S, Liu Q. Phosphorylation of the human microRNA-generating complex mediates MAPK/Erk signaling. Cell. 2009;139(1):112-122.

Partin AW, Yoo J, Carter HB, Pearson JD, Chan DW, Epstein JI, Walsh PC. The use of prostate specific antigen, clinical stage and Gleason score to predict pathological stage in men with localized prostate cancer. J Urol. 1993;150(1):110-114.

Pettersen K, Monsen VT, Hakvåg Pettersen CH, Overland HB, Pettersen G, Samdal H, Tesfahun AN, Lundemo AG, Bjørkøy G, Schønberg SA. DHA-induced stress response in human colon cancer cells - Focus on oxidative stress and autophagy. Free Radic Biol Med. 2016;90:158-172.

Pfeifer U, Warmuth-Metz M. Inhibition by insulin of cellular autophagy in proximal tubular cells of rat kidney. Am J Physiol. 1983;244(2):E109-114.

Polson HE, de Lartigue J, Rigden DJ, Reedijk M, Urbé S, Clague MJ, Tooze SA. Mammalian Atg18 (WIPI2) localizes to omegasome-anchored phagophores andpositively egulates LC3 lipidation. Autophagy. 2010;6(4):506-522.

Qi HH, Ongusaha PP, Myllyharju J, Cheng D, Pakkanen O, Shi Y, Lee SW, Peng J, Shi Y. Prolyl 4-hydroxylation regulates Argonaute 2 stability. Nature. 2008;455(7211):421-424.

Quinlan, JR. Induction of decision trees. Machine learning 1. 1986: 81-106, Kluwer Academic Publishers

Rajaguru P, Vaiphei K, Saikia B, Kochhar R. Increased accumulation of dendritic cells in celiac disease associates with increased expression of autophagy protein LC3. Indian J Pathol Microbiol. 2013;56(4):342-348.

Rampertab SD, Pooran N, Brar P, Singh P, Green PH. Trends in the presentation of celiac disease. Am J Med. 2006;119(4):355.e9-14.

Ravikumar B, Sarkar S, Davies JE, Futter M, Garcia-Arencibia M, Green-Thompson ZW, Jimenez-Sanchez M, Korolchuk VI, Lichtenberg M, Luo S, Massey DC, Menzies FM, Moreau K, Narayanan U, Renna M et al. Regulation of mammalian autophagy in physiology and pathophysiology. Physiol Rev. 2010;90(4):1383-1435.

Regazzo G, Terrenato I, Spagnuolo M, Carosi M, Cognetti G, Cicchillitti L, Sperati F, Villani V, Carapella C, Piaggio G, Pelosi A, Rizzo MG. A restricted signature of serum miRNAs distinguishes glioblastoma from lower grade gliomas. J Exp Clin Cancer Res. 2016;35(1):124.

Reinhart BJ, Slack FJ, Basson M, Pasquinelli AE, Bettinger JC, Rougvie AE, Horvitz HR, Ruvkun G. The 21-nucleotide let-7 RNA regulates developmental timing in Caenorhabditis elegans. Nature. 2000;403(6772):901-906.

Rishi AR, Rubio-Tapia A, Murray JA. Refractory celiac disease. Expert Rev Gastroenterol Hepatol. 2016;10(4):537-546.

Rokach L, Maimon O. Data mining with decision tree. Theory and applications. 2nd ed. 2014

Rosenberg N, Shimoni Y, Altschuler Y, Levanony H, Volokita M, Galili G. Wheat (Triticum aestivum L.) [gamma]-gliadin accumulates in dense protein bodies within the endoplasmic reticulum of yeast. Plant Physiol. 1993;102(1):61-69.

Rossin F, D'Eletto M, Macdonald D, Farrace MG, Piacentini M. TG2 transamidating activity acts as a reostat controlling the interplay between apoptosis and autophagy. Amino Acids. 2012;42(5):1793-1802.

Rubio-Tapia A, Hill ID, Kelly CP, Calderwood AH, Murray JA; American College of Gastroenterology. ACG clinical guidelines: diagnosis and management of celiac disease. Am J Gastroenterol. 2013;108(5):656-676.

Ruderman NB, Xu XJ, Nelson L, Cacicedo JM, Saha AK, Lan F, Ido Y. AMPK and SIRT1: a long-standing partnership? Am J Physiol Endocrinol Metab. 2010;298(4):E751-760.

Safdie FM, Dorff T, Quinn D, Fontana L, Wei M, Lee C, Cohen P, Longo VD. Fasting and cancer treatment in humans: A case series report. Aging (Albany NY). 2009;1(12):988-1007.

Safdie F, Brandhorst S, Wei M, Wang W, Lee C, Hwang S, Conti PS, Chen TC, Longo VD. Fasting enhances the response of glioma to chemo- and radiotherapy. PLoS One. 2012;7(9):e44603.

Saitoh T, Fujita N, Jang MH, Uematsu S, Yang BG, Satoh T, Omori H, Noda T,

Yamamoto N, Komatsu M, Tanaka K, Kawai T, Tsujimura T, Takeuchi O, Yoshimori T et al. Loss of the autophagy protein Atg16L1 enhances endotoxin-induced IL-1beta production. Nature. 2008;456(7219):264-268.

Sakamoto S, Aoki K, Higuchi T, Todaka H, Morisawa K, Tamaki N, Hatano E, Fukushima A, Taniguchi T, Agata Y. The NF90-NF45 complex functions as a negative regulator in the microRNA processing pathway. Mol Cell Biol. 2009;29(13):3754-3769.

Sambuy Y, De Angelis I, Ranaldi G, Scarino ML, Stammati A, Zucco F. The Caco-2 cell line as a model of the intestinal barrier: influence of cell and culture-related factors on Caco-2 cell functional characteristics. Cell Biol Toxicol. 2005;21(1):1-26.

Sánchez E, Laparra JM, Sanz Y. Discerning the role of Bacteroides fragilis in celiac disease pathogenesis. Appl Environ Microbiol. 2012;78(18):6507-6515.

Santambrogio L, Cuervo AM. Chasing the elusive mammalian microautophagy. Autophagy. 2011;7(6):652-654.

Sbalchiero E, Azzalin A, Palumbo S, Barbieri G, Arias A, Simonelli L, Ferretti L, Comincini S. Altered cellular distribution and sub-cellular sorting of doppel (Dpl) protein in human astrocytoma cell lines. Cell Oncol. 2008;30(4):337-347.

Schanen BC, Li X. Transcriptional regulation of mammalian miRNA genes. Genomics. 2011;97(1):1-6.

Scharl M, Rogler G. Inflammatory bowel disease: dysfunction of autophagy? Dig Dis. 2012;30 Suppl 3:12-19.

Schumann M, Richter JF, Wedell I, Moos V, Zimmermann-Kordmann M, Schneider T, Daum S, Zeitz M, Fromm M, Schulzke JD. Mechanisms of epithelial translocation of the alpha(2)-gliadin-33mer in coeliac sprue. Gut. 2008;57(6):747-754.

Schippa S, Iebba V, Barbato M, Di Nardo G, Totino V, Checchi MP, Longhi C, Maiella G, Cucchiara S, Conte MP. A distinctive 'microbial signature' in celiac pediatric patients. BMC Microbiol. 2010;10:175.

Schirru E, Jores RD, Congia M. Prudence is necessary in the application of the new ESPGHAN criteria for celiac disease omitting duodenal biopsy: a case report. Eur J Gastroenterol Hepatol. 2014;26(6):679-680.

Schuppan D, Pickert G, Ashfaq-Khan M, Zevallos V. Non-celiac wheat sensitivity: differential diagnosis, triggers and implications. Best Pract Res Clin Gastroenterol.

2015;29(3):469-476.

Sen GL, Blau HM. Argonaute 2/RISC resides in sites of mammalian mRNA decay known as cytoplasmic bodies. Nat Cell Biol. 2005;7(6):633-636.

Shan L, Molberg Ø, Parrot I, Hausch F, Filiz F, Gray GM, Sollid LM, Khosla C. Structural basis for gluten intolerance in celiac sprue. Science. 2002;297(5590):2275-2279.

Shang L, Chen S, Du F, Li S, Zhao L, Wang X. Nutrient starvation elicits an acute autophagic response mediated by Ulk1 dephosphorylation and its subsequent dissociation from AMPK. Proc Natl Acad Sci U S A. 2011;108(12):4788-4793.

Shi CS, Kehrl JH. Traf6 and A20 differentially regulate TLR4-induced autophagy by affecting the ubiquitination of Beclin 1. Autophagy. 2010;6(7):986-987.

Shi CS, Shenderov K, Huang NN, Kabat J, Abu-Asab M, Fitzgerald KA, Sher A, Kehrl JH. Activation of autophagy by inflammatory signals limits IL-1β production by targeting ubiquitinated inflammasomes for destruction. Nat Immunol. 2012;13(3):255-263.

Siegel M, Strnad P, Watts RE, Choi K, Jabri B, Omary MB, Khosla C. Extracellular transglutaminase 2 is catalytically inactive, but is transiently activated upon tissue injury. PLoS One. 2008;3(3):e1861.

Sollid LM, Thorsby E. HLA susceptibility genes in celiac disease: genetic mapping and role in pathogenesis. Gastroenterology. 1993;105(3):910-922.

Sollid LM, Markussen G, Ek J, Gjerde H, Vartdal F, Thorsby E. Evidence for a primary association of celiac disease to a particular HLA-DQ alpha/beta heterodimer. J Exp Med. 1989;169(1):345-350.

Stolz A, Ernst A, Dikic I. Cargo recognition and trafficking in selective autophagy. Nat Cell Biol. 2014;16(6):495-501.

Stoven S, Murray JA, Marietta EV. Latest in vitro and in vivo models of celiac disease. Expert Opin Drug Discov. 2013;8(4):445-457.

Sui X, Fang Y, Lou H, Wang K, Zheng Y, Lou F, Jin W, Xu Y, Chen W, Pan H, Wang X, Han W. p53 suppresses stress-induced cellular senescence via regulation of autophagy under the deprivation of serum. Mol Med Rep. 2015;11(2):1214-1220.

Takamizawa J, Konishi H, Yanagisawa K, Tomida S, Osada H, Endoh H, Harano T, Yatabe Y, Nagino M, Nimura Y, Mitsudomi T, Takahashi T. Reduced expression of the let-7 microRNAs in human lung cancers in association with shortened

postoperative survival. Cancer Res. 2004;64(11):3753-3756.

Tang D, Kang R, Livesey KM, Cheh CW, Farkas A, Loughran P, Hoppe G, Bianchi ME, Tracey KJ, Zeh HJ 3rd, Lotze MT. Endogenous HMGB1 regulates autophagy. J Cell Biol. 2010;190(5):881-892.

Thomson M, Tringali A, Landi R, Dumonceau JM, Tavares M, Amil-Dias J, Benninga M, Tabbers MM, Furlano R, Spaander M, Hassan C, Tzvinikos C, Ijsselstijn H, Viala J, Dall'Oglio L et al. Pediatric Gastrointestinal Endoscopy: European Society of Pediatric Gastroenterology Hepatology and Nutrition (ESPGHAN) and European Society of Gastrointestinal Endoscopy (ESGE) Guidelines. J Pediatr Gastroenterol Nutr. 2016.

Tokumaru S, Suzuki M, Yamada H, Nagino M, Takahashi T. let-7 regulates Dicer expression and constitutes a negative feedback loop. Carcinogenesis. 2008;29(11):2073-2077.

Tong J, Yan X, Yu L. The late stage of autophagy: cellular events and molecular regulation. Protein Cell. 2010;1(10):907-915.

Trabucchi M, Briata P, Garcia-Mayoral M, Haase AD, Filipowicz W, Ramos A, Gherzi R, Rosenfeld MG. The RNA-binding protein KSRP promotes the biogenesis of a subset of microRNAs. Nature. 2009;459(7249):1010-1014.

Tsukada M, Ohsumi Y. Isolation and characterization of autophagy-defective mutants of Saccharomyces cerevisiae. FEBS Lett. 1993;333(1-2):169-174.

Tsutsumi A, Kawamata T, Izumi N, Seitz H, Tomari Y. Recognition of the pre-miRNA structure by Drosophila Dicer-1. Nat Struct Mol Biol. 2011;18(10):1153-1158.

Tjon JM, van Bergen J, Koning F. Celiac disease: how complicated can it get? Immunogenetics. 2010;62(10):641-651.

Vader W, Stepniak D, Kooy Y, Mearin L, Thompson A, van Rood JJ, Spaenij L, Koning F. The HLA-DQ2 gene dose effect in celiac disease is directly related to the magnitude and breadth of gluten-specific T cell responses. Proc Natl Acad Sci U S A. 2003;100(21):12390-12395.

Vaira V, Roncoroni L, Barisani D, Gaudioso G, Bosari S, Bulfamante G, Doneda L, Conte D, Tomba C, Bardella MT, Ferrero S, Locatelli M, Elli L. microRNA profiles in coeliac patients distinguish different clinical phenotypes and are modulated by gliadin peptides in primary duodenal fibroblasts. Clin Sci (Lond). 2014;126(6):417-423.

Van Belzen MJ, Meijer JW, Sandkuijl LA, Bardoel AF, Mulder CJ, Pearson PL, Houwen RH, Wijmenga C. A major non-HLA locus in celiac disease maps to chromosome 19. Gastroenterology. 2003;125(4):1032-1041.

van Heel DA, Franke L, Hunt KA, Gwilliam R, Zhernakova A, Inouye M, Wapenaar MC, Barnardo MC, Bethel G, Holmes GK, Feighery C, Jewell D, Kelleher D, Kumar P, Travis S et al. A genome-wide association study for celiac disease identifies risk variants in the region harboring IL2 and IL21. Nat Genet. 2007;39(7):827-829.

van Rooij E, Marshall WS, Olson EN. Toward microRNA-based therapeutics for heart disease: the sense in antisense. Circ Res. 2008;103(9):919-928.

Verdu EF, Galipeau HJ, Jabri B. Novel players in coeliac disease pathogenesis: role of the gut microbiota. Nat Rev Gastroenterol Hepatol. 2015;12(9):497-506.

Vilppula A, Collin P, Mäki M, Valve R, Luostarinen M, Krekelä I, Patrikainen H, Kaukinen K, Luostarinen L. Undetected coeliac disease in the elderly: a biopsy-proven population-based study. Dig Liver Dis. 2008; 40(10):809-813.

Vilppula A, Kaukinen K, Luostarinen L, Krekelä I, Patrikainen H, Valve R, Mäki M, Collin P. Increasing prevalence and high incidence of celiac disease in elderly people: a population-based study. BMC Gastroenterol. 2009;9:49.

Wang J, Chen J, Sen S. MicroRNA as Biomarkers and Diagnostics. J Cell Physiol. 2016;231(1):25-30.

Wang J, Yu JT, Tan L, Tian Y, Ma J, Tan CC, Wang HF, Liu Y, Tan MS, Jiang T, Tan L. Genome-wide circulating microRNA expression profiling indicates biomarkers for epilepsy. Sci Rep. 2015;5:9522.

Wieser H. Chemistry of gluten proteins. Food Microbiol. 2007;24(2):115-119.

Wieser H. Relation between gliadin structure and coeliac toxicity. Acta Paediatr Suppl. 1996;412:3-9.

Wilson EN, Bristol ML, Di X, Maltese WA, Koterba K, Beckman MJ, Gewirtz DA. A switch between cytoprotective and cytotoxic autophagy in the radiosensitization of breast tumor cells by chloroquine and vitamin D. Horm Cancer. 2011;2(5):272-285.

Winslow AR, Chen CW, Corrochano S, Acevedo-Arozena A, Gordon DE, Peden AA, Lichtenberg M, Menzies FM, Ravikumar B, Imarisio S, Brown S, O'Kane CJ, Rubinsztin DC. α-Synuclein impairs macroautophagy: implications for Parkinson's disease. J Cell Biol. 2010;190(6):1023-1037.

Wirawan E, Vanden Berghe T, Lippens S, Agostinis P, Vandenabeele P. Autophagy: for better or for worse. Cell Res. 2012;22(1):43-61.

Wu F, Zhang S, Dassopoulos T, Harris ML, Bayless TM, Meltzer SJ, Brant SR, Kwon JH. Identification of microRNAs associated with ileal and colonic Crohn's disease. Inflamm Bowel Dis. 2010;16(10):1729-1738.

Yang Z, Huang J, Geng J, Nair U, Klionsky DJ. Atg22 recycles amino acids to link the degradative and recycling functions of autophagy. Mol Biol Cell. 2006;17(12):5094-5104.

Yu WH, Cuervo AM, Kumar A, Peterhoff CM, Schmidt SD, Lee JH, Mohan PS, Mercken M, Farmery MR, Tjernberg LO, Jiang Y, Duff K, Uchiyama Y, Näslund J, Mathews PM et al. Macroautophagy--a novel Beta-amyloid peptide-generating pathway activated in Alzheimer's disease. J Cell Biol. 2005;171(1):87-98.

Zahm AM, Thayu M, Hand NJ, Horner A, Leonard MB, Friedman JR. Circulating microRNA is a biomarker of pediatric Crohn disease. J Pediatr Gastroenterol Nutr. 2011;53(1):26-33.

Zalckvar E, Berissi H, Mizrachy L, Idelchuk Y, Koren I, Eisenstein M, Sabanay H, Pinkas-Kramarski R, Kimchi A. DAP-kinase-mediated phosphorylation on the BH3 domain of beclin 1 promotes dissociation of beclin 1 from Bcl-XL and induction of autophagy. EMBO Rep. 2009;10(3):285-292.

Zanotto-Filho A, Braganhol E, Klafke K, Figueiró F, Terra SR, Paludo FJ, Morrone M, Bristot IJ, Battastini AM, Forcelini CM, Bishop AJ, Gelain DP, Moreira JC. Autophagy inhibition improves the efficacy of curcumin/temozolomide combination therapy in glioblastomas. Cancer Lett. 2015;358(2):220-131.

Zhang J, Li S, Li L, Li M, Guo C, Yao J, Mi S. Exosome and exosomal microRNA: trafficking, sorting, and function. Genomics Proteomics Bioinformatics. 2015;13(1):17-24.

Zhang H, Kolb FA, Jaskiewicz L, Westhof E, Filipowicz W. Single processing center models for human Dicer and bacterial RNase III. Cell. 2004;118(1):57-68.

Zeng Y, Sankala H, Zhang X, Graves PR. Phosphorylation of Argonaute 2 at serine-387 facilitates its localization to processing bodies. Biochem J. 2008;413(3):429-436.

Zeng X, Overmeyer JH, Maltese WA. Functional specificity of the mammalian Beclin-Vps34 PI 3-kinase complex in macroautophagy versus endocytosis and lysosomal enzyme trafficking. J Cell Sci. 2006;119(Pt 2):259-270.

Zhao Y, Yang J, Liao W, Liu X, Zhang H, Wang S, Wang D, Feng J, Yu L, Zhu WG. Cytosolic FoxO1 is essential for the induction of autophagy and tumour suppressor activity. Nat Cell Biol. 2010;12(7):665-675.

Zhao ZQ, Yu ZY, Li J, Ouyang XN. Gefitinib induces lung cancer cell autophagy and apoptosis via blockade of the PI3K/AKT/mTOR pathway. Oncol Lett. 2016;12(1):63-68.

Zhu H, Wu H, Liu X, Li B, Chen Y, Ren X, Liu CG, Yang JM. Regulation of autophagy by a beclin 1-targeted microRNA, miR-30a, in cancer cells. Autophagy. 2009;5(6):816-823.

Zimmer KP, Fischer I, Mothes T, Weissen-Plenz G, Schmitz M, Wieser H, Büning J, Lerch MM, Ciclitira PC, Weber P, Naim HY. Endocytotic segregation of gliadin peptide 31-49 in enterocytes. Gut. 2010;59(3):300-310.

Zimmermann C, Rudloff S, Lochnit G, Arampatzi S, Maison W, Zimmer KP. Epithelial transport of immunogenic and toxic gliadin peptides in vitro. PLoS One. 2014;9(11):e113932.

Collaborations

During the PhD period I have collaborated on three projects which involved the Oncogenomics laboratory group. Two of these projects concerned the modulation of autophagy as a therapeutic approach for glioblastoma and Alzheimer's disease (AD). Particularly, these projects were focused on glioblastoma therapy and on the treatment of AD with low-frequency electomagnetic fields (LF-EMF). In the last project a genetic association between SNPs in the oxytocin receptor gene (*OXTR*) and congenital prosopagnosia (CP) was investigated. In this section a description of the results of the AD project is reported. The other two projects are described by the relative publications in the next section.

A Low-Frequency Electromagnetic (LF-EMF) Exposure Scheme Induces Autophagy Activation to Counteract in Vitro β-Amyloid Neurotoxicity

This project was in collaboration with the Department of Industrial and Information Engineering, the Department of Drug Sciences – Section of Pharmacology and the IDR "Santa Margherita" – Department of Internal Medicine and Therapeutics – Section of Geriatrics and Gerontology.

The aim of this research was to clarify how a specific LF-EMF treatment induces autophagy leading to Aβ peptides degradation, thus increasing cell viability. In our laboratory it was demonstrated that LF-EMF treatments can modulate *in vitro* the expression of Beclin 1 through a significant reduction of his negative regulator miR-30a (Marchesi *et al.* 2014). The human neuroblastoma cell line SHSY5Y in presence of Aβ(1-40) or Aβ(1-42) was used as AD model. Cells were exposed for 1 hour to LF-EMF generated by a bioreactor consisted of a carrying structure custom-machined in a tube of polymethylmethacrylate. The tube carried two parallel solenoids that generated an EMF with 2 ± 0.2 mT of intensity, 75 ± 2 Hz of frequency and pulse duration of 1.3 ms. Firstly, toxic effects of Aβ peptides were confirmed through MTT assays (data not shown) and cells were visualized using an inverted fluorescence microscope because Aβ is autofluorescent at 300 nm. As reported in **Figure A**, Aβ(1-40) generated intracellular round-

shaped aggregates 24 hours after the administration of the peptide.

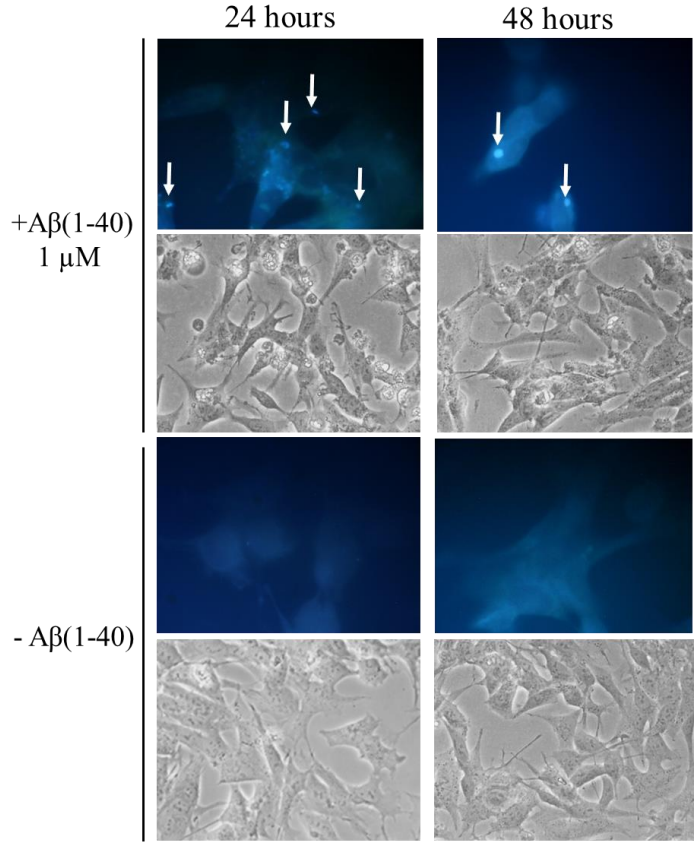

Figure A: Aβ(1-40) aggregates after 24 and 48 hours (white arrows).

Subsequently, it was demonstrated that LF-EMF treatment after Aβ administration induces the clearance of the peptides (**Figure B**). As reported, 4 hours p.t. Aβ was entirely localized on the plasma membrane of the cells, suggesting that the process of internalization was still ongoing. After 24 p.t. round-shaped aggregates were detected in the cytoplasm of SHSY5Y cells and their number was higher compared with untreated cells, suggesting that the exposure to LF-EMF enhanced the aggregation of Aβ in vesicular structure. These intracellular Aβ deposits were cleared after 48 p.t. compared with untreated cells, which showed large vesicular aggregates. Same results were obtained pre-treating cells with LF-EMF 4 hours before

Aβ administration.

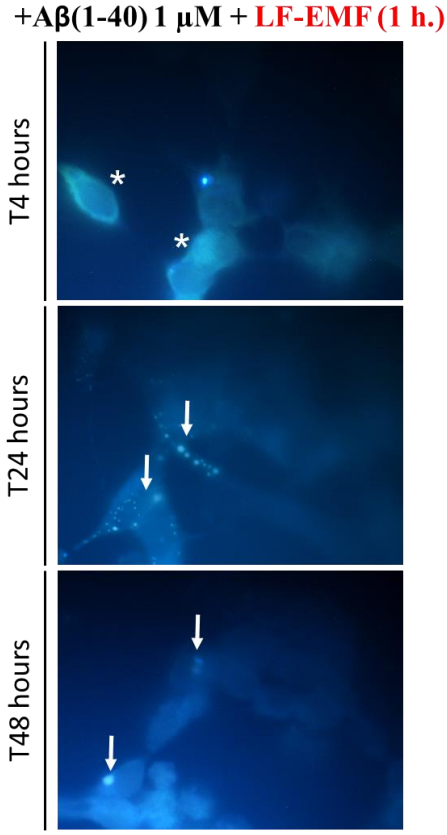

Figure B: Aβ(1-40) clearance after LF-EMF treatment. White asterisks highlight the internalization of the peptide. White arrows indicate intracellular aggregates. Same results were obtained with Aβ(1-42).

These evidence suggested that LF-EMF exposure promoted Aβ metabolism through internalization of the peptide in vesicles. According to the perspective of future application, our attention was focused on LF-EMF pre-treatment. In order to understand the nature of these vesicular aggregates and the mechanisms of Aβ degradation, Hydrolyte Fluor 388 Aβ(1-42) and the Lysotracker probe were used 4 hours after LF-EMF pre-treatment. Hydrolyte Fluor 388 is a fluorophore labeled β-amyloid peptide that emitted in the green when excited at 388 nm, while Lysotracker is a fluorescent probe that stained in red acidic organelles, such as lysosomes, at 584 nm.

Results visualized 24 hours after LF-EMF pre-treatment (**Figure C**) showed co-localization of Aβ aggregates with acidic vesicles compared with untrated cells.

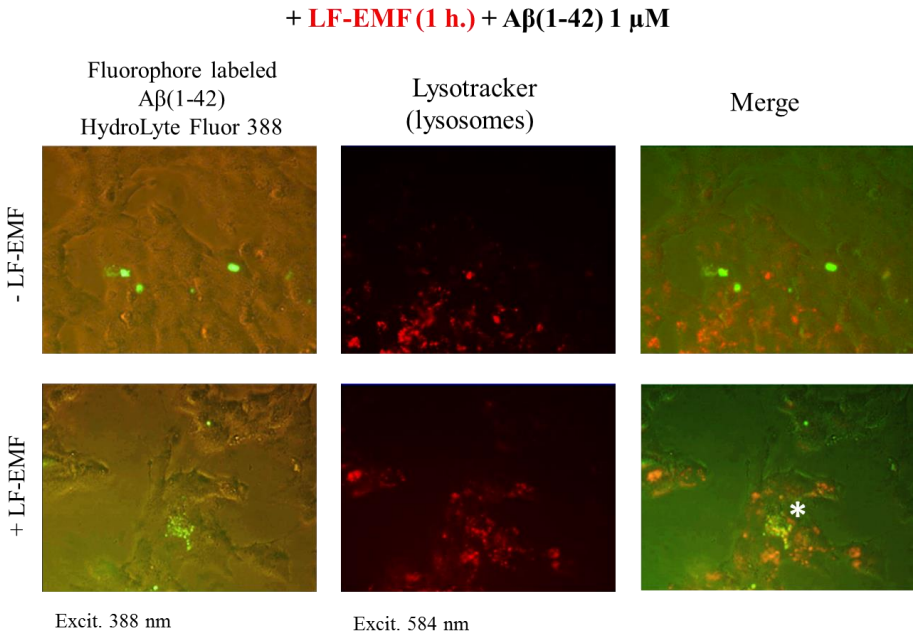

Figure C: Co-localization of Aβ aggregates with acidic vesicles. White asterisk highlights the area of co-localization.

According to the findings that EMF exposure leads to an increased expression of Beclin 1, autophagomes induction was monitored in living cells by transduction with a baculovirus expressing LC3B-GFP, known to be localized in correspondence of nascent membranes of the autophagosomes. Both baculovirus and Aβ were administered to cells 4 hours after the activation of Aβ metabolism through LF-EMF pre-exposure and visualization occurred 24 hours p.t.

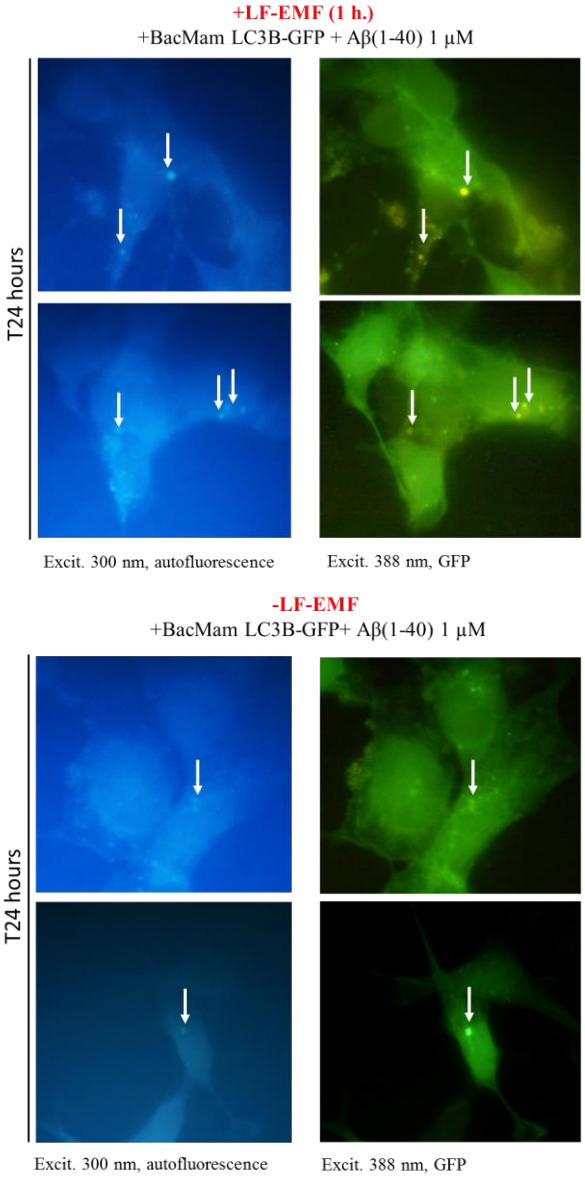

Figure D: Co-localization of autophagosomes and Aβ(1-40) aggregates through the use of baculovirus expressing LC3B-GFP. White arrows indicate the vesicles. The upper panel refers to LF-EMF treated cells while the lower panel to untreated cells. Same results obtained for Aβ(1-42).

As evidenced by the results (**Figure D**), LF-EMF treatment increased the levels of autophagic vesicles that co-localized with intracellular Aβ aggregates (upper panel) compared with untreated cells (lower panel). All the findings suggested that LF-EMF exposure promoted Aβ degradation increasing the levels of autophagy, which is impaired in AD. Moreover, it seemed that the treatment could be perform before or after Aβ administration without differences in the induction levels of autophagy. In order to quantify the beneficial effects of LF-EMF exposure to cell viability, a 24 hours MTT assay was performed on SHSY5Y cells treated with Aβ(1-40) or both Aβ(1-40) and Aβ(1-42).

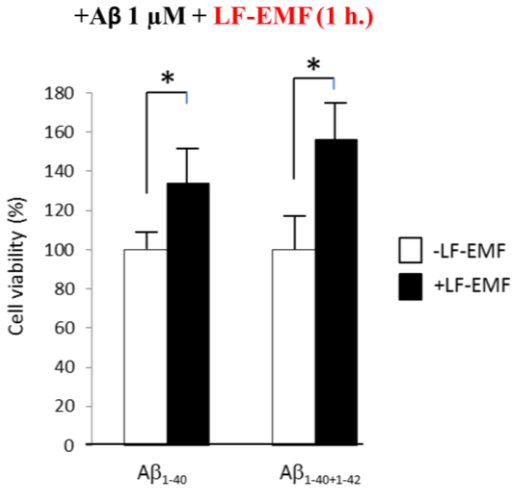

Figure E: MTT assay performed on cells treated with Aβ(1-40) or with the combination of both the peptides. Bars indicate SD. Asterisks indicate statistical significant differences (ANOVA, One-way, P<0.0001).

As reported in **Figure E**, LF-EMF treatment improved cell viability thus confirming that the induction of autophagy was able to degrade Aβ peptides counteracting their toxic effects. The same experiment was perfomed testing the pre-exposure and the post-exposure schemes in order to study differences in cell viability.

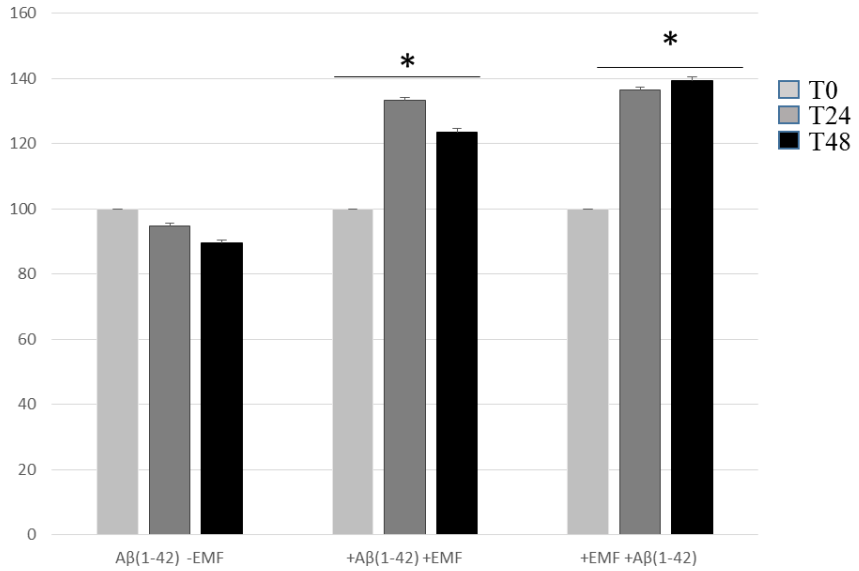

Figure F: MTT assay perfomed on both the exposure schemes. Bars indicate SD. Asterisks indicate statistical significant differences (ANOVA, One-way, P<0.0001).

The MTT assay showed that both LF-EMF treatments significantly increased of ~40% cells viability from 24 to 48 hours after the exposure compared with T0 (**Figure F**). Moreover, at T48 LF-EMF pre-exposure scheme resulted to be more effective in counteracting Aβ toxicity, leading to a difference of ~16% compared with LF-EMF post-treatment (data not shown). Furthermore, it was demonstrated that both the exposure schemes reduce serial cell-to-cell Aβ toxicity. These experiments were conducted using the fluorophore labelled TAMRA Aβ(1-42), which emits in red when excited at 584 nm. Particularly, cells treated with a condition medium derived from another experiment and containing TAMRA Aβ(1-42) showed severe morphological alterations and the presence of Aβ fibrils. On the other hand cells treated with a condition medium derived by a cell culture previously exposed to LF-EMF and containing TAMRA Aβ(1-42) preserved a good morphology, an increasing in cell viability and the presence of autophagic vesicles (**Figure G**).

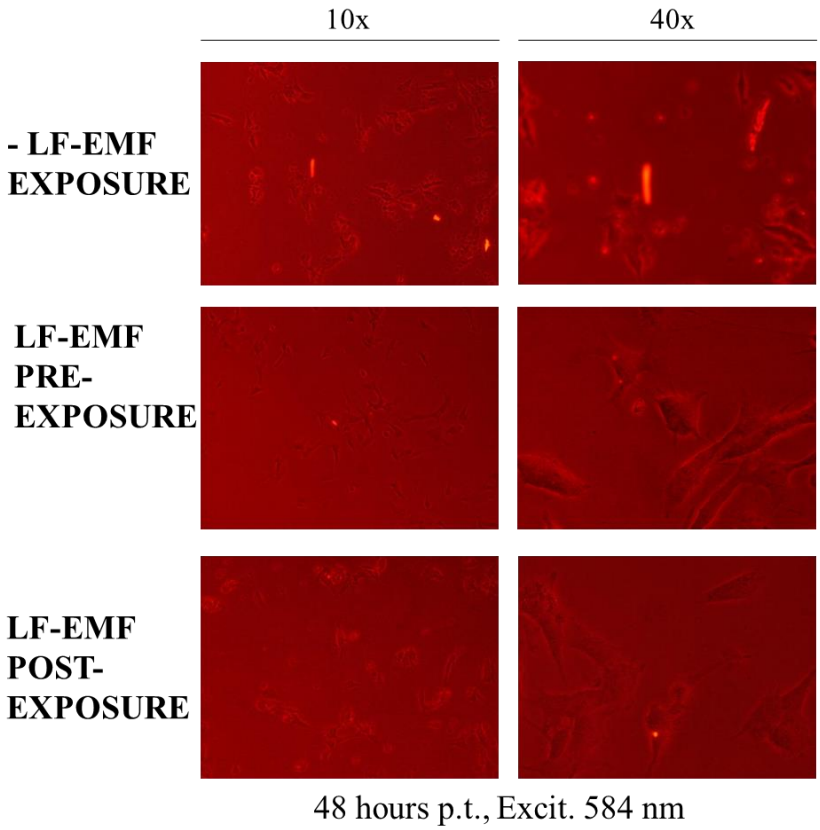

Figure G: Evaluation of cell-to-cell toxicity reduction of Aβ(1-42) due to both the LF-EMF exposure schemes. Visualization was performed after 48 hours the administration of the conditioned medium through an inverted fluorescent microscope.

Consistent with previous results, this study assesses that LF-EMF exposure directs Aβ(1-40) and Aβ(1-42) aggregates into autophagic vesicles leading to the degradation of these peptides thus counteracting their toxic effect and increasing cell viability. Moreover, LF-EMF exposure promotes autophagy induction and different LF-EMF protocols significantly increase cells viability and Aβ intracellular turn-over, reducing also Aβ cell-to-cell toxicity.

List of original manuscripts

Palumbo S, Tini P, Toscano M, Allavena G, Angeletti F, Manai F, Miracco C, Comincini S, Pirtoli L. Combined EGFR and autophagy modulation impairs cell migration and enhances radiosensitivity in human glioblastoma cells. J Cell Physiol. 2014;229(11):1863-1873.

Pdf is reported below

Cattaneo Z, Daini R, Malaspina M, Manai F, Lillo M, Fermi V, Schiavi S, Suchan B, Comincini S. Congenital prosopagnosia is associated to a genetic variation in the oxytocin receptor (OXTR) gene: an exploratory study. Neuroscience. 2016. pii: S0306-4522(16)30487-0.

Pdf is reported below

ORIGINAL RESEARCH ARTICLE

1863

Journal of Cellular Physiology

Combined EGFR and Autophagy Modulation Impairs Cell Migration and Enhances Radiosensitivity in Human Glioblastoma Cells

SILVIA PALUMBO,[1]* PAOLO TINI,[2] MARZIA TOSCANO,[2] GIULIA ALLAVENA,[4] FRANCESCA ANGELETTI,[1] FEDERICO MANAI,[1] CLELIA MIRACCO,[3,5] SERGIO COMINCINI,[1] AND LUIGI PIRTOLI[2,3]

[1]Department of Biology and Biotechnology, University of Pavia, Pavia, Italy

[2]Department of Medicine, Surgery and Neuroscience (Radiotherapy Unit), University Hospital of Siena, Siena, Italy

[3]Istituto Toscano Tumori, Florence, Italy

[4]Department of Molecular and Developmental Biology, University of Siena, Siena, Italy

[5]Department of Medicine, Surgery and Neuroscience (Pathological Anatomy Unit), University Hospital of Siena, Siena, Italy

Glioblastoma (GBM) remains the most aggressive and lethal brain tumor due to its molecular heterogeneity and high motility and invasion capabilities of its cells, resulting in high resistance to current standard treatments (surgery, followed by ionizing radiation combined with Temozolomide chemotherapy administration). Locus amplification, gene overexpression, and genetic mutations of epidermal growth factor receptor (*EGFR*) are hallmarks of GBM that can ectopically activate downstream signaling oncogenic cascades such as PI3K/Akt/mTOR pathway. Importantly, alteration of this pathway, involved also in the regulation of autophagy process, can improve radioresistance in GBM cells, thus promoting the aggressive phenotype of this tumor. In this work, the endogenous EGFR expression profile and autophagy were modulated to increase radiosensitivity behavior of human T98G and U373MG GBM cells. Our results primarily indicated that *EGFR* interfering induced radiosensitivity according to a decrease of the clonogenic capability of the investigated cells, and an effective reduction of the in vitro migratory features. Moreover, *EGFR* interfering resulted in an increase of Temozolomide (TMZ) cytotoxicity in T98G TMZ-resistant cells. In order to elucidate the involvement of the autophagy process as pro-death or pro-survival role in cells subjected to *EGFR* interfering, the key autophagic gene *ATG7* was silenced, thereby producing a transient block of the autophagy process. This autophagy inhibition rescued clonogenic capability of irradiated and *EGFR*-silenced T98G cells, suggesting a pro-death autophagy contribution. To further confirm the functional interplay between EGFR and autophagy pathways, Rapamycin-mediated autophagy induction during *EGFR* modulation promoted further impairment of irradiated cells, in terms of clonogenic and migration capabilities. Taken together, these results might suggest a novel combined EGFR-autophagy modulation strategy, to overcome intrinsic GBM radioresistance, thus improving the efficacy of standard treatments.

J. Cell. Physiol. 229: 1863–1873, 2014.

The epidermal growth factor receptor (EGFR) is the cell-surface receptor for members of the epidermal growth factor family (EGF-family) of extracellular protein ligands (Herbst, 2004). EGFR signaling promotes multiple physiological processes, and contributes to uncontrolled cell proliferation, cell invasiveness, and angiogenesis in cancer (Lynch et al., 2004). Mutations involving *EGFR*, leading to its constant activation, are a major driver for tumorigenesis and have been identified in many cancer types (Lynch et al., 2004; Mitsudomi and Yatabe, 2010). Amplification, overexpression, and mutation of *EGFR* are a hallmark of glioblastoma (GBM), being found in about 50% of cases (Chakravarti et al., 2004). The most frequent mutant of *EGFR*, expressed in about 30% of GBM, is the EGFR variant III (EGFRvIII). Playing a key role in GBM genesis and progression, the RAS-RAF-MEK-ERK-MAPK and PI3K-Akt-mTOR pathways are among the major effectors of activated *EGFR* (Narita et al., 2002; Ciardiello and Tortora, 2008).

Moreover, EGFR signaling induces phosphorylation of STAT3, Erk1/2, and Akt in GBM cells (Zhu et al., 2009) promoting aberrant PI3K/Akt/mTOR signaling and elevated STAT3 activation, which contributes significantly to GBM cell proliferation and survival. The EGFR signaling network thus represents an attractive domain to be addressed by research on GBM therapy, and a considerable effort is focused to

The authors declared that they have no conflict of interest.

Contract grant sponsor: PRIN 2008-2009.

*Correspondence to: Silvia Palumbo, Department of Biology and Biotechnology, University of Pavia, Via Ferrata 1, 27100 Pavia, Italy. E-mail: silvia.palumbo@unipv.it

Manuscript Received: 16 December 2013
Manuscript Accepted: 28 March 2014

Accepted manuscript online in Wiley Online Library (wileyonlinelibrary.com): 1 April 2014.
DOI: 10.1002/jcp.24640

inhibit the receptor using antibodies, tyrosine kinase inhibitors (TKIs), or vaccines (Mendelsohn and Baselga, 2000; Heimberger et al., 2003). The subject of TKIs in the clinical setting has been largely addressed by prospective trials with unsatisfactory results, consisting of response rates between 10% and 20%, across a variety of human malignancies (Fukuoka et al., 2002; Kris et al., 2002; Cohen et al., 2003; Dancey and Freidlin, 2003). To this reason, researchers have been focusing their efforts to overcome these hurdles, improving the treatment of GBM beyond the present standard of care, consisting of post-surgical concurrent irradiation (IR) and Temozolomide (TMZ), followed by adjuvant TMZ (Omuro and DeAngelis, 2013). Autophagy, known as "type II programmed cell-death," has been recognized as related to a major type of non-apoptotic death in GBM, both in vivo (Sarkaria et al., 2011) and in vitro (Barbieri et al., 2011; Palumbo et al., 2012), occurring either spontaneously or induced by radio- and chemotherapy (including TMZ), (Kanzawa et al., 2004; Zhuang et al., 2009). Autophagy is a complex process responsible for degrading long-lived proteins and cytoplasmic organelles, the products of which are recycled to generate macromolecules and ATP, crucial in maintaining cellular homeostasis (Levine and Klionsky, 2004). Although these metabolic features makes autophagy an effective mechanism for cell survival, several recent studies suggested that the stress-induced exacerbation of this process may also lead to a pro-death shift of the cellular fate (Nelson and White, 2004; Wang et al., 2005). Importantly, signaling pathways activated by EGFR and other receptor tyrosine *kinases* (RTKs), the downstream effectors of which converge to PI3K/Akt/mTOR pathway, are strictly involved in the regulation of autophagy, indicating a potential link between the activity of cell surface receptors and a specific activation of the endogenous autophagy process.

In this study, the interplay between EGFR pathway and autophagy has been investigated in two human GBM cell lines, namely T98G and U373MG. We here report that autophagy may act as a pro-death process following *EGFR* interfering, thus sensitizing these cells to subsequent IR or TMZ treatments. Autophagy inhibition decreased the effect of combined IR and *EGFR* interfering, and contrarily Rapamycin-mediated autophagy induction was able to enhance the effect of combined EGFR/IR treatment.

Materials and Methods

Cell cultures

T98G and U373MG established human GBM cell lines (provided by ECACC) were cultivated in D-MEM medium supplemented with 10% FBS, 100 U/ml penicillin, 0.1 mg/ml streptomycin and 1% L-glutamine (Invitrogen), at 37°C and 5% CO_2 atmosphere.

EGFR silencing

To inhibit expression of EGFR gene, a pool of specific siRNAs was provided by Riboxx and transfected using NEON Transfection System (Invitrogen, Carlsbad, CA). In details, 4×10^5 cells were transfected with a 100 µl-tip at 1 µM concentration of siRNA pool, or with mock transfection buffer alone. After electroporation, cells were seeded into cell culture six-well plates and incubated for at least 48 h before additional treatments.

IR treatment

For IR treatment, cells were seeded into six-well plates, subsequently placed in a water phantom for dose homogeneity as previously reported (Palumbo et al., 2012). Cells were irradiated with a 6-MV X-ray linear accelerator (Varian, Clinac 600, Palo Alto, CA) at a dose-rate of 244.5 cGy/min, with a dose of 2 Gy.

TMZ treatment

TMZ (Schering-Plough) was employed as a chemotherapeutic agent, resuspended in DMSO. For experiments using TMZ, cells were seeded into cell culture six-well plates, and after 24 h TMZ was added at the concentration of 100 µM, as already documented (Palumbo et al., 2012).

Clonogenic assay

To evaluate re-plating efficiency, clonogenic assay was performed as previously described (Palumbo et al., 2012). Briefly, 24 h before experiment, cells were seeded into 30 mm^2 culture dishes (10^3 cells per dish). After each treatment, cells were incubated two weeks at 37°C, then fixed with ethanol and stained with 0.5% Crystal Violet (Sigma). Colonies that contained more than 50 cells were counted using clono-counter software (http://www.ansci.wisc.edu/equine/parrish/index.html); the clonogenic capability was calculated as a ratio between treated counted clones and the corresponding control plate. Each experiment was performed in triplicate.

Scratch-wound assay

To evaluate cell migration capability, a scratch-wound or migration assay was performed in both T98G and U373MG cells, as documented (Cory, 2011). In detail, cells were seeded into 24-well plates at high cellular density, and immediately after each treatment, a scratch-wound was performed in the middle of the well, using a 200 µl-tip. Light optical microscopy photographs (Nikon, Eclipse TS100) were collected at different times after scratch-wound performing. Cell migration (in µm) was calculated measuring the scratch-wound area immediately after its performing and during the analyzed time. Percentage of cell migration was obtained dividing the cell migration of each sample, collected at 24 (T24) and at 72 hours (T72) by the cell migration of the MOCK untreated sample at T72 (corresponding to the completely scratch-wound closing).

Autophagy inhibition

To inhibit the autophagy process, a knockdown of the autophagic gene *ATG7* was performed using specific siRNAs pools (Riboxx), transfected by NEON Transfection System (Invitrogen). In details, 4×10^5 cells were transfected using a 100 µl-tip with 600 nM of siRNA ATG7, or with mock transfection buffer alone. When autophagy inhibition was combined with *EGFR* silencing, both specific siRNAs pools, at the corresponding concentrations, were co-transfected into the cells. After electroporation, cells were seeded into cell culture 6-well plates and incubated for 48 h, before IR treatment.

Rapamycin-mediated autophagy induction

Autophagy induction was carried out adding Rapamycin (Sigma), resuspended in DMSO, at different concentrations (5–10 µM) to the cultured cells. Cells were further incubated for 24 h according to previously established protocols (Takeuchi et al., 2005).

Immunoblotting analysis

Immunoblotting was employed to evaluate protein expression of analyzed markers. Before loading in SDS–PAGE, protein extracts were quantified using Quantit-IT Protein Assay Kit

(Invitrogen). Proteins were then boiled in Laemmli sample buffer (2% SDS, 6% glycerol, 150 mM B-mercaptoethanol, 0.02% bromophenol blue and Tris–HCl pH 6.8 62.5 mM) and denatured for 5′ at 95°C. SDS–PAGE gels were used to separate proteins by size in the presence of electric current. Gels were run in running buffer (TrisOH pH 8.3 25 mM, Glycine 192 mM, SDS 1%) at 90V for 3 h. After electrophoresis, proteins were transferred onto nitro-cellulose membrane Hybond-C Extra (GE Healthcare), using the semi-dry blotters TE70 PWR (GE Healthcare, Sciences, UK). Transfer was performed at 60 mA for 1 h and 15′, in presence of transfer buffer (25 mM TrisOH pH 8.3, 192 mM Glycine, Methanol 20%, v/v). Membranes were blocked 1 h with 8% non-fat milk in TBS (138 mM NaCl, 20 mM TrisOH pH 7.6) containing 0.1% Tween-20 and incubated over-night at 4°C with primary antibodies. The following primary antibodies were employed: EGFR, Atg-7,

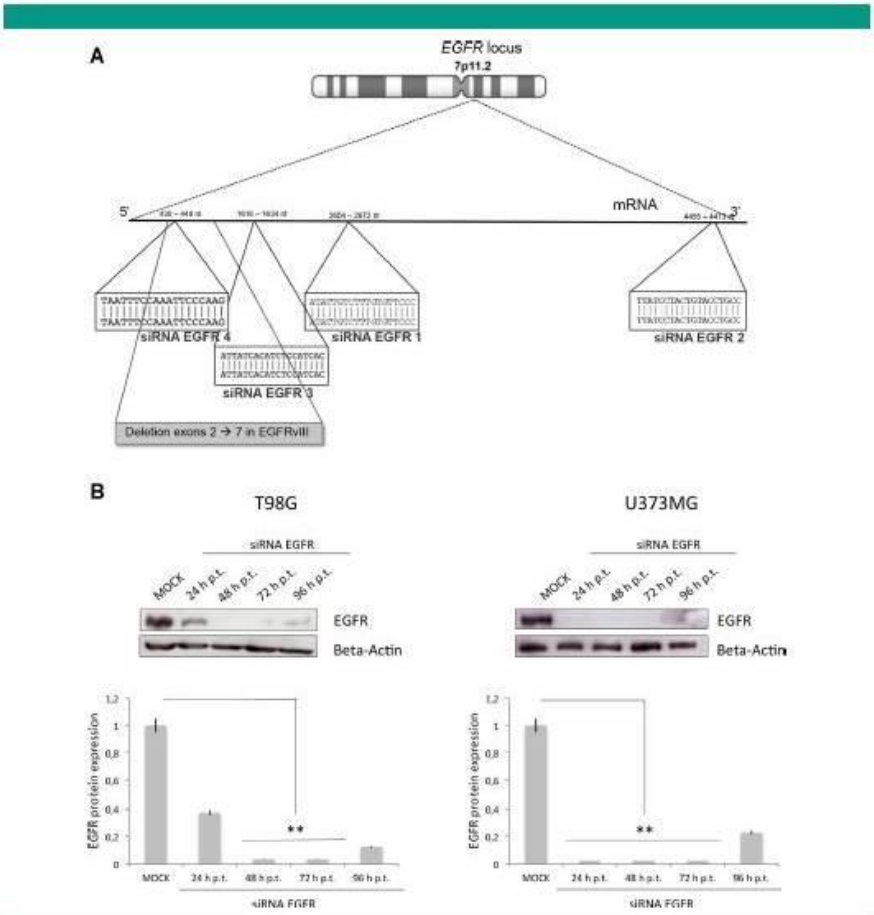

Fig. 1. *EGFR* silencing by siRNA transfection in T98G and U373MG cells. A: Localization of the single siRNA EGFR molecules along human *EGFR* transcript. B: EGFR protein expression in T98G and U373MG cells. A pool of siRNAs EGFR (1 μM) was transfected and EGFR protein expression was assayed at 24, 48, 72, 96 h p.t. For densitometric analysis, EGFR expression was normalized with β-actin (ImageJ software) and referred to the expression of not transfected (MOCK) cells. Normalized protein expression is reported in the histogram as average of three independent experiments (**$P < 0.01$).

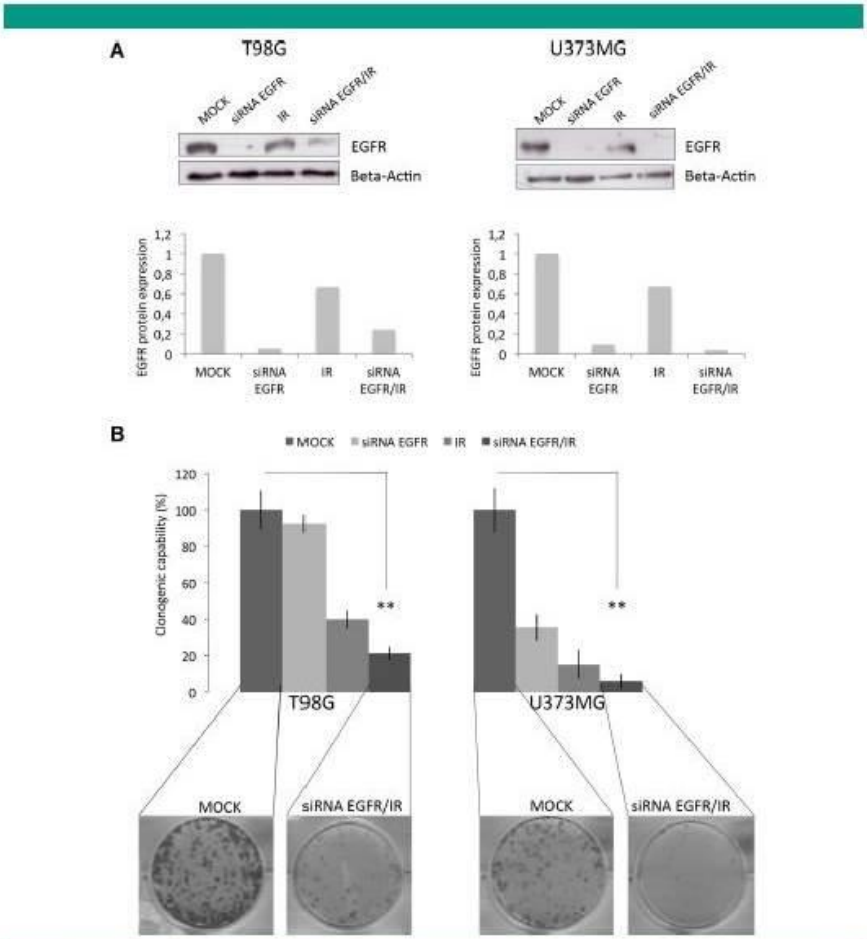

Fig. 2. Effect of IR on clonogenic capability after *EGFR* silencing in T98G and U373MG cells. A: Expression immunoblotting analysis of EGFR expression after *EGFR* silencing and IR treatment. A pool of EGFR siRNAs (1 μM) was transfected and after 48 h, cells were exposed to IR (2 Gy). EGFR expression was evaluated after additional 24 h. For densitometric analysis, protein expression was normalized with β-actin as above. **B:** Clonogenic capability after *EGFR* silencing and IR administration. Cells were transfected with a pool of siRNA EGFR (1 μM) and seeded for clonogenic assay. After 48 h, cells were exposed to IR (2 Gy). Clonogenic capability was calculated as described in the Materials and Methods Section, and reported as percentage into the graph. Results of three independent experiments are indicated with error bars. Light optical microscopy photographs of the different treatments (10× magnification) are reported (**$P < 0.01$).

Phospho-p70 S6 Kinase, p70 S6 Kinase, β-actin (Cell Signalling Technology, Beverley, MD). Species-specific peroxidase-labeled ECL secondary antibodies (GE Healthcare) were employed. Protein signals were revealed using the "ECL Advance Western Blotting Detection Kit" (GE Healthcare).

Statistical analysis

Statistical analysis was performed by ANOVA-one way for repeated measures, using SPSS 14.0 software. All *P* values lower than 0.05 were considered statistically significant.

Results

EGFR silencing in T98G and U373MG human GBM cell lines

Immunoblotting analysis showed that T98G and U373MG cells had constitutive EGFR protein expression, in particular that the former exhibited twofold higher expression compared with the latter (data not shown). Thus, to silence EGFR gene in both cell lines, a pool of siRNAs (siRNA EGFR) was transfected, as described in the Materials and Methods Section. This pool consists of four siRNAs, in identical stoichiometric amount, directed against different regions of *EGFR* transcript, as schematized in Figure 1A. Specifically, within this pool, siRNA EGFR4 is directed against a part of the region deleted in the EGFRvIII variant (exon skipping from 2 to 7). Both cell lines were firstly transfected with 1 μM of siRNA EGFR pool and, subsequently, EGFR protein expression was evaluated by immunoblotting at different post-transfection (p.t.) times (from 24 to 96 h p.t.). As reported in Figure 1B, EGFR expression was significantly decreased in both cell lines. As expected, at the longest p.t. time (i.e., 96 h) EGRF partially recovered its expression levels.

Effect of IR after *EGFR* silencing in T98G and U373MG human GBM cells

Next, cells were transfected with siRNA EGFR pool and, at 48 h p.t., irradiated with 2 Gy; after additional 48 h, EGFR protein expression was assayed by immunoblotting. As highlighted in Figure 2A, EGFR expression was almost completely abrogated in siRNA EGFR transfected cells, compared to the untreated samples; however, in T98G cells the effect of siRNA in *EGFR* silencing resulted less efficient when combined with IR treatment. Afterwards, the effect of the combined treatments (siRNA EGFR/IR) on long-term viability was evaluated in both cell lines by a clonogenic assay. A

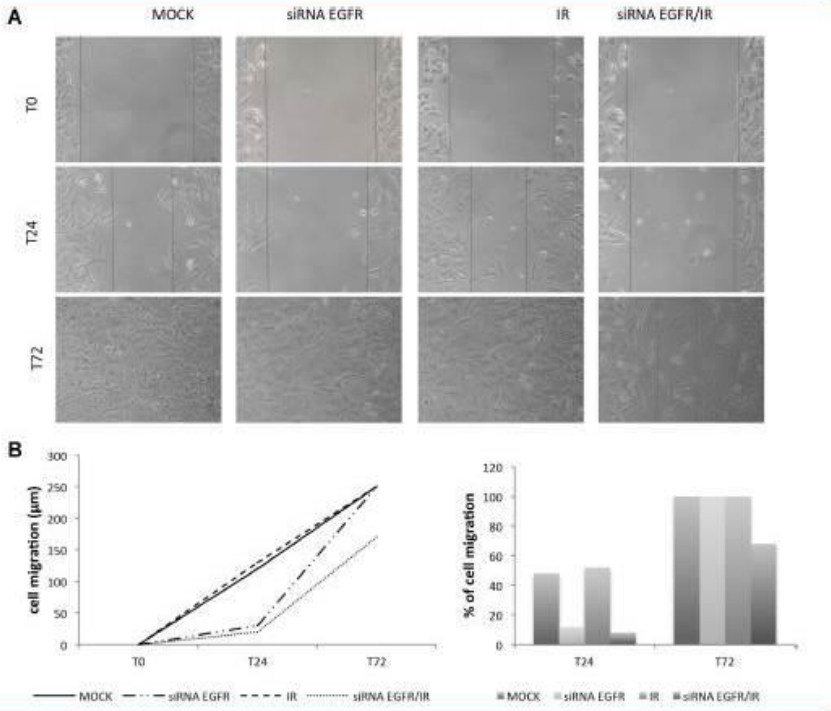

Fig. 3. Effect of IR on cell migration after *EGFR* silencing in T98G cells. A: Cells were transfected with a pool of siRNA EGFR (1 μM) and seeded for migration assay. After 48 h, cells were exposed to IR (2 Gy), and subjected to a scratch-wound assay. Light optical microscope photographs (10× magnification) were collected at different time after scratch-wound performing (T0, T24, T72). **B:** Cell migration rates expressed in micrometer, evaluated by measuring the area of the scratch-wound at the analyzed time (T0, T24, T72). **C:** Percentage of cell migration, as ratio of migrated cells on MOCK untreated sample at T72 (roughly corresponding to the completely scratch-wound closing).

significant decrease of clonogenic capability was detected in IR treated cells, and further in the combined treatment. Overall, U373MG resulted more sensitive to the combined treatment than T98G cells (Fig. 2B).

It was then evaluated how these treatments might interfere on tumor cell migration capabilities, by means of a scratch-wound assay, in T98G (Fig. 3) and in U373MG (Fig. 4) cells, in order to further explore the functional effects of *EGFR* interfering alone or combined with IR. Twenty-four hours after the beginning of migration assay (T24), *EGFR* silencing induced a marked decrease in cell migration rates, compared to MOCK and IR-treated cells, as highlighted from re-population of wound areas (Figs. 3–4, part A), measurement of migration rates (Figs. 3–4, part C) and percentage of cell migration (Figs. 3–4, part C). Interestingly, in T98G cells, 72 h after scratch-wound performing, the combined siRNA EGFR/IR treatment resulted in a significant time-extended impaired migration.

Effect of TMZ after *EGFR* silencing in the TMZ-resistant T98G human GBM cell line

The effect of TMZ was tested in the TMZ-resistant T98G cell line (Kanzawa et al., 2004) after *EGFR* silencing. TMZ was added to the culture 24 h after siRNA EGFR transfection, at the final concentration of 100 μM; 48 h after TMZ administration, cells were assessed for EGFR protein expression. As a result, EGFR protein expression was highly down-regulated after siRNA EGFR transfection, also in combination with TMZ treatment; differently, TMZ alone did not influence EGFR expression (Suppl. Fig. S1A). Importantly, as shown in Suppl. Figure S1B, clonogenic capability of TMZ-treated T98G cells resulted

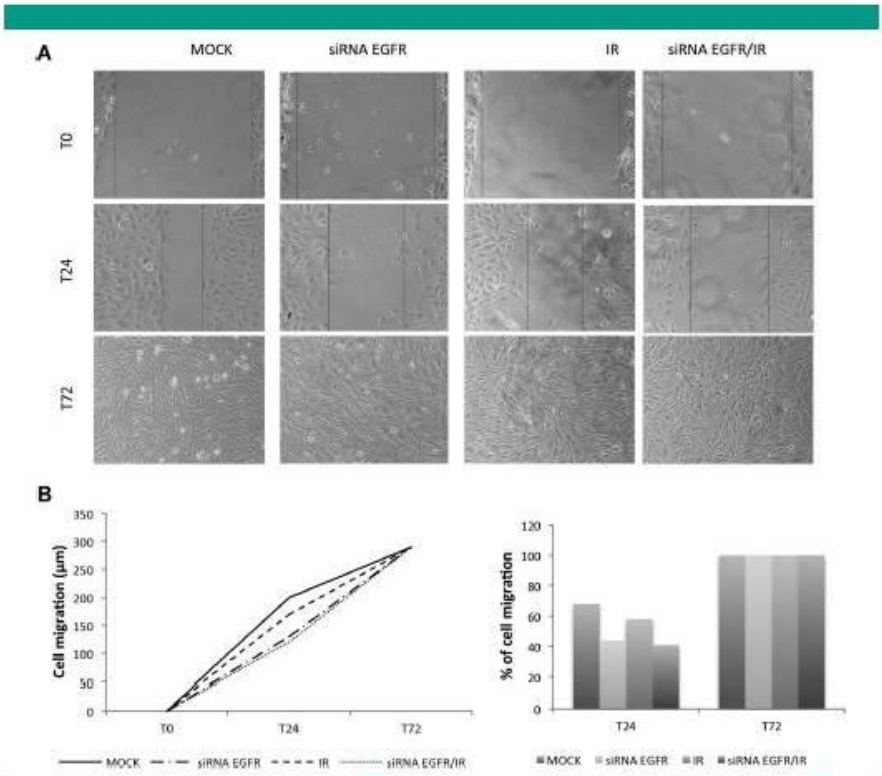

Fig. 4. Effect of IR on cell migration after *EGFR* silencing in U373MG cells. A: Cells were transfected with a pool of siRNA EGFR (1 μM) and seeded for migration assay. After 48 h, cells were exposed to IR (2 Gy), and subjected to a scratch-wound assay. Light optical microscopy photographs of the different treatments (10× magnification) were reported. B: Cell migration rates expressed in micrometer, evaluated measuring the area of the scratch-wound at the analyzed time (T0, T24, T72). C: Percentage of cell migration, as ratio of migrated cells to MOCK untreated sample at T72 (roughly corresponding to the completely scratch-wound closing).

significantly decreased after *EGFR* silencing (32.1% of clonogenic capability, compared to the control sample).

Autophagy investigation in T98G cells after *EGFR* silencing

Given the above described results, showing that in T98G cells EGFR modulation impaired different cancer functional signatures (i.e., viability, migration, and resistance to TMZ administration), the autophagy process was investigated in order to discern its contribute within the described effects. To this purpose, autophagy was inhibited interfering with one of the major autophagic genes, *ATG7*, by means of siRNA technology, as recommended (Klionsky et al., 2008). In detail, cells were transfected with siRNA ATG7 or siRNA EGFR alone, or in combination (siRNA ATG7/EGFR), and after 48 h, cells were assessed for ATG7 and EGFR expression by immunoblotting (Fig. 5A). A significant reduction of EGFR and ATG7 protein expression in the corresponding transfected samples was highlighted. Interestingly, a marked over-expression of EGFR was scored after siRNA ATG7 transfection.

Subsequently, T98G cells were irradiated with 2 Gy, 48h after siRNA EGFR/ATG7 transfection, and analyzed in long-term viability. Overall, the clonogenic capability of EGFR- and ATG7-silenced not-irradiated T98G cells was similar to the MOCK (Fig. 5B); differently, re-plating efficacy resulted significantly affected after IR treatment and further after IR treatment combined to EGFR silencing (respectively 33.6% and 17.7% of clonogenic capability, compared to the control). Importantly, re-plating efficacy of these samples was partly rescued after *ATG7* interfering (50.2% in siRNA ATG7/IR and 53.1% in siRNA ATG7/EGFR/IR combined treatment).

Effect of IR combined with Rapamycin after *EGFR* silencing in both T98G and U373MG human GBM cell lines

According to previous results (Fig. 5), *ATG7* interfering was able to partly rescue clonogenic capability of EGFR-silenced T98G cells additionally subjected to IR treatment. Thus, these data suggest a putative autophagy involvement, mainly as a cell-death process, during EGFR silencing. To verify this hypothesis, a Rapamycin-mediated autophagy induction was performed in T98G and in U373MG cells. Firstly, the phosphorylation of p70 S6 kinase protein was evaluated in order to confirm the effect of Rapamycin, that acts blocking mTOR pathway. As shown in Suppl. Figure S2, the level of ph-p70 S6 kinase significantly decreased after incubation with Rapamycin (at 5 and 10 nM concentration) in both cell lines, suggesting an effective mTOR inhibition. Thus, Rapamycin (at the lowest effective concentration of 5 nM) was employed for the next experiments; in detail, cells were firstly transfected with siRNA EGFR, then treated with Rapamycin for 24 h and, after additional 24 h incubation, irradiated with 2 Gy. Figure 6 reported the results of clonogenic assays showing that Rapamycyn induced a significant decrease in clonogenic capability rates. Furthermore, the combined *EGFR* silencing and Rapamycin treatment enhanced the IR effect on long-term viability compared to the Rapamycin untreated corresponding samples (siRNA EGFR/IR); more specifically, 5.5% of clonogenic capability in siRNA EGFR/Rapamycin/IR and 14.1 % in siRNA EGFR/IR were scored in T98G cells, compared to 4.0 % and 12.6 % in U373MG cells.

As before, cell migration was evaluated in both cell lines, as reported in Figure 7 (T98G) and in Figure 8 (U373MG), along with the combined treatments for autophagy activation, *EGFR* interfering and IR exposure. As a result, the migration of T98G cells transfected with siRNA EGFR and treated with both

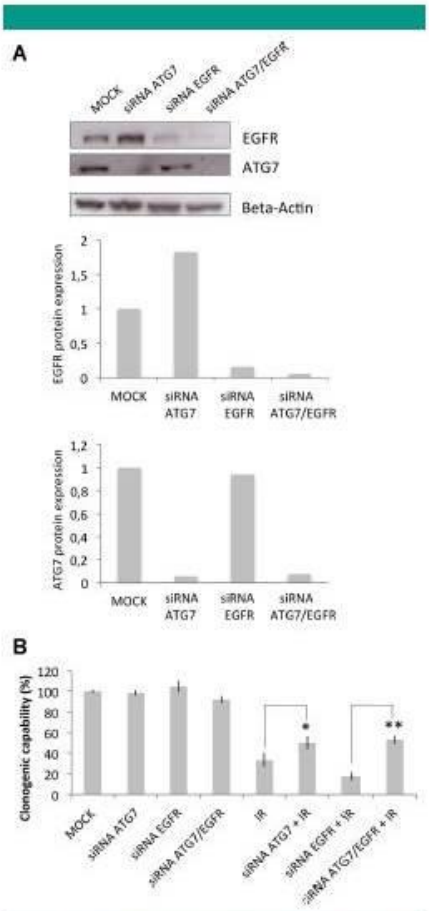

Fig. 5. Effect of IR on clonogenic capability after *EGFR* and *ATG7* silencing in T98G cells. A: Immunoblotting analysis of EGFR and ATG7 expression after *EGFR* and *ATG7* silencing. Both siRNAs pools, specific for EGFR (1 μM) or ATG7 (0.6 μM), were transfected alone or concomitantly into the cells, and after 48 h, protein levels were analyzed. For densitometric analysis, protein expression was normalized with β-actin (ImageJ software) and referred to the expression of not transfected (MOCK) cells. B: Clonogenic capability after *EGFR* and *ATG7* silencing in IR treated T98G cells. Cells were transfected, as above, and seeded for clonogenic assay. After 48 h, cells were exposed to IR (2 Gy). Clonogenic capability was calculated as described in the Materials and Methods Section, and reported as percentage into the graph. Results of three independent experiments are reported with error bars. Light optical microscopy photographs of the different treatments (10× magnification) are reported (*$P < 0.5$; **$P < 0.01$).

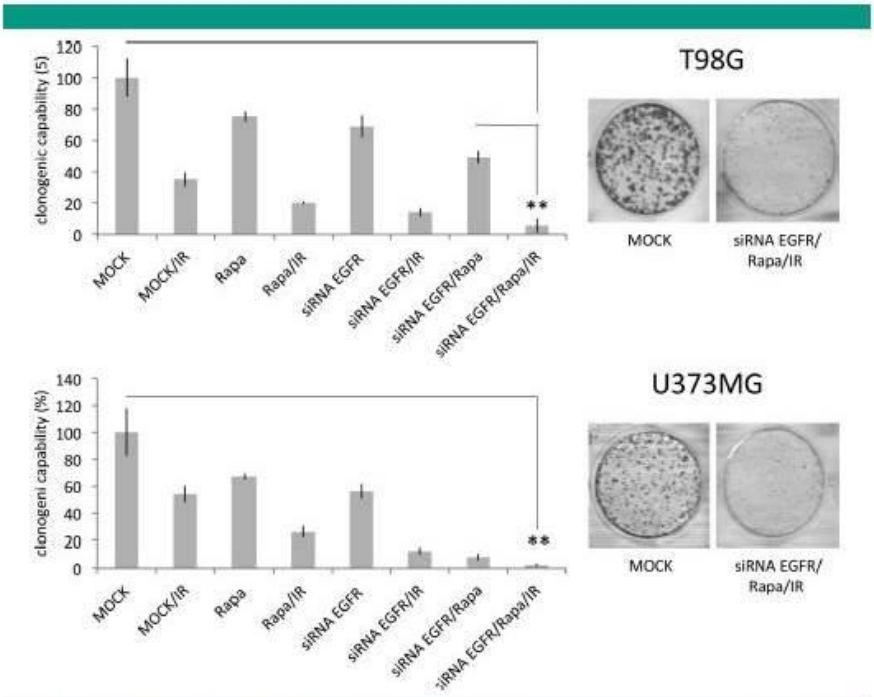

Fig. 6. Effect of IR combined with Rapamycin administration, after *EGFR* silencing in T98G and U373MG cells. Both siRNAs pools, specific for *EGFR* (1 μM) or *ATG7* (0.6 μM), were transfected alone or concomitantly into the cells, and after 24 h, Rapamycin at (5 nM) was added to the culture. After additional 24 h, cells were irradiated at 2 Gy. Clonogenic capability was calculated as described in the Materials and Methods Section, and reported as percentage into the graph. Results of three independent experiments are indicated with error bars. Light optical microscopy photographs of the different treatments (10× magnification) are reported ($P < 0.01$).**

Rapamycin and IR was significantly impaired, compared to the corresponding samples without Rapamycin (Fig. 7A). In detail, in T98G cells, the slowest migration rate in terms of migration distances (Fig. 7B) and percentage (Fig. 7C) was scored in correspondence of Rapamycin, siRNA EGFR and IR combined treatment, at both the investigated times (i.e., 24 and 72 h). More specifically, after 72 h from scratch-wound performing, a cell migration rate of 120 μm, compared to 250 μm of the control, was detected, with therefore a percentage of cell migration of 48.0% compared to the control. In U373MG cells (Fig. 8), the combined treatment exhibited a less significant reduction in migration rates, only in correspondence of the longest investigated interval time, showing a migration rate (Fig. 8B) of 210 μm (compared to 270 μm measured in the control) and a 77.0% of cell migration (Fig. 8C).

Discussion

Despite the significant biological and clinical efforts during the past decades, GBM (the most common and lethal primary central nervous system neoplasm) has an extremely poor prognosis (Cloughesy et al., 2014). After surgery removal, IR combined with TMZ chemotherapy is presently considered the most effective therapeutic option. However, GBM heterogeneity and its high number of genetic alterations make this tumor elusive, in respect to any known therapeutic strategy. Interfering with molecular pathways is an appealing strategy, as the resulting cytostatic effect might enhance IR and chemotherapy cytotoxicity. A critical factor that affects IR-sensitivity of GBM seems to be *EGFR*, which is overexpressed in up to 50% of malignant GBM cells (Chakravarti et al., 2004). When bound by its ligands (e.g., epidermal growth factor and transforming growth factor-alpha), EGFR is activated and triggers downstream signaling cascades, such as PI3K/Akt/mTOR pathway, involved also in the regulation of autophagy, that in turn can improve radiosensitivity in GBM cells (Palumbo et al., 2012). In addition, clinical studies have also shown that EGFR promotes resistance to radiation in many tumor types, including GBM (Li et al., 2004).

In agreement with these experimental assumptions, EGFR expression combined with the endogenous autophagy status was here investigated in its capability to enhance IR in vitro

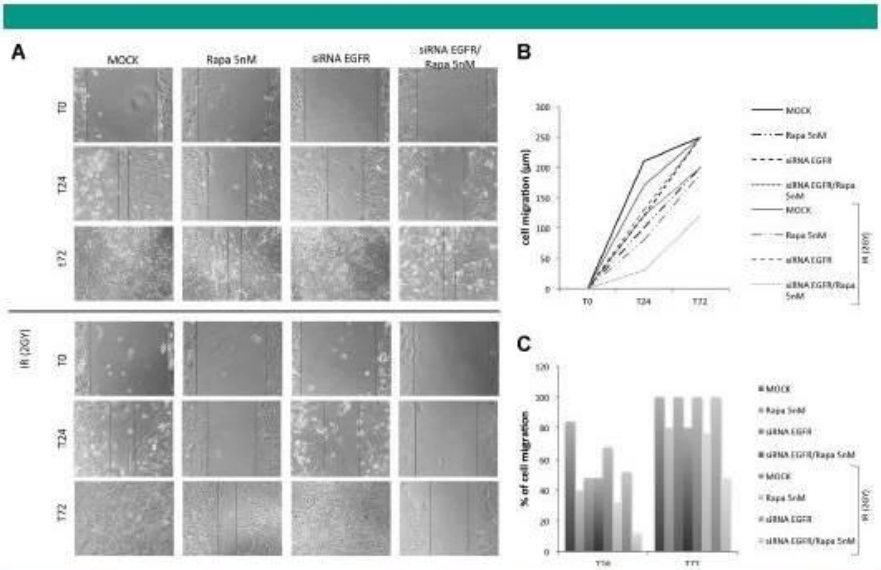

Fig. 7. Effect of IR on cell migration after *EGFR* silencing in Rapamycin-treated T98G cells. A: Both siRNAs pools, specific for *EGFR* (1 µM) or *ATG7* (0.6 µM), were transfected alone or co-transfected into the cells, and after 24 h Rapamycin (5nM) was added to the culture. After additional 24 h, cells were exposed to IR (2 Gy), and subjected to a scratch-wound assay. Light microscopy photographs were collected at different times after scratch-wound performing (T0, T24, T72). B: Cell migration rates expressed in micrometer, evaluated measuring the area of the scratch-wound at the analyzed time (T0, T24, T72). C: Percentage of cell migration, obtained by dividing the cell migration of each sample by that of the MOCK untreated sample at T72 (corresponding to the completely scratch-wound closing).

sensitivity in GBM cells. After *EGFR* silencing through transfection of a pool of siRNAs, IR sensitivity was evaluated in human T98G and U373MG GBM cells, by testing their clonogenic and migration capabilities. An impaired clonogenic rate was shown in both cell lines, mostly in U373MG cells, demonstrating that *EGFR* interfering enhanced IR sensitivity in long-term viability assays. In accordance with these results, mAb 806, an EGFR-specific antibody, was found able to enhance the efficacy of IR in glioma xenografts, reducing the volume of the tumor mass (Johns et al., 2010).

Furthermore, it is interesting to note how in T98G, but not in U373MG cells, IR counteracted the induced *EGFR* silencing. In this respect, it was found that *EGFR* could be activated by irradiation in various cancer cells, including GBM (Dent et al., 2003; Schmidt-Ullrich et al., 2003; Chakravarti et al., 2004), and this effect is believed to be one of the major causes of intrinsic radioresistance in GBM cells. Conversely to clonogenic results, the effect of the combined siRNA EGFR/IR treatment on cell migration resulted more effective in T98G cells, probably due to the better response of these cells after EGFR silencing alone, in which cell migration was much more impaired, compared to U373MG ones. In particular, U373MG cells showed a constitutive higher migration rate compared to T98G cells. Our results are in line with Ramis et al. (2012) observation of a decreased GBM cell mobility after *EGFR* inhibition, which the authors attributed to the formation of actin stress fibers.

TMZ administration, concurrent and sequential besides IR, represents the standard therapy for GBM patients in agreement with several clinical studies (Stupp et al., 2005). In the present report, the effect of *EGFR* silencing on T98G cells, described as a prototype of TMZ-resistant cells (Kanzawa et al., 2004), was evaluated in respect of TMZ cell toxicity. As a result, a significant reduction of clonogenic capability was scored after TMZ treatment in siRNA EGFR transfected T98G cells, suggesting that *EGFR* modulation might enhance also chemo-sensitivity of GBM cells.

Subsequently, down-regulation of ATG7 was employed to discern the role of autophagy process in radio-sensitizing EGFR-silenced cells. From the literature (Kim and Choi, 2008; Macintosh et al., 2012; Misirkic et al., 2012; Shin et al., 2013), transfection of siRNA directed versus *ATG7*, or other *ATGs*, provides a useful approach to inhibit autophagy process, through a blockade of autophagosome formation and the consequent degradation by lysosome (Klionsky et al., 2008). Moreover, this approach provides a functional evidence to discern between the pro-survival or the pro-death contribution of the process, as recommended by Klionsky et al. (2012).

In the present manuscript, autophagy inhibition (by means of siRNA *ATG7* transfection) in irradiated and EGFR-silenced cells resulted in a general reduction of radio-sensitivity, in

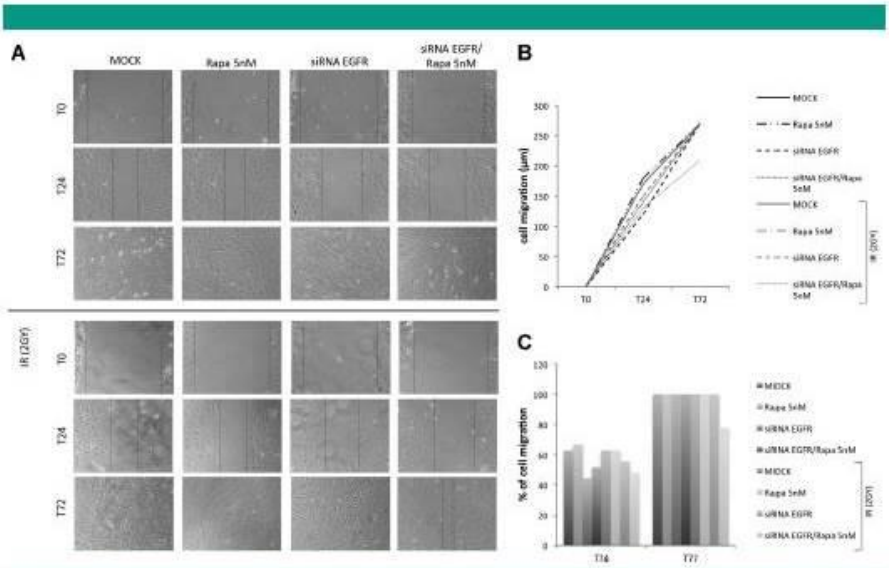

Fig. 8. Effect of IR on cell migration after *EGFR* silencing in Rapamycin-treated U373G cells. A: Both siRNAs pools, specific for *EGFR* (1 μM) or *ATG7* (0.6 μM), were transfected alone or co-transfected into the cells, and after 24 h, Rapamycin (5 nM) was added to the culture. After additional 24 h, cells were exposed to IR (2 Gy), and subjected to a scratch-wound assay. Light microscopy photographs were collected at different times after scratch-wound performing (T0, T24, T72). B: Cell migration rates expressed in micrometer, evaluated measuring the area of the scratch-wound at the analyzed time (T0, T24, T72). C: Percentage of cell migration, obtained dividing the cell migration of each sample with that of the MOCK untreated sample at T72 (corresponding to the completely scratch-wound closing).

comparison with the corresponding not transfected samples. This evidence supports a major contribution of autophagy as a cell-death promoting process.

Furthermore, it is well established that *EGFR* amplification promotes hyperactivation of the downstream PI3K/Akt-1/mTOR pathway, one of the hallmarks of GBMs (Furnari et al., 2007; McLendon et al., 2008; Parsons et al., 2008), conferring an IR-resistant phenotype (Kao et al., 2007). To contrast this unfavorable phenotype, the specific EGFR-inhibitor AG1478 was employed to prevent IR-induced Akt activation, thus enhancing IR sensitivity (Li et al., 2009). Moreover, it has been demonstrated that PI3K/Akt-1/mTOR signaling blockage, using small molecule inhibitors, promoted radiation sensitivity in GBM (Kao et al., 2007) and in breast cancer cells (Friedmann et al., 2004). In addition, the PI3K/AKT/mTOR axis inhibits autophagy, thus stimulating cell growth and proliferation (Chen et al., 2009; Kroemer et al., 2009). Taken these evidences and due to the fact that therapeutic resistance of EGFR-inhibitors alone has emerged, it has been investigated here whether strategies for targeting EGFR-associated downstream signaling would radiosensitize GBM cell lines. Specifically, in the present report, Rapamycin was combined with *EGFR* interfering during GBM cells irradiation. In detail, Rapamycin is an autophagy-inducing drug in human malignant GBM cells able to promote a blockage of the PI3K/Akt/mTOR pathway, without any alteration of the up-stream EGFR status (Iwamaru et al., 2007). Rapamycin binds to the intracellular FKBP12 protein to form a drug–receptor complex that then interacts with and suppresses mTOR, resulting in inactivation of its downstream molecule p70S6 kinase (p70S6K) (Huang and Houghton et al., 2003; Sawyers, 2003). In both T98G and U373MG cells, Rapamycin enhanced IR-sensitivity, and further decreased the clonogenic capability of the EGFR-silenced cells. Thus, combining *EGFR* silencing and autophagy induction, two different GBM cell lines showed an improved response to a specific IR scheduled treatment. Moreover, not only clonogenic capability but also cell migration was impaired, especially in T98G cells. In this cell line, the effect of the Rapamycin-only treatment in control and irradiated cells is more marked than in U373MG cells, probably due to the different basal sensitivity of these cell lines to the drug (Takeuchi et al., 2005). To improve the efficacy of autophagy induction in U373MG cells, other inducers, such as Berberine (Wang et al., 2010) or 2-Hydroxyde acid (Marcilla-Etxenike et al., 2012) might deserve consideration for future experiments.

In conclusion, in our hands, a combined *EGFR* interfering and an autophagy modulation combined scheme pointed at new promising approaches in GBM therapy to enhance IR effects.

Literature Cited

Barbieri G, Palumbo S, Gabrusiewicz K, Stoichevo E, Marchesi N, Mazzini C, Spedito A, Biggiogera M, Azzalin A, Kaminska B, Cominelli S. 2011. Interference with the cellular prion protein (PrPC) expression by DNAantisense molecules induces autophagic death in glioma cells. Autophagy 7:840–853.

Chakravarti A, Dicker A, Mehta M. 2004. The contribution of epidermal growth factor receptor (EGFR) signaling pathway to radioresistance in human gliomas: A review of preclinical and correlative clinical data. Int J Radiat Oncol Biol Phys 58:927–931.

Chen N, Karantza-Wadsworth V. 2009. Role and regulation of autophagy in cancer. Biochim Biophys Acta 1793:1516–1523.
Ciardiello F, Tortora G. 2008. EGFR antagonists in cancer treatment. N Engl J Med 358:1160–1174.
Cloughesy TF, Cavenee WK, Mischel PS. 2014. Glioblastoma: from molecular pathology to targeted treatment. Annu Rev Pathol 9:1–25.
Cohen EE, Rosen F, Stadler WM, Recant W, Stenson K, Huo D, Vokes EE. 2003. Phase II trial of ZD1839 in recurrent or metastatic squamous cell carcinoma of the head and neck. J Clin Oncol 21:1980–1987.
Cory G. 2011. Scratch-wound assay. Methods Mol Biol 769:25–30.
Dancey JE, Freidlin B. 2003. Targeting epidermal growth factor receptor—Are we missing the mark? Lancet 362:62–64.
Dent P, Yacoub A, Contessa J, Caron R, Amorino G, Valerie K, Hagan MP, Grant S, Schmidt-Ullrich R. 2003. Stress and radiation-induced activation of multiple intracellular signaling pathways. Radiat Res 159:283–300.
Friedman B, Caplin M, Hardee JA, Hochhauser D. 2004. Modulation of DNA repair in vitro after treatment with chemotherapeutic agents by the epidermal growth factor receptor inhibitor gefitinib (ZD1839). Clin Cancer Res 10:6476–6486.
Fukuoka M, Yano S, Giaccone G. 2002. Final results from a phase II trial of ZD for patients with advanced non-small lung cancer. Proc Am Soc Clin Oncol 21:298a.
Furnari FB, Fenton T, Bachoo RM, Mukasa A, Stommel JM, Stegh A, Hahn WC, Ligon KL, Louis DN, Brennan C, Chin L, DePinho RA, Cavenee WK. 2007. Malignant astrocytic glioma: Genetics, biology, and paths to treatment. Genes Dev 21:2683–2710.
Heimberger AB, Crotty LE, Archer GE, Hess KR, Wikstrand CJ, Friedman AH, Friedman HS, Bigner DD, Sampson JH. 2003. Epidermal growth factor receptor VIII peptide vaccination is efficacious against established intracerebral tumors. Clin Cancer Res 9:4247–4254.
Herbst RS. 2004. Review of epidermal growth factor receptor biology. Int J Radiat Oncol Biol Phys 59:21–26.
Huang S, Houghton PJ. 2003. Targeting mTOR signaling for cancer therapy. Curr Opin Pharmacol 3:371–377.
Iwamaru A, Kondo Y, Iwado E, Aoki H, Fujiwara K, Yokoyama T, Mills GB, Kondo S. 2007. Silencing mammalian target of rapamycin signaling by small interfering RNA enhances rapamycin-induced autophagy in malignant glioma cells. Oncogene 26:1840–1851.
Johns TG, McKay MJ, Cvrljevic AN, Carr HK, Taylor C, Xu H, Smyth FE, Scott AM. 2010. MAb 806 enhances the efficacy of ionizing radiation in glioma xenografts expressing the de2-7 epidermal growth factor receptor. Int J Radiat Oncol Biol Phys 78:572–578.
Karasawa T, Germino IM, Komata T, Ito H, Kondo Y, Kondo S. 2004. Role of autophagy in temozolomide-induced cytotoxicity for malignant glioma cells. Cell Death Differ 11:448–457.
Kao GD, Jiang Z, Fernandes AM, Gupta AK, Maity A. 2007. Inhibition of phosphatidylinositol-3-OH kinase/Akt signaling impairs DNA repair in glioblastoma cells following ionizing radiation. J Biol Chem 282:21206–21212.
Kim EH, Choi KS. 2008. A critical role of superoxide anion in selenite-induced mitophagic cell death. Autophagy 4:76–78.
Klionsky DJ, Abeliovich H, Agostinis P, Agrawal DK, Aliev G, Askew DS, Baba M, Baehrecke EH, Bahr BA, Ballabio A, Bamber BA, Bashmm DC, Bergamini E, Bi X, Biard-Piechaczyk M, Blum JS, Bredesen DE, Brodsky JL, Brumell JH, Brunk UT, Bursch W, Camougrand N, Cebollero E, Cecconi F, Chen Y, Chin LS, Choi A, Chu CT, Chung J, Clarke PG, Clark RS, Clarke SG, Clavé C, Cleveland JL, Codogno P, Colombo MI, Coto-Montes A, Cregg JM, Cuervo AM, Debnath J, Demarchi F, Dennis PB, Dennis PA, Deretic V, Devenish RJ, Di Sano F, Dice JF, Difiglia M, Dinesh-Kumar S, Distelhorst CW, Djavaheri-Mergny M, Dorsey FC, Dröge W, Dron M, Dunn WA, Jr., Duszenko M, Eissa NT, Elazar Z, Esclatine A, Eskelinen EL, Fésüs L, Finley KD, Fuentes JM, Fueyo J, Fujisaki K, Galliot B, Gao FB, Gewirtz DA, Gibson SB, Gohla A, Goldberg AL, Gonzalez R, González-Estévez C, Gorski S, Gottlieb RA, Häussinger D, He YW, Heidenreich K, Hill JA, Höyer-Hansen M, Hu X, Huang WP, Iwasaki A, Jäättelä M, Jackson WT, Jiang X, Jin S, Johansen T, Jung JU, Kadowaki M, Kang C, Kelekar A, Kessel DH, Kiel JA, Kim HP, Kimchi A, Kinsella TJ, Kiselyov K, Kitamoto K, Knecht E, et al. 2008. Guidelines for the use and interpretation of assays for monitoring autophagy in higher eukaryotes. Autophagy 4:151–175.
Kris MG, Natale RB, Herbst RS. 2002. A Phase II trial of ZD1839 in advanced non-small cell lung cancer patients who had failed platinum- and docetaxel-based regimens. Proc Am Soc Clin Oncol 21:292a.
Kroemer G, Levine B. 2008. Autophagic cell death: The story of a misnomer. Nature Rev Mol Cell Biol 9:1004–1010.
Levine B, Klionsky DJ. 2004. Development by self-digestion: Molecular mechanisms and biological functions of autophagy. Dev Cell 6:463–477.
Li B, Yuan M, Kim IA, Chang CM, Bernhard EJ, Shu HK. 2004. Mutant epidermal growth factor receptor displays increased signaling through the phosphatidylinositol-3 kinase/AKT pathway and promotes radioresistance in cells of astrocytic origin. Oncogene 23:4594–4602.
Li HF, Kim JS, Waldman T. 2009. Radiation-induced Akt activation modulates radioresistance in human glioblastoma cells. Radiat Oncol 4:43.
Lynch TJ, Bell DW, Sordella R, Gurubhagavatula S, Okimoto RA, Brannigan BW, Harris PL, Haserlat SM, Supko JG, Haluska FG, Louis DN, Christiani DC, Settleman J, Haber DA. 2004. Activating mutations in the epidermal growth factor receptor underlying responsiveness of non-small-cell lung cancer to gefitinib. N Engl J Med 350:2129–2139.
Macintosh RL, Timpson P, Thorburn J, Anderson KI, Thorburn A, Ryan KM. 2012. Inhibition of autophagy impairs tumor cell invasion in an organotypic model. Cell Cycle 11:2022–2029.
Mandila-Eleankka A, Martín ML, Noguera-Salvá MA, García-Verdugo JM, Soriano-Navarro M, Dey I, Escribá PV, Busquets X. 2012. 2-Hydroxyoleic acid induces ER stress and autophagy in various human glioma cell lines. PLoS ONE 7:e48233.
McLendon R, Friedman A, Bigner D, Cancer Genome Atlas Research Network. 2008. Comprehensive genomic characterization defines human glioblastoma genes and core pathways. Nature 455:1061–1068.
Mendelsohn J, Baselga J. 2000. The EGF receptor family as targets for cancer therapy. Oncogene 19:6550–6565.
Mizushimi T, Yatabe Y. 2010. Epidermal growth factor receptor in relation to tumor development: EGFR gene and cancer. FEBS J 277:301–308.
Misirkic M, Janjetovic K, Vucicevic L, et al. 2012. Inhibition of AMPK-dependent autophagy enhances in vitro antiglioma effect of simvastatin. Pharmacol Res 65:111–119.
Narita Y, Nagane M, Mishima K, Huang HJ, Furnari FB, Cavenee WK. 2002. Mutant epidermal growth factor receptor signaling down-regulates p27 through activation of the phosphatidylinositol 3-kinase/Akt pathway in glioblastomas. Cancer Res 62:6764–6769.
Nelson DA, White E. 2004. Exploiting different ways to die. Genes Dev 18:1223–1226.
Omuro A, DeAngelis LM. 2013. Glioblastoma and other malignant gliomas: A clinical review. JAMA 310:1842–1850.
Palumbo S, Pirtoli L, Tini P, Cevenini G, Calderaro F, Toscano M, Miracco C, Comincini S. 2012. Different involvement of autophagy in human malignant glioma cell lines undergoing irradiation and temozolomide combined treatments. J Cell Biochem 113:2308–2318.
Parsons DW, Jones S, Zhang X, Lin JC, Leary RJ, Angenendt P, Mankoo P, Carter H, Siu IM, Gallia GL, Olivi A, McLendon R, Rasheed BA, Keir S, Nikolskaya T, Nikolsky Y, Busam DA, Tekleab H, Diaz LA, Jr, Hartigan J, Smith DR, Strausberg RL, Marie SK, Shinjo SM, Yan H, Riggins GJ, Bigner DD, Karchin R, Papadopoulos N, Parmigiani G, Vogelstein B, Velculescu VE, Kinzler KW. 2008. An integrated genomic analysis of human glioblastoma multiforme. Science 321:1807–1812.
Ramis G, Thomàs-Moyà E, Fernández de Mattos S, Rodriguez J, Villalonga P. 2012. EGFR inhibition in glioma cells: oddities in Rho signaling to inhibit cell motility and invasion and cooperation with temozolomide to reduce cell growth. PLoS ONE 7:e38770.
Sarkaria JN, Galanis E, Wu W, Peller PJ, Giannini C, Brown PD, Uhm JH, McGraw S, Jaeckle KA, Buckner JC. 2011. NCCTG Phase I trial N057K of everolimus (RAD001) and temozolomide in combination with radiation therapy in newly diagnosed glioblastoma multiforme patients. Int J Radiat Oncol Biol Phys 81:468–475.
Sawyers CL. 2003. Will mTOR inhibitors make it as cancer drugs. Cancer Cell 4:343–348.
Schmidt-Ullrich RK, Contessa JN, Lammering G, Amorino G, Lin PS. 2003. ERBB receptor tyrosine kinases and cellular radiation responses. Oncogene 22:5835–5845.
Shin SY, Lee KS, Choi YK, et al. 2013. The antipsychotic agent chlorpromazine induces autophagic cell death by inhibiting the Akt/mTOR pathway in human U-87MG glioma cells. Carcinogenesis 34:2080–2089.
Stupp R, Mason WP, van den Bent MJ, Weller M, Fisher B, Taphoorn MJ, Belanger K, Brandes AA, Marosi C, Bogdahn U, Curschmann J, Janzer RC, Ludwin SK, Gorlia T, Allgeier A, Lacombe D, Cairncross JG, Eisenhauer E, Mirimanoff RO. 2005. European Organisation for Research and Treatment of Cancer Brain Tumor and Radiotherapy Groups; National Cancer Institute of Canada Clinical Trials Group. Radiotherapy plus concomitant and adjuvant temozolomide for glioblastoma. N Engl J Med 352:987–996.
Takeuchi H, Kondo Y, Fujiwara K, Kanzawa T, Aoki H, Mills GB, Kondo S. 2005. Synergistic augmentation of rapamycin-induced autophagy in malignant glioma cells by phosphatidylinositol 3-kinase/protein kinase B inhibitors. Cancer Res 65:3336–3346.
Wang X, Bhagden C, Fan J, Nowak SJ, Tamuchi I, Uittmen DR, Burden SJ. 2005. Runx1 prevents wasting, myofibrillar disorganization, and autophagy of skeletal muscle. Genes Dev 19:1715–1722.
Wang N, Feng Y, Zhu M, Tsang CM, Man K, Tong Y, Tsao SW. 2010. Berberine induces autophagic cell death and mitochondrial apoptosis in liver cancer cells: The cellular mechanism. J Cell Biochem 111:1426–1436.
Zhu H, Acquaviva J, Ramachandran P, Boskovitz A, Woolfenden S, Pfannl R, Bronson RT, Chen JW, Weissleder R, Housman DE, Chernet A. 2009. Oncogenic EGFR signaling cooperates with loss of tumor suppressor gene functions in gliomagenesis. Proc Natl Acad Sci USA 106:2712–2716.
Zhuang W, Qin Z, Liang Z. 2009. The role of autophagy in sensitizing malignant glioma cells to radiation therapy. Acta Biochim Biophys Sin 41:341–351.

Supporting Information

Additional supporting information may be found in the online version of this article at the publisher's web-site.

Neuroscience 339 (2016) 162–173

CONGENITAL PROSOPAGNOSIA IS ASSOCIATED WITH A GENETIC VARIATION IN THE OXYTOCIN RECEPTOR (*OXTR*) GENE: AN EXPLORATORY STUDY

ZAIRA CATTANEO, [a,b*†] **ROBERTA DAINI,** [a,c] **MANUELA MALASPINA,** [a,c] **FEDERICO MANAI,** [d] **MARIARITA LILLO,** [d] **VALENTINA FERMI,** [d] **SUSANNA SCHIAVI,** [a,c] **BORIS SUCHAN** [e] **AND SERGIO COMINCINI** [d*†]

[a] *Department of Psychology, University of Milano-Bicocca, Milano, Italy*

[b] *Brain Connectivity Center, C. Mondino National Neurological Institute, Pavia, Italy*

[c] *Milan Center for Neuroscience (NeuroMI), Milano, Italy*

[d] *Department of Biology and Biotechnology, University of Pavia, Pavia, Italy*

[e] *Clinical Neuropsychology, Institute of Cognitive Neuroscience, Faculty of Psychology, Ruhr-University Bochum, Bochum, Germany*

Abstract—Face-recognition deficits, referred to with the term *prosopagnosia* (i.e., face blindness), may manifest during development in the absence of any brain injury (from here the term congenital prosopagnosia, CP). It has been estimated that approximately 2.5% of the population is affected by face-processing deficits not depending on brain lesions, and varying a lot in severity. The genetic bases of this disorder are not known. In this study we tested for genetic association between single-nucleotide polymorphisms (SNPs) in the oxytocin receptor gene (*OXTR*) and CP in a restricted cohort of Italian participants. We found evidence of an association between the common genetic variants rs53576 and rs2254298 *OXTR* SNPs and prosopagnosia. This association was also found when including an additional group of German individuals classified as prosopagnosic in the analysis. Our preliminary data provide initial support for the involvement of genetic variants of *OXTR* in a relevant cognitive impairment, whose genetic bases are still largely unexplored.

Key words: congenital prosopagnosia, oxytocin receptor gene, face blindness.

INTRODUCTION

Deficits in face recognition – usually referred to with the term *prosopagnosia* or face-blindness – that do not derive from brain injury seem to affect about 2.5% of the population (Kennerknecht et al., 2006). Individuals affected by this disorder (that may be present at different levels of severity) have spared sensory visual abilities and normal intelligence but are likely to have developed suboptimal visual mechanisms implied in face processing (Behrmann and Avidan, 2005; Susilo and Duchaine, 2013). Moreover, in spite of a (possibly) severe face-recognition deficit, individuals with prosopagnosia may show normal social abilities thanks to highly developed compensatory alternative strategies to effectively recognize people (Daini et al., 2014; Malaspina et al., 2016).

A number of studies demonstrated the recurring presence of the deficit in relatives, pointing to a possible genetic contribution (also from here the term *congenital* prosopagnosia, CP) reflected by a simple autosomal inheritance pattern (Duchaine et al., 2007; Schmalzl et al., 2008; Lee et al., 2010; Wilmer et al., 2010; Zhu et al., 2010). In particular, it has been suggested that CP may have a polygenic basis as most neurodevelopmental disorders (Susilo and Duchaine, 2013). A recent contribution reported that the substantial heritability of face-recognition capacity is due to genetic influences that are mostly specific to this ability, rather than shared either with general object recognition or general intelligence: in particular, it has been estimated that face recognition displays a substantial heritability of 61% (Shakeshaft and Plomin, 2015).

The genetic investigation of perceptual and cognitive disorders is quite complex, since there are several genes that can differently contribute to a specific ability. Nonetheless, we were driven in our investigation by accumulating evidence on the effects of the hormone oxytocin on face-processing abilities. In fact, inhalation of oxytocin has been found to improve face-processing abilities in both healthy (Savaskan et al., 2008; Rimmele et al., 2009) and prosopagnosic individuals (Bate et al., 2014). Indeed, oxytocin has been reported to increase the time spent looking at the eye region of the face (Guastella et al., 2008), an area that provides critical information for face identification. Oxytocin has also been shown to enhance the ability to infer the mental state of others on a task that requires sensitivity to subtle information from the eye region (Domes et al., 2007). Further supporting the link between oxytocin and facial recognition ability, a recent study of 178 families with at least one autistic child found that variation in *OXTR* was

*Corresponding authors.
E-mail addresses: zaira.cattaneo@unimib.it (Z. Cattaneo), sergio.comincini@unipv.it (S. Comincini).
† These authors contributed equally to this work.

http://dx.doi.org/10.1016/j.neuroscience.2016.09.040
0306-4522/

strongly associated with face-recognition performance in a face-memory test (Skuse et al., 2014).

To identify possible genetic determinants involved in CP, we performed a study in a restricted cohort of Italian participants evaluating if *OXTR* single-nucleotide polymorphisms (SNPs), alone or in combination, would be associated with deficits in face-recognition. We designed our study on a highly stringent and homogeneous cohort of cases and controls. Criteria to classify an individual as prosopagnosic are indeed highly debated (see Duchaine and Nakayama, 2004, 2006) and we opted for strict selection criteria based on performance in multiple tests measuring face-recognition abilities (beyond self-reported experience of deficit, see also Palermo et al., 2016). The use of stringent criteria is also recommended in light of a recent meta-analysis of *OXTR* genotype effects in humans showing that demographic composition and ethnic backgrounds can originate inconsistent results (Bakermans-Kranenburg and van Ijzendoorn, 2014). After completion of analysis on the Italian cohort of participants, we were able to get DNA samples of six additional German individuals with CP (some of them described in Minnebusch et al., 2007, 2009). Notwithstanding the quite limited size of this additional sample, we report some preliminary genetic analyses on this sample as well, this additional exploratory evidence being possibly informative in guiding future research with larger samples.

METHODS

Participants and classification criteria

Italian sample. Eighteen Italian CP participants (mean age 25.42 ± 8 years) took part in the study and were selected from a larger sample of participants (n = 23) in response to paper and online advertisements recruiting subjects with face-recognition impairment. All individuals that replied to advertisements were interviewed and underwent a battery of tests diagnostic for face-recognition abilities (see Fig. 1): the Cambridge Face Memory Test (CFMT; Duchaine and Nakayama, 2006; Bowles et al., 2009), the Benton Facial Recognition Test (BFRT; Benton et al., 1994), and an Italian version of the Famous faces test (consisting in the presentation of 42 grayscale face ovals of recent Italian or international celebrities; each face remains visible till participants verbally provide the exact name or relevant information about the celebrity proving recognition; maximum score: 42). The CFMT has been shown to be the most sensitive test in detecting face-recognition impairment (Duchaine and Nakayama, 2004, 2006). This test has been widely used in studies of CP and has impressive internal and test–retest reliability (Bowles et al., 2009; Wilmer et al., 2010, 2012). The inversion effect in the CMFT (i.e., the difference in accuracy between the total score of the upright and inverted faces, Yin, 1969) was considered as an additional diagnostic index (the inversion "cost" for recognition being frequently absent in CP, see Behrmann and Avidan, 2005). The BFRT (Benton et al., 1994) allows to test face-recognition ability in absence of any memory component, while the Famous faces test allows to assess the association between a face and the person's identity. Participants were also administered two (control) tests not related to face-recognition abilities: the Boston Naming test (Kaplan et al., 1983), and an Italian test measuring Famous monuments recognition (consisting in the presentation of 30 pictures of Italian and international monuments in their most conventional perspective; each monument remains visible till participants name the monument or provide as much information as possible about it in order to prove correct recognition; max score = 30). Participants were classified as having CP only if they met all the following criteria: (1) they had come to the lab spontaneously reporting face-recognition deficits in response to our advertisements and the interview revealed their difficulties were present since early childhood and did not start at a specific moment of life (according to their self-reports); (2) their performance was below 2 SD compared to the mean performance of the normative sample (n = 70, see Table 1) in at least two of the following face processing measures: CFMT upright faces, BFRT, Famous faces test, and in the face inversion index of the CFMT; 3) they had normal performance in Boston naming and in the Famous Monuments tests. All CP participants had normal or corrected-to normal vision and no neurological damage and they were all right-handed.

Eighteen Italian participants (mean age 24.0 ± 3.4 years) were recruited as controls. None of them in a pre-screening phase reported to experience any face-recognition deficits. Control participants underwent the same battery of tests described for the CP group. All control participants were right-handed and had normal or corrected-to normal vision. None of them reported any neurological damage.

Demographic features of the CP and control Italian participants and their performance scores (raw data and z scores) to neuropsychological tests used are shown in Table 2. All participants (included those acting as normative sample) gave written informed consent and were treated in accordance with the declaration of Helsinki. The study was approved by Ethics Committee of the University of Milano-Bicocca.

German sample. A second group of CP participants (n = 6, mean age 45.83 ± 15.87 years) of German nationality was recruited. Participants' age (ys) at taking saliva samples and sex were: 51 ys old, male (#1); 47 ys old, male (#2); 48 ys old, female (#3); 67 ys old, female (#4); 44 ys old, male (#5); 18 ys old, female (#6). Two of them (#5, #6) were family-related members (father–daughter). The prosopagnosic subjects (#1, #2, #3) have been described in detail in previous reports (Minnebusch et al., 2007, 2009). Subject #5 accepted to give his saliva sample but refused to take part in the behavioral assessment: he and his family declared that he suffers of severe face-recognition abilities, comparable to that of his daughter, and he considered as pointless to undergo parametric assessment of his performance. All subjects were right-handed and had normal or corrected-to-normal vision. Face-processing and -recognition abilities were assessed using the

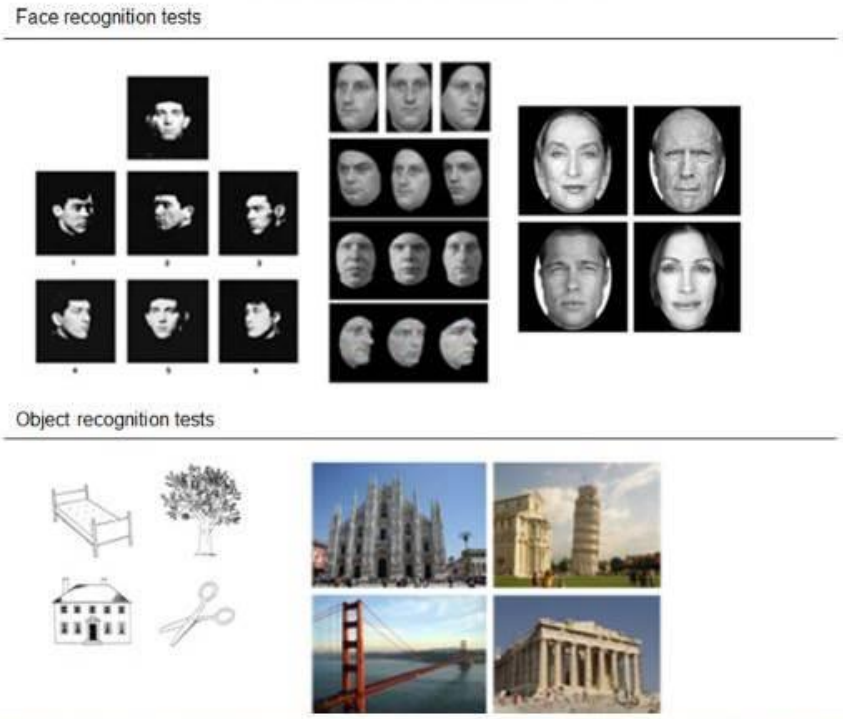

Fig. 1. Examples of stimuli used in the behavioral assessment. The upper panel shows examples of stimuli used in the face-recognition tests, specifically, from left to right: (i) faces from the Benton Facial Recognition Test; (ii) faces presented in the Cambridge Face Memory Test; (iii) famous faces of the Famous Face recognition test. The lower panel shows examples of stimuli used in the object-recognition tasks, in particular, from left to right: (i) object drawings taken from the Boston naming task; and (ii) pictures of monuments presented in the Famous Monuments recognition test.

Table 1. Mean performance of the normative Italian sample in the tests used to classify Italian participants as having congenital prosopagnosia (CP) vs. controls. The normative sample in each test consisted of 70 right-handed participants (60F, 10 M, age range: 19–43 ys; mean education range: 13–22 ys). Note that the sample differed for a few participants between the Benton, Cambridge and Boston tests (10 M, mean age = 23.4 ys ± 3.69; mean education: 17.21 ys ± 2.38), the Famous faces test (10 M, mean age = 24.0 ys ± 4.46, mean education: 16.76 ys ± 2.05) and the Famous monuments test (10 M, mean age = 23.4 ys ± 3.65, mean education: 16.85 ys ± 2.07).

		Mean scores ± SD (range)	Cut-off z-score
Face-recognition tests			
Benton facial recognition test		47.17 ± 2.86 (41–54)	41.45
Cambridge face memory test	Upright	57.86 ± 8.44 (44–72)	40.98
	Inverted	42.56 ± 5.59 (27–54)	31.38
	Inversion effect	15.33 ± 6.5 (1–28)	2.33
Famous faces test		29.97 ± 5.95 (14–42)	18.07
Control tests			
Famous monuments test		20.72 ± 4.94 (6–30)	10.84
Boston naming test		55.69 ± 2.96 (45–60)	49.77

Recognition Memory Test for faces (RMT-F; Warrington, 1984), the Benton Facial Recognition Test (BFRT; Benton et al., 1983), the Bochum test of face-processing skills (Minnebusch et al., 2007) and the Famous Face Recognition Test (Minnebusch et al., 2007). The ability to discriminate face identity and to recognize emotions in facial expressions was assessed using five subtests of the Tübinger Affect Battery (TAB, Breitenstein et al., 1996, 1998). Table 3 also reports participants' scores in basic-level object recognition that was assessed by digitized

Table 2. Demographic characteristics of prosopagnosic (CP) and control (C) participants and their performance in the different tests. Age and Education (Ed.) are in years. Raw data, z scores and ranks are reported. Participants were classified as prosopagnosic only if their scores fell below 2 SD (cases indicated with an asterisk) compared to the normative sample in at least two measures within Benton, CFMT upright version, CFMT Inversion effect and Famous Faces. An additional z value (z2) that refers to the normative sample provided by Duchaine and Nakayama (2006) is also reported. BFRT: Benton Facial Recogniton Test; CFMT: Cambridge Face Memory Test; BNT: Boston naming test.

	Age	Ed.	Face recognition tests							Famous faces		Control tests			
			BFRT		CFMT							BNT		Famous monuments	
					Upright			Inversion effect							
			raw	z	raw	z	z2	raw	z	raw	z	raw	z	raw	z
CP															
1	24	18	49	0.64	37	−2.47*	−2.65*	−8	−3.59*	31	0.17	57	0.44	24	0.66
2	25	18	41	−2.16*	38	−2.35*	−2.52*	5	−1.59	18	−2.01*	56	0.10	23	0.46
3	28	20	45	−0.76	38	−2.35*	−2.52*	−4	−2.97*	33	0.51	57	0.44	28	1.47
4	25	19	40	−2.51*	36	−2.59*	−2.77*	6	−1.44	11	−3.19*	58	0.78	17	−0.75
5	20	15	46	−0.41	37	−2.47*	−2.65*	−7	−3.44*	16	−2.35*	57	0.44	24	0.66
6	20	14	50	0.99	37	−2.47*	−2.65*	6	−1.44	17	−2.18*	54	−0.57	17	−0.75
7	21	16	41	−2.16*	43	−1.76	−1.89	−1	−2.51*	4	−4.36*	60	1.46	24	0.66
8	20	15	40	−2.51*	36	−2.59*	−2.77*	1	−2.20*	14	−2.68*	56	0.10	18	−0.55
9	19	14	47	−0.06	34	−2.83*	−3.03*	−3	−2.82*	18	−2.01*	58	0.78	27	1.27
10	30	22	47	−0.06	37	−2.47*	−2.65*	−1	−2.51*	18	−2.01*	57	0.44	21	0.06
11	23	17	47	−0.06	40	−2.12*	−2.27*	−1	−2.51*	16	−2.35*	54	−0.57	19	−0.35
12	24	17	44	−1.11	35	−2.71*	−2.90*	0	−2.36*	15	−2.52*	55	−0.23	20	−0.15
13	26	18	38	−3.21*	40	−2.12*	−2.27*	1	−2.20*	8	−3.69*	55	−0.23	21	0.06
14	46	22	45	−0.76	31	−3.18*	−3.41*	3	−1.90	13	−2.85*	58	0.78	26	1.07
15	20	13	48	0.29	40	−2.12*	−2.27*	0	−2.36*	28	−0.33	57	0.44	26	1.07
16	20	13	47	−0.06	32	−3.06*	−3.28*	−2	−2.67*	22	−1.34	51	−1.58	22	0.26
17	22	14	46	−0.41	40	−2.12*	−2.27*	−4	−2.97*	7	−3.86*	55	−0.23	17	−0.75
18	47	16	41	−2.16*	36	−2.59*	−2.77*	−9	−3.74*	28	−0.33	52	−1.25	28	1.47
C															
1	19	14	51	1.34	69	1.32	1.41	20	0.72	36	1.01	55	−0.23	25	0.87
2	23	18	49	0.64	71	1.56	1.66	17	0.26	33	0.51	59	1.12	18	−0.55
3	29	22	51	1.34	72	1.68	1.78	23	1.18	40	1.69	57	0.44	24	0.66
4	28	20	48	0.29	66	0.96	1.03	29	2.10	33	0.51	56	0.10	27	1.27
5	27	21	48	0.29	59	0.14	0.14	18	0.41	35	0.85	58	0.78	20	−0.15
6	33	22	52	1.69	58	0.02	0.01	14	−0.20	41	1.85	57	0.44	25	0.87
7	25	18	47	−0.06	65	0.85	0.90	7	−1.28	34	0.68	59	1.12	21	0.06
8	23	16	49	0.64	60	0.25	0.27	15	−0.05	29	−0.16	50	−1.92	20	−0.15
9	22	16	49	0.64	55	−0.34	−0.37	10	−0.82	30	0.01	53	−0.91	22	0.26
10	23	16	48	0.29	62	0.49	0.52	27	1.80	42	2.02	53	−0.91	26	1.07
11	25	21	52	1.69	67	1.08	1.15	8	−1.13	39	1.52	53	−0.91	21	0.06
12	22	16	49	0.64	70	1.44	1.53	17	0.26	25	−0.84	52	−1.25	13	−1.56
13	22	16	47	−0.06	57	−0.10	−0.11	10	−0.82	24	−1.00	57	0.44	19	−0.35
14	20	13	49	0.64	58	0.02	0.01	20	0.72	28	−0.33	50	−1.92	27	1.27
15	23	16	46	−0.41	60	0.25	0.27	15	−0.05	35	0.85	54	−0.57	26	1.07
16	25	18	52	1.69	58	0.02	0.01	15	−0.05	40	1.69	54	−0.57	26	1.07
17	22	13	49	0.64	51	−0.81	−0.87	11	−0.67	39	1.52	54	−0.57	21	0.06
18	22	16	47	−0.06	56	−0.22	−0.24	13	−0.36	42	2.02	57	0.44	29	1.68

versions of 100 line drawings from the pictures of Snodgrass and Vanderwart (1980) (see Minnebusch et al., 2007, for details). The Rey Complex Figure test (RCFT; Osterrieth, 1944) was also used to assess visuospatial and constructional abilities as well as visual/non-verbal memory. For detailed description of the behavioral assessment and the specificity of the impairment pattern (for subjects #1, #2, and #3) see Minnebusch et al. (2007). To sum up, none of the prosopagnosic subjects that underwent behavioral assessment were impaired in tests of low-level vision and basic-level object recognition whereas they presented selective impairments in tests measuring face-processing abilities. Note that in Minnebusch et al. (2007) participants #1, #2, #3 also performed additional tests. The study was approved by the Ethics Committee of the Medical Faculty of the Ruhr-University, Bochum (Germany) and written informed consent was obtained from all subjects. The study was performed in accordance with the guidelines of the Declaration of Helsinki.

Sample processing, PCR and sequencing

Genomic DNA was collected from buccal cells. DNA from 18 controls and 18 Italian CP participants was extracted from freshly obtained buccal washes using 30 ml of a

Table 3. Performance of the German prosopagnosic participants in the behavioral assessment. Data of #5 are not available (see text). Mean performance (±SD) of the control participants described in Minnebusch et al. (2007, 2009) is also reported. Further details on the behavioral tests used and participants' samples are reported in Minnebusch et al. (2007, 2009). Asterisks indicate performance below average ($z < 1.65$ relative to control group). Control data for the BFRT and RMT–F are based on the tests' manual. RMT–F: Recognition Memory Test for faces (Warrington, 1984); BFRT: Benton Facial Recognition Test (Benton et al., 1994).

Tests	Subtests/scores	#1	#2	#3	#4	#6	Controls
Snodgrass	% correct	96	99	96	96	99	96 (±2.5)
Rey figure	Copy	34	29.5	36	36	36	31.3 (±4.5)
	Recall	17.5/36	5/36*	14.5/36	30/36	22.5	16.4 (±7.1)
Tübinger affect battery	Identity discrimination	93.33*	91.6*	100	100	100	98.8 (±2.7)
	Affect discrimination	91.6	85.71*	92.86	64.3*	100	91.6 (±5.6)
	Affect naming	94.81	66.7*	93.33	80	73.33*	94.8 (±5.8)
	Affect identification	86.6*	93.3	93.33	80*	86.6*	96.5 (±3.7)
	Affect matching	94.3	46.7*	93.33	66.6*	93.3	94.3 (±5.3)
Famous faces-Test 1	% correct	35.71*	13.63*	10*	14*	33.3*	76 (±14)
Famous faces-Test 2	% correct	44.8*	28.95*	13.9*	11*	16.6*	84 (±12)
BFRT	Total correct	45	40*	42	28*	43	Normal range 41–54
RMT–F	Total correct	38*	33*	34*	13*	45	Age-related test scores 35–39 ys: 43.9 (±3.7) 40–44 ys: 44.8 (±3.3)
Bochum Test of Face	d'	0.6*	0.09*	1.3	0.4*	Unable to	2.1 (±0.7)
Processing	RT for hits (ms)	117	380*	430*	98	perform the test	187 (±99)

commercial mouth washer. Suspensions were centrifuged (1500 rpm × 10 min at 4 °C), washed twice with PBS to remove salts and finally residual cells were resuspended into 500 μl of DNAzol Reagent (Thermofisher). DNA extraction was performed according to the manufacturer's specification. DNA was then resuspended in 20 μl sterile water and quantified using Qubit DNA High Sensitive kit (Thermofisher). Total DNA yield was in general 20–150 ng per sample. Due to logistic reasons, genomic DNA from German samples was extracted from buccal swabs kits sent by express courier, following a previously reported protocol (Vai et al., 2015). In this case, genomic DNA total yield was 50–200 ng per sample.

Primers for PCR and sequencing were: P1-U: 5′-GCTCTCCACATCACTGGGTC and P1-L: 5′-TCACTGGGGCAACCAAACAT; P2-U: 5′-TTTTGGAGTGAATGACTTAG and P2-L: 5′-GCATGGTAGGATATTTAACA; P3-U: 5′-TCAAGGTTAAGAACCACTA and P3-L: 5′-TGAACAGATAAGATTGTGC (see Fig. 2).

PCR was performed using 1–5 ng of genomic DNA, in the presence of 10 pmol of each primer and adopting mineral oil to avoid aerosol contaminations. Samples were subjected to 35 cycles at: 94 °C × 10 s, 58 °C × 30 s, 72 °C × 60 s. PCR products were purified (GenElute PCR Purification kit, Sigma) and sequenced on both DNA strands by Eurofins Genomics (Ebersberg, Germany).

Single-nucleotide polymorphism (SNP) selection and analysis

We selected eighteen SNPs in *OXTR* intron 3 (human chromosome 3 from 8754861 to 8762685 coordinates, spanning a 7824-nucleotide region) (Table 4). SNPs genotyping was performed by Sanger's sequencing on both DNA strands using the primers mapped in Fig. 2. Hardy–Weinberg (HWE) equilibrium was tested using the HWE calculator located at http://www.oege.org/software/hwe-mr-calc.shtml (Rodriguez et al., 2009). Odd ratios, upper and lower limits (at 0.95 Confidence interval), Fisher's Exact test probabilities (P) were calculated using Vassarstats calculator (http://vassarstats.net/) where the resulted three possible genotypes for each SNP were analyzed in 2 × 2 contingency tables as homozygous for ancestral allele vs absence of ancestral allele in normal and prosopagnosic condition. Clustering, nomograms and classification analyses were performed using Orange

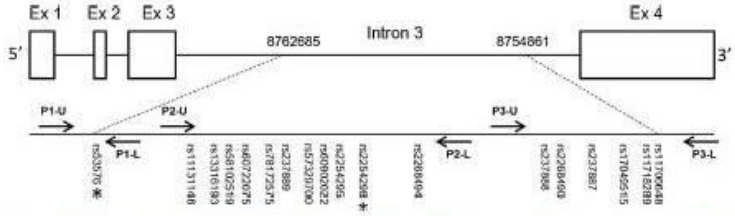

Fig. 2. *OXTR* gene architecture and the investigated intron region with human chromosome 3 nucleotide coordinates. Selected SNPs (MAF > 0.01) were amplified and sequenced with the indicated primers (arrows). Asterisks indicated SNPs variations that resulted associated with CP condition.

Table 4. SNPs into the *OXTR* gene analyzed in the current study are reported alongside their chromosomal position and minor allele frequency (MAF).

SNP ID	Pos. Chr.3	Alleles	MAF
rs53576	8762685	A/G	A = 0.40
rs11131148	8761059	C/T	C = 0.39
rs13316193	8761057	C/T	C = 0.40
rs58102519	8760982	C/T	C = 0.06
rs60722075	8760904	-/A	A = 0.38
rs78172575	8760848	A/G	A = 0.04
rs237889	8760797	C/T	T = 0.30
rs57329700	8760793	A/G/T	T = 0.14
rs60902022	8760717	C/T	C = 0.39
rs2254295	8760606	C/T	C = 0.21
rs2254298	8760542	A/G	A = 0.21
rs2268494	8760360	A/T	A = 0.07
rs237888	8755409	C/T	C = 0.13
rs2268490	8755399	C/T	T = 0.26
rs11706648	8754861	A/C	C = 0.29
rs11718289	8755176	C/T	T = 0.31
rs237887	8755356	A/G	G = 0.40
rs17049515	8755327	C/T	C = 0.01

Canvas 3.2 data-mining tool (Demsar et al., 2013). To identify putative functional effects of the identified variations, Consite (http://consite.genereg.net/) and Transfac (http://www.gene-regulation.com/index2.html) transcription-binding sites predicting tools were employed.

RESULTS

As detailed above, we sequenced a 7824-nucleotide region of human *OXTR* containing 18 SNPs (Table 4); for SNP rs53576, genotype GG and its allele G were associated with facial recognition deficits (both $P = 0.03$), while for SNP rs2254298, a significant association with prosopagnosic condition was scored for genotypes AG and AA and its allele A (respectively, $P = 0.04$ and $P = 0.01$) (Table 5).

Next, to highlight the connectivity between the above-mentioned nucleotide variations and the face-recognition performance, an unsupervised hierarchical clustering was performed (Fig. 3). This analysis was performed on all samples irrespective of participants' classification (based on the behavioral performance and self-report, see above) as prosopagnosic vs. control, but only considering participants' rs53576/rs2254298 genotypes and their scores in the face-recognition tests. An Euclidean distance matrix was then computed to cluster participants. Finally, we compared the output of the unsupervised computation with the status (CP vs. C) of each participant as established on the basis of the behavioral criteria defined above and described in Table 2. The dendrogram showed two main clusters: the former including 22 subjects (18 prosopagnosic and 4 controls) and the latter 14 subjects (all controls). The association between the identified clusters and the two categorical variables (i.e. CP vs. C) was highly significant ($P = 0.0001$, Fisher exact test). Notably, control participants number 2, 4, 5 and 7 that clusterized within the CP cluster, did not exhibit peculiar face-recognition scores compared to the other control participants (see Table 2), rather they all had G allele at rs53576 that might explain similarity with the CP group.

Then, to evaluate the effects of rs53576 and rs2254298 genotypes on the performance in the behavioral tests we used, nomograms analyses were performed. In this context, nomogram models may be used to predict the probability of an individual to be classified as CP when her/his performance in the tests we used and specific genotypes are known. Therefore, the introduced variables were the *z* scores of the various tests (Table 2) and rs53576 and rs2254298 genetic condition (Table 5) for each CP and C participant. For each test, diagrams representative of the investigated alleles/genotypes with their associated probabilities to predict the CP condition were produced (Figs. 4 and 5). One of the mainly consistent graphical signatures was the relative higher probabilities of R/G (rs53576) and R/A (rs2254298) genotypes to be associated with the CP rather than with the C condition when considering overall the face-recognition tests (Fig. 4; average probabilities 0.84 and 0.67, respectively for CP and C groups). In turn, no graphical and statistical differences in mean probabilities were reported between CP and C groups when considering performance in cognitive tests unrelated to face-recognition ability (i.e. Boston Naming test and Famous Monuments test) (Fig. 5).

To evaluate the capability of the two identified SNPs to correctly classify CP individuals, further *OXTR* sequencing analyses of rs53576 and rs2254298 were carried out with the second group of six participants of German nationality with prosopagnosia. A test learner using Receiver Operating Characteristics (ROC) analysis, based on a Naive Bayes classifying algorithm (Bradley, 1997), was used to establish the accuracy of CP classification in cross-validation supervised tests. Within the Italian samples, the CP-predicted cluster exhibited a relatively high value of area under curve (AUC = 0.8333). The AUC did not significantly vary when we introduced the additional outgroup of German prosopagnosic participants (AUC = 0.8195) (Fig. 6).

Finally, to identify putative functional effects of the identified variations at those SNPs that exhibited an association with congenital prosopagnosia, i.e. rs53576 and rs2254298, an *in silico* analysis using transcription-binding sites predicting tools was performed. Consite software predicted a reliable score for the binding of p53 transcription factor with allele A of rs53576 as DNA scaffold, while this interaction was not sustained with the G allele. Differently, alleles A and G of rs2254298 showed possible interactions predicted by Transfact tool with Heat Shock Transcriptional Factor (HSF) or Ikaros 2 (Ik-2), respectively (data not shown).

DISCUSSION

Impaired face-recognition ability in the absence of brain injury classifies individuals as having congenital prosopagnosia (e.g., Behrmann and Avidan, 2005;

Table 5. Genotypes-alleles frequency and association studies. The investigated SNPs genotypes (Gen) and alleles (all) are reported in number (*n*) and frequencies (Freq). Hardy–Weinberg equilibrium (HWE) is highlighted (χ^2, with $P > 0.05$). Association studies with Odd ratios (OR), lower and upper limits at 0.95 confidential intervals and P (Fisher exact test, significance at $P < 0.05$ indicated with asterisks) are reported.

SNP	Gen/all	Control				Prosopagnosia							
				HWE				HWE		Association			
		n	Freq	χ^2	*P*	*n*	Freq	χ^2	*P*	OR	Low	Upp	*P*
rs53576	GG	2	0.11	1.21	0.27	8	0.44	0.13	0.72	6.40	1.12	36.44	0.03*
	AA	11	0.61			2	0.11						
	R	5	0.28			8	0.44						
	G	7	0.39			16	0.89			3.66	1.11	10.01	0.03*
	A	16	0.89			10	0.56						
rs237889	TT	11	0.61	0.02	0.88	10	0.56	0.52	0.47	0.80	0.21	3.00	0.50
	CC	1	0.06			2	0.11						
	Y	6	0.33			6	0.33						
	C	7	0.39			8	0.44			1.21	0.36	4.12	0.50
	T	17	0.94			16	0.72						
rs2254295	TT	14	0.78	1.66	0.20	13	0.72	0.72	0.40	0.74	0.16	3.38	0.50
	CC	1	0.06			1	0.06						
	Y	3	0.16			4	0.22						
	T	17	0.94			17	0.94			0.80	0.18	3.50	0.53
	C	4	0.22			5	0.28						
rs2254298	GG	13	0.72	0.72	0.40	7	0.39	0.13	0.72	0.25	0.06	0.99	0.04*
	AA	1	0.06			2	0.11						
	R	4	0.22			9	0.50						
	A	5	0.28			11	0.61			4.95	1.41	17.41	0.01*
	G	17	0.94			16	0.89						
rs2268490	CC	12	0.66	0.23	0.63	12	0.66	0.23	0.63	1.00	0.25	4.00	0.64
	TT	1	0.06			1	0.06						
	Y	5	0.28			5	0.28						
	C	17	0.94			17	0.94			1.00	0.27	3.72	0.63
	T	6	0.33			6	0.33						
rs237887	GG	7	0.39	1.90	0.17	6	0.33	0.18	0.67	0.67	0.18	2.59	0.41
	AA	5	0.28			4	0.22						
	R	6	0.33			8	0.44						
	G	13	0.72			14	0.78			0.99	0.32	3.00	0.60
	A	11	0.61			12	0.66						
	CC	9	0.50	0.13	0.72	10	0.66	0.52	0.47	1.53	0.42	5.50	0.37
	TT	2	0.11			2	0.11						
	Y	7	0.39			6	0.33						
	C	16	0.89			16	0.89			1.13	0.35	3.65	0.54
	T	9	0.50			8	0.44						
rs11706648	AA	12	0.66	0.23	0.63	10	0.66	0.52	0.47	0.63	0.16	2.41	0.30
	CC	1	0.06			2	0.11						
	M	5	0.28			6	0.33						
	A	17	0.94			16	0.89			0.71	0.20	2.49	0.41
	C	6	0.33			8	0.44						

Shah, 2016). The term *congenital* refers explicitly to the absence of a lesion acquired in any period of development and calls for a genetic origin associated to a certain trait. In this study, we have identified specific DNA polymorphisms within the *OXTR* gene that might contribute to affect the performance on face-recognition tests in individuals in which prosopagnosia is present since development (congenital) and is not due to brain lesions.

It is well established that the functional effects of the different neuropeptides, including oxytocin, depend on the expression of their receptors. To this regard, Mizumoto et al. (1997) demonstrated that the third intronic region of *OXTR* is associated with transcriptional regulation of the gene itself. In their pioneristic study, the differential methylation of a CpG island within this region was associated with differences in gene expression in peripheral blood and myometrial cells; furthermore, recent studies showed that these epigenetic processes may also affect *OXTR* expression in human cortex (Gregory et al., 2009). Besides methylation, transcriptional regulation, in particular the affinity binding of transcriptional regulatory proteins within specific DNA regions, might be influenced by DNA variations. Compared with other SNPs, those located in the third intron of *OXTR* (i.e.,

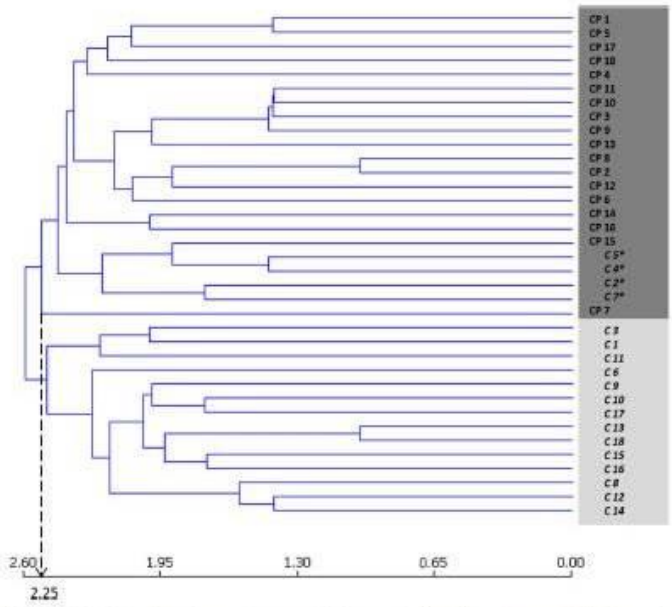

Fig. 3. Unsupervised hierarchical clustering based on genotypes and tests scores. Groups' items were created using a hierarchical unsupervised clustering algorithm. Subjects were analyzed according to their SNPs genotypes (rs53576 and rs2254298) as well as to their score in the different visual tests reported in Table 2 (but irrespective of their classification as CP or C). The analysis showed two main clusters, the inferior (light gray) composed of only control subjects and the superior (dark gray) containing mainly CP subjects with the excepton of four control subjects (i.e., control subject number 2, 4, 5, and 7, indicated with asterisks). Dissimilarity index scale is indicated (2.25 was the cut-off value that separated CP and C clusters).

rs53576, rs2254298, rs2264293, etc) have been considered in several genetics behavior studies and found to modulate various aspects of social behavior, including mind-reading and face-recognition capacities (e.g., Lucht et al., 2013; Skuse et al., 2014; Slane et al., 2014; Massey et al., 2015). In line with these evidences, our exploratory study indicated a significant association between the common genetic variants rs53576 and rs2254298 SNPs and prosopagnosia. These SNPs have been suggested to be particularly promising candidates to explain differences in oxytocinergic functioning (Meyer-Lindenberg et al., 2011). Furthermore, a combined contribution of the rs53576 and rs2254298 SNPs has been reported in disorders such anorexia (Acevedo et al., 2015), high-functioning autism (Nyffeler et al., 2014), and schizophrenia (Montag et al., 2012). In children with autism spectrum disorder, carriers of the "G" allele of rs53576 showed impaired affect recognition performance and carriers of the "A" allele of rs2254298 exhibited greater global social impairments (Parker et al., 2014). Similarly, Slane and collaborators (2014) reported that in typically developing children these SNPs consistently interacted such that the GG/AG allele combination was associated with poorer performance on neurocognitive measures, including face-processing tasks. In analogy, we have reported that the G and A alleles of rs53576 and rs2254298 are significantly associated with impaired face-processing performance, indicative of a prosopagnosic condition.

Considering our results, it is worth noting that available evidence is still controversial about whether variation in the oxytocin receptor gene may in fact explain (at least in part) individual differences in (oxytocin-related) social behavior. In particular, a recent meta-analysis in a Caucasian population considering variations in rs53576 and rs2254298 and their combined effects on different outcomes such as personality, social behavior, psychopathology, and autism, reported that *OXTR* SNPs (rs53576 and rs2254298) failed to explain significant part of human social behavior considered (Bakermans-Kranenburg and van Ijzendoorn, 2014). In a different meta-analysis study, Li et al. (2015) reported a positive association between the rs53576 polymorphism (G allele) and "general sociality" skills (i.e., how an individual responds to other people in general), but no association with "close relationships" skills (i.e., how an individual responds to individuals with closed connections, like parent–child or romantic relationship).

Rs53576 and rs2254298 are included, as all investigated SNPs, in intron 3 of *OXTR*: they respectively localize 4581 and 6724 bp upstream of the intron 3-exon 4 splice junction. Functional analysis of

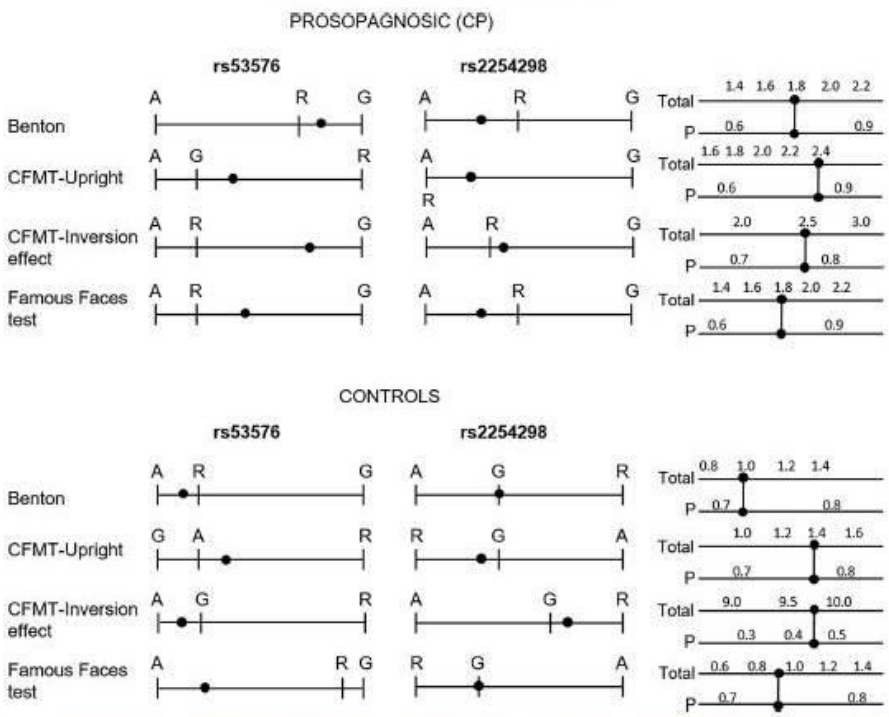

Fig. 4. Nomogram analysis for participants with congenital prosopagnosia (CP, upper panel) and control participants (lower panel). Total scores (Total) produced by the algorithm and corresponding mean probabilities (P) are reported in right columns, each related to rs53576/rs2254298 genotypes, according to participants' score in each face-recognition test. CFMT: Cambridge Face Memory Test.

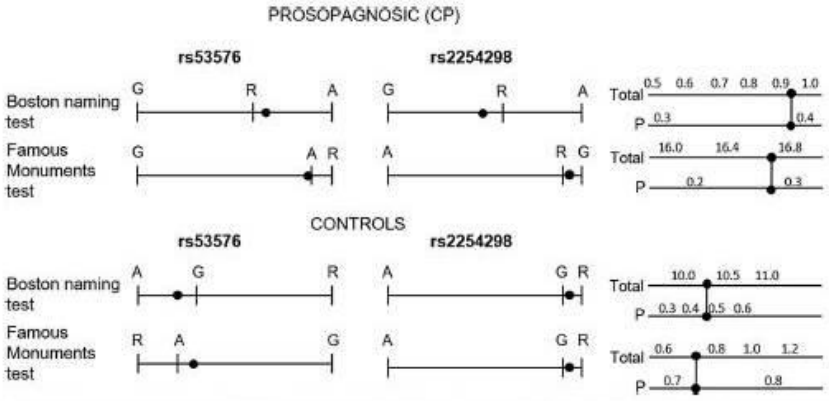

Fig. 5. Nomogram analysis for participants with congenital prosopagnosia (CP, upper panel) and control participants (lower panel). Total scores (Total) and mean probabilities (P) are reported in right columns, each related to rs53576/rs2254298 genotypes, according to participants' scores in the control behavioral tests (Boston Naming test and Famous Monuments test, respectively).

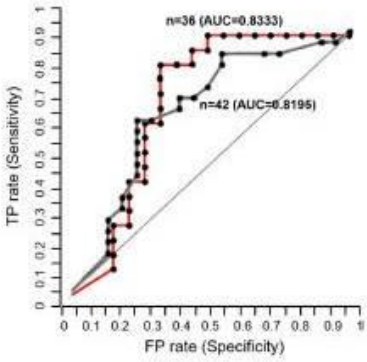

Fig. 6. Test-learners validation to predict Congenital prosopagnosia (CP) status in the investigated Italian subjects (n = 36; red line, Classification accuracy (CA) = 0.6357; sensitivity (Sens) = 0.5000; specificity (Spec) = 0.778) or with the addition of the German outgroup (total n = 42; gray line, CA = 0.7338; Sens = 0.8422; Spec = 0.6105).

these SNPs performed with transcription-binding predicting tools indicated that these genetic variations might alter transcription factor-binding sites. Specifically, DNA variations at rs53576 might influence the binding of p53. This tumor suppressor protein is widely known for its role as a transcription factor that regulates the expression of stress response genes (May and May, 1999). Furthermore, p53 has a role in controlling secretory activity, being able to suppress growth factor secretion (Hassan et al., 2006) and insulin-like growth factor-binding proteins (Grinberg et al., 2012), and to promote vasopressin and catecholamine secretion (Chernigovskaya et al., 2005). In addition, Sirotkin and colleagues (2008) reported that p53 controls ovarian oxytocin and prostaglandin secretion. In relation to the identified variations in rs2254298 SNP, we highlighted that these might influence the interaction of Heat Shock Factor (HSF), a widely recognized transcription element that regulates the expression of the heat shock proteins (Sorger, 1991) and alternatively of Ikaros-2 (Ik-2), a zinc-finger protein that strongly stimulates transcription (Agoston et al., 2007). Altogether, DNA variations at rs53576 and rs2254298 that our exploratory analyses indicated to be significantly associated with face-processing deficits, might therefore directly contribute to the regulation of the neuropeptide expression. However, deeper studies on larger samples are needed to directly prove the effect of the identified nucleotide variations in affecting *OXTR* gene expression and to clarify how these transcriptional profiles can influence the neuro-functional mechanisms mediating face processing.

Indeed, it remains to be clarified how the genetic variations we observed in CP participants affect brain structure and functional mechanisms involved in face processing. In a prior study, Bate et al. (2014) found that intranasal inhalation of the hormone oxytocin significantly improved face processing in developmental prosopagnosic participants, and argued that this effect was possibly mediated by oxytocin modulating activity in the fusiform face area and in the amygdala (the latter, part of extended face-network, see Haxby et al., 2000). A recent neuroimaging study (Andari et al., 2016) offers critical support to this hypothesis, showing that activity in the inferior occipital gyrus (comprising the occipital face area, fundamental in early stages of face perception, see Pitcher et al., 2011) and in the fusiform gyrus were significantly more activated for faces as compared to non-social cues after inhalation of oxytocin. Indeed, as noted by Andari et al. (2016), oxytocin may influence complex social behaviors partially via more basic early sensory processes of attention to social cues, as suggested by a selective neuroanatomical distribution of oxytocin receptors mainly in visual attention areas (Loup et al., 1991). In a developmental perspective, OXTR is likely to play a key role in experience-dependent programing of sensory systems during development (with neocortical OXTR for instance modulating signal-to-noise ratio in sensory processing) (see Hammock, 2015, for an extensive developmental perspective on the effects of oxytocin and vasopressin on brain and behavior). Available neuroimaging evidence indicates that congenital face-processing deficits are associated with both functional and anatomical abnormalities in the face core regions (e.g., Behrman et al., 2007; Furl et al., 2011; Gomez et al., 2015; Song et al., 2015), as well as with differences in connectivity within face-core regions and between these regions and other areas outside the core face network, including the early visual cortex (e.g., Avidan et al., 2014; Lohse et al., 2016). Although our data cannot be directly informative about the mechanisms through which genetic variations in *OXTR* affect face-recognition abilities later in life, we may speculate that oxytocin receptor genotype may affect the development of visual circuits specifically drawn up to process faces (see Hammock, 2015).

CONCLUSION

Behavioral assessment through adequate tests is critical in revealing possible deficits in face-recognition capacity. Still, the high heterogeneity in test performance, even within the same family tree (e.g. Schmalzl et al., 2008), suggests that the diagnostic criteria might suffer of a certain arbitrariness. In light of this, the genetic difference that we found between individuals with face-recognition deficits and controls, is critical not only in suggesting the relevance of specific genes in determining CP, but also in enforcing the validity of a complementary psychological/genetic approach for the diagnosis of this (not so rare) impairment. As a pioneering contribution of the effect of specific variations within *OXTR* gene and the performance on face-recognition tests, we deliberately selected a restricted but highly stringent and homogeneous cohort of cases and controls, since the demographic composition and ethnic backgrounds can originate inconsistent results as documented in oxytocin-biology studies (Bakermans-Kranenburg and van Ijzendoorn, 2014). While we stress the need to use

stringent criteria to select CP participants, we are aware that the statistical output reported in our exploratory study is limited by the small sample size considered. Nonetheless, our aim was not to offer conclusive evidence but to provide useful information for future research comprising much larger samples, possibly via a synergic collaboration among several research groups working on face-recognition deficits. Testing *OXTR* SNPs rs53576 and rs2254298 for association with additional endophenotypes related to congenital prosopagnosia, as well as considering other genes possibly involved in the predisposition for CP, will be interesting next steps to deepen our understanding of the genetic underpinning of congenital face-recognition deficits.

Acknowledgments—We are extremely grateful to Prof. Silvia Pellegrini, to Prof. Lucio Tremolizzo, to Prof. Camilo Cela-Conde and to Prof. Francisco Ayala for their critical comments on a prior version of our study and to Dr. Andrea Albonico for his precious help in data recruitment. This work was supported by a Fund for Investments on Basic Research (FIRB), Italian Ministry of Education, University and Research (RBFR12F0BD) to Z.C.

REFERENCES

Acevedo SF, Valencia C, Lutter M, McAdams CJ (2015) Severity of eating disorder symptoms related to oxytocin receptor polymorphisms in anorexia nervosa. Psychiatry Res 228 (3):641–648.

Agoston DV, Szemes M, Dobi A, Palkovits M, Georgopoulos K, Gyorgy A, Ring MA (2007) Ikaros is expressed in developing striatal neurons and involved in enkephalinergic differentiation. J Neurochem 102(6):1805–1816.

Andari E, Richard N, Leboyer M, Sirigu A (2016) Adaptive coding of the value of social cues with oxytocin, an fMRI study in autism spectrum disorder. Cortex 76:79–88.

Avidan G, Tanzer M, Hadj-Bouziane F, Liu N, Ungerleider LG, Behrmann M (2014) Selective dissociation between core and extended regions of the face processing network in congenital prosopagnosia. Cereb Cortex 24:1565–1578.

Bakermans-Kranenburg MJ, van Ijzendoorn MH (2014) A sociability gene? Meta-analysis of oxytocin receptor genotype effects in humans. Psychiatry Genet 24(2):45–51.

Bate S, Cook SJ, Duchaine B, Tree JJ, Burns EJ, Hodgson TL (2014) Intranasal inhalation of oxytocin improves face processing in developmental prosopagnosia. Cortex 50:55–63.

Behrmann M, Avidan G, Gao F, Black S (2007) Structural imaging reveals anatomical alterations in inferotemporal cortex in congenital prosopagnosia. Cereb Cortex 17:2354–2363.

Behrmann M, Avidan G (2005) Congenital prosopagnosia: face-blind from birth. Trends Cogn Sci 9(4):180–187.

Benton AL, Sivan AB, Hamsher K, Varney NR, Spreen O (1994) Contributions to neuropsychological assessment. New York: Oxford University Press.

Bowles DC, McKone E, Dawel A, Duchaine B, Palermo R, Schmalzl L, Rivolta D, Wilson CE, Yovel G (2009) Diagnosing prosopagnosia: effects of ageing, sex, and participant- stimulus ethnic match on the Cambridge Face Memory Test and Cambridge Face Perception Test. Cogn Neuropsychol 26 (5):423–455.

Bradley AP (1997) The use of the area under the roc curve in the evaluation of machine learning algorithms. Pattern Recogn 30:1145–1159.

Breiterstein C, Daum I, Ackermann H, Lutgehetmann R, Muller E (1996) Erfassung der Emotionswahrnehmung bei zentralnervosen Lasionen und Erkrankungen: Psychometrische Gutekriterien der 'Tubinger Affekt Batterie'. Neurologische Rehabilitation 2:93–101.

Breitenstein C, Daum I, Ackermann H (1998) Emotional processing following cortical and subcortical brain damage: contribution of the frontostriatal circuitry. Behav Neurol 11:29–42.

Chernigovskaya EV, Taranukhin AG, Glazova MV, Yamova LA, Fedorov LM (2005) Apoptotic signaling proteins: possible participation in the regulation of vasopressin and catecholamines biosynthesis in the hypothalamus. Histochem Cell Biol 124(6):523–533.

Daini R, Comparetti CM, Ricciardelli P (2014) Behavioral dissociation between emotional and non-emotional facial expressions in congenital prosopagnosia. Front Hum Neurosci 8:974.

Demsar J, Curk T, Erjavec A, Gorup C, Hocevar T, Milutinovic M, Mozina M, Polajnar M, Toplak M, Staric A, Stajdohar M, Umek L, Zagar L, Zbontar J, Zitnik M, Zupan B (2013) Orange: data mining toolbox in Python. J Mach Learn Res 14:2349–2353.

Domes G, Heinrichs M, Glascher J, Buchel C, Braus DF, Herpertz SC (2007) Oxytocin attenuates amygdala responses to emotional faces regardless of valence. Biol Psychiatry 62:1187–1190.

Duchaine BC, Nakayama K (2004) Developmental prosopagnosia and the Benton facial recognition test. Neurology 62:1219–1220.

Duchaine BC, Nakayama K (2006) Developmental prosopagnosia: a window to content-specific face processing. Curr Opin Neurobiol 16(2):166–173.

Duchaine BC, Germine L, Nakayama K (2007) Family resemblance: ten family members with prosopagnosia and within-class object agnosia. Cogn Neuropsychol 24:419–430.

Furl N, Garrido L, Dolan RJ, Driver J, Duchaine B (2011) Fusiform gyrus face selectivity relates to individual differences in facial recognition ability. J Cogn Neurosci 23:1723–1740.

Gomez J, Pestilli F, Witthoft N, Golarai G, Liberman A, Poltoratski S, Yoon J, Grill-Spector K (2015) Functionally defined white matter reveals segregated pathways in human ventral temporal cortex associated with category-specific processing. Neuron 85:216–227.

Gregory SG, Connelly JJ, Towers AJ, Johnson J, Biscocho D, Markunas CA, Lintas C, Abramson RK, Wright HH, Ellis P, Langford CF, Worley G, Delong GR, Murphy SK, Cuccaro ML, Persico A, Pericak-Vance MA (2009) Genomic and epigenetic evidence for oxytocin receptor deficiency in autism. BMC Med 7:62.

Grinberg YY, van Dongelen W, Kraig RP (2012) Insulin-like growth factor-1 lowers spreading depression susceptibility and reduces oxidative stress. J Neurochem 122(1):221–229.

Guastella AJ, Mitchell PB, Dadds MR (2008) Oxytocin increases gaze to the eye region of human faces. Biol Psychiatry 63(1):3–5.

Hammock EA (2015) Developmental perspectives on oxytocin and vasopressin. Neuropsychopharmacology 40(1):24–42.

Hassan I, Wunderlich A, Burchert A, Hoffmann S, Zielke A (2006) Antisense p53 oligonucleotides inhibit proliferation and induce chemosensitivity in follicular thyroid cancer cells. Anticancer Res 26(2A):1171–1176.

Haxby JV, Hoffman EA, Gobbini MI (2000) The distributed human neural system for face perception. Trends Cogn Sci 4 (6):223–233.

Kaplan E, Goodglass H, Weintraub S (1983) The Boston Naming Test. Philadelphia, PA: Lea and Febiger.

Kennerknecht I, Grueter T, Welling B, Wentzek S, Horst J, Edwards S, Grueter M (2006) First report on the prevalence of non-syndromic hereditary prosopagnosia (HPA). Am J Med Genet 140A:1617–1622.

Lee Y, Duchaine B, Wilson HR, Nakayama K (2010) Three cases of developmental prosopagnosia from one family: Detailed neuropsychological and psychophysical investigation of face processing. Cortex 46:949–964.

Li J, Zhao Y, Li R, Broster LS, Zhou C, Yang S (2015) Association of Oxytocin Receptor Gene (OXTR) rs53576 polymorphism with sociality: a meta-analysis. PLoS One 10(6):e0131820.

Lohse M, Garrido L, Driver J, Dolan RJ, Duchaine BC, Furl N (2016) Effective connectivity from early visual cortex to posterior

occipitotemporal face areas supports face selectivity and predicts developmental prosopagnosia. J Neurosci 36(13):3821–3828.
Loup F, Tribollet E, Dubois-Dauphin M, Dreifuss JJ (1991) Localization of high-affinity binding sites for oxytocin and vasopressin in the human brain. An autoradiographic study. Brain Res 555(2):220–232.
Lucht MJ, Barnow S, Sonnenfeld C, Ulrich I, Grabe HJ, Schroeder W, Völzke H, Freyberger HJ, John U, Herrmann FH, Kroemer H, Rosskopf D (2013) Associations between the oxytocin receptor gene (OXTR) and "mind-reading" in humans–an exploratory study. Nord J Psychiatry 67(1):15–21.
Malaspina M, Albonico A, Daini R (2016) Right perceptual bias and self-face recognition in individuals with congenital prosopagnosia. Laterality 21(2):118–142.
Massey SH, Estabrook R, O'Brien TC, Pine DS, Burns JL, Jacob S, Cook EH, Wakschlag LS (2015) Preliminary evidence for the interaction of the oxytocin receptor gene (OXTR) and face processing in differentiating prenatal smoking patterns. Neurosci Lett 584:259–264.
May P, May E (1999) Twenty years of p53 research: structural and functional aspects of the p53 protein. Oncogene 18 (53):7621–7636.
Meyer-Lindenberg A, Domes G, Kirsch P, Heinrichs M (2011) Oxytocin and vasopressin in the human brain: social neuropeptides for translational medicine. Nat Rev Neurosci 12:524–538.
Minnebusch DA, Suchan B, Ramon M, Daum I (2007) Event-related potentials reflect heterogeneity of developmental prosopagnosia. Eur J Neurosci 25(7):2234–2247.
Minnebusch DA, Suchan B, Köster O, Daum I (2009) A bilateral occipitotemporal network mediates face perception. Behav Brain Res 198(1):179–185.
Mizumoto Y, Kimura T, Ivell RA (1997) A genomic element within the third intron of the human oxytocin receptor gene may be involved in transcriptional suppression. Mol Cell Endocrinol 135 (2):129–138.
Montag C, Brockmann EM, Lehmann A, Müller DJ, Rujescu D, Gallinat J (2012) Association between oxytocin receptor gene polymorphisms and self-rated 'empathic concern' in schizophrenia. PLoS One 7(12):e51882.
Nyffeler J, Walitza S, Bobrowski E, Gundelfinger R, Grünblatt E (2014) Association study in siblings and case-controls of serotonin- and oxytocin-related genes with high functioning autism. J Mol Psychiatry 2(1):1.
Osterrieth PA (1944) Le test de copie d'une figure complexe. Arch Psychologie 30:206–356.
Palermo R, Rossion B, Rhodes G, Laguesse R, Tez T, Hall B, Albonico A, Malaspina M, Daini R, Irons J, Al-Janabi S, Taylor LC, Rivolta D, McKone E (2016) Do people have insight into their face recognition abilities? Q J Exp Psychol (Hove) 23:1–16.
Parker KJ, Garner JP, Libove RA, Hyde SA, Hornbeak KB, Carson DS, Liao CP, Phillips JM, Hallmayer JF, Hardan AY (2014) Plasma oxytocin concentrations and OXTR polymorphisms predict social impairments in children with and without autism spectrum disorder. Proc Natl Acad Sci U S A 111 (33):12258–12263.
Pitcher D, Walsh V, Duchaine B (2011) The role of the occipital face area in the cortical face perception network. Exp Brain Res 209:481–493.
Rimmele U, Hediger K, Heinrichs M, Klaver P (2009) Oxytocin makes a face in memory familiar. J Neurosci 29(1):38–42.
Rodriguez S, Gaunt TR, Day INM (2009) Hardy-Weinberg equilibrium testing of biological ascertainment for Mendelian randomization studies. Am J Epidemiol 169(4):505–514.
Savaskan E, Ehrhardt R, Schulz A, Walter M, Schachinger H (2008) Post-learning intranasal oxytocin modulates human memory for facial identity. Psychoneuroendocrinology 33(3):368–374.
Schmalzl L, Palermo R, Coltheart M (2008) Cognitive heterogeneity in genetically based prosopagnosia: a family study. J Neuropsychol 2(Pt 1):99–117.
Shah P (2016) Identification, diagnosis and treatment of prosopagnosia. Br J Psychiatry 208(1):94–95.
Shakeshaft NG, Plomin R (2015) Genetic specificity of face recognition. Proc Natl Acad Sci U S A 112(41):12887–12892.
Sirotkin AV, Benco A, Tandlmajerova A, Vasicek D, Kotwica J, Darlak K, Valenzuela F (2008) Transcripiton factor p53 can regulate proliferation, apoptosis and secretory activity of luteinizing porcine ovarian granulosa cell cultured with and without ghrelin and FSH. Reproduction 136(5):611–618.
Skuse DH, Lori A, Cubells JF, Lee I, Conneely KN, Puura K, Lehtimaki T, Binder EB, Young LJ (2014) Common polymorphism in the oxytocin receptor gene (OXTR) is associated with human social recognition skills. Proc Natl Acad Sci U S A 111 (5):1987–1992.
Slane MM, Lusk LG, Boomer KB, Hare AE, King MK, Evans DW (2014) Social cognition, face processing, and oxytocin receptor single nucleotide polymorphisms in typically developing children. Dev Cogn Neurosci 9:160–171.
Snodgrass JG, Vanderwart MA (1980) A standardised set of 260 pictures: norms for name agreement, familiarity, and visual complexity. J Exp Psychol Gen 6:174–215.
Song S, Garrido L, Nagy Z, Mohammadi S, Steel A, Driver J, Dolan RJ, Duchaine B, Furl N (2015) Local but not long-range microstructural differences of the ventral temporal cortex in developmental prosopagnosia. Neuropsychologia 78:195–206.
Sorger PK (1991) Heat shock factor and the heat shock response. Cell 65(3):363–366.
Susilo T, Duchaine B (2013) Advances in developmental prosopagnosia research. Curr Opin Neurobiol 23(3):423–429.
Vai S, Ghirotto S, Pilli E, Tassi F, Lari M, Rizzi E, Matas-Lalueza L, Ramirez O, Lalueza-Fox C, Achilli A, Olivieri A, Torroni A, Lancioni H, Giostra C, Bedini E, Pejrani Baricco L, Matullo G, Di Gaetano C, Piazza A, Veeramah K, Geary P, Caramelli D, Barbujani G (2015) Genealogical relationships between early medieval and modern inhabitants of Piedmont. PLoS One 10(1): e0116801.
Warrington EK (1984) Recognition Memory Test. Windsor, UK: NFER-Nelson.
Wilmer JB, Germine L, Chabris CF, Chatterjee G, Williams M, Loken E, Nakayama K, Duchaine B (2010) Human face recognition ability is specific and highly heritable. Proc Natl Acad Sci U S A 107(11):5238–5241.
Wilmer JB, Germine L, Chabris CF, Chatterjee G, Gerbasi M, Nakayama K (2012) Capturing specific abilities as a window into human individuality: The example of face recognition. Cogn Neuropsychol 29(5–6):360–392.
Yin RK (1969) Looking at upside-down faces. J Exp Psychol 81 (1):141–145.
Zhu Q, Song Y, Hu S, Li X, Tian M, Zhen Z, Dong Q, Kanwisher N, Liu J (2010) Heritability of the specific cognitive ability of face perception. Curr Biol 20(2):137–142.

(Accepted 22 September 2016)
(Available online 28 September 2016)

Cover image modified from:
Nicolle Rager Fuller – Sayo Art LLC Studio